

Methods in Molecular Biology™

VOLUME 161

Cytoskeleton Methods and Protocols

Edited by

Ray H. Gavin



HUMANA PRESS

Cytoskeleton Methods and Protocols

METHODS IN MOLECULAR BIOLOGY™

John M. Walker, SERIES EDITOR

175. **Genomics Protocols**, edited by Michael P. Starkey and Ramath Elasarapu, 2001
174. **Epstein-Barr Virus Protocols**, edited by Joanna B. Wilson and Gerhard H. W. May, 2001
173. **Calcium-Binding Protein Protocols, Volume 2: Methods and Techniques**, edited by Hans J. Vogel, 2001
172. **Calcium-Binding Protein Protocols, Volume 1: Reviews and Case Histories**, edited by Hans J. Vogel, 2001
171. **Proteoglycan Protocols**, edited by Renato V. Iozzo, 2001
170. **DNA Arrays: Methods and Protocols**, edited by Jang B. Rampil, 2001
169. **Neurotrophin Protocols**, edited by Robert A. Rush, 2001
168. **Protein Structure, Stability, and Folding**, edited by Kenneth P. Murphy, 2001
167. **DNA Sequencing Protocols, Second Edition**, edited by Colin A. Graham and Alison J. M. Hill, 2001
166. **Immunotoxin Methods and Protocols**, edited by Walter A. Hall, 2001
165. **SV40 Protocols**, edited by Leda Raptis, 2001
164. **Kinesin Protocols**, edited by Isabelle Vernos, 2001
163. **Capillary Electrophoresis of Nucleic Acids, Volume 2: Practical Applications of Capillary Electrophoresis**, edited by Keith R. Mitchelson and Jing Cheng, 2001
162. **Capillary Electrophoresis of Nucleic Acids, Volume 1: The Capillary Electrophoresis System as an Analytical Tool**, edited by Keith R. Mitchelson and Jing Cheng, 2001
161. **Cytoskeleton Methods and Protocols**, edited by Ray H. Gavin, 2001
160. **Nuclease Methods and Protocols**, edited by Catherine H. Schein, 2001
159. **Amino Acid Analysis Protocols**, edited by Catherine Cooper, Nicole Packer, and Keith Williams, 2001
158. **Gene Knockout Protocols**, edited by Martin J. Tymms and Ismail Kola, 2001
157. **Mycotoxin Protocols**, edited by Mary W. Trucksess and Albert E. Pohland, 2001
156. **Antigen Processing and Presentation Protocols**, edited by Joyce C. Solheim, 2001
155. **Adipose Tissue Protocols**, edited by Gérard Ailhaud, 2000
154. **Connexin Methods and Protocols**, edited by Roberto Bruzzone and Christian Giaume, 2001
153. **Neuropeptide Y Protocols**, edited by Ambikaipakan Balasubramanian, 2000
152. **DNA Repair Protocols: Prokaryotic Systems**, edited by Patrick Vaughan, 2000
151. **Matrix Metalloproteinase Protocols**, edited by Ian M. Clark, 2001
150. **Complement Methods and Protocols**, edited by B. Paul Morgan, 2000
149. **The ELISA Guidebook**, edited by John R. Crowther, 2000
148. **DNA-Protein Interactions: Principles and Protocols (2nd ed.)**, edited by Tom Moss, 2001
147. **Affinity Chromatography: Methods and Protocols**, edited by Pascal Bailon, George K. Ehrlich, Wen-Jian Fung, and Wolfgang Berthold, 2000
146. **Mass Spectrometry of Proteins and Peptides**, edited by John R. Chapman, 2000
145. **Bacterial Toxins: Methods and Protocols**, edited by Otto Holst, 2000
144. **Calpain Methods and Protocols**, edited by John S. Elce, 2000
143. **Protein Structure Prediction: Methods and Protocols**, edited by David Webster, 2000
142. **Transforming Growth Factor-Beta Protocols**, edited by Philip H. Howe, 2000
141. **Plant Hormone Protocols**, edited by Gregory A. Tucker and Jeremy A. Roberts, 2000
140. **Chaperonin Protocols**, edited by Christine Schneider, 2000
139. **Extracellular Matrix Protocols**, edited by Charles Streuli and Michael Grant, 2000
138. **Chemokine Protocols**, edited by Amanda E. I. Proudfoot, Timothy N. C. Wells, and Christine Power, 2000
137. **Developmental Biology Protocols, Volume III**, edited by Rocky S. Tuan and Cecilia W. Lo, 2000
136. **Developmental Biology Protocols, Volume II**, edited by Rocky S. Tuan and Cecilia W. Lo, 2000
135. **Developmental Biology Protocols, Volume I**, edited by Rocky S. Tuan and Cecilia W. Lo, 2000
134. **T Cell Protocols: Development and Activation**, edited by Kelly P. Kearsse, 2000
133. **Gene Targeting Protocols**, edited by Eric B. Kmieciak, 2000
132. **Bioinformatics Methods and Protocols**, edited by Stephen Misener and Stephen A. Krawetz, 2000
131. **Flavoprotein Protocols**, edited by S. K. Chapman and G. A. Reid, 1999
130. **Transcription Factor Protocols**, edited by Martin J. Tymms, 2000
129. **Integrin Protocols**, edited by Anthony Howlett, 1999
128. **NMDA Protocols**, edited by Min Li, 1999
127. **Molecular Methods in Developmental Biology: Xenopus and Zebrafish**, edited by Matthew Guille, 1999
126. **Adrenergic Receptor Protocols**, edited by Curtis A. Machida, 2000
125. **Glycoprotein Methods and Protocols: The Mucins**, edited by Anthony P. Corfield, 2000
124. **Protein Kinase Protocols**, edited by Alastair D. Reith, 2001
123. **In Situ Hybridization Protocols (2nd ed.)**, edited by Ian A. Darby, 2000
122. **Confocal Microscopy Methods and Protocols**, edited by Stephen W. Paddock, 1999
121. **Natural Killer Cell Protocols: Cellular and Molecular Methods**, edited by Kerry S. Campbell and Marco Colonna, 2000
120. **Eicosanoid Protocols**, edited by Elias A. Lianos, 1999
119. **Chromatin Protocols**, edited by Peter B. Becker, 1999
118. **RNA-Protein Interaction Protocols**, edited by Susan R. Haynes, 1999
117. **Electron Microscopy Methods and Protocols**, edited by M. A. Nasser Hajibagheri, 1999
116. **Protein Lipidation Protocols**, edited by Michael H. Gelb, 1999
115. **Immunocytochemical Methods and Protocols (2nd ed.)**, edited by Lorette C. Javois, 1999
114. **Calcium Signaling Protocols**, edited by David G. Lambert, 1999

METHODS IN MOLECULAR BIOLOGY™

Cytoskeleton Methods and Protocols

Edited by

Ray H. Gavin

*Department of Biology, Brooklyn College,
The City University of New York, NY*

Humana Press



Totowa, New Jersey

© 2001 Humana Press Inc.
999 Riverview Drive, Suite 208
Totowa, New Jersey 07512

All rights reserved. No part of this book may be reproduced, stored in a retrieval system, or transmitted in any form or by any means, electronic, mechanical, photocopying, microfilming, recording, or otherwise without written permission from the Publisher. Methods in Molecular Biology™ is a trademark of The Humana Press Inc.

The content and opinions expressed in this book are the sole work of the authors and editors, who have warranted due diligence in the creation and issuance of their work. The publisher, editors, and authors are not responsible for errors or omissions or for any consequences arising from the information or opinions presented in this book and make no warranty, express or implied, with respect to its contents.

This publication is printed on acid-free paper. 
ANSI Z39.48-1984 (American Standards Institute) Permanence of Paper for Printed Library Materials.

Cover design by Patricia F. Cleary.

Cover image: Structural synergy of three cytoskeletal polymers: microtubules, actin microfilaments, and cytokeratin. Cover art courtesy of Dr. William Bement.

For additional copies, pricing for bulk purchases, and/or information about other Humana titles, contact Humana at the above address or at any of the following numbers: Tel: 973-256-1699; Fax: 973-256-8341; E-mail: humana@humanapr.com, or visit our Website at www.humanapress.com

Photocopy Authorization Policy:

Authorization to photocopy items for internal or personal use, or the internal or personal use of specific clients, is granted by Humana Press Inc., provided that the base fee of US \$10.00 per copy, plus US \$00.25 per page, is paid directly to the Copyright Clearance Center at 222 Rosewood Drive, Danvers, MA 01923. For those organizations that have been granted a photocopy license from the CCC, a separate system of payment has been arranged and is acceptable to Humana Press Inc. The fee code for users of the Transactional Reporting Service is: [0-89603-771-1/01 \$10.00 + \$00.25].

Printed in the United States of America. 10 9 8 7 6 5 4 3 2 1

Library of Congress Cataloging in Publication Data

Main entry under title:

Cytoskeleton methods and protocols / edited by Ray H. Gavin.

p. cm. -- (Methods in molecular biology ; v. 161)

Includes bibliographical references and index.

ISBN 0-89603-771-1 (alk. paper)

1. Cytoskeleton--Laboratory manuals. 2. Cytoskeletal proteins--Laboratory manuals. I. Gavin, Ray H. II. Methods in molecular biology (Clifton, N.J.) ; v.161.

QH603.C96 C974 2000
571.6'54--dc21

00-035020

Preface

Over the past two decades experimental studies have solidified the interpretation of the cytoskeleton as a highly dynamic network of microtubules, actin microfilaments, intermediate filaments, and myosin filaments. Rather than a network of disparate fibers, these polymers are often interconnected and display synergy, which is the combined action of two or more cytoskeletal polymers to achieve a specific cellular structure or function. Cross-communication among cytoskeletal polymers is thought to be achieved through cytoskeletal polymer accessory proteins and molecular motors that bind two or more cytoskeletal polymers.

Development of the modern concept of the cytoskeleton is a direct outgrowth of advances in experimental tools and reagents that are available to cell and molecular biologists. Technological advances and refinements in cell imaging have made it possible to selectively image a single cytoskeletal polymer and monitor its dynamics through the use of fluorescence probes *in vitro* and *in vivo*. Two decades ago, cytoskeletal research was limited to a few perturbation reagents that included colchicine and cytochalasin. Today, the perturbation arsenal has expanded to a highly selective group of reagents that includes Taxol, nocodazole, benomyl, latrunculin, jasplakinolide, and such endogenous proteins as gelsolin. These reagents enable the investigator to selectively perturb or destroy a cytoskeletal polymer while leaving other cytoskeletal polymers intact. Site-specific monoclonal antibodies that target a specific cytoskeletal polymer have proven to be highly selective affinity tools for cytoskeletal research. PCR technology has been effectively used to identify new cytoskeletal polymer accessory proteins, and interrelationships among these proteins are being explored through the use of two-hybrid screens. Techniques for targeted gene disruption or gene replacement through site-directed mutagenesis, genetic recombination, or transient transfections are widely used with diverse groups of organisms. Increasingly, cytoskeletal research has taken advantage of the unique features of certain organisms and developed them as model experimental systems. Such model systems have been developed in fungi, protists, mollusks, insects, and flowering plants. These varied research tools and model systems enable investigators to use diverse approaches to cytoskeletal studies.

Cytoskeleton Methods and Protocols, a new volume in the *Methods in Molecular Biology* series, focuses on a select number of topics aimed at providing investigators with easy-to-read, up-to-date protocols based on several model experimental systems. An international panel of experienced investigators presents detailed protocols that combine biochemistry, immunology, genetics, microscopy, and image analysis in integrative approaches for investigations of cytoskeleton structure and function. Each protocol contains step-by-step instructions that enable both novice and experienced investigators to successfully use the technique. These protocols utilize several model systems in a variety of organisms, including *Saccharomyces*, *Micrasterias*, *Tetrahymena*, *Drosophila*, *Spisula*, and *Xenopus*. Each chapter includes a “Notes” section, containing additional, often unpublished, information that can provide solutions to anticipated problems and further serves to enhance the success of first-time users of the technique.

I thank John Walker for carefully reviewing the initial drafts of the manuscripts and for instructing me in the stylistic requirements of Humana Press. Trudy Trotta, Office Manager in the Department of Biology at Brooklyn College, and David L. Rice provided editorial assistance. *Cytoskeleton Methods and Protocols* belongs to its contributors, and I thank them for their fine contributions and their professionalism.

Ray H. Gavin

Contents

Preface	v
Contributors	xi
PART I. IDENTIFICATION OF CYTOSKELETON PROTEINS	
1 Using an Inverse PCR Strategy to Clone Large, Contiguous Genomic DNA Fragments Jorge A. Garcés and Ray H. Gavin	3
2 Microsequencing of Myosins for PCR Primer Design Elaine L. Bearer	9
3 Evaluating the Dynein Heavy Chain Gene Family in <i>Tetrahymena</i> Gangadhara Sailaja, Leslie M. Lincoln, Jifan Chen, and David J. Asai	17
PART II. MICROSCOPY APPLICATIONS	
4 Video-Enhanced Microscopy for Analysis of Cytoskeleton Structure and Function George M. Langford	31
5 Computer-Assisted Systems for the Analysis of Amoeboid Cell Motility David R. Soll, Deborah Wessels, Edward Voss, and Olof Johnson	45
6 Evaluation of Individual-Cell Motility Peter S. Walmod, Rasmus Hartmann-Petersen, Anton Berezin, Søren Prag, Vladislav V. Kiselyov, Vladimir Berezin, and Elisabeth Bock	59
7 Evaluation of Cell Morphology Eugene A. Lepekhin, Peter S. Walmod, Anton Berezin, Vladimir Berezin, and Elisabeth Bock	85
8 A Quantitative Assay for Measurement of Chemokinesis in <i>Tetrahymena</i> Uffe Koppelhus, Per Hellung-Larsen, and Vagn Leick	101

PART III. REAGENTS FOR STUDYING CYTOSKELETON PROTEIN FUNCTION

- 9 Jasplakinolide: *An Actin-Specific Reagent that Promotes Actin Polymerization*
Andreas Holzinger 109
- 10 Site-Directed Antibodies as Tools For Investigating Structure and Function of Cytoskeleton Proteins
Walter Steffen and Julie L. Hodgkinson 121
- 11 Direct Labeling of Components in Protein Complexes by Immuno-Electron Microscopy
Julie L. Hodgkinson and Walter Steffen 133
- 12 Tat-Mediated Delivery of Antibodies into Cultured Cells
Walter Steffen 141

PART IV. CYTOSKELETON DYNAMICS

- 13 Studying Cytoskeletal Dynamics in Living Cells Using Green Fluorescent Protein
Yisang Yoon, Kelly R. Pitts, and Mark A. McNiven 151
- 14 Use of Green Fluorescent Protein to Study Cellular Dynamics: *Constructing GFP-Tagged Motor Enzymes*
Hong Cao, Heather M. Thompson, Eugene W. Krueger, and Mark A. McNiven 165
- 15 Transient Transfections and Heterokaryons as Tools for the Analysis of Keratin IF Dynamics
Jesús M. Paramio and José L. Jorcano 189

PART V. CELLULAR SYSTEMS AS TOOLS FOR INVESTIGATING CYTOSKELETON STRUCTURE AND FUNCTION

- 16 Chromatophores as Tools for the Study of Organelle Transport
Bruce R. Telzer and Leah T. Haimo 201
- 17 Centriole Duplication, Centrosome Maturation, and Spindle Assembly in Lysates of *Spisula solidissima* Oocytes
Andrew W. Suddith, Eugeni A. Vaisberg, Sergei A. Kuznetsov, Walter Steffen, Conly L. Rieder, and Robert E. Palazzo 215
- 18 *Xenopus* Egg Extracts as a Model System for Analysis of Microtubule, Actin Filament, and Intermediate Filament Interactions
Craig A. Mandato, Kari L. Weber, Anna J. Zandy, Thomas J. Keating, and William M. Bement 229

19 Detergent-Extracted Models for the Study of Cilia or Flagella
Charles B. Lindemann and Kathleen A. Schmitz 241

PART VI. GENETIC APPROACHES FOR STUDIES OF CYTOSKELETON PROTEIN FUNCTION

20 A Yeast Two-Hybrid Approach for Probing Cytoskeletal
 Protein Interactions
Jin-jun Meng and Wallace Ip 255

21 Manipulating Dynein Genes in *Tetrahymena*
**David J. Asai, K. Mark DeWall, Leslie M. Lincoln,
 and Renotta K. Smith 269**

22 Functional Analysis of Cytoskeletal Components in the Developing
 Visual System of *Drosophila*
Qi He 279

Index **285**

Contributors

- DAVID J. ASAI • *Department of Biological Sciences, Purdue University, West Lafayette, IN*
- ELAINE L. BEARER, MD • *Department of Pathology and Laboratory Medicine, Brown University Medical School, Providence, RI*
- WILLIAM M. BEMENT • *Program in Cellular and Molecular Biology, Department of Zoology, University of Wisconsin, Madison, WI*
- ANTON BEREZIN • *Protein Laboratory, Institute of Molecular Pathology, University of Copenhagen, Copenhagen, Denmark*
- VLADIMIR BEREZIN • *Protein Laboratory, Institute of Molecular Pathology, University of Copenhagen, Copenhagen, Denmark*
- ELISABETH BOCK • *Protein Laboratory, Institute of Molecular Pathology, University of Copenhagen, Copenhagen, Denmark*
- HONG CAO • *Center for Basic Research in Digestive Diseases, Department of Gastroenterology and Hepatology, Mayo Clinic, Rochester, MN*
- JIFAN CHEN • *Department of Biological Sciences, Purdue University, West Lafayette, IN*
- ELISE DARGELOS • *Laboratoire de Biochimie et Technologie des Aliments, Université Bordeaux, Talence, France*
- K. MARK DEWALL • *Department of Biological Sciences, Purdue University, West Lafayette, IN*
- JORGE A. GARCÉS • *Athena Diagnostics Inc., Division of Elan Pharmaceuticals, Worcester, MA*
- RAY H. GAVIN • *Department of Biology, Brooklyn College, City University New York, Brooklyn, NY*
- LEAH T. HAIMO • *Department of Biology, University of California, Riverside, CA and Marine Biological Laboratory, Woods Hole, MA*
- RASMUS HARTMANN-PETERSEN • *Protein Laboratory, Institute of Molecular Pathology, University of Copenhagen, Copenhagen, Denmark*
- QI HE • *Department of Biology, City University New York, Brooklyn College, Brooklyn, NY*

- PER HELLUNG-LARSEN • *Department of Medical Biochemistry and Genetics Biochemistry Laboratory B, University of Copenhagen, The Panum Institute, Copenhagen, Denmark*
- JULIE L. HODGKINSON • *National Heart and Lung Institute, Cardiac Medicine, Imperial College of Science, Technology, and Medicine, London, UK*
- ANDREAS HOLZINGER • *Institute for Plant Physiology, University of Salzburg, Salzburg, Austria*
- WALLACE IP • *Department of Cell Biology, Neurobiology and Anatomy, Vontz Center for Molecular Studies, University of Cincinnati College of Medicine, Cincinnati, OH*
- OLOF JOHNSON • *WM Keck Dynamic Image Analysis Facility, Department of Biological Sciences, University of Iowa, Iowa City, IA*
- JOSÉ L. JORCANO • *Department of Cell and Molecular Biology, CIEMAT, Madrid, Spain*
- THOMAS J. KEATING • *Laboratory of Molecular Biology, University of Wisconsin, Madison, WI*
- VLADISLAV V. KISELYOV • *Protein Laboratory, Institute of Molecular Pathology, University of Copenhagen, Copenhagen, Denmark*
- UFFE KOPPELHUS • *Center for Biomolecular Recognition, Department of Medical Biochemistry and Genetics Biochemistry Laboratory B, University of Copenhagen, Copenhagen, Denmark*
- EUGENE W. KRUEGER • *Center for Basic Research in Digestive Diseases, Department of Gastroenterology and Hepatology, Mayo Clinic and Foundation, Rochester, MN*
- SERGEI A. KUZNETSOV • *Institute of Cell Biology and Biosystems Technology, University of Rostock, Rostock, Germany*
- GEORGE M. LANGFORD • *Department of Biological Sciences, Dartmouth College, Hanover, NH*
- VAGN LEICK • *Department of Medical Biochemistry and Genetics Biochemistry Laboratory B, University of Copenhagen, The Panum Institute, Copenhagen, Denmark*
- EUGENE A. LEPEKHIN • *Protein Laboratory, Institute of Molecular Pathology, University of Copenhagen, Copenhagen, Denmark*
- LESLIE M. LINCOLN • *Interdepartmental Genetics Program, Iowa State University, IA*
- CHARLES B. LINDEMANN • *Department of Biological Sciences, Oakland University, Rochester, MI*

- CRAIG A. MANDATO • *Department of Zoology, University of Wisconsin, Madison, WI*
- MARK A. MCNIVEN • *Center for Basic Research in Digestive Diseases, Department of Gastroenterology and Hepatology, Department of Biochemistry and Molecular Biology, Mayo Clinic and Foundation, Rochester, MN*
- JIN-JUN MENG • *Department of Cell Biology, Neurobiology and Anatomy, Vontz Center for Molecular Studies, University of Cincinnati College of Medicine, Cincinnati, OH*
- ROBERT E. PALAZZO • *The Department of Molecular Biosciences, University of Kansas, Lawrence, KS*
- JESÚS M. PARAMIO • *Department of Cell and Molecular Biology, CIEMAT, Madrid, Spain*
- KELLY R. PITTS • *Department of Biochemistry and Molecular Biology, Mayo Graduate School, Mayo Clinic and Foundation, Rochester, MN*
- SØREN PRAG • *Protein Laboratory, Institute of Molecular Pathology, University of Copenhagen, Copenhagen, Denmark*
- CONLY L. RIEDER • *Wadsworth Center for Laboratories and Research, Albany, NY*
- GANGADHARA SAILAJA • *Department of Veterinary Pathobiology, Purdue University, West Lafayette, IN*
- KATHLEEN A. SCHMITZ • *Department of Biological Sciences, Oakland University, Rochester, MI*
- RENOTTA K. SMITH • *Department of Biological Sciences, Purdue University, West Lafayette, IN*
- DAVID R. SOLL • *Director, WM Keck Dynamic Image Analysis Facility, Department of Biological Sciences, University of Iowa, Iowa City, IA*
- WALTER STEFFEN • *FB Biologie, Institut für Zellphysiologie und Biosystemtechnik, Universität Rostock, Rostock, Germany*
- ANDREW W. SUDDITH • *The Department of Molecular Biosciences, University of Kansas, Lawrence, KS*
- BRUCE R. TELZER • *Department of Biology, Pomona College, Claremont, CA and Marine Biological Laboratory, Woods Hole, MA*
- HEATHER M. THOMPSON • *Department of Biochemistry and Molecular Biology, Mayo Graduate School, Mayo Clinic and Foundation, Rochester, MN*
- EUGENI A. VAISBERG • *The Department of Molecular, Cell, and Developmental Biology, University of Colorado, Boulder, CO*
- EDWARD VOSS • *WM Keck Dynamic Image Analysis Facility, Department of Biological Sciences, University of Iowa, Iowa City, IA*

PETER S. WALMOD • *Protein Laboratory, Institute of Molecular Pathology,
University of Copenhagen, Copenhagen, Denmark*

KARI L. WEBER • *Department of Zoology, University of Wisconsin,
Madison, WI*

DEBORAH WESSELS • *WM Keck Dynamic Image Analysis Facility, Department
of Biological Sciences, University of Iowa, Iowa City, IA*

YISANG YOON • *Center for Basic Research in Digestive Diseases, Department
of Gastroenterology and Hepatology, Mayo Clinic and Foundation,
Rochester, MN*

ANNA J. ZANDY • *Department of Zoology, University of Wisconsin,
Madison, WI*

I _____

Identification of Cytoskeleton Proteins

Using an Inverse PCR Strategy to Clone Large, Contiguous Genomic DNA Fragments

Jorge A. Garcés and Ray H. Gavin

1. Introduction

Conventional PCR screens of genomic DNA will often yield a substantial fragment of the gene of interest. However, identification of flanking sequences on either side of a known sequence can be problematic with conventional PCR, in which primers extend a complementary chain in a 5' → 3' direction. However, if the template DNA is circularized and then used with primers that are oriented with their 3' ends directed away from each other, amplification around the circular template results in a linear PCR product consisting of uncharacterized DNA fragments flanked by the known DNA sequences (**Fig. 1**). This variation of the conventional PCR strategy is known as inverse PCR (**1,2**), and we have used the technique to amplify myosin sequences in *Tetrahymena* (**3**). In this chapter we describe protocols that enable the investigator to apply the inverse PCR technique to clone contiguous sequences upstream and downstream of a known DNA sequence.

1.1. General Scheme for Cloning Contiguous Sequences

1. Purify and cut genomic DNA sample with appropriate restriction enzyme. EcoR1 is shown in **Fig. 1**. Black box shows region of initially known sequence.
2. Perform inverse PCR reactions as described using primer sequences within the region of known sequence.
3. After the inverse PCR product has been cloned and sequenced, a full-length contiguous fragment may be amplified by conventional PCR using primer sequences at or adjacent to the EcoR1 sites from a genomic DNA template. Search for new restriction sites within this latest cloned stretch of DNA. A Hind III site is shown in **Fig. 1**.

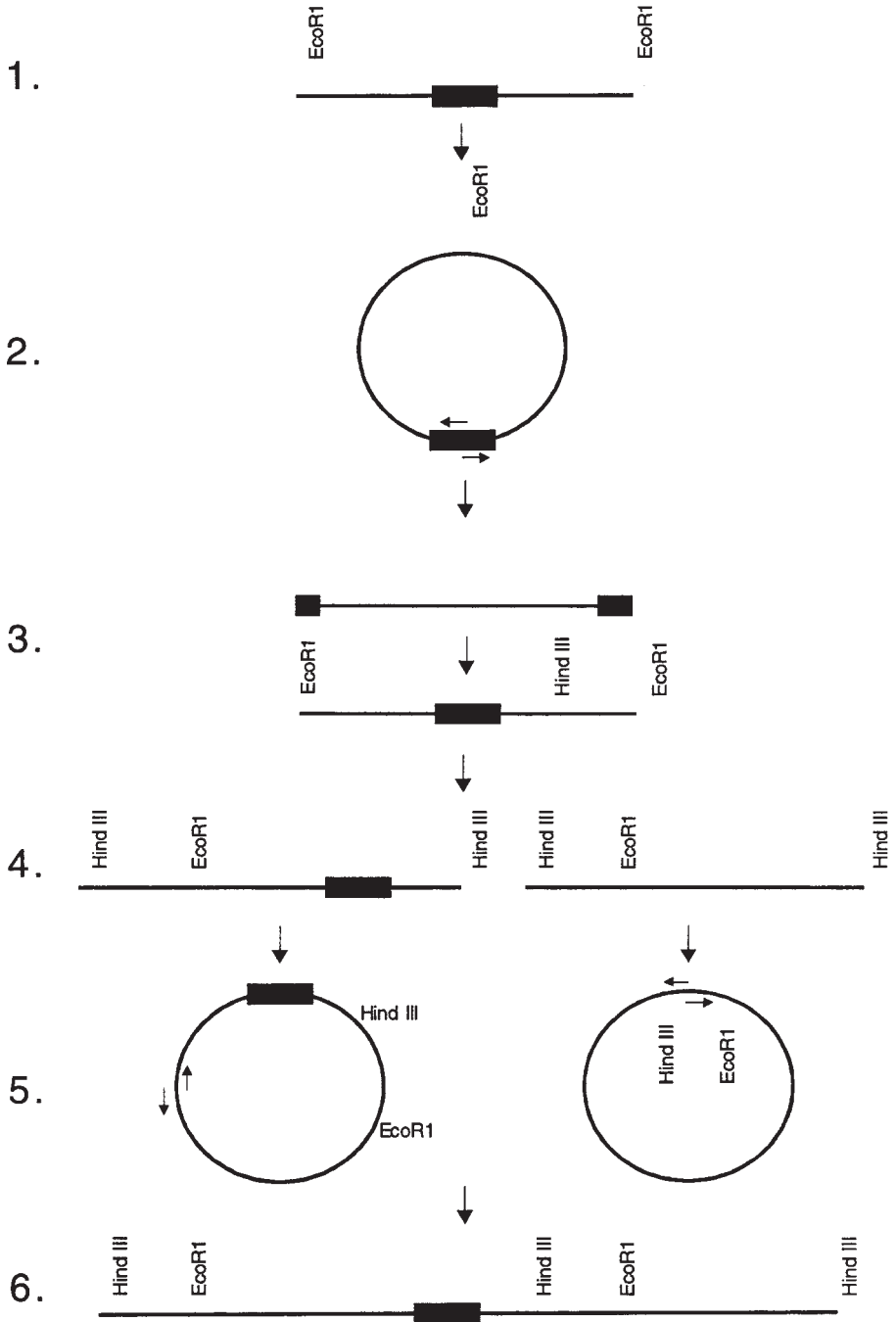


Fig. 1. General scheme for cloning contiguous sequences.

4. Cut genomic DNA sample with the second restriction enzyme. This creates two fragments that will serve as template for the inverse PCR reaction and facilitates amplification of novel sequences both upstream and downstream of the known sequence.
5. Obtain additional clones by inverse PCR. The overlap between the new and old clones allows for proper orientation of the inverse PCR fragments and prevents the creation of gaps in a contiguous sequence. PCR primers are designed from regions of known sequence as depicted in the diagram.
6. Amplify full-length contiguous DNA fragment by conventional PCR using primer sequences at or adjacent to the outermost Hind III sites. Using this strategy, between 5 and 10kb of novel contiguous DNA sequence information can be obtained after only two rounds of inverse PCR. Further inverse PCR cycles using fragments left and right of the starting fragment will yield more sequence. This strategy may be repeated to “walk” both upstream and downstream of a known DNA sequence.

2. Materials

1. Chroma-Spin column (Clontech) with an exclusion limit of 1000 bp.
2. T4 Ligase.
3. Ligase Buffer: 66 mM Tris-HCl (pH 7.6), 6.6 mM MgCl₂, 0.1 mM ATP, 0.1 mM spermidine, 10 mM DTT and stabilizers.
4. PCR Buffer: 25 mM Tricine, pH 8.7, 85 mM KOAc, 8–10% glycerol, 2% DMSO, dNTP mix: 10 mM dNTP mix [200 μM final concentration for each dNTP].
5. rTth polymerase-XL (Perkin-Elmer). (*see Note 1*).
6. Glycerol reagent.
7. Dimethylsulfoxide (DMSO) reagent.
8. Agarose gel electrophoresis reagents.
9. Clean, sharp razor blades.

3. Methods

3.1. Designing PCR Primers

Design primers suitable for your application (*see Note 2*).

3.2. Digestion and Purification of Template DNA

1. Mix the following components in a microfuge tube:
 - a. 30 μg genomic DNA.
 - b. 30 units of a suitable restriction enzyme (*see Note 3*).
 - c. Enzyme buffer according to supplier’s directions.
 - d. Distilled water to 50 μL.
2. Incubate at 37°C for 1 h.
3. Purify digestion products from **step 2** by using a Chroma-Spin column. (*see Note 4*).

3.3. Circularizing the DNA

1. Make serial dilutions of the purified DNA prepared in **Subheading 3.2**.
2. Set-up the ligation reaction in small PCR tubes as follows (*see* **Notes 5** and **6**):
 - a. Diluted DNA.
 - b. 6 Weiss units of T4 ligase in ligation buffer.
 - c. Incubate at 16°C for 60 min. (*see* **Note 7**).
3. Purify circularized fragments by using a Chromaspin column.
4. Use the purified, circularized DNA for inverse PCR as described in **Subheading 3.4**.

3.4. Inverse PCR

3.4.1. DNA Template

Make serial dilutions of the circularized DNA prepared in **Subheading 3.3**.

3.4.2. PCR Reaction Mixtures (*see* **Notes 8–10**)

3.4.2.1. LOWER LAYER OF PCR MIXTURE

1. Add the following reagents to a PCR tube:
 - a. 14 μL distilled water
 - b. 12 μL PCR buffer
 - c. 1 μL primers [0.5 μM each]
 - d. 8 μL of dNTP mix
 - e. 5.0 μL Mg (OAc)₂ = 1.25 mM final Mg concentration.
2. Place an AmpliWax bead on top of the mixture.
3. Heat the tube at 80°C for 5 min.
4. Resolidify the wax by returning the tube to room T_m for 5 min.

3.4.2.2. UPPER LAYER PCR MIXTURE

Add the following reagents to the PCR tube:

1. 18 μL PCR buffer.
2. 1 μg circularized DNA.
3. 20 μL of rTth polymerase-XL.
4. Distilled water to total a 60 μL volume.

3.4.2.3. PCR CYCLE

Select suitable cycling parameters and initiate the reaction (*see* **Note 11**).

3.4.3. Analyzing the PCR Products

1. Analyze the PCR products using agarose gel electrophoresis.
2. Excise the band of interest and clone into a suitable vector for sequencing and expression.

4. Notes

1. This approach has been successfully used to amplify *Tetrahymena* DNA fragments ranging from 2–8 kb. It is important to use a cocktail mixture of DNA polymerase enzymes such as rTth polymerase-XL (Perkin-Elmer) or *Taq*/pfu (Stratagene), which are proportionally premixed to enhance amplification of long PCR products and allow for proofreading activity to minimize random mutagenesis of amplification products.
2. For amplification of ciliated protozoan sequences, recommended characteristics for primers include: oligomers consisting of 21–24 nucleotides, a T_m between 60–68°C, and 50% G-C rich composition. The T_m of the primers should not differ by more than 3–5° from each other. If the T_m of the primers varies by 5–10°, use a touch down approach from the highest to the lowest T_m value. For example, in a two-step PCR reaction in which the T_m of one primer is 68° and the T_m of the second primer is 62°, start with a cycle consisting of a 94-degree denaturation step followed by a 68 degree combined annealing/extension step. Subtract 0.5°C from the annealing/extension step in each subsequent PCR cycle. A 5 s time increment should be added to the annealing/extension step of each subsequent cycle to compensate for a slight decrease in the DNA polymerase's rate of nucleotide incorporation as the reaction progresses. The last eighteen of thirty cycles consist of a 94-degree denaturation step followed by a 62 degree combined annealing/extension step.
3. A suitable restriction enzyme should generate fragments about 2–3 kb (*see Note 5*) with a four base overhang to facilitate ligation. Select an enzyme that has a recognition site compatible with the template DNA based on G-C/A-T content. For example, in *Tetrahymena*, A-T content of genomic DNA is high, and enzymes such as EcoRI and Hind III, which cut at A-T rich sites, yield fragments in the desired size range. In contrast, enzymes such as BamHI, which cuts at G-C rich sites, yield fragments that are too long for efficient use in inverse PCR. Hybridization blotting can be used to confirm the identity of the restriction fragments.
4. Alternatively, gel electrophoresis can be used to purify the digestion products and to identify components of optimum size for circularization (*see Note 5*). Use a sharp clean razor blade to excise the band of interest from the gel and purify fragments using the Gel Extraction Kit (Qiagen).
5. Many of the problems encountered with inverse PCR can often be traced to characteristics of the template DNA. In creating the circular DNA template, there is competition between concatamer formation and circularization of DNA fragments. The optimum DNA concentration that promotes circularization varies with the length of the DNA to be circularized and must be determined empirically for each template. In general, the optimum size range for efficient circularization is 2–3 kb. Fragments outside this range fail to circularize efficiently.
6. Perform a range of ligation reactions with varying concentrations (10 ng–1.0 µg) of the purified, digested DNA.
7. A 1 h incubation period is used instead of the standard overnight incubation because it appears optimal for biasing circularization over concatamer formation.

8. Use a hot start approach to minimize mispriming. For hot start PCR, a wax bead (AmpliWax PCR Gem 100; Perkin Elmer) is used as a barrier between layers consisting of different PCR components. Melting and subsequent solidification of the wax bead allows PCR components to be mixed at a T_m higher than the highest annealing T_m in the PCR cycle. The wax also eliminates the need for oil or a heated lid to minimize condensation at the top of the tube.
9. In order to lower the high melting temperatures required for denaturation of closed circular DNA, the DNA can be linearized at a site between primers. Alternatively, a PCR buffer containing DMSO and glycerol as solvents can be used to overcome difficult secondary structure restrictions.
10. Magnesium concentration can be varied as desired.
11. A recommended cycle consists of a pre-PCR hold at 94° for 10–15 s and 12 rounds of a two step PCR-cycling program that combines annealing and extension steps. Each cycle consist of a denaturation step at 94° for 12 s, an annealing/extension step at 65° for 5–12 min (1 kb/min), and 18 cycles of the same two-step process with time increments of 12 s per cycle added to the annealing/extension step. An extension at 72° for 10–15 min is used as the final step in the reaction.

Acknowledgments

This work was supported by Grant MCB 9808301 from the National Science Foundation to RHG.

References

1. Ochman, H., Gerber, A. S., and Hartl, D. L. (1988) Genetic applications of an inverse polymerase chain reaction. *Genetics* **120**, 621–625.
2. Triglia, T., Peterson, M. G., and Kemp, D. J. (1988) A procedure for in vitro amplification of DNA segments that lie outside the boundaries of known sequences. *Nucleic Acids Res.* **16**, 8186.
3. Garcés, J. and Gavin, R. H. (1998) A PCR screen identifies a novel, unconventional myosin heavy chain gene (*MYO1*) in *Tetrahymena thermophila*. *J. Euk. Microbiol.* **45**, 252–259.

Microsequencing of Myosins for PCR Primer Design

Elaine L. Bearer

1. Introduction

1.1. Background

Their large size and their relative resistance to proteolytic cleavage (1) make myosins particularly difficult substrates for the acquisition of their peptide sequences by standard protocols. For this reason, instead of identifying myosins first according to their biochemical activity and then obtaining their sequences, PCR and other DNA-based techniques exploiting the highly conserved sequences in the amino end, the “head” domain, have been used to find new myosins (2–5). However, such identification of myosins by sequence leaves open the question of their function. If peptide sequence could be obtained from myosin proteins whose biochemical behavior was known, then the gap between function and sequence could be bridged. We describe here a method that enabled us to acquire peptide sequences of semi-purified myosins (6).

1.2. Rationale for the Strategy

There are several difficulties that must be overcome to obtain peptide sequences from myosins. First, a sufficient amount of protein that is reasonably pure must be obtained. For muscle and non-muscle myosin IIs this is rarely a problem, although it can pose problems if the organism or the tissue to be studied is small, rare or otherwise difficult to obtain in large quantities—as is the case for axoplasm from the squid giant axon (6–10) or the organism *Tetrahymena* (2). This chapter will not address problems of abundance since they pertain to individual applications.

Once sufficient amounts (micrograms) of a myosin have been obtained, the protein must be proteolytically cleaved into peptide fragments. These fragments must then be purified to homogeneity for Edman digestion to

produce readable sequence. Myosin is relatively protease resistant. The coil-coil region in the tail and the tight packing of the amino head domain prevent cleavage at all but the neck region that links the two domains. Chymotrypsin, trypsin and pronase all produce cleavage in the neck and leave the rest of the molecule intact even under conditions when other proteins would be reduced to peptide fragments. Since tight packing of these domains in myosin is likely responsible for this protease resistance, we unwind the myosin before proteolysis with sodium dodecyl sulfate (SDS), although other chaotropic agents may work as well. While low levels of SDS unwind myosin, the proteolytic enzyme endolys C, a serine protease, remains active in SDS. This strategy results in sensitivity to proteolysis throughout the myosin molecule.

After proteolytic cleavage, the resultant peptide fragments must be separated. For a large molecule this is particularly difficult as complete digestion results in a very large number of small peptides, often with very similar properties making them difficult to separate. Hence, chromatographic separation must be performed in two steps in order to obtain adequately pure peptides. Several factors including inadequate amount of starting material, incomplete digestion of proteins, or loss of peptides during the chromatographic separations, can lead to insufficient quantities of each purified peptide for the final sequencing reaction.

The following protocol was first developed using squid muscle myosin as starting material. At the time, that myosin had not been purified, and its sequence had not been obtained. The sequence of squid muscle myosin II was ultimately obtained by a combination of two approaches: (1) PCR sequencing using primers to hypothetically homologous domains from scallop muscle myosin, a myosin from a related species, and (2) PCR sequencing using degenerate PCR primers based on the peptide sequences we obtained from the purified squid protein (*11,12*). After devising a strategy applicable to muscle myosins, we then applied this strategy to the identification of a squid brain myosin not so easily obtained in large amounts (*6,10,13,14*). Others have since applied our strategy to obtain sequences from other squid optic lobe myosins (*15*). This strategy is therefore likely to be of use for most myosins even those that are significantly less abundant than muscle myosin. This method can be applied to purified myosin in solution or semi-pure myosin excised from a Coomassie-stained SDS-PAGE gel. The strategy as we applied it was a compilation and modification of previously reported methods (*16–18*).

2. Materials

2.1. Reagents and Glassware

1. Endoproteinase Lys-C (Wako Chemicals, Richmond, VA).
2. Guanadinium hydrochloride (Sigma Chemicals, St. Louis, MO).

3. Biospin-30 chromatography column (BioRad, Hercules, CA).
4. Millex HV filter (Millipore, Bedford, MA).
5. Vydac 218TP52 column (Separations Industries, Metuchen, NJ).
6. YMC ODS AQ column (YMC, Willmington, NC).
7. Briobrene-treated glass fiber filter (Applied Biosystems, Foster City, CA).

2.2. Buffers

1. Myosin storage buffer (MS): 0.5M KCl, 3 mM NaN₃, 2 mM MgCl₂, 1 mM DTT, 2 mM EGTA, 4 mM NaHCO₃ (pH 7.0), 50% glycerol.
2. NED: 0.1 mM NaHCO₃, 0.1 mM EGTA, 0.1 mM DTT.
3. Digestion buffer (DB): 0.1 % SDS, 100 mM NH₄HCO₃.
4. Solvent A: 0.1% trifluoroacetic acid in water.
5. Solvent B: 0.1% trifluoroacetic acid in acetonitrile.

2.3. Equipment

1. Beckman System Gold HPLC equipped with an autosampler (model 507), diode array detector (model 168), and programmable solvent module (model 126).
2. Applied Biosystems pulsed-liquid protein sequencer (model 477A) equipped with PTH analyzer (model 120A).
3. Applied Biosystems data analysis system (model 610A).

3. Methods

3.1. Proteolytic Digestion of Myosins (see Notes 1–4)

1. Precipitate purified myosin out of buffer (MS) by adding a tenfold volume of NED to 40 µg of the myosin suspension.
2. Incubate for 1–4 h on ice.
3. Collect the precipitate by centrifugation at 16,000g in a microfuge for 30 min (see Note 1).
4. While the myosin is precipitating, equilibrate the BioSpin 30 column. First remove the packing buffer by centrifuging in the 2 mL tube (comes with the kit from BioRad) for 1 min at 1,000g or until the entire amount has passed through the column. Discard the buffer. Next add 100 µL of DB to the top of the column and centrifuge again. It is best to use a swinging bucket rotor, but you can also do this with a benchtop microfuge. After the DB has passed through the column, remove it, and let the tube sit on the bench until loading.
5. Resuspend the myosin precipitate in 80 µL of DB. Heat to boiling (95–100°C) for 5 min.
6. Apply 80 µL of denatured protein solution to the DB-equilibrated BioSpin 30 column and centrifuge the tube for 4 min at 1000g. This removes light chains that are released during the denaturation process, and any other contaminating proteins smaller than 40 kDa which are retained in the column. Dispose of the column, and use the solution that passed through it for subsequent steps.
7. Add to the column eluate 6 µL of DB containing 1.5 µg of endoproteinase Lys C. Put samples in 37°C water bath and allow to digest overnight (16 h).

8. Add 150 μL of DB and 150 μL of 1M guanidinium hydrochloride to the digests. The SDS will precipitate. Clarify the protein suspension by centrifugation for 15 min in a microfuge at full speed, room temperature.
9. Pass the supernatant through a Millex HV filter unit to remove any residual SDS precipitates.
10. While the SDS is precipitating, prepare HPLC Vydac 218TP52 column by equilibrating in 1.6% Solvent B in Solvent A.

3.2. Isolation of Peptides

1. Load the entire 300 μL sample into the loop of the input line to the HPLC column.
2. Elute column at 0.25 mL/min with a three step gradient. We used a binary solvent delivery system. Step 1: 1.6–29.6% Solvent B in Solvent A (0–63 min, 15.75 mL). Step 2: 29.6–60% Solvent B in Solvent A (64–95 min, 7.75 mL). **Step 3:** 60–80% Solvent B in Solvent A (95–105 min, 2.5 mL).
3. After the final elution, wash the column for 12 min in 80% Solvent B in Solvent A and then re-equilibrate in 1.6% Solvent B in Solvent A.
4. Monitor protein concentration at 215 and 280 nm wavelength. Collect fractions at 30 s intervals and store them at -70°C . Select one fraction from each of the highest, narrow peaks that eluted at least several minutes apart. The fractions selected should be as symmetric (up slope similar to down slope) as possible. Such symmetric, sharp, high peaks are most likely to contain one or only a few peptides species.
5. Pool the separated peaks for loading on the second column. This eliminates the peptides eluting between these higher peaks. By loading these fractions onto a second, different C18 (18 carbon-chain) reverse phase column peptides whose elution is overlapping through the first chromatographic step, can be separated into the empty intervening elution. Even though the second column is also a C18 column, it behaves differently enough to separate the same set of peptides that were not separated on the first column.
6. Remove the acetonitrile by evaporation in a Savant Speed Vac (centrifuge for 1 h/100 μL of sample). While the sample is in Speed Vac, equilibrate the second column, YMC ODS AQ column, in 1.6% Solvent B in Solvent A.
7. Load the sample (max 500 μL) into the loop of the HPLC and elute with the same series of step gradients as for the first column, at the same rate (0.25 mL/min) at 35°C .
8. Monitor protein concentrations as before. Collect 0.125 mL fractions at 30 s intervals and store them at -70°C (see **Note 5**).

3.3. Peptide Sequencing

1. Select a fraction from a narrow high peak and thaw rapidly. Apply 30 μL onto a Briobrene-treated glass fiber filter loaded into the drying arm of the 477a sequencer.

2. Lower the drying arm. When the 30 μL is dried down onto the filter, load another 30 μL and dry and so on until the entire sample has been dried down onto the fiber filter.
3. Load the filter into the cartridge of the sequencer and then activate the machine.
4. Collect amino acid profiles amino acid profiles and analyze on the data analysis machine.

4. Notes

1. Myosins that do not precipitate in NED can also be pelleted with addition of 1/10 volume of trichloroacetic acid for 15 min on ice. The resultant precipitate is collected by centrifugation in a microfuge at 16,000g for 15 min at 4°C.
2. To increase the yield of protein from a protein purification preparation, we decreased the number of solution purification steps and used gel electrophoresis as the final step at an earlier stage in the purification protocol. This strategy also helps eliminate contamination of the soluble purified myosin with proteins of different molecular weights, although it allows higher levels of contamination with proteins of similar molecular weight. Many of the more abundant proteins in most systems have been cloned and sequenced, and such contaminants can usually be eliminated by databank identification as a non-myosin. By digesting in the gel and eluting the resultant peptide fragments, we were able to overcome the problems encountered by poor transfer of intact myosins out of the gel onto PDVF membranes.
3. For in-gel digestion: Protein is electrophoretically purified through a 6% polyacrylamide-SDS gel to facilitate separation of high molecular weight species and to increase the yield of peptides eluting from the gel after digestion. We use 0.8% *bis*-acrylamide, not 1% as recommended in Maniatis. Sometimes better separation can be obtained with 0.6% *bis*. The gel is stained with Commassie, destained, and mounted in water on an acid-cleaned glass plate. A razor, cleaned with ethanol and rinsed in bleach, is used to excise the band of interest. Gel bands are stored in distilled water and can be stored at -70°C . A high protein to acrylamide ratio results in a better yield from the digest. Twenty gel slices with 0.5–10 μg of protein each are digested in 140 μL of DB with 1.5 μg of endoproteinase Lys-C overnight at 37°C. The solution is removed from the tube and another 150 μL of DB added and allowed to soak for 1 h at room temperature. This second “wash” is pooled with the digest and 50 μL of 6M guanidinium added and the sample vortexed to precipitate the SDS. The precipitate is removed by passage through the Millex filter and then processed by HPLC as described above.
4. To improve proteolytic digestion, SDS is used to open proteolytic sites in the myosin, particularly in the head and coil-coiled domains in the tail. Alkylation and reduction do not improve digestion for these particular proteins. However, other myosins or other high molecular weight proteins may expose protease sensitive sites if they are alkylated and reduced. Alkylation/reduction can be achieved by addition of an equal volume of 45 mM dithiothreitol (DTT) to the sample and incubating for 15 min at 40°C before digestion.

5. To improve the separation of co-eluting peptides, two C18 hydrophobic columns can be used in sequence. Although these columns retain and elute peptides under similar conditions, they are made by different manufacturers. The YMC ODS AQ column differs enough from the 218TP52 column that it successfully separates peptides that co-elute on the 218TP52 column. By removing the smaller peaks between the major peaks, a blank in elution space is provided such that the newly separated peptides do not co-elute with some other species. Even with this strategy, some co-elution of peptides is still encountered. Since we obtained so many peaks, we were able to obtain many peptide sequences of clean peaks and could ignore those with overlapping amino acid sequences (6). However, if there are not many peaks, one approach might be to take smaller fractions that elute at greater distance from each other. If no peptides are separated by this sequence of columns, a C18 column from a different manufacturer could be tried, or a C16 column be substituted. The advantage of using two similar columns is that the same solvent conditions that are known to work in the first column can be reapplied in the second and the peptides that were initially isolated will be recovered at high efficiency.

Acknowledgments

I thank Nelson Medeiros for his work in purifying the myosins used to develop this strategy, Howard Jaffe for trying many different digestion and isolation approaches before finding this one that worked for myosins, and Tom Reese of the National Institute for Neurological Disease and Stroke for his support and involvement in all aspects of this myosin project. This work was supported in part by National Institutes of Health Grant GM47368 (ELB).

References

1. Bálint, M., Szilágyi, L., Fekete, G., Blazsó, M., and Biró, N. A. (1968) Studies on proteins and protein complexes of muscle by means of proteolysis: V. Fragmentation of light meromyosin by trypsin. *J. Mol. Biol.* **37**, 317–330.
2. Garces, J. and Gavin, R. H. (1998) A PCR screen identifies a novel, unconventional myosin heavy chain gene (MYO1) in *Tetrahymena thermophyla*. *J. Euk. Micro.* **45**, 252–259.
3. Goodson, H. and Spudich, J. A. (1995). Identification and molecular characterization of a yeast myosin I. *Cell Motil Cytoskeleton* **30**, 73–84.
4. Bement, W. M., Hasson, T., Wirth, J. A., Cheney, R. E., and Mooseker, M. S. (1994) Identification and overlapping expression of multiple unconventional myosin genes in vertebrate cell types. *Proc. Natl. Acad. Sci. USA* **91**, 6549–6553.
5. Titus, M. A., Kuspa, A., and Loomis, W. F. (1994) Discovery of myosin genes by physical mapping in *Dictyostelium*. *Proc. Natl. Acad. Sci. USA* **91**, 9446–9450.
6. Medeiros, N., Reese, T. S., Jaffe, H., DeGiorgis, J. A., and Bearer, E. L. (1998) Primary peptide sequences from squid muscle and optic lobe myosin IIs: A strategy to identify an organelle motor. *Cell. Biol. Int.* **22**, 161–173.

7. Bearer, E. L., DeGiorgis, J. A., Bodner, R. A., Kao, A., and Reese, T. S. (1993) Evidence for myosin motors on organelles in squid axoplasm. *Proc. Natl. Acad. Sci. USA* **90**, 11,252–11,256.
8. Bearer, E. L., DeGiorgis, J. A., Jaffe, H., Medeiros, N. A., and Reese, T. S. (1996) An axoplasmic myosin with a calmodulin-like light chain. *Proc. Natl. Acad. Sci. USA* **93**, 6064–6068.
9. Bearer, E. L., DeGiorgis, J. A., Medeiros, N. A., and Reese, T. S. (1996) Actin-based motility of isolated axoplasmic organelles. *Cell. Motil. Cytoskel.* **33**, 106–114.
10. Bearer, E. L., Jaffe, H., Medeiros, N., and Reese, T. S. (1996) Purification and amino acid sequencing of two high molecular weight myosins from squid muscle and brain. *Molec. Biol. Cell* **7**, 37a.
11. Nyitray, L., Goodwin, E. B., and Szent-Györgyi, A. G. (1991) Complete primary structure of a scallop striated muscle myosin heavy chain. Sequence comparison with other heavy chains reveals regions that might be critical for regulation. *J. Biol. Chem.* **266**, 18,469–18,476.
12. Matulef, K., Sirokman, K., Perreault-Micale, C. L., and Szent-Györgyi, A. G. (1998) The amino acid sequence of squid syphon muscle myosin heavy chain. *J. Musc. Res. Cell. Motil.* **19**, 705–712.
13. Medeiros, N. A., DeGiorgis, J. A., Reese, T. S., and Bearer, E. L. (1997) Obtaining primary amino acid sequences from squid brain myosins. *Biol. Bull.* **193**, 198.
14. DeGiorgis, J. A., Reese, T. S., and Bearer, E. L. (2000) Myosin II and V: Implications for exonal transport, submitted.
15. Tabb, J. S., Molyneaux, B. J., Cohen, D. L., Kuznetsov, S. A., and Langford, G. M. (1998) Transport of ER vesicles on actin filaments in neurons by myosin V. *J. Cell Sci.* **111**, 3221–3234.
16. Stone, K. L., Lopresti, M. B., and Williams, K. R. (1990) Enzymatic digestion of proteins and HPLC isolation in the subnanomole range. In *Laboratory Methodology in Biochemistry* (edited by Fini, C. F.), pp. 181–205. Boca Raton, FL: CRC Press.
17. Riviere, L. R., Fleming, M., Elicone, C., and Tempst, P. (1991) Study and applications of the effects of detergents and chaotropes on enzymatic proteolysis. In *Techniques in Protein Chemistry II* (edited by Villafranca, J. J.), pp. 171–179. San Diego, CA: Academic Press.
18. Fernandez, J., Demott, M., Atherton, D., and Mische, S. M. (1992) Internal protein sequence analysis: Enzymatic digestion for less than 10 μ g of protein bound to polyvinylidene difluoride or nitrocellulose membranes. *Anal. Biochem.* **201**, 255–264.

Evaluating the Dynein Heavy Chain Gene Family in *Tetrahymena*

Gangadhara Sailaja, Leslie M. Lincoln,
Jifan Chen, and David J. Asai

1. Introduction

In this chapter, we describe our methods to evaluate the dynein heavy chain genes expressed in a cell. Dynein is the high molecular weight molecular motor that produces directed movement along microtubules. All known dyneins travel to the proximal or minus end of the microtubule. The large dynein complex (M_r 1200–2000K) is comprised of several different polypeptides. The smaller subunits mediate the attachment of the dynein to its cargo and regulate dynein activity. The heavy chains (M_r >500K) contain the motor activity. Each heavy chain folds into a short flexible tail, which associates with other subunits and with the cargo, and a compact globular head, which transduces the chemical energy derived from ATP hydrolysis into mechanical motion.

Many organisms utilize multiple dynein heavy chain isoforms, and each protein isoform is encoded by a separate gene (*I*). In organisms with cilia or flagella, approximately 15 separate heavy chain genes are expressed. These isoforms are divided into two functional classes. The approximately one dozen axonemal dynein heavy chains are assembled into the inner and outer dynein arms to produce the active sliding between adjacent outer doublet microtubules that underlies ciliary and flagellar bending. The few non-axonemal or “cytoplasmic” dyneins are responsible for the directional trafficking of membrane-bounded vesicles and other organelles. Biochemical and genetic evidence lead to the “multi-dynein hypothesis” which states that each dynein heavy chain is functionally specialized and that there is little or no functional redundancy among the isoforms (2–4).

As the first step in connecting isoform structure with function, it is necessary to obtain a clear picture of the number and diversity of the dynein genes expressed. Ideally, this assessment should involve cataloguing all of the expressed dynein genes, and it should by-pass conventional cloning and sequencing of these enormous genes. Each heavy chain gene is ca. 15 kb. We have refined the strategy originally developed with Ian Gibbons's laboratory to evaluate the dynein heavy chain gene family expressed in a given organism (5–7). The strategy utilizes standard protocols (8) and is as follows: (a) Use reverse transcriptase to synthesize cDNA from cellular RNA; (b) utilize the cDNA as the template in polymerase chain reactions (PCR), employ degenerate oligonucleotide primers to amplify a short fragment of each expressed dynein heavy chain gene; (c) clone and sequence the PCR-amplified fragments; and (d) utilize Southern blotting to estimate the size of the dynein gene family in the organism by hybridizing genomic DNA with a mixture of the PCR-amplified fragments.

Our laboratory has focussed on the dynein genes expressed in the ciliated protozoan *Tetrahymena thermophila*. While we use *Tetrahymena* as the example when explaining the methods in this chapter, the same strategy has been employed to characterize the dynein genes expressed in several other model organisms (6,9–14).

The organization of the dynein heavy chain is unique among the well-characterized molecular motors (15). Dynein has four nucleotide-binding sites located in the middle of the heavy chain sequence, rather than the single nucleotide-binding site usually located near one end of the heavy chain of the myosins and kinesins. The first phosphate-binding P-loop is the dynein catalytic site, and its sequence is absolutely conserved among all the dynein heavy chain sequences determined: GPAGTGKT. In addition to the catalytic P-loop, there are a few other highly conserved sequences located nearby. These are shown in **Fig. 1**. It is to these conserved sequences we have aimed the degenerate oligonucleotide primers.

2. Materials

2.1. Culturing *Tetrahymena*

Neff's medium: 0.25% proteose peptone, 0.25% yeast extract, 0.55% glucose, 33 μM ferric chloride. We supplement the medium with penicillin and streptomycin (250 $\mu\text{g}/\text{mL}$ each) and 1.25 $\mu\text{g}/\text{mL}$ amphotericin B (FungizoneTM, Gibco).

2.2. RNA Isolation

1. Solution D: 4M guanidinium thiocyanate supplemented with 8 $\mu\text{L}/\text{mL}$ 2-mercaptoethanol, 0.5% sarkosyl, 25 mM sodium citrate, pH 7.0.
2. Phenol buffered with pH 5.2 citrate.
3. CHISAM: Chloroform and Isoamyl alcohol (49:1).
4. 2 M sodium acetate, pH 5.2.

8. X-Gal and Amp agar plates.
9. In a 2 L flask, make a 1 L solution: 10 g tryptone, 5 g NaCl, 5 g yeast extract, pH 7.4.
10. Add 15 g Bacto agar; autoclave.
11. Cool solution to ca. 50°C; then add in order: (1) 1 mL of ampicillin (stock of 100 mg/mL in sterile water); (2) 0.5 mL of IPTG (isopropyl β -D-thiogalactopyranoside: Sigma I5502) (stock of 240 mg/mL in water, then filter sterilized); (3) 4 mL X-Gal (5-bromo-4-chloro-3-indolyl β -D-galactopyranoside; Sigma B9146) (stock of 20 mg/mL dissolved in dimethyl formamide). Swirl solution and pour into Petri dishes.
12. LB-Amp: Luria-Bertani medium (per 1 L): 10 g bacto-tryptone, 5 g bacto-yeast extract, 10 g NaCl, pH 7.0 with NaOH; supplemented with 100 μ g/mL ampicillin.
13. Wizard™ miniprep DNA purification system (Promega).
14. ThermoSequenase™ (Amersham).

2.6. Genomic DNA Isolation

1. NDS: 1% SDS, 0.5M EDTA, 10 mM Tris-HCl, pH 9.5.
2. Proteinase K (Fisher).
3. PEG: 12% polyethylene glycol (M.W. 8000) in 1.2M NaCl.
4. TE: 10 mM Tris-HCl, pH 8.0, 1 mM EDTA.
5. DNase-free RNase: 10 mg/mL RNAase in 0.01M NaAcetate, pH 5.2. Heat at 100°C for 15 min, adjust pH to 7.4, store at -20°C.
6. Phenol equilibrated with Tris pH 8.0 (USB).
7. Chloroform.
8. 100% and 75% ethanol, stored at -20°C.

2.7. Southern Blotting

1. Appropriate restriction enzyme(s); use reaction buffers and supplements provided by vendor.
2. Labeling kit: Random Primers DNA labeling system (GibcoBRL), [³²P]-dTTP.
3. SSC (20X): 1 L: 175.3 g NaCl, 88.2 g NaCitrate, pH 7.0.
4. Phosphate buffer (1M): 1 L: 71 g Na₂HPO₄, 69 g NaH₂PO₄·H₂O.
5. Denhardt's solution (50X): 500 mL: 5 g Ficoll, 5 g polyvinylpyrrolidone, 5 g bovine serum albumin.
6. SET (1X): 0.15M NaCl, 2 mM EDTA, 30 mM Tris-HCl, pH 8.

2.8. Electrophoresis

1. Agarose gel solution: 1.5% agarose in 0.5X TBE.
2. Sequencing gel solution: 7% acrylamide/bisacrylamide, 8M urea.

3. Methods

3.1. Culturing Cells

1. Culture *Tetrahymena thermophila* strain B2086 cells in Neff's medium at 30°C on a shaker. Harvest exponentially growing cells at a density of 3–5 \times 10⁵ cells/mL.

Collect cells by centrifugation at 1500 rpm for 1 min at room temperature in pear-shaped oil tubes (HN-S II centrifuge, International Equipment Company). Beginning with a 100 mL culture, approximately 0.2 mL of pelleted cells are obtained.

3.2. RNA Isolation (see Note 1)

1. Resuspend pelleted cells in an equal volume of sterile water; transfer to a sterile 30 mL glass Corex tube.
2. For ca. 0.2 mL cells, add 4 mL Solution D; immediately mix.
3. Add 1/10 vol (0.4 mL) 2M sodium acetate.
4. Add equal vol (4 mL) citrate-buffered phenol, swirl gently.
5. Add equal vol (4 mL) CHISAM, mix, on ice for 10 min; then centrifuge 12,000g for 10 min, 4°C.
6. Transfer aqueous phase into a fresh Corex tube; avoid contaminating with the interphase precipitants; measure the volume.
7. Add 0.5 vol 100% cold ethanol, mix, precipitate overnight at -20°C.
8. Centrifuge 12,000g for 10 min at 4°C; decant supernatant.
9. Resuspend pellet in 0.5 vol (2 mL) Solution D; if necessary, warm to 60–65°C for a few minutes in order to hasten solubilization of pellet.
10. Add 0.2 mL 2M sodium acetate.
11. Add 0.5 vol 100% cold ethanol, mix, precipitate overnight at -20°C.
12. Repeat **steps 8–11**.
13. Dissolve final RNA pellet (should be translucent) in 1 mL DEPC-H₂O.
14. Quantify RNA by absorption at 260 nm and store at -70°C in ethanol.

3.3. cDNA Synthesis

1. Add the following reagents to a sterile 500- μ L Eppendorf tube: (1) 0.5 μ g polyA+ RNA or 5 μ g total RNA dissolved in 18 μ L DEPC-H₂O and (2) 2 μ L random hexamers.
2. Heat to 70°C for 10 min; then immediately plunge into liquid nitrogen.
3. After sample returns to room temperature, add in order: (1) 8 μ L 5X reaction buffer; (2) 4 μ L 0.1 M DTT; (3) 4 μ L 10 mM dNTPs. Mix; pulse in a microcentrifuge.
4. Warm to 40°C.
5. Add 2 μ L (400 units) RT Superscript II™; allow the reaction to proceed at 40–42°C for 1.5–2 h.
6. Stop reaction by addition of 100 μ L 0.5X TE; store at -20°C.

3.4. Polymerase Chain Reaction with Degenerate Primers (see Note 2)

1. Mix 10 μ L of diluted cDNA with 40 μ L sterile water. Boil the mixture for 10 min, then plunge into wet ice.
2. Use the following per reaction: 10 μ L 10X Taq buffer, 1.5 mM Mg²⁺, 16 μ L 1.25 mM dNTPs, 100–500 pmols (1–5 μ L) of each degenerate primer, sterile water to 50 μ L, 1 μ L Taq DNA polymerase (5 units).

3. Mix DNA and master mix together (100 μ L each reaction), pulse in microcentrifuge.
4. Use the following cycles for PCR amplification: (1) 5 cycles: 94°C, 1 min; 50°C, 2 min; 72°C, 2 min; (2) 40 cycles: 94°C, 1 min; 35°C, 2 min; 72°C, 2 min; (3) 1 cycle: 72°C, 10 min.
5. At the end of the amplification, remove 10 μ L to check on an agarose gel. The A2 and S2 primers should amplify a ca. 180 bp fragment. Precipitate the remaining PCR product by adding 25 μ L polyacrylamide and 250 μ L ethanol, overnight at -20°C.

3.5. Cloning and Sequencing of PCR-Amplified Fragments (see Note 3)

1. Dissolve the precipitated PCR-amplified product in TE; digest with the appropriate restriction enzymes (in the case of the S2 and A2 primers, BamHI and EcoRI).
2. Gel-purify the digested DNA from a 1.5% low-melting point agarose gel made in TAE.
3. After electrophoresis, carefully excise the band trimming away excess agarose, add 200 μ L sterile water.
4. Melt the agarose in a heating block. Add 300 μ L phenol, mix, centrifuge at room temperature for 5 min.
5. Transfer the upper aqueous layer to a fresh sterile eppendorf tube and add 300 μ L chloroform, shake vigorously, centrifuge at room temperature for 5 min.
6. Recover upper layer, add 300 μ L isopropanol and 30 μ L 3M KoAC, plunge into liquid nitrogen.
7. Centrifuge at 4°C for 10 min.
8. Recover DNA pellet, wash with 70% cold ethanol, air-dry pellet.
9. Ligate the gel-purified PCR-amplified DNA into pUC118 (see Note 4).
10. Transform DH5 α -competent cells according to the vendor's protocol. Plate the bacteria onto X-Gal indicator plates and incubate at 37°C overnight. Transformants with inserts should give rise to white colonies; transformants without inserts should be blue.
11. Pick individual colonies, grow bacteria overnight in LB-Amp, and isolate plasmid DNA using the Wizard™ miniprep DNA purification system according to the manufacturer's instructions.
12. Digest the plasmid DNA with BamHI and EcoRI and use electrophoresis to detect the ca. 180 bp. Colonies with the appropriate-sized insert are numbered and stored at -70°C as glycerol stocks (15% final vol glycerol).
13. Use the Wizard purification kit to purify the plasmid.
14. Use the purified plasmid DNA as the template for cycle sequencing in which the universal forward and reverse oligonucleotides, corresponding to sequences in pUC118, are utilized as primers.
15. Use the ThermoSequenase™ terminator cycle sequencing kit with [³³P]dNTPs (dGTP termination mix; 95°C, 30 s; 50°C, 30 s; 72°C, 1 min; 30 cycles) in the sequencing reactions.
16. Setup the sequencing gel and perform the electrophoresis according to standard protocols.

3.6. Genomic DNA Isolation (see Note 5)

1. Harvest 200 mL cells in pear-shaped oil tubes.
2. Resuspend pellet of cells in 10 mL NDS.
3. Add 100 µg/mL proteinase K; incubate at 65°C overnight.
4. Add 10 mL PEG solution; on ice for >1.5 h; centrifuge at 12,000g, 15 min.
5. Discard the supernatant, wash the pellet twice with 70% cold ethanol.
6. Resuspend the pellet in 10 mL TE; add 100 µg of DNase-free RNase; incubated at 37°C for 1 h.
7. Extract once with 10 mL phenol and twice with 10 mL chloroform.
8. Precipitate DNA with 2 vol 100% ethanol, wash pellet with cold 70% ethanol; dry pellet.
9. Resuspend pellet in 1 mL TE; estimate yield by absorption at 260 nm.

3.7. Southern Blotting (see Notes 6 and 7)

3.7.1. Preparation of Probes

1. Separate individual clones of the 180-bp dynein fragments from the pUC118 by digestion with BamHI and EcoRI, then gel-purify.
2. Denature DNA by boiling for 5 min, then immediately plunge into wet ice.
3. Label DNA with [³²P] dTTP using random primers DNA labelling system.

3.7.2. Genomic DNA

1. Digest 10 µg genomic DNA with the appropriate enzyme. In the example shown in **Fig. 3** (see **Note 7**), we used EcoRI. Perform the digestion in a large (100 µL) volume overnight. After digestion, precipitate the DNA with ethanol and resuspend in a small (20 µL) volume of sterile water.
2. Separate the digested genomic DNA on a 1% agarose gel, treat the gel in order to nick and denature the DNA according to standard methods (8), transfer to nylon GeneScreen Plus™ (NEN Life Sciences) membrane in 10X SSC overnight. Crosslink the transferred DNA with UV illumination.
3. Wash filter in 0.2M phosphate buffer, 10X Denhardt's, 0.1% SDS, and 5X SET at 65°C for 1 h.

3.7.3. Hybridization

1. Perform pre-hybridization in a seal-a-meal bag containing: filter, 20 mM phosphate buffer, 1X Denhardt's, 0.25% SDS, and 5X SET at 65°C for 1 h.
2. Open the bag, add the labeled probe, reseal the bag. Incubate overnight in the hybridization solution at 65°C.
3. Wash the filters three times, 30 min each wash, in 25 mM phosphate buffer, 0.1% sodium pyrophosphate, 0.1% SDS, and 0.2X SET at 65°C. Expose blots to X-ray film.

4. Notes

1. These methods are based on a standard protocol (17).
2. Choice of primers (see **Fig. 1** in ref. 7): We have used various combinations of the following degenerate oligonucleotide primers to: (1) ITPLTDR (primer S1);

DYH 1	GPAGTGKTESVKALGSQ LGRFVLVFNCD E T F D F H A M G R I F V G L C Q V G A W G C F D E F N R	(0)
DYH 2	GPAGTGKTESVKALGQA FGRQVLVFNCD E G L D F K S M G R I F I G L V K C G A W G C F D E F N R	(3)
DYH 3	GPAGTGKTE TVKDLGRTLG V F V V V T N C S D Q H R Y R D M A K I F K G L V Q S G L W G C F D E F N R	(2)
DYH 4	GPAGTGKTE T T K D L G R A I G I P V M V F N C S D Q M N K D S M A Q I F M G L S Q S G A W G C F D E F N R	(10)
DYH 5	GPAGTGKTE T T K D L A N A L A K A C Y V F N C S S E M N Y E S M G N I Y K G L A S S G C W G C F D E F N R	(44)
DYH 9	GPAGTGKTE S T K D L A K A L A K Q C V V F N C S D S M D Y I M I G K F F K G L A S A G A W C C F D E F N R	(25)
DYH 11	GPAGTGKTE T V K D L A K A L A V Q C V V F N C S D G L N Y V A M R K F F K G L A S S G A W C C F D E F N R	(11)
DYH 14	GPAGTGKTE T T K D L A K A I A K H C V V F N C S D A L D Y T A M G K F F K G L S S C G S W A C F D E F N R	(5)

Fig. 2. Deduced amino acid sequences of PCR-amplified fragments of eight *Tetrahymena* dynein heavy chain genes. The numbering of the DYH genes is that established for *Tetrahymena* (see ref. 21). DYH1 encodes the ubiquitous cytoplasmic dynein also called 1a. DYH2 encodes the second cytoplasmic dynein also called 1b. DYH3 encodes the outer arm dynein heavy chain that is the homologue of *Chlamydomonas* γ heavy chain and sea urchin α heavy chain. DYH4 encodes the outer arm β heavy chain. DYH5 encodes the outer arm dynein heavy chain that is the homologue of *Chlamydomonas* α heavy chain. In the survey of 100 randomly selected clones, the number of individual clones recovered for each DYH gene is indicated in parentheses to the right of each sequence.

- (2) PAGTGKT (primer S2); (3) CFDEFNR (primer A2); (4) FITMNPG (primer A1); and (5) HYDFGLRA (primer A3). We have utilized primers based on the universal genetic code as well as biasing the sequences according to *Tetrahymena* codon usage (18); we have detected little difference between primers derived by the two methods. The primers listed in this chapter are based on the universal genetic code. Here we describe PCR amplification with the S2 and A2 primers. At the 5' end of S2 is an added BamHI site; at the 5' end of A2 is an added EcoRI site.
- We PCR-amplified the expressed dynein heavy chain genes in *Tetrahymena*. Four separate RNA preparations were individually reverse-transcribed. Each of the four cDNA mixtures was then subjected to three separate PCR reactions utilizing the degenerate S2 and A2 primers. The PCR-amplified products from each template were then pooled, digested, cloned into pUC118, and transformed into bacteria. One hundred randomly selected clones were sequenced. Seven different sequences were obtained (Fig. 2). The sequence of an eighth, DYH1, was added to Fig. 2. Even though DYH1 was not one of the 100 randomly selected clones, we had previously identified and characterized this cytoplasmic dynein isoform (20). Our eight sequences were then compared to the partial genomic sequences of 13 dynein genes obtained by Xu et al. (21), and we have organized our sequences according to their numbering system. DYH14 was not identified by Xu et al. DYH1 and DYH2 encode two cytoplasmic dyneins and have been extensively sequenced and characterized (20). DYH3-5 encode the three heavy chains of ciliary outer arm dynein; DYH4 (β heavy chain) has been completely sequenced (22).

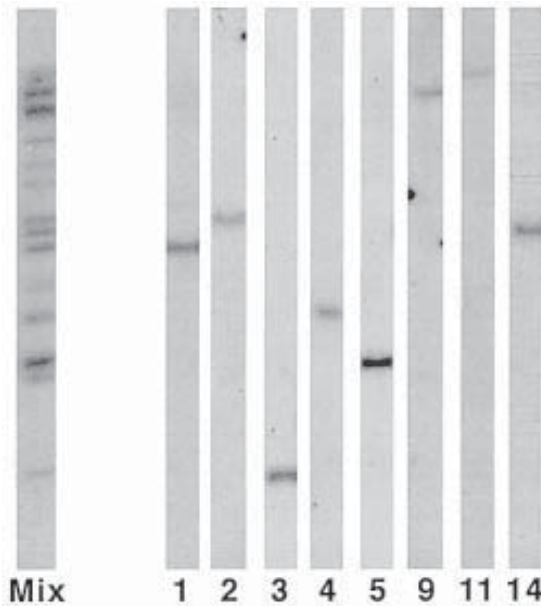


Fig. 3. Southern blot analysis suggests that *Tetrahymena* expresses 13-14 dynein heavy chain genes. *Tetrahymena* genomic DNA was digested with EcoRI, separated in a 1% agarose gel, transferred to nitrocellulose, and probed with labelled dynein fragments. Strip marked “Mix” was probed with the mixture of PCR products. The other strips were hybridized with individual cloned PCR-amplified fragments, the number of the strip corresponds to the DYH gene.

4. It is a good idea to also attempt to ligate the cut vector without insert—since the insert will be directionally cloned (i.e., two different restriction sites), the vector without insert should not ligate to itself. The extent of ligation is sensitive to the proportion of insert and vector; therefore, it is a good idea to set up two or three ligations varying the insert-to-vector ratio.
5. This protocol is based on a procedure described by Meng-Chao Yao’s laboratory (19).
6. These methods are based on standard protocols (8).
7. A Southern blot of EcoRI-digested genomic DNA was probed with the mixture of PCR-amplified fragments. The result is shown in the far left lane of Fig. 3. Approximately 13–14 hybridizing bands were seen in this blot. Each of the cloned individual dynein fragments was also used to probe identical Southern blots (Fig. 3). Each individual fragment hybridized to a single band, and the band corresponded to one of the 13–14 bands hybridizing with the mixed probe. We conclude that, under these conditions, the Southern blot probed with the PCR mixture provides a good estimate of the number of dynein genes expressed in *Tetrahymena*.

Acknowledgments

We thank David Pennock for sharing his laboratory's unpublished results and Jim Forney for his good advice. This work was supported by a grant from the National Science Foundation, MCB 9728207.

References

1. Asai, D. J. (1996) Functional and molecular diversity of dynein heavy chains. *Sem. Cell Biol.* **7**, 311–320.
2. Piperno, G. (1990) Functional diversity of dyneins. *Cell Motil. Cytoskel.* **17**, 147–149.
3. Brokaw, C. J. (1994) Control of flagellar bending: a new agenda based on dynein diversity. *Cell Motil. Cytoskel.* **28**, 199–204.
4. Asai, D. J. (1995) Multi-dynein hypothesis. *Cell Motil. Cytoskel.* **32**, 129–132.
5. Asai, D. J., Tang, W. J. Y., Ching, N. S., and Gibbons, I. R. (1991) Cloning and sequencing of the ATP-binding domains of novel isoforms of sea urchin dynein. *J. Cell Biol.* **115**, 369a.
6. Gibbons, B. H., Asai, D. J., Tang, W.-J. Y., Hays, T. S., and Gibbons, I. R. (1994) Phylogeny and expression of axonemal and cytoplasmic dynein genes in sea urchins. *Mol. Biol. Cell* **5**, 57–70.
7. Asai, D. J. and Criswell, P. S. (1995) Identification of new dynein heavy chain genes by RNA-directed PCR. *Meth. Cell Biol.* **47**, 579–585.
8. Sambrook, J., Fritsch, E. F., and Maniatis, T. (1989) *Molecular Cloning: A Laboratory Manual, 2nd ed.* Cold Spring Harbor Laboratory Press, Cold Spring Harbor, NY.
9. Rasmusson, K., Gepner, J., Serr, M., Gibbons, I., and Hays, T. S. (1994) A family of dynein genes in *Drosophila melanogaster*. *Mol. Biol. Cell* **5**, 45–55.
10. Wilkerson, C. G., King, S. M., and Witman, G. B. (1994) Molecular analysis of the α heavy chain of *Chlamydomonas* flagellar outer-arm dynein. *J. Cell Sci.* **107**, 497–506.
11. Porter, M. E., Knott, J. A., Myster, S. H., and Farlow, S. J. (1996) The dynein gene family in *Chlamydomonas reinhardtii*. *Genetics* **144**, 569–585.
12. Tanaka, Y., Zhang, Z., and Hirokawa, N. (1995) Identification and molecular evolution of new dynein-like protein sequences in rat brain. *J. Cell Sci.* **108**, 1883–1893.
13. Andrews, K. K., Nettesheim, P., Asai, D. J., and Ostrowski, L. E. (1996) Identification of seven rat axonemal dynein heavy chain genes: expression during ciliated cell differentiation. *Mol. Biol. Cell* **7**, 71–79.
14. Asai, D. J., Beckwith, S. M., Kandl, K. A., Keating, H. H., Tjandra, H., and Forney, J. D. (1994) The dynein genes of *Paramecium tetraurelia*: sequences adjacent to the catalytic P-loop identify cytoplasmic and axonemal heavy chain isoforms. *J. Cell Sci.* **107**, 839–847.
15. Gibbons, I. R., Gibbons, B. H., Mocz, G., and Asai, D. J. (1991) Multiple nucleotide-binding sites in the sequence of dynein β heavy chain. *Nature* **352**, 640–743.
16. Gibbons, I. R., Asai, D. J., Tang, W. J. Y., and Gibbons, B. H. (1992) A cytoplasmic dynein heavy chain in sea urchin embryos. *Biol. Cell* **76**, 303–309.

17. Chirgwin, J. M., Przybyla, A. E., MacDonald, R. J., and Rutter, W. J. (1979) Isolation of biologically active ribonucleic acid from sources enriched in ribonuclease. *Biochemistry* **18**, 5294–5299.
18. Wuitschick, J. D. and Karrer, K. M. (1999) Analysis of genomic G + C content, codon usage, initiator codon context and translation termination sites in *Tetrahymena thermophila*. *J. Euk. Microbiol.* **46**, 239–247.
19. Austerberry, C. F. and Yao, M. C. (1987) Nucleotide sequence structure and consistency of a developmentally regulated DNA deletion in *Tetrahymena thermophila*. *Mol. Cell. Biol.* **7**, 435–443.
20. Lee, S.-w., Wisniewski, J. C., Dentler, W. L., and Asai, D. J. (1999) Gene knockouts reveal separate functions for two cytoplasmic dyneins in *Tetrahymena thermophila*. *Mol. Biol. Cell* **10**, 771–784.
21. Xu, W., Royalty, M. P., Zimmerman, J. R., Angus, S. P., and Pennock, D. G. (1999) The dynein heavy chain gene family in *Tetrahymena thermophila*. *J. Euk. Microbiol.* **46**, 606–611.
22. Lincoln, L. M., Gibson, T. M., Lee, S.-w., Forney, J. D., and Asai, D. J. (1998) The characterization and targeted disruption of the dynein beta heavy chain in *Tetrahymena thermophila*. *Mol. Biol. Cell* **9**, 155a.

II

MICROSCOPY APPLICATIONS

Video-Enhanced Microscopy for Analysis of Cytoskeleton Structure and Function

George M. Langford

1. Introduction

1.1. Cytoskeletal Dynamics and AVEC-DIC Microscopy

The cytoskeleton is a dynamic network of filaments in the cytoplasm of cells and functions as the roadways for vesicular transport. Of the three types of cytoskeletal filaments, both microtubules and actin filaments have been shown to support vesicle transport. The transport of vesicles is mediated by molecular motors and members of all three super-families of molecular motors—myosin, kinesin and cytoplasmic dynein—have been shown to function as vesicle motors (*1–4*). The specific types of vesicles transported by some of the molecular motors have been identified (*4–6*).

To assay motor activity *in vitro* and to determine the cargo transported by them, motility assays have been devised (*7–9*). The development of these assays was aided by the discovery that microtubules and small vesicles, both of which are smaller than the limit of resolution of the light microscope, can be detected by video-enhanced DIC microscopy (*10*). The aim of this chapter is to describe the Allen Video-Enhanced-Contrast Differential Interference Contrast (AVEC-DIC) protocol, one of the principal techniques for visualizing dynamic cytoskeletal filaments and the movement of vesicles on them. Allen and colleagues developed the AVEC-DIC method (*10,11*). The theoretical basis for this technique was developed simultaneously in the laboratories of Allen (*10,11*) and Inoué (*12,13*) and has been codified in the two editions of the authoritative text on video microscopy by Inoué (*14,15*). The AVEC-DIC protocol provides a sophisticated but practical and easy-to-use method for assaying vesicle transport on microtubules and actin filaments.

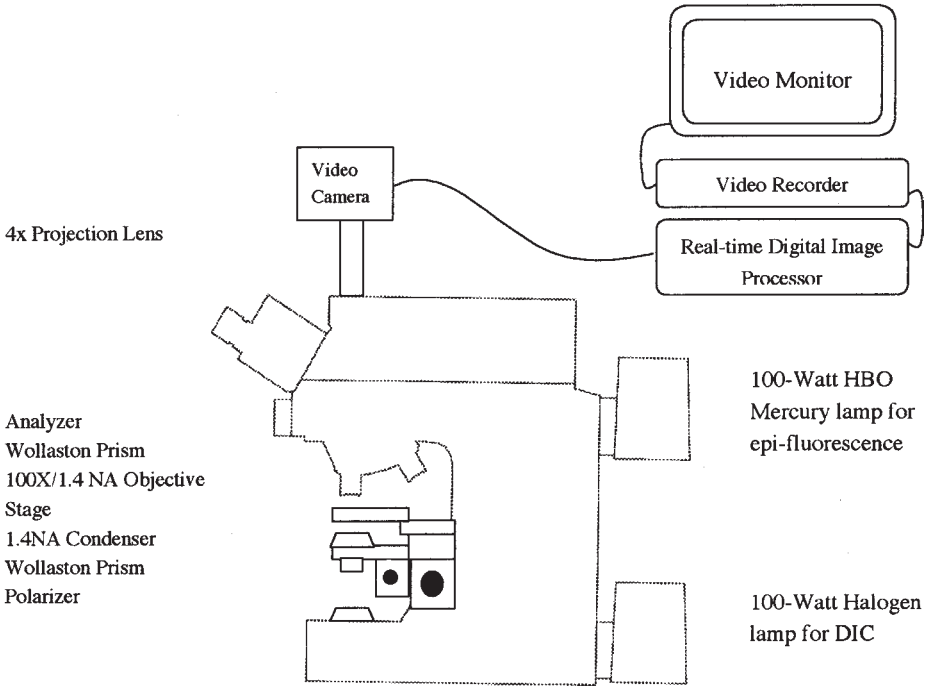


Fig. 1. Diagram of a high-resolution video microscope equipped with differential interference contrast (DIC) optics for motility assays. A 100W halogen lamp is mounted at the base of the microscope for transmitted light and a 100W HBO mercury lamp is located in the epi-fluorescence light path. A polarizer and a beam splitter (Wollaston Prism) are located below the 1.4 NA condenser and a beam recombining prism (Wollaston Prism) and analyzer are located above the 100 \times /1.4 NA objective. The video camera is mounted on the microscope using a 4 \times -projection lens for additional magnification. The images, acquired at 30 frames per s by the video camera, are transferred in realtime to the digital image processor and the final processed image is recorded on videotape using a super VHS video recorder. The processed images captured on videotape are displayed on the video monitor.

The AVEC-DIC method requires a high quality research microscope with DIC optics, a high-resolution video camera and a real-time image processor (15–19) (Fig. 1). With the addition of fluorescence filter sets, this microscope system can be used to track green fluorescent protein (GFP)-tagged proteins in living cells or cell extracts. Co-localization of fluorescent signals at two different wavelengths, a technique that requires the precise registration of images obtained with two different fluorophores or co-localization of a DIC image and an image of fluorescent structures in cells or extracts can be performed with this microscopic setup.

1.2. Theory of AVEC-DIC Microscopy

Video-enhanced contrast microscopy is a technique that allows one to detect objects that are below the resolving power of the light microscope by improving the contrast in the image. The structural details detectable by video microscopy are not visible when the specimen is viewed by eye through the eyepieces of the microscope. The detection of fine detail in specimens depends upon the high sensitivity of video cameras and the contrast enhancement features of digital image processors. The video camera, an analog device, improves image contrast by subtracting background light and amplifying the remaining weak signal. The effect is equivalent to the experience of leaving the city for the countryside to observe the stars in the nighttime sky. Subtracting the background glare of the city lights and allowing the eyes to adjust to dim light permit one to see the stars. The image produced by the video camera is digitized and contrast enhanced by the image processor through mathematical manipulation of the image pixel-by-pixel. One of the major advantages of the digital processor is the ability to amplify small differences in shades of gray so that these differences become visible to the eye. In addition, dust spots on lenses or other fixed pattern mottle can be subtracted and video frames can be averaged to reduce background and electronic noise. The final processed image reveals objects in the 20–100 nm range, a form of superresolution (*13*).

Video-enhanced contrast methods work especially well with light microscopic images generated by DIC microscopy. DIC microscopy produces high-contrast images of objects in cell extracts as well as the fine structural detail within unstained living cells. One of the advantages of DIC optics is its very shallow depth of field and therefore its ability to produce clear optical sections of relatively thick but transparent specimens. A specimen placed in a DIC microscope is illuminated with a polarized beam of light (**Fig. 2**). Before reaching the specimen, the polarized beam of light is split into two divergent polarized light waves whose planes of polarization are at right angles to each other. The divergent waves produced by the beam splitter are separated laterally by a very small amount. Differences in the optical path of the two waves, produced by differences in the refractive index and thickness of features within the specimen, introduce bias retardation and hence phase differences between the two waves. When the two waves are recombined in the objective by the Wollaston prism, the amplitude of the resultant wave will be greater or lesser than the amplitude of the waves in the background. The net effect of the interference created upon recombination of the two waves passing through closely adjacent points in the specimen is to cause one edge of the object to appear brighter than the background and the other edge to appear darker than the background. The object therefore takes on a “shadow-cast” appearance. The direction of the shadow depends on the setting of the Wollaston prism, which controls the sign of retardation. The prism

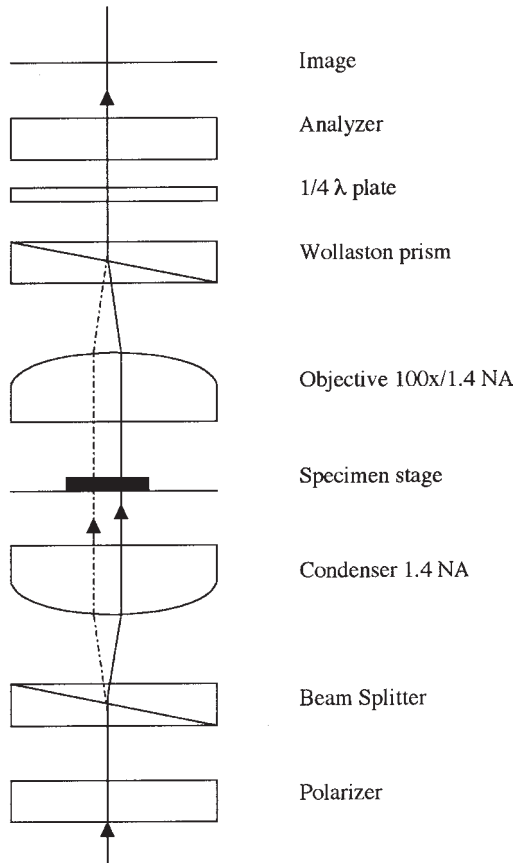


Fig. 2. Details of the optical components and their placement in a DIC microscope (21).

is usually set so that the shadow appears on the lower edge and the object appears raised to the eye.

The net effect of acquiring images with a video camera and processing the images in real-time with an image processor is to enhance the inherent contrast in the image generated by the DIC optics. After image processing, the ability to detect structural detail is improved tenfold over conventional light microscopy. The specimens most suitable for video microscopy are unstained living cells or cell extracts. Objects that are detectable by this method include small vesicles (50 nm), microtubules (25 nm) and latex beads as small as 20 nm in diameter. The video microscopic procedure described in this chapter will include protocols for sample preparation, alignment of the microscope, analog contrast enhancement via the video camera and digital contrast enhancement with an image processor.

2. Materials

2.1. High-Resolution Light Microscope with Optics for DIC and Fluorescence

The basic component of a high-resolution video microscope system is a research quality microscope (**Fig. 1**) such as the Zeiss Axioplan with DIC and epi-fluorescence optics. The microscope must be equipped with a high-resolution video camera (e.g., Hamamatsu Newvicon tube camera) and with an image processor (e.g., Hamamatsu Argus-20 real-time image processor). Optional components include a low light-level camera for imaging fluorescent specimens (e.g., Hamamatsu ORCA-2 dual scan cooled digital “charge-coupled device” or CCD camera) and computer software to drive the CCD camera.

The elements needed for DIC microscopy are a polarizer, analyzer, beam splitter, beam combining prism (Wollaston prism), and a quarter wave-plate (**Fig. 2**). On a standard brightfield microscope, the polarizer is located in the light path below the condenser and the adjustable analyzer is located above the objective in the optical tube. These two elements convert the brightfield microscope into a polarizing light microscope. To convert the polarizing light microscope into a DIC microscope, a prism beam splitter is placed in the light path near the condenser diaphragm and a removable Wollaston prism or DIC slider is inserted just above the objective (**Fig. 1**). The Wollaston prism functions to recombine the two beams of light produced by the beam splitter below the condenser. A quarter wave-plate ($1/4 \lambda$) is inserted just below the analyzer to create a de Sénarmont compensator design as specified for AVEC-DIC (**10**). The settings for the adjustable components (analyzer and Wollaston prism) will be given in the Methods section of this chapter.

The principal objective lens for high-resolution DIC and fluorescence microscopy is a strain-free plan-apochromat 100 \times /1.3 or 1.4 NA oil objective. An optional objective for the microscope is a strain-free plan-apochromat 63 \times /1.4 NA oil. The DIC condenser should have a 1.4 NA strain-free, oil-immersion achromatic top lens to match the high NA oil objectives.

The microscope base should have a 100 W quartz halogen lamp for DIC applications and a 100W HBO mercury lamp for epi-fluorescence microscopy (**Fig. 1**). The power supplies for both lamps should have a variable control to adjust the intensity of the light and thereby extend the lifetime of the bulb as well as protect cells from excessive brightness. The microscope stage should be equipped with a heating element to maintain slides at 30–37°C. The body of the research microscope should be motorized for precision switching of optical components. A motorized light shutter should be installed to prevent exposure of the specimen to light when not being imaged. A motorized nosepiece for

changing objectives is optional but a motorized Z-focus drive capable of producing a step-size of 50 nm in the z-axis is highly desirable. A precision motorized focusing drive is needed to acquire stacks of images for deconvolution and 3-D reconstruction of fluorescent specimens.

The filter magazine containing the fluorescence filter cubes should be motorized if possible. A motorized filter wheel is an alternate solution to a motorized filter cube turret and may be a better choice for experiments in which imaging of dynamic events in cells or extracts are required. If a filter cube turret is used, it should move and seat precisely to prevent misalignment of identical points in images due to the faulty positioning of fluorescent filters. Any offset that occurs reproducibly between images acquired with different fluorescent filters can be corrected through software applications that have the ability to shift images by one or more pixels to restore image registration. For imaging BFP- or GFP-tagged proteins, the blue and green filter cubes should be specifically adapted for BFP and GFP excitation and emission.

A binocular phototube with 2-exit ports for the video and cooled CCD cameras is required. The two exit ports should have identical magnification. A 4 \times -magnification adapter is required for the video camera.

2.2. Video Camera and CCD Camera

The high-resolution video camera is a key part of the hardware for the microscope (**Fig. 1**). The video camera (e.g., the Hamamatsu C2400-07 Newvicon tube camera) should have a separate control unit that permits control of gain and offset or black level. The real-time image processor (e.g., Hamamatsu Argus-20) should be capable of real-time background subtraction, averaging and digital contrast enhancement.

An optional camera is the cooled CCD camera such as the Hamamatsu ORCA-2 dual scan cooled digital camera. This camera is cooled to -45°C by air radiation peltier device. An image processing software package is needed to control the exposure time of the cooled CCD camera. Software packages that control both the microscope and the cameras should be chosen (e.g., Inovision ISEE CM Analytical Imaging System (Raleigh, NC) and Universal Imaging MetaMorph Imaging System (West Chester, PA). The software should include modules for digital image acquisition from the cooled CCD camera, acquisition module for video camera, control module for motorized stage and z-axis focus and data analysis including particle tracking program for automatic tracking of vesicles in real-time. The software should be designed to produce 3-D deconvolution images based on a constrained iterative algorithm.

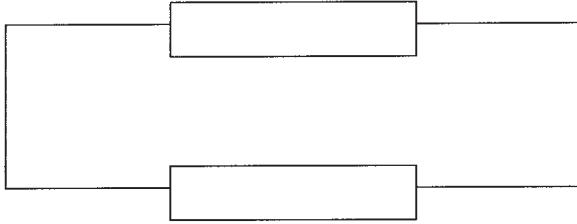
2.3. Monitor and Tape Recorder

A high quality super VHS (S-VHS) VCR cassette recorder is desirable to store images in real-time. Excellent S-VHS models are available from both Sony and Panasonic. A 13-inch black and white monitor with contrast and brightness controls is needed for displaying images. It is important to connect the monitor to the output of the tape recorder to ensure that the recorder is properly set and images of interest are being recorded. A color monitor is also useful for displaying images in pseudocolor.

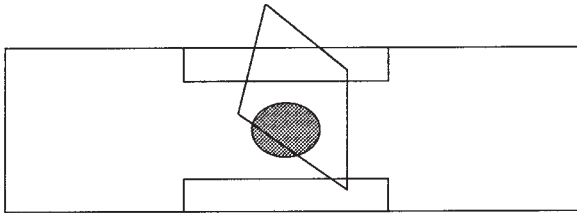
3. Methods

3.1. Preparation of Observation Chamber for Motility Assays of Cell Extracts or Purified Components (filaments, motors, vesicles, and the like)

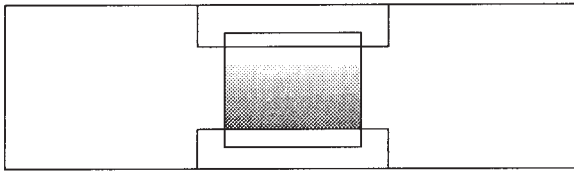
1. Prepare an observation chamber on a glass slide with transparent tape as illustrated in **Fig. 3**. Place a strip of tape along each of the two long edges of a glass slide. The tape functions as a spacer (about 70 μm thick) and controls the volume of the observation chamber. The length of the tape strips should be determined by the length of the coverslip (22mm) and the distance between the two strips of tape should be adjusted to maximize the observation area and to accommodate the volume of the sample (5–10 μL). For most samples, a spacing of about 10–15 mm will accommodate coverslips of 22 \times 22 mm. It is best to attach the strips of tape to the glass slide at the appropriate spacing and then remove the tape overhang with a sharp razor blade.
2. Apply the droplet of sample (5–10 μL) to the center of the chamber with a pipette. The volume of solution should be sufficient to fill the chamber. Air space remaining in the chamber after sealing may cause the coverslip to bow or flex during focusing.
3. Place a coverslip (22 \times 22 mm) over the droplet of solution. Touch the droplet with the coverslip at an angle and lower the coverslip onto the tape spacers. The solution should not spread onto the tape. If the volume of the droplet is greater than the chamber, wick away the excess at the open edges with a triangle of filter paper. The edges must be dry for sealing.
4. Seal the chamber on all four sides with VALAP (1:1:1 Vaseline: lanolin: paraffin) using a cotton swab. First tack down the corners with a small spot of valap then streak a thin line of valap along each edge with the cotton swab. Valap is solid at room temperature, heat to melt before using. The sealing process should be practiced. The chamber will not seal properly if the edges are wet with solution. One clean stroke along each edge is best. The valap at the edges should be a thin flat line to avoid accidentally soiling the microscope objectives with valap when rotating the nosepiece.
5. The observation chamber is now complete and the preparation should be viewed immediately in the microscope.



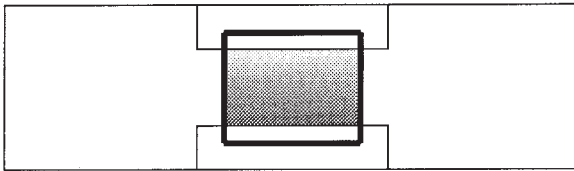
1. Place strips of transparent tape along 2 edges of glass slide.



2. Add droplet of sample with pipette.



3. Place coverslip over the droplet.



4. Seal the chamber with Valap.

Fig. 3. Steps for preparing a microscope observation chamber for motility assays.

3.2. Microscope Alignment (Kohler Illumination) for DIC (see Notes 1–5)

1. Place a drop of immersion oil on the bottom and the top of the observation chamber.
2. Place the slide on the microscope stage and secure in place with the stage clips. The condenser should be positioned near the top of its travel to contact the oil

droplet. The light source should be centered and focused following the manufacturer's instructions.

3. Focus on the specimen (the inner surface of the coverslip) with the 100×1.4 or 1.3 NA oil immersion objective. Follow proper microscopic technique for focusing. Lower the objective into the oil droplet before viewing through the eyepieces. View through the eyepieces and focus the objective on the specimen. Adjust the halogen lamp intensity for comfortable viewing. Focusing is one of the very tedious steps. The specimen is transparent and can be seen with the video camera only, therefore knowledge of the approximate focal plane is helpful. Imperfections in the glass, a fingerprint place at one corner of the coverslip and/or dust particles or other cellular debris are useful guides for finding the proper focal plane. Practice with an object that is visible by eye such as a cheek cell or artificial beads.
4. After the specimen is in focus, complete the steps for Kohler illumination as follows.
5. Close the field diaphragm so that a narrow beam of light is visible. As a practical guide, close the field diaphragm so that only half of the field of view is illuminated.
6. Focus the field diaphragm by adjusting the height of the condenser. If the image of the field diaphragm is astigmatic or difficult to focus, an air bubble may be present in the oil or the objective lens may need cleaning. Center the field diaphragm with the condenser centering screws.
7. Open the field diaphragm slightly to fill the field of view. The field of view is ultimately determined by the video camera. Always keep the field diaphragm as small as possible to reduce scattered light and to enhance contrast.
8. Adjust the condenser diaphragm to the fully open position or to a diameter that matches the diameter of the back focal plane of the objective. To view the back focal plane of the objective, remove one of the eyepieces and replace with a focusing telescope. If the microscope has a built-in optivar, switch to the optivar setting. Focus the telescope or optivar to bring the back focal plane into sharp focus then adjust the condenser diaphragm so that the edges match the focal plane in view.
9. Set the polarizer to the zero degree position and the analyzer to the 90-degree position (extinction). Insert the 543 nm quarter-wave plate and the Wollaston Prism (DIC slider) above the objective. View the back focal plane of the objective with the telescope or optivar and adjust the Wollaston prism to the extinction point by rotating the adjustment knob. Extinction is the position where the brightness is minimal and the image at the back aperture should appear as a dark X. If an X is not visible or appears asymmetric set the slider to the darkest position. Replace the eyepiece and view the specimen.
10. The final step is to rotate the analyzer by 18–20 degrees from the 90-degree setting (off extinction). The direction of rotation should ensure that the dark shadows of the objects appear on the lower side of the object rather than the upper side of the object. Ensuring that shadows appear below rather than above the object produce images in which the object appears as a raised structure or bump rather than a depression or pit. The 18–20 degree setting (one-ninth wavelength)

is the optimal setting for AVEC-DIC microscopy. At this setting, the smallest objects especially small vesicles less than 50 nm in diameter and microtubules can be detected. After the DIC settings are established they do not need to be adjusted during a session at the microscope but should be checked before each session.

3.3. Video Image

1. Switch the light from the eyepieces to the video camera with the beam splitter. An image should appear on the video monitor but may be very dim.
2. Adjust the light intensity of the microscope to saturate the video camera and to bring up the image on the monitor. First slowly increase the light intensity by turning the rheostat on the microscope until the green indicator light on the camera control module begins to glow brightly. Continue to increase light intensity until the red (over saturation) indicator light begins to glow dimly. This is the best light intensity for video microscopy. If the camera is under-saturated (green indicator light does not light or glows dimly), the light intensity is too low and the image on the monitor will appear grainy, a sign of electronic noise. If the intensity is too high, camera will over-saturated and the image will appear washed out. Over-saturation should be avoided because it will damage the camera. If the highest setting of the lamp does not trigger the green indicator light to glow brightly and the red indicator light to glow dimly, more light has to be made available to the camera. The two options are to increase light throughput of the optics (clean optics, realign microscope, change bulb, and so on) or switch to a brighter lamp such as a 50 or 100W mercury lamp.
3. Set the gain and offset or black level of the camera for best image contrast and brightness. Increase the black level by a small amount until the image grows dark then increase the gain to bring back image brightness. This step has to be repeated several times to achieve the optimal setting. The changes should be made in small increments until the best contrast is obtained. Optimal contrast has been achieved when submicroscopic detail becomes visible and the video image is not grainy. Objects in the 20–25 nm size range should be detected clearly. A test specimen should be used such as a preparation of microtubules or small artificial beads. The analog settings of the camera can be saved and do not have to be readjusted if the specimen conditions do not change. The contrast settings have to be optimized for each kind of specimen.
4. Use the image processor to enhance contrast and remove electronic noise and background mottle. For the Argus-10 or 20, select background subtraction in the menu displayed on the monitor. Defocus and acquire the background. Defocus only slightly so that the specimen features are not visible but the variations in brightness across the field is visible. After the background image has been acquired, refocus and select start to begin background subtraction in real time. The image should be free of fixed pattern mottle and shading. A new background has to be acquired each time the field is changed if shading is significant and the specimen is heterogeneous.

5. Reduce electronic noise in the image by averaging successive frames in real time. Set the number of frames to be averaged to 4. A setting of 4 frames allows one to record objects moving at speeds of $1\ \mu\text{m/s}$ or faster. Slower moving objects ($< 0.5\ \mu\text{m/s}$) can be captured with an average of 8 frames but 4 frames are sufficient to remove most of the electronic noise.
6. Finally adjust the contrast of the image digitally with the image processor as follows. Display a histogram of the 256 gray levels in the image if this feature is available. Find the lowest and highest gray values and set the black and white levels to these gray values. The settings may have to be adjusted slightly to give the image less contrast and to make it more pleasing to the eye. The setting of the monitor is important at this step. Set the monitor to the mid-range for brightness and contrast. Then use the digital enhancement control to enhance contrast in the image. If a display of the gray level histogram is not possible set the high and low values of the 256 gray scale to display about 40 gray levels i.e., high of 125 and low of 85.

4. Notes

1. Immersion oils; use only the oil recommended by the manufacturer and do not mix types of oil. Oil should be use with both the condenser and objective.
2. Center the light source as follows. Place an index card in the light path at the condenser diaphragm. An image of the lamp filament should be visible. Focus and center the filament using the centering screws in the lamp housing to the center of the condenser diaphragm. The image of the filament may not be visible if the light path has a glass diffuser. Remove this component before centering the lamp.
3. To focus the specimen, put a fingerprint on one corner of the coverslip to serve as a reference marker.
4. After the microscope, camera and image processor are properly set, adjust the field diaphragm to fit the size of the image. It is important to keep the field diaphragm as small as possible to reduce scattered light.
5. The AVEC-DIC protocol requires the introduction of additional bias retardation by setting the analyzer away from extinction to gain a high input signal from the specimen. The technique calls for a de Sénarmont compensator Bennett (20) by the addition of a 546 nm quarter-wave plate in front of the analyzer. The recommended bias retardation is one-quarter to one-ninth of a wavelength from extinction, with one-ninth (21 degrees) the best setting for high signal and minimal image anomaly.

References

1. Langford, G. M. and Molyneaux, B. J. (1998) Myosin V in the brain: mutations lead to neurological defects, *Brain Res. Rev.* **28**, 1–8.
2. Mermall, V., Post, P. L., and Mooseker, M. S. (1998) Unconventional myosins in cell movement, membrane traffic, and signal transduction. *Science* **279**, 527–533.

3. Karki, S. and Holzbaur, E. L. (1999) Cytoplasmic dynein and dynactin in cell division and intracellular transport. *Curr. Opin. Cell. Biol.* **11**, 45–53.
4. Hirokawa, N. (1998) Kinesin and dynein superfamily proteins and the mechanism of organelle transport. *Science* **279**, 519–526.
5. DePina, A. S. and Langford, G. M. (1999) Vesicle Transport: the role of actin filaments and myosin motors. *Microsc. Res. Tech.* **47**, 93–106.
6. Wu, X., Bowers, B., Rao, K., Wei, Q., and Hammer, J. A., 3rd. (1998) Visualization of melanosome dynamics within wild-type and dilute melanocytes suggests a paradigm for myosin V function In vivo. *J. Cell. Biol.* **143**, 1899–1918.
7. Allen, R. D., Weiss, D. G., Hayden, J. H., Brown, D. T., Fujiwake, H., and Simpson, M. (1985) Gliding movement of and bidirectional transport along single native microtubules from squid axoplasm: Evidence for an active role of microtubules in cytoplasmic transport. *J. Cell. Biol.* **100**, 1736–1752.
8. Vale, R. D., Schnapp, B. J., Reese, T. S., and Sheetz, M. P. (1985) Organelle, bead, and microtubule translocations promoted by soluble factors from the squid giant axon. *Cell* **40**, 559–569.
9. Kuznetsov, S. A., Langford, G. M., and Weiss, D. G. (1992) Actin-dependent organelle movement in squid axoplasm. *Nature* **356**, 725–727.
10. Allen, R. D., Allen, N. S., and Travis, J. L. (1981) Video-enhanced contrast, differential interference contrast (AVEC-DIC) microscopy: A new method capable of analyzing microtubule-related motility in the reticulopodial network of *Allogromia laticollaris*. *Cell Motil.* **1**, 291–302.
11. Allen, R. D., Travis, J. L., Allen, N. S., and Yilmaz, H. (1981b) Video-enhanced contrast polarization (AVEC-POL) microscopy: A new method applied to the detection of birefringence in the motil reiculopodial network of *Allogromia laticollaris*. *Cell Motil.* **1**, 275–288.
12. Inoué, S. (1981) Video image processing greatly enhances contrast, quality and speed in polarization-based microscopy. *J. Cell. Biol.* **89**, 346–356.
13. Inoué, S. (1989) Imaging of unresolved objects, superresolution and precision of distance measurement with video microscopy. In “Methods in Cell Biology” (Eds. D. L. Taylor and Y.-L. Wang) Vol. 30, Pp. 85–112. Academic Press, New York.
14. Inoué, S. (1986) Video Microscopy, 1st edition, Plenum Press, New York.
15. Inoué, S. and Spring, K. (1997) Video Microscopy, 2nd edition, Plenum Press, New York.
16. Weiss, D. G. (1998) Video-enhanced contrast microscopy. In “Cell Biology: A Laboratory Handbook” Vol. 3, 2nd Edition, Pp. 99–108, Academic Press, New York.
17. Weiss, D. G. and Maile, W. (1993) Principles, practices and applications of video-enhanced contrast microscopy. In “Electronic Light Microscopy” (Ed. D. Shotton), Pp. 105–140. Wiley-Liss, New York.
18. Weiss, D. G., Maile, W., and Wick, R. A. (1989) Video microscopy. In “Light Microscopy in Biology. A Practical Approach” (Ed. A. J. Lacey), Pp. 221–278. IRL Press, Oxford.

19. Weiss, D. G., Meyer, M., and Langford, G. M. (1990) Studying axoplasmic transport by video microscopy and using the squid giant axon as a model system. In "Squid as Experimental Animal" (Eds. D. L. Gilbert, W. J. Adelman, Jr., and J. M. Arnold), Pp. 303–321. Plenum Press, New York.
20. Bennett, H. S. (1950) Methods applicable to the study of both fresh and fixed materials: The microscopical investigation of biological materials with polarized light. In "Handbook of Microscopical Technique" (Ed. C.E. McClung) Pp. 591–677, Harper and Row, New York.
21. Salmon, E. D. and Tran, P. (1998) High-resolution video-enhanced differential interference contrast (VE-DIC) light microscopy. In "Video Microscopy" Eds. G. Sluder and D. E. Wolf, *Methods Cell. Biol.* **56**, 153–184, Academic Press, New York.

Computer-Assisted Systems for the Analysis of Amoeboid Cell Motility

David R. Soll, Deborah Wessels, Edward Voss, and Olof Johnson

1. Introduction

Almost all eukaryotic cells move or are moved sometime in their life time. In the evolution of eukaryotic cells, two forms of single cell locomotion have evolved, flagellar or ciliary locomotion, and amoeboid locomotion. The latter represents the more general method of cellular locomotion. Amoeboid locomotion in the past has been trivialized. The view, strengthened by bad science fiction movies, was of a cytoplasmic mass, or blob, rolling blindly forward across a substratum, consuming things in its path. Because of a variety of static and dynamic 2D and 3D imaging methods, and newly developed computer-assisted 2D and 3D dynamic image reconstruction and analysis systems (*1-6*), we now know that amoeboid locomotion is not simple. Amoeboid cells move across a substratum by extending pseudopods on and off the substratum, making soft turns by biasing pseudopod expansion to the left or right (*7,8*), and making sharp turns through lateral pseudopod formation (*9-11*). Animal cells spanning the eukaryotic world, from *Dictyostelium discoideum* amoeba to human white blood cells, also exhibit a one minute behavior cycle that, in some cases, has a z-axis component (*3,10,12,13*).

Because the behavioral phenotype of crawling cells in complex, it is unacceptable to characterize behavior in an anecdotal, qualitative fashion, and in some cases it is inaccurate to describe the cell in two dimensions. This is especially true when the behavior of normal cells and abnormal cells (e.g., metastasizing cells, cytoskeletal mutants, regulatory mutants, cells infected with pathogens, cells treated with a drug) are compared e.g., (*14*). In this chapter, we will describe methods for analyzing cells with the most advanced computer-assisted 2D and 3D dynamic image analysis systems, 2D-DIAS and 3D-DIAS.

For 2D analysis (*1–6*), the images of living, crawling cells are digitized directly into the data base of 2D-DIAS. The perimeter of the image is then automatically identified and converted into a beta spline model. From this model, the centroid is automatically determined. Cell images can be digitized and analyzed as frequently as every thirtieth of a second. 2D-DIAS software then computes over forty parameters of motility and dynamic cell morphology, based on the dynamics of the centroid in the former case and the changing contour in the latter case. For 3D analysis (*3–6*), the cell is optically sectioned in a 0.5 to 2.0 s period. The optical sections are automatically outlined, and the outlines stacked and processed to form a faceted image at intervals as short as the time it takes for sectioning. 4D computer presentations of the reconstructed cells can then be visualized at any angle. 3D-DIAS also provides the capabilities of “direct image” reconstruction, the simultaneous reconstruction of the plasma membrane, pseudopodial regions containing nonparticulate cytoplasm and nucleus, and the tracking of vesicles in 3D (*3–6,14*).

2. Materials

In selecting the equipment, we have considered the average experiment in which a typical amoeboid cell is being analyzed. Variations on the themes followed in the subsequent descriptions can be acquired by examining the latest research papers employing 2D-DIAS and 3D-DIAS.

2.1. 2D-DIAS Experiment

1. Sykes-Moore perfusion chamber (Bellco Glass, Inc, Vineland, NJ).
2. Upright microscope with brightfield optics at 10× or 25× magnification.
3. Video camera with contrast and brightness adjustment (MTI Television).
4. Half inch VCR.
5. Time Base Corrector TBC/FREEZE II (Prime Image Inc, San Jose, CA).
6. Late model Macintosh computer (Apple Computer Inc., Cupertino, CA).
7. Data Translation DT3155 framegrabber board (Data Translation Inc, Marlboro, MA).
8. 2D-DIAS software (Solltech Inc, Oakdale, IA).
9. Chemotaxis chamber (*15–17*).

2.2. 3D-DIAS (DIC) Experiment

1. Dvorak-Stotler chamber (Lucas-Highland, Burnsville, VA).
2. Zeiss Axioplan or Axiovert microscope with differential interference (DIC), or Nomarski, optics (Carl Zeiss Inc, Thornwood, NY).
3. 63× Planapo objective (Carl Zeiss Inc).
4. Computer-regulated microstepper motor with character generator.
5. Cooled CCD camera (Optronics Inc, Galeta, CA); optional 3/4 inch VCR.
6. Media 100QX framegrabber board (Media 100 Inc, Marlboro, MA).

7. Late model Macintosh computer (Apple Computer Inc).
8. Adobe Premiere software (Adobe Systems Inc, San Jose, CA).
9. 3D-DIAS Software (Solltech Inc).
10. Crystal Eyes 3D display system (Stereographics, San Raphael, CA).

2.3. 3D-DIAS (Confocal) Experiment

1. Dvorak-Stotler perfusion chamber (Lucas-Highland).
2. Zeiss Axiovert S100TV inverted microscope (Carl Zeiss).
3. Noran Oz Laser Scanning Confocal Microscope (LSCM) (Noran Corporation, Middleton, WI).
4. 100× Plan-Neofluar oil immersion objective (Carl Zeiss).
5. Optional 3/4 inch VCR.
6. Media 100QX framegrabber board (Media 100 Inc).
7. Late model Macintosh computer (Apple Computer Inc).
8. Adobe Premiere software (Adobe Systems Inc).
9. 3D-DIAS Software (Solltech Inc).
10. Crystal Eyes 3D display system (Stereographics).

3. Methods

3.1. 2D-DIAS Experiment (see Notes 1 and 2)

3.1.1. Videomicroscopy

The two dimensional dynamics image analysis system, 2D-DIAS, is diagrammed in **Fig. 1**. For the 2D analysis of cell behavior in the absence of chemoattractant, samples are inoculated into a perfusion chamber, and allowed to adhere to the wall of the chamber for 5 min. The chamber is perfused with buffer or media at a rate of 4 mL per min in order to continuously refresh the environment (**16**). Images are videorecorded onto half inch or three quarter inch videotape, or digitized directly, for at least 10 min at 25× magnification using brightfield optics. Additional magnification is provided by the camera system; therefore, the final magnification is determined by recording a stage micrometer at the precise settings used for the experiment and then measuring a scale factor using DIAS software. In order to automatically outline the image using the threshold method of edge detection in 2D DIAS, the image is slightly defocused and processed by adjusting the gain and offset settings on the camera controls to achieve a uniformly dark cell against a lighter background.

For analyzing cells in a spatial gradient of test attractant, cells are deposited on the bridge of a chemotaxis chamber (**15–17**). In this chamber, a 2 mm wide bridge separates the source and sink troughs. Solution containing the appropriate concentration of chemoattractant (for example, 10^{-6} M cAMP for *Dictyostelium discoideum*, 5×10^{-8} M fMLP for human polymorphonuclear leukocytes; (**17**) is placed in the source trough and solution without the test

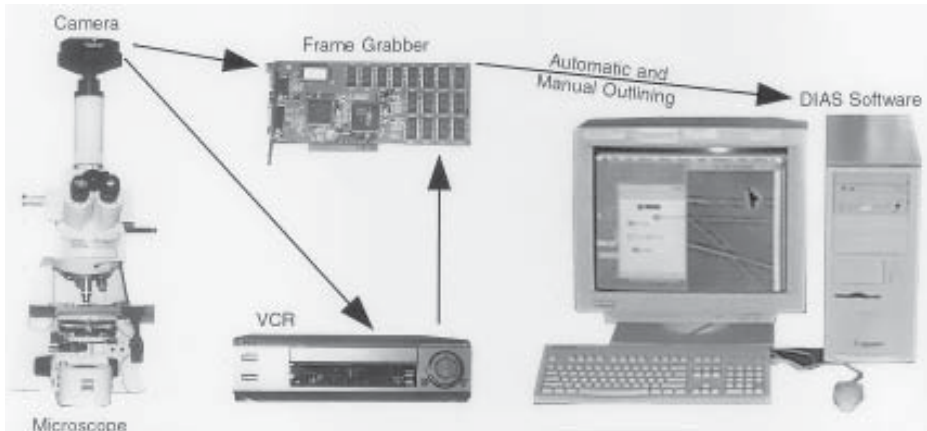


Fig. 1. The 2D dynamic image analysis system (2D-DIAS) is based on a Macintosh computer and uses a frame-grabber board both for automatic and manual digitization.

attractant in the sink trough. Cells are dispersed on the bridge, incubated for 5 min, and then videorecorded. Images are processed at the time of recording as described above. Stage warmers and CO₂ environmental chambers are used when necessary.

For analyzing the behavior of *Dictyostelium discoideum* amoebae in natural aggregation territories (18,19), log phase cells are washed 3 times in BSS (BSS: 20 mM KCl, 2.5 mM MgCl₂, 20 mM KH₂PO₄, pH 6.4), vortexed into a single cell suspension, resuspended in BSS at a concentration of 2.5×10^6 per ml, and 2 mL dispersed onto an agar film generated by coating the bottom of a 35 mm Petri dish with 300 μ L of 1% Noble agar in BSS. After 30 min, 1 mL of the overlying BSS is removed, the preparation placed on the stage of an inverted microscope and the cell layer continuously videorecorded throughout early development and aggregation using brightfield optics at 10 \times magnification.

3.1.2. Digitizing and Automatic Outlining of Recorded Images

Using 2D-DIAS software, videorecorded images are standardly digitized at a rate of 15 frames per min onto the hard disc of a computer equipped with a framegrabber board and 2D-DIAS software. The frame rate may be increased or decreased for faster or slower moving cells.

2D-DIAS automatically detects the edge of the cell image in each frame employing a gray scale threshold, converts the detected perimeter to a mathematically precise beta-spline replacement image, and from this final shape computes the centroid, or geometric center, at each time point.

3.1.3. Motility and Dynamic Morphology Parameters Computed by 2D-DIAS

The user may select up to 40 parameters from the standard 2D-DIAS menu, or enter other functions as desired (163, 195). Parameters such as instantaneous velocity, direction of travel, and direction change are computed from the position of the cell centroid. For example, “instantaneous velocity” for a cell in frame n is computed by drawing a line from the cell centroid in frame $n-1$ to the cell centroid in frame $n+1$, and then dividing the length of that line by $2t$, where t is the time interval between analyzed frames. “Directional change” for the interval between n and $n+1$ is computed as the direction in the interval $(n-1, n)$ minus the direction in the interval $(n, n+1)$. If the directional change for an interval is greater than 180° , it is subtracted from 360° . Parameters that quantify cell shape are computed from the beta-spline replacement image. For example, “maximum length” is computed as the longest chord between any two points along the perimeter. “Maximum width” is computed as the longest chord between any two points along the perimeter drawn perpendicular to the initial longest chord. “Roundness” is computed by the formula $100 \times 4\pi \times \text{area}/\text{perimeter}^2$. “Convexity” is computed by first drawing line segments connecting the vertices of the final cell shape, and then measuring the angles of turning from one segment to the next. Counterclockwise turns are considered positive and clockwise turns negative. Convexity is the absolute value of the sum of positive turn angles, in degrees. The “chemotactic index” is computed as the net distance moved towards the source of chemoattractant divided by the total distance moved in a set period of time (195). These data can then be displayed in graphic form (**Fig. 2**) or tabular form (**Fig. 3**). Several display modes allow the user to visualize cell movement either as a static image or as a movie. An example of a centroid track and stacked perimeter plots of a crawling amoeboid cell are presented in **Fig. 4**. DIAS data files can be exported into other spreadsheet software for additional statistical analyses. Static images can be saved as PICT files for use in graphics software such as PhotoShop, and movies can be converted to QuickTime for presentation purposes.

3.2. 3D-DIAS (DIC) Experiment (see Notes 3 and 4)

3.2.1. Videomicroscopy

The three-dimensional dynamic image analysis system, 3D-DIAS, is diagrammed in **Fig. 5**. For the 3D reconstruction of cells crawling in the absence of attractant, cells are inoculated into a Dvorak-Stotler chamber (Lucas-Highland, Burnsville, VA) positioned on the stage of an inverted microscope equipped with DIC optics and a high numerical aperture objective such as the Zeiss 63 \times Planapo. Cells are allowed to adhere to the coverslip for 5 min and

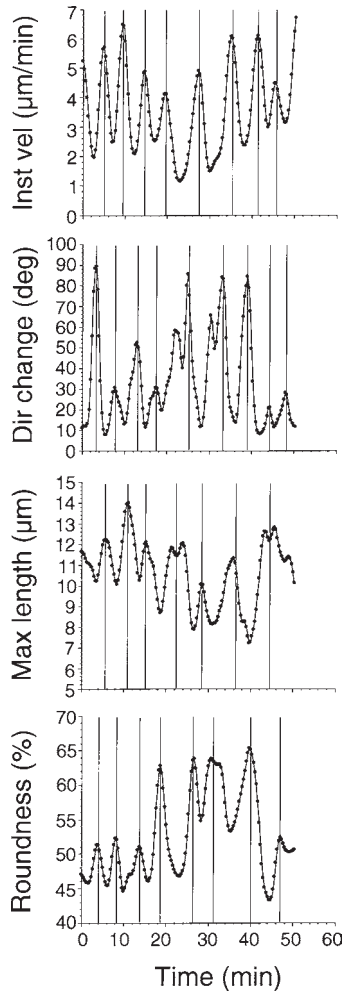


Fig. 2. Graphic presentation of parameters calculated by 2D-DIAS.

the chamber is then perfused with buffer or media. To obtain optical sections, the coarse focus knob of the microscope is connected to a computer-regulated microstepper motor programmed to move the focus from the substratum through the desired z -axis height, generally 10–20 μm for single cells. The user determines the z -axis height and the time period of optical sectioning and enters the appropriate instructions when prompted by the stepper motor software. Images are acquired with a videocamera, such as a cooled CCD camera, and either recorded onto 3/4 inch videotape, or directly digitized. In the case of motile single cells such as *Dictyostelium discoideum*, PMNs and T cells, thirty

A

Title: Spatial Gradient
 9/18/98. Trial 1. 152 Frames. 1 Objects
 Frame Rate: 30 fr/min Scale: 0.25 um/pixel
 Pre-spline resolution: 33 % Post-spline resolution: 50 % Spline bias: 1 Spline tension: 1
 Centroid Method: Center of perimeter

Frame	Time	Speed	Direct	Dir Ch	Accel	Persis	X Cent	Y Cent	Tilt	Length	AvgWid	MaxWid	CenWid	etc...
	(min)	(um/min)	(deg)	(deg)	um/sqmin	um/min	(pix)	(pix)	(deg)	(um)	(um)	(um)	(um)	
1	0	22.605	-88.266	0	-282.995	22.605	345.952	191.405	-73.725	15.067	3.416	6.49	4.91	
2	0.033	13.172	-77.336	10.93	-288.285	3.264	346.043	194.417	-73.577	15.12	3.447	6.49	4.98	
3	0.067	3.386	-17.818	59.517	-150.328	0.193	346.722	194.832	-73.539	14.988	3.262	6.49	4.91	
4	0.1	3.15	-90.695	72.877	38.135	0.148	346.903	194.694	-74.397	14.923	3.29	6.731	4.911	
5	0.133	5.928	-87.154	3.541	43.609	2.989	346.712	195.672	-72.865	15.013	3.358	6.562	4.981	
6	0.167	6.057	-98.255	11.101	71.871	1.483	346.981	196.273	-73.322	14.799	3.405	6.489	0	
7	0.2	10.72	-88.93	9.325	190.832	2.986	346.48	197.27	-74.347	14.775	3.419	6.731	5.393	
8	0.233	18.779	-61.484	27.447	176.234	2.178	347.035	199.131	-76.982	14.428	3.473	6.671	5.94	
9	0.267	22.469	-57.282	4.202	-9.571	10.368	348.871	201.67	-74.982	14.34	3.566	6.49	6.249	
10	0.3	18.141	-68.045	10.764	-86.515	4.547	350.273	204.172	-74.546	14.01	3.572	6.731	0	
11	0.333	16.701	-79.157	11.111	-60.537	4.087	350.68	206.157	-80.925	14.022	3.762	6.823	5.342	
12	0.367	14.106	-82.904	3.747	-131.814	6.911	351.111	208.546	-80.925	14.022	3.734	6.823	4.809	
13	0.4	7.14	-86.406	3.502	-129.914	4.012	351.144	209.89	-84.117	14.635	3.665	6.543	5.025	
14	0.433	5.445	-80.97	5.436	-40.658	2.169	351.243	210.652	-82.304	14.809	3.813	7.071	4.031	
15	0.467	5.203	-81.801	0.931	36.56	4.228	351.372	211.324	-83.116	14.611	3.875	7.318	5.798	
16	0.5	7.882	-95.14	13.339	72.149	1.675	351.441	212.025	-85.802	14.492	3.824	7.018	5.771	
17	0.533	10.013	-86.846	8.294	31.76	3.031	351.184	213.417	-84.774	13.978	3.965	6.519	5.772	
18	0.567	9.999	-71.28	15.566	33.494	1.878	351.588	214.691	-83.959	13.928	4.003	6.792	6.543	
19	0.6	12.246	-77.083	5.803	-8.644	4.689	352.04	215.943	-85.659	13.564	3.95	6.768	6.519	
20	0.633	9.423	-88.725	11.642	-47.159	2.226	352.318	217.874	-98.699	12.493	4.118	5.797	3.288	
21	0.667	9.102	-108.022	19.297	-8.546	1.431	352.095	218.455	-91.086	13.113	4.021	5.754	3.254	
22	0.7	8.853	-97.222	10.801	12.806	2.213	351.567	220.182	-104.098	13.027	3.956	5.14	3.335	
23	0.733	9.956	-90.059	7.163	51.846	3.33	351.799	220.797	-103.915	13.352	3.918	4.911	3.335	
24	0.767	12.31	-91.104	1.046	32.708	9.539	351.565	222.837	-98.345	13.781	3.804	4.772	3.783	
25	0.8	12.136	-94.72	3.616	23.667	6.055	351.735	224.079	-95.159	13.902	3.716	4.776	3.508	
26	0.833	13.887	-100.554	5.834	12.705	5.299	351.298	226.063	-100.506	13.687	3.737	5.053	3.824	
27	0.867	12.983	-101.071	0.517	-81.045	11.352	351.057	227.72	-107.67	14.572	3.59	4.981	4.429	
28	0.9	8.484	-101.176	0.104	-72.627	8.246	350.633	229.46	-109.504	14.624	3.468	5.297	0	
29	0.933	8.141	-106.817	5.641	86.438	3.172	350.619	229.939	-107.61	14.648	3.403	5.533	4.191	
30	0.967	14.247	-101.177	5.64	79.756	5.551	350.005	231.538	-107.036	14.237	3.424	5.532	4.742	
31	1	13.458	-100.585	0.593	-18.888	11.556	349.882	233.666	-107.607	14.173	3.572	5.533	5.322	
32	1.033	12.988	-116.775	16.19	4.466	2.363	349.346	235.066	-113.24	13.939	3.63	5.482	0	
33	1.067	13.756	-125.597	8.822	-56.761	3.987	348.322	236.758	-123.364	13.737	3.74	5.408	0	
34	1.1	9.204	-111.219	14.378	-32.601	1.843	347.211	238.049	-122.122	14.033	3.672	5.406	0	
35	1.133	11.583	-89.842	21.377	17.449	1.669	347.434	239.064	-112.252	14.355	3.603	5.385	5.385	
36	1.167	10.367	-101.752	11.91	-129.948	2.406	347.219	241.138	-117.261	15.576	3.434	5.145	0.115	
37	1.2	2.92	-90.818	10.935	-91.452	0.723	346.871	241.753	-113.742	15.951	3.473	4.924	4.696	
38	1.233	4.27	-115.879	25.061	102.564	0.536	347.208	241.916	-106.06	16.427	3.522	4.67	4.67	
39	1.267	9.757	-131.391	15.512	76.493	1.838	346.374	242.777	-107.512	16.616	3.515	4.505	0	
40	1.3	9.37	-129.958	1.434	-45.846	6.701	345.488	243.868	-106.797	16.514	3.469	4.43	3.951	

B

SUMMARY:
 Object 1, Frames: 1 to 40
 Time: 0 to 1.3 min, Total Elapsed Time: 1.3 min
 Total path length: 14.2363 um Net path length: 13.1165 um
 Directionality - Total: 0.921338 Upward: -0.921302 Rightward: -0.00815281
 Speed (um/min): 10.7778 +/- 4.6587
 Direction (deg): 267.852 +/- 19.3537
 Direction Change (deg): 0.951718 +/- 0.13098
 Acceleration (um/sq min): -14.4648 +/- 98.8204
 Persistence (um/min-deg): 4.38687 +/- 4.1172
 Centroid: X (pix): 349.346 +/- 2.2125
 Centroid: Y (pix): 218.379 +/- 16.1214
 Axis Tilt (deg): 86.3441 +/- 15.5618
 Maximum Length (um): 14.457 +/- 0.88941
 Mean width (um): 3.63963 +/- 0.219318
 Maximum width (um): 5.90002 +/- 0.836986
 Central width (um): 3.84022 +/- 2.08837
 X Bounding width (um): 7.67915 +/- 0.615616
 Y Bounding width (um): 14.0338 +/- 0.821489
 X Maximum width (um): 5.975 +/- 0.675001
 Y Maximum width (um): 12.1562 +/- 1.45955
 Area (sq um): 52.4841 +/- 2.49942
 Perimeter (um): 36.6172 +/- 3.0052
 Roundness (%): 49.9262 +/- 6.62899
 Predicted Volume (cu um): 187.209 +/- 25.2283
 Predicted Surface Area (sq um): 133.756 +/- 6.37606
 Mean Radial Length (um): 4.5643 +/- 0.195384
 Radial Deviation (%): 37.9844 +/- 2.42342
 Mean Convexity (deg): 602.622 +/- 92.2348
 Mean Concavity (deg): 242.622 +/- 92.2349
 Positive Flow (%): 5.6522 +/- 2.68502
 Negative Flow (%): 5.37175 +/- 2.23185
 Area Sec 1 (sq um): 52.0578 +/- 2.3524
 Perimeter Sec 1 (um): 44.0312 +/- 3.03634
 Pos Flow Sec 1 (%): 5.6522 +/- 2.68502
 Neg Flow Sec 1 (%): 5.37175 +/- 2.23185
 Area Sec 2 (sq um): 52.0578 +/- 2.3524
 Area Sec 3 (sq um): 52.0578 +/- 2.3524
 Area Sec 4 (sq um): 52.0578 +/- 2.3524
 Perimeter Sec 2 (um): 44.0312 +/- 3.03634
 Perimeter Sec 3 (um): 44.0312 +/- 3.03634
 Perimeter Sec 4 (um): 44.0312 +/- 3.03634
 Pos Flow Sec 2 (%): 5.6522 +/- 2.68502
 Pos Flow Sec 3 (%): 5.6522 +/- 2.68502
 Pos Flow Sec 4 (%): 5.6522 +/- 2.68502
 Neg Flow Sec 2 (%): 5.37175 +/- 2.23185
 Neg Flow Sec 3 (%): 5.37175 +/- 2.23185
 Neg Flow Sec 4 (%): 5.37175 +/- 2.23185

Fig. 3. Data generated for one cell by 2D-DIAS presented in tabular form.



Fig. 4. Stacked perimeters and centroid track of a translocating *Dictyostelium discoideum* amoeba generated by 2D-DIAS.

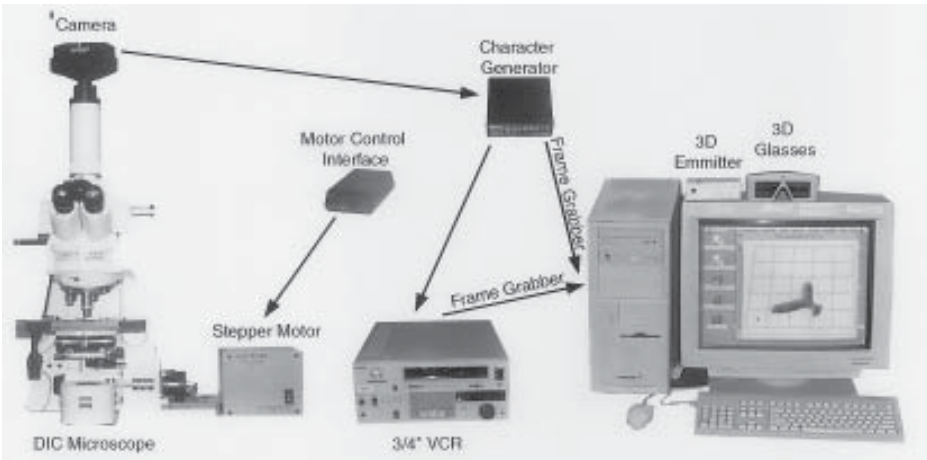


Fig. 5. The 3D-DIAS system operates in a Macintosh platform and a StereoGraphics CrystalEyes stereo workstation for 3D-reconstruction and quantitative motion analysis of the dynamics of cellular and intracellular motility.

optical sections are recorded at $0.6 \mu\text{m}$ increments in the z -axis over a 2 s period for a single reconstruction, and this procedure is repeated at 4 s intervals. The error in reconstruction due to movement was previously estimated by comparison of 3D-DIAS and confocal reconstruction to be approximately 2% of volume (20).

For the 3D reconstruction of cells responding to a spatial gradient of cAMP, a chamber developed for the analysis of T cell chemotaxis (17) that includes a quartz bridge and glass walls for DIC imaging (21) is employed. Cells are placed on the glass coverslip chamber wall that can be pre-conditioned if necessary. The coverslip is then clamped over the bridge and troughs of the chamber, and the chamber is inverted. One trough is filled with solution containing the test attractant (source) and the other with the solution or buffer alone (sink). The second glass wall of the chamber is then lowered over the troughs and the bridge. The apparatus is then placed on the stage of an inverted microscope for optical sectioning.

3.2.2. Optical Sectioning, Outlining and Reconstructing Crawling Cells in 3D

The videorecorded optical sections are then digitized at 30 frames per s with a framegrabber board. The perimeter of the in-focus portion of the cell image in each optical section is automatically outlined by the 3D-DIAS program using the pixel complexity measurement (3,4,6). Perimeters are stacked at distance intervals proportional to those of the original optical sections. After automatic outlining, the 3D-DIAS data file contains both the interpreted perimeter and the original averaged DIC image of each optical section. To generate a “direct image” reconstruction, 3D-DIAS superimposes the automatically interpreted perimeter over the original averaged DIC image of each optical section and subtracts those portions of the averaged DIC image outside the interpreted perimeter. The optical sections containing all interval pixel complexity are then stacked to generate a direct image reconstruction. Edge points along each perimeter corresponding to a 2D x,y -coordinate grid can also be connected to generate transparent faceted reconstructions of the cell surface. Alternatively, the faceted image can be smoothed and presented as a shadowed, nontransparent “wrapped” image. Faceted, wrapped or direct image reconstructions can then be viewed at any angle in 3D through a 3D display system, and converted to a time series for dynamic 3D display.

To reconstruct the nucleus of a crawling cell in 3D, the perimeter of the nucleus in each optical section is manually outlined, and the collection of perimeters stacked and wrapped. The wrapped image at each time point can then be colored, shadowed and inserted into the faceted 3D reconstruction of the cell surface. To reconstruct the pseudopods of crawling cells, the interfaces between the particulate cytoplasm of the main cell body and the nonparticulate cytoplasm of pseudopodial extensions can be manually outlined in each optical section. The interface plus the peripheral outline of each pseudopodial extension is used to encapsulate the nonparticulate zones in each optical section. These zones are stacked and a wrapped image of the pseudo-

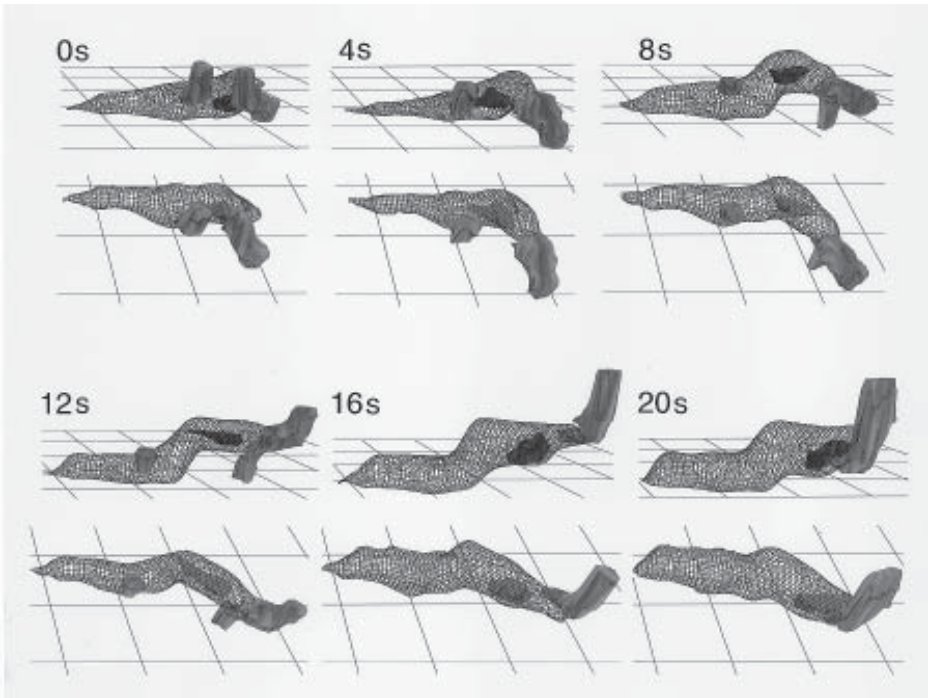


Fig. 6. Three-dimensional reconstruction of a *Dictyostelium discoideum* amoeba translocating in buffer. The faceted surface of the cell body is represented as a transparent blue cage, non-particulate pseudopodial extensions are color-coded red, and the nucleus is color-coded green. The cellular reconstructions, presented at 4 s intervals, are viewed at 15° (top panel) and 45° (bottom panel).

pod generated. The wrapped pseudopodial regions can then be colored, shadowed and inserted at their resident positions in faceted or wrapped images of the entire cell surface in a time series. 3D reconstruction of a crawling *Dictyostelium* cell is presented in **Fig. 6** with the plasma membrane displayed as a transparent blue faceted surface, the pseudopods color-coded red and the nucleus color-coded green.

3.2.3. Motility and Dynamic Morphology Parameters Computed by 3D-DIAS

3D-DIAS computes more than 100 parameters based upon the 3D position of the cell centroid and the 3D contours of the cell body. It generates centroid track based on the 3D positions of the cell centroid, which are plotted in 4D and must be viewed in stereo. 3D-DIAS also provides 2D parameters on any planar slice of the cell. Since the 3D reconstructions of the nucleus and pseudo-

pod are encapsulated, all 3D parameters computed for the entire 3D cell surface can also be computed for the 3D reconstructions of the nucleus and pseudopodia of a crawling cell.

3.3. 3D-DIAS (Confocal) Experiment

3.2.4. Microscopy

Fluorescently labeled cells (e.g., DiI stained, green fluorescent protein-tagged, and the like) are inoculated into the Dvorak-Stotler perfusion chamber, allowed to adhere to the coverslip for 5 min and then placed on the stage of an inverted microscope coupled to a Noran Oz Laser Scanning Confocal Microscope (LSCM). The coverslip may be pre-conditioned or coated with a matrix protein if necessary. Stage warmers and CO₂ environmental chambers can also be used. The LSCM is set to a time rate that generates 30 optical sections per s. This corresponds to a laser dwell time of 100 ns per image pixel. The resolution of the scans in this mode is 512 × 480 image pixels. A confocal slit of 25 microns is used to reduce out-of-focus light. A 100 × Plan-Neofluar oil immersion objective and a digital zoom factor in the LSCM software results in a final scale factor of 0.08 μm per image pixel. Thirty optical sections can be acquired during both the down-scan and 30 during the up-scan. A version of 3D-DIAS modified for the LSCM is used for reconstructions. Synchronization software insures proper registration (in the z direction) of alternate up/down scans, and a customized stepper-motor constructed specifically for this task provides near-linear motion and stable pauses in the up/down phases. The effectiveness of this method was verified by using trial runs with fixed samples. The z-axis registration error proved to be less than one slice per min, that is < 0.5 μm. Of the 30 optical sections acquired in one sec scan in either direction, the 20 to 25 midsections are chosen (omitting the first and last 2 to 5 frames) to remove artifacts resulting from abrupt changes in direction at the end of the up-scan and at the end of the down-scan. This process yields one 3D reconstruction per sec containing 20 to 25 optical slices at 0.5 μm increments, resulting in a total height of 10 to 15 μm. Because the Silicon Graphics O2 workstation attached to the Noran Oz LSCM can not save images at a speed of 30 frames per second (fps), one of its analog buffer outputs is connected either to a 3/4 inch VCR so that the optical sections are recorded onto videotape, or to a framegrabber. Images are captured with a framegrabber board and processed using the “image inversion” and “brightness contrast” image processing features of 3D-DIAS.

For the analysis of DiI-stained vesicles, vesicles are first outlined in the optical section in which they exhibit their widest diameter. Newly developed software then automatically adds outlines to slices above and below the marked

circle to form a sphere. Each particle outline is then placed in its own ‘trace-slot’. Organelles and structures with sufficient contrast can likewise be automatically outlined; others may require manual tracing. DiI, a stain used to visualize intracellular vesicles, also stains the plasma membrane lightly. The cell outline in each optical section can, therefore, be traced automatically by 3D-DIAS. From the outlines of the cell perimeter and the reconstructed particles, a faceted representation with color-coded particles is created. The vesicles and cell centroid are then motion-analyzed simultaneously with 3D-DIAS software. Data files as described above are generated. Faceted movies of the cell with intracellular vesicles and/or organelles can also be displayed at any angle and viewed in 3D through a display system. This system is now being optimized for molecular complexes stained with fluorescent tags, such as green fluorescent protein.

4. Notes

1. Two-dimensional analyses rely heavily on the level of image resolution. Automatic edge detection, although highly optimized, depends on the quality of the microscopic image. Even so, 2D-DIAS can automatically trace outlines of cells in soft images, such as those visualized with DIC optics.
2. Caution must always be applied to the level of light used to image. Tests must be performed to assess the effects of photodamage.
3. 2D-DIAS and 3D-DIAS can be used to reconstruct and motion analyze cells crawling in tissue or in a 3D matrix, so long as the cell is visible to the researcher. In many of these cases, manual outlining is necessary.
4. A critical element in the creation of a 3D movie is the registration of the optical sections from one 3D frame to the next. This specification is referred to as synchronization. Potential problems include: oscillations in Z motor speed, movement or pumping of the imaging chamber, z motion of the sample under study, and motion due to the perfusion system.
 - a. Oscillations in Z motor speed are most often caused by having a focus system that is too massive. A higher torque motor can help to compensate for this problem. Another source of motor oscillation is a phenomenon called mid-range resonance. This can cause variations in motor speed and motor stall at certain rotation speeds. The solution to this problem is to use a more sophisticated bipolar motor driver that suppresses midrange resonance.
 - b. With water or oil immersion optics, the movement of the objective lens is coupled to the imaging chamber cover slip by the immersion medium. When the objective is moved it can pick up the chamber or pump the chamber volume rhythmically. The use of stiff cover glass which is supported along the entire perimeter by a solid structure will usually solve this problem. Often it is necessary to remanufacture the chamber holder on the microscope stage since they are not designed with rapid focusing in mind.

- c. The problem of the z motion of the sample under study is formidable. The most simple solution is to allow extra space in the z scan to account for potential motion or growth in the z axis. Another solution is to adjust the z scan limits as the sample moves. A near-real time system that accomplishes this automatically is now under construction.
- d. Most perfusion pumps have cyclic action. Diastolic pumps are quite smooth for large volumes but oscillate at low flow rates. Even syringe pumps, which are relatively light, can oscillate as the feed screw turns. The best solution for this problem is to build a perfusion system which is powered by a pressure bottle. This system gives smooth flow and excellent flow control over long time scales.
- e. The cost of the equipment for 2D-DIAS will include microscope, computer plus framegrabber and 2D-DIAS software. The software is the least expensive item. 3D-DIAS (DIC) will include microscope (very expensive in the case of confocal), computer-driven microstepper motor, computer and framegrabber, and 3D-DIAS software. The cost of this complete system may be prohibitive to most researchers. This technology can be accessed by visiting the W.M. Keck Dynamic Image Analysis Facility at Iowa www.miowa.edu/~keck.

Acknowledgments

The development of 2D-DIAS and 3D-DIAS was supported in part by grants HD18577 and AI40040 from the National Institutes of Health and a generous facility grant from the W.M. Keck Foundation.

References

1. Soll, D. R. (1988) "DMS", a computer-assisted system for quantitating motility, the dynamics of cytoplasmic flow and pseudopod formation: its application to *Dictyostelium* chemotaxis, in *Optical Approaches to the Dynamics of Cellular Motility* (ed. J. Condeelis, J., ed.). Supplement to *Cell Motil. Cytoskel.* **10**, 91–106.
2. Soll, D. R., Voss, E., Varnum-Finney, B., and Wessels, D. (1988) The "Dynamic Morphology System": a method for quantitating changes in shape, pseudopod formation and motion in normal mutant amoebae of *Dictyostelium discoideum*. *J. Cellular Biochem.* **37**, 177–192.
3. Soll, D. R. (1995) The use of computers in understanding how cells crawl. *Int. Rev. of Cytology* **163**, 43–104.
4. Soll, D. R. and Voss, E. (1998) Two and three dimensional computer systems for analyzing how cells crawl, in *Motion Analysis of Living Cells* (Soll, D. R. and Wessels, D., eds.), John Wiley, Inc., pp.25–52.
5. Soll, D. R. (1998) 3D reconstruction and motion analysis of the surface and internal architecture of live, crawling cells: 3D-DIAS. *Comp. Med. Imag. Graph.* **23**, 3–14.
6. Wessels, D., Voss, E., Von Bergen, N., Burns, R., Stites, J., and Soll, D. R. (1998) A computer-assisted system for reconstructing and interpreting in three dimensions the relationships of the cell surface, the nucleus and pseudopods in living cells. *Cell Motil. Cytoskel.* **41**, 225–246.

7. Royal, D., Royal, M.-A., Italiano, J., Roberts, T., and Soll, D. R. (1995) In *Ascaris* Sperm Pseudopods, MSP Fibers Move Proximally at a Constant Rate Regardless of the Forward Rate of Cellular Translocation. *Cell Motil. Cytoskel.* **31**, 241–253.
8. Royal, D., Royal, M. A., Wessels, D., L'Hernault, S., and Soll, D. R. (1997) Quantitative analysis of *Caenochabditis elegans* sperm motility and how it is affected by mutants *spell* and *unc54*. *Cell Motil. Cytoskel.* **37**, 98–110.
9. Varnum-Finney, B., Voss, E., and Soll, D. R. (1987) Frequency and orientation of pseudopod formation of *Dictyostelium discoideum* amoebae chemotaxing in a spatial gradient: Further evidence for a temporal mechanism. *Cell Motil. Cytoskeleton* **8**, 18–26.
10. Wessels, D., Vawter-Hugart, H., Murray, J., and Soll, D. R. (1994) Three dimensional dynamics of pseudopod formation and turning during the motility cycle of *Dictyostelium*. *Cell Motil. Cytoskel.* **27**, 1–12.
11. Wessels, D., Titus, M., and Soll, D. R. (1996) A *Dictyostelium* myosin I plays a crucial role in regulating the frequency of pseudopods formed on the substratum. *Cell Motil. Cytoskel.* **33**, 64–79.
12. Murray, J., Vawter-Hugart, H., Voss, E., and Soll, D. R. (1992) A three-dimensional motility cycle in leukocytes. *Cell Motil. Cytoskel.* **22**, 211–223.
13. Sylwester, A., Shutt, D., Wessels, D., Stapleton, J. T., Stites, J., Kennedy, R., and Soll, D. R. (1995) T cells and HIV-induced T cell syncytia exhibit the motility cycle. *J. Leuk. Biol.* **57**, 643–650.
14. Wessels, D. and Soll, D. R. (1998) Computer-assisted analysis of cytoskeleton mutants of *Dictyostelium*, in *Motion Analysis of Living Cells* (Soll, D. R. and Wessels, D., eds.), John Wiley, Inc., pp. 101–140.
15. Zigmond, S. H. (1978) A new visual assay of leukocyte chemotaxis, in *Leukocyte Chemotaxis: Methods, Physiology and Clinical Implication* (Gallin, J. I. and Quie, P. G., eds.), Raven Press, New York, NY, pp. 57–66.
16. Varnum, B. and Soll, D. R. (1984) Effect of cAMP on single cell motility in *Dictyostelium*. *J. Cell Biol.* **99**, 1151–1155.
17. Shutt, D. C., Jenkins, L. M., Carolan, E. J., Stapleton, J., Daniels, K. J., Kennedy, R. C., and Soll, D. R. (1998) T cell syncytia induced by HIV release T cell chemoattractants: demonstration with a newly developed single cell chemotaxis chamber. *J. Cell Science* **111**, 99–109.
18. Wessels, D., Murray, J., and Soll, D. R. (1992) The complex behavior cycle of chemotaxing *Dictyostelium* amoebae is regulated primarily by the temporal dynamics of the natural wave. *Cell Motil. Cytoskel.* **23**, 145–156.
19. Escalante, R., Wessels, D., Soll, D. R., and Loomis, W. F. (1997) Chemotaxis to cAMP and slug migration in *Dictyostelium* both depend on MigA, a BTB protein. *Molec. Biol. Cell.* **8**, 1763–1775.
20. Shutt, D., Wessels, D., Chandrasekhar, A., Luna, B., Hitt, A., and Soll, D. R. (1995) Ponticulin plays a role in the spatial stabilization of pseudopods. *J. Cell Biol.* **131**, 1495–1506.
21. Shutt, D. and Soll, D. R. (1999) HIV-induced T-cell syncytia release a two component T-helper cell chemoattractant composed of Nef and Tat. *J. Cell Sci.* **112**, 3931–3941.

Evaluation of Individual-Cell Motility

**Peter S. Walmod, Rasmus Hartmann-Petersen,
Anton Berezin, Søren Prag, Vladislav V. Kiselyov,
Vladimir Berezin, and Elisabeth Bock**

1. Introduction

The coordinated displacement of a cell is a highly complex process which relies on the integration of a series of signaling pathways and on the function of a large number of molecular components including all main structures of the cytoskeleton (1,2). Thus, a detailed knowledge of the regulation and function of the cytoskeleton is of central importance for the understanding of cell motility, and conversely, investigations of cell motility may shed light on the function of cytoskeletal components.

Quantitative evaluations of cell motility comprise two main approaches, individual-cell assays and cell-population assays (3). The latter include methods such as the Boyden chamber assay (4) and the in vitro “wound healing” assay (5) in which motility generally is evaluated by measuring the fraction of cells that have traveled a certain distance during a predetermined time interval. In contrast, individual-cell assays are based on the tracking of individual cells, typically performed by means of time-lapse video microscopy.

A major part of published cell motility studies is based on cell-population assays, since individual-cell assays generally are more laborious and require more sophisticated and expensive equipment. However, the revolution in computer technology and advances in microscope technology within the last decade have now made large-scale individual-cell assays a realistic task.

The present chapter evaluates some of the most common parameters used for the characterization of the motile behavior of cells, and describes ways of detecting biological or physical instabilities during recordings of cell motility. The chapter deals exclusively with data derived from time-lapse video micros-

copy of individual cells moving in two dimensions under uniform conditions i.e., in the absence of a chemotactic gradient.

1.1. Quantification of Individual-Cell Motility (see Notes 1 and 2)

Time-lapse investigations of cell motility date back to the 1920's and '30's (6–8), but no major study in which the phenomenon was quantified was undertaken until the mid-1950's (9) when the motility of fibroblasts was estimated by measuring the cell speed, i.e., the cell-displacement divided by the time interval between observations. However, since cells do not move along straight lines, such velocity-measurements depend on the employed time intervals between observations (see **Subheadings 2.3.2.** and **3.2.**).

Quantitative parameters independent of the time interval between observations were not developed until the 1970's when cell motility was described mathematically according to a “random walk”-model. Traditionally, a random walk (such as Brownian motions of small particles) is (for movements in two dimensions) described by the equation $\langle d^2 \rangle = 4Dt$, where $\langle d^2 \rangle$ is the mean-squared displacement of the particles, t is the time and D is the “diffusion coefficient” (measured as area/time). Under a given set of conditions D is a constant, and thus the area covered by random diffusion of particles is proportional to the time, whereas random displacement, d , of the particles is proportional to the square root of the time (10). Gail and Boone (11) modified the random walk equation by correcting it for cellular persistence in direction, i.e., the tendency of a cell to move in approximately the same direction for a certain amount of time, and demonstrated that motility of fibroblasts could be described as a “persistent random walk”. The equation was later modified by Dunn (12) to include estimates of the instantaneous velocity (termed the root-mean-square speed), S , of cells as well as the persistence time in direction, P , and the rate of diffusion, R .

More recently, cell motility has been described by a Langevin equation, in which the process is characterized by the two parameters α and β , describing “magnitude of random fluctuations” and “velocity decay rate”, respectively. The equation was formulated for a discrete process (displacements observed at uniform time increments) for one-dimensional motion by Doob (13) in 1942, and was later modified to describe two-dimensional motion in the 1980s (14–16) (see **Subheading 2.3.3.**).

2. Materials (see Notes 3–5)

2.1. Cell Culture

The cell lines used for experiments presented in this chapter include 1321N1 (human astrocytoma cells), BT4Cn (rat glioma cells), CHO (Chinese hamster ovary cells), COS7 (African Green Monkey kidney cells), HeLa (human cer-

vix carcinoma cells), L929 and Swiss 3T3 (both mouse fibroblasts). All cell lines were grown in Dulbecco's Modified Eagle's Medium (DMEM) supplemented with 10% fetal calf serum, penicillin (100 U/mL), streptomycin (100 μ g/mL) and fungizone (2.5 μ g/mL).

When replating cells for recordings of cell motility these were dislodged with 0.5 mg/mL trypsin, 0.54 mM EDTA in a modified Puck's saline and seeded in 6-well tissue culture plates in DMEM containing 25 mM HEPES. Cells were incubated for 24–48 h (37°C, 5% CO₂) before video recordings were initiated.

2.2. Video Recording

Requirements for a microscope workstation for recordings of cell motility have been described in detail elsewhere (17,18) including Chapter 5 in this book. Briefly, the workstation utilized for the present study comprised a Nikon Diaphot 300 inverted microscope equipped with a heated, movable, computer controlled microscope stage (Lincam Scientific Instruments LTD, Surrey, UK) and a plexiglass incubator (Nikon, Yokohama, Japan) with a thermostatically controlled heating fan (DFA, Copenhagen, Denmark). Digital phase-contrast micrographs of cells were obtained with the aid of a black and white CCD video camera (Burle, Lancaster, PA, USA) and a frame grabber coupled to a conventional PC. Recordings were performed using PRIGRA software (developed at the Protein Laboratory, Copenhagen, Denmark).

Long-term recordings of cell motility were performed by grabbing images of several microscopic fields within a cell culture dish with a uniform time interval between series of recordings, t , of 15 min for a total recording-time, t_{tot} , of 10 h. In some cases, 21 min long recordings with 3 min intervals were performed at selected time-points within the long-term recordings. The total number of cells measured, N , in the individual experiments was between 50 and 157.

The positions of individual cells in consecutive video frames were determined by semi-automatic marking of their nuclear centers using PRIMA image processing software (developed at the Protein Laboratory).

2.3. Determination of Motility Parameters

2.3.1. Overlapping vs Nonoverlapping Calculations

When making video recordings of cells for motility studies, the observations can be performed either continuously or (as it has been done in our study) at selected time intervals. In the following the time interval (of uniform length) between discrete observations is denoted τ . For example, during a given recording positions of a cell are observed at time-points $\tau = 0, t = \tau, t = 2\tau, t = 3\tau$ etc. The time elapsed from the first to the last image constituting a recording is referred to as the “total time of observation”, t_{tot} .

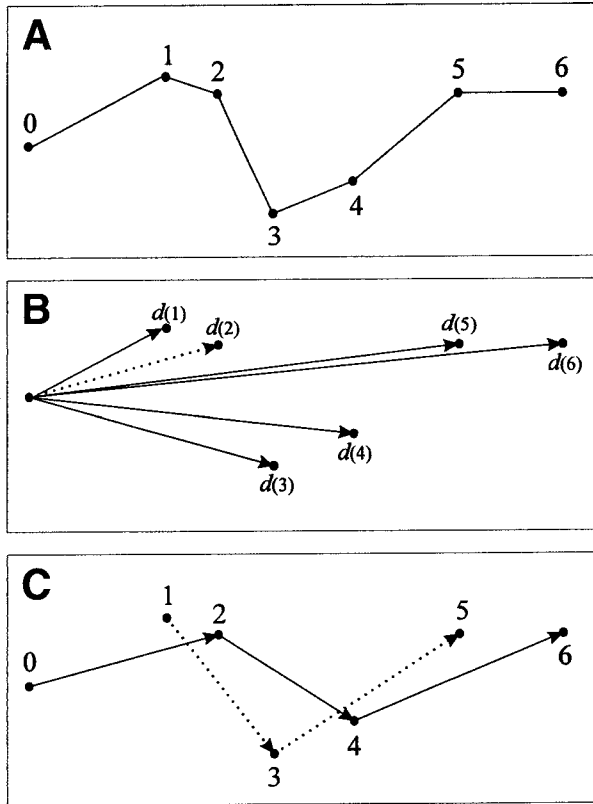


Fig. 1. Schematic presentation of the different methods used for calculating the dispersion of a cell. (A) The positions of a single cell observed for six time intervals of uniform duration τ . The initial position of the cell (at $t_{obs} = 0$) is indicated by 0, the position at $t_{obs} = 1\tau$ is indicated by 1 and so on. The total length of the six lines corresponds to the total path-length of the cell. (B) The dispersions of the cell (from panel A) calculated according to the simple method for $t_{obs} = \tau, 2\tau, 3\tau$ etc. The dispersion corresponding to $t_{obs} = 2t$ is indicated by a dotted line. C: The dispersions of the cell calculated according to the complex methods for $t_i = 2\tau$. When using the complex, non-overlapping method the dispersion of the cell for the selected $t_i = 2\tau$, is an average of the length of the vectors indicated with a solid line. When using the complex, overlapping method, the dispersion at this time interval is the average of solid as well as dotted vectors.

In principle the displacement of a cell during a given time period can be calculated in three different ways, here denoted the “simple”, “complex, non-overlapping” and “complex, overlapping” method.

According to the “simple” method the displacement of a cell is calculated as the displacement from its position at the initiation of the recording to its posi-

tion at later time-points. In the following such a time-point will be referred to as the “time of observation”, t_{obs} . Thus, when using the simple method of calculation the cellular displacement is measured from $t = 0$ to $t = t_{obs}$ (see also **Subheadings 2.3.2.** and **2.3.4.**).

The term “complex” refers to the situation where the calculated displacement is an average value of displacements occurring in several, different time intervals of identical duration. In the following these time intervals will be referred to as the “time interval of interest”, t_i . When using the complex, nonoverlapping method, the displacement during, e.g., a time $t_i = 4\tau$ will be the average displacement for all non-overlapping intervals of the length $t = 4\tau$ i.e., from $t = 0$ to $t = 4\tau$, $t = 4\tau$ to $t = 8\tau$, $t = 8\tau$ to $t = 12\tau$ and so on. When using the complex, overlapping method the displacement at $t_i = 4\tau$ will be the average displacement for all intervals of the length $t = 4\tau$ (i.e. from $t = 0$ to $t = 4\tau$, $t = \tau$ to $t = 5\tau$, $t = 2\tau$ to $t = 6\tau$ and so on).

The differences in calculation procedure are presented graphically in **Fig. 1**. **Figure 1A** illustrates the movements of a single cell over six time-intervals of uniform duration τ . The individual lines in **Fig. 1A** represent the displacements of the cell during the individual time-intervals. The sum of the length of these displacements from time $t = 0$ to any given time-point represents the “path length”, L , (see **Subheading 2.3.4.**). **Figure 1B** demonstrates the displacements of the cell calculated according to the “simple” method. When using this procedure, the displacements are exclusively measured from the position at the initiation of the recording, and the time during which a given displacement has taken place, t_{obs} , corresponds to the actual recording time. For instance, the dotted line in **Fig. 1B** corresponds to the displacement at $t_{obs} = 2\tau$. For comparison **Fig. 1C** illustrates the displacements occurring within a time interval of interest corresponding to $t_i = 2\tau$. When using the complex, non-overlapping method, the displacement of the cell at $t_i = 2\tau$ will be the average value of the length of the solid lines. When using the complex, overlapping method, the displacements indicated with dotted lines will also be included in the calculation.

The complex methods of calculation reduce random noise but mask systematic instabilities, and from a statistical point of view calculations based on the complex, overlapping method are difficult to evaluate, since the averaged values are not statistically independent. The complex methods should therefore be used with caution. In the following sections both simple and complex, overlapping calculations have been utilized.

2.3.2. Mean-Cell Speed

The speed of a cell can be estimated simply by dividing the displacement, Δd , of the cell by the time interval, Δt , within which the displacement took place.

$$S_{\Delta t} = \frac{\Delta d}{\Delta t} \quad (\text{I})$$

The dispersion of a cell is simply an Euclidean distance between two points on a plane; measured in μm . For example the dispersion of a single cell after a given time of observation is calculated as

$$d_{t_{obs}} = \sqrt{(x(t_{obs}) - x(t_0))^2 + (y(t_{obs}) - y(t_0))^2} \quad (\text{II})$$

where $x(\cdot)$ and $y(\cdot)$ are the x - and y -coordinates of the cell, respectively.

The average speed of a sample of a population of cells calculated for a given time of observation (i.e., according to the simple method, in which the displacements of the individual cells are measured from the positions of the cells at the initiation of the recording to the positions at a given t_{obs}) can therefore be calculated using the following equation,

$$S_{t_{obs}} = \frac{1}{N} \cdot \sum_{k=1}^N \frac{\sqrt{(x_k(t_{obs}) - x_k(t_0))^2 + (y_k(t_{obs}) - y_k(t_0))^2}}{t_{obs}} \quad (\text{III})$$

where k denotes a given cell, and N is the size of investigated sample of a population of cells. Since the speed is an average value for a sample of a population of cells it is most correctly denoted, e.g., $\langle S_{obs} \rangle$ or $\langle S_{t_i} \rangle$. However, for convenience the simpler notations S_{obs} and S_{t_i} are being used in the following. Thus, e.g., for $t_{obs} = 15$ min the speed is denoted S_{15} .

Since cells do not move with a constant velocity, but tend to cycle between periods of high and low velocity, it is advisable to estimate the average speed of the individual cells by calculating the mean displacement of each cell for several time intervals with different starting points. This can be done using either the complex, non-overlapping method (equation IV), or the complex, overlapping method (equation V).

$$S_{t_i} = \frac{1}{N} \cdot \frac{1}{\left[\frac{t_{tot}}{t_i} \right]} \sum_{k=1}^N \sum_{t=t_i \text{ by } t_i}^{t \leq t_{tot}} \frac{\sqrt{(x_k(t) - x_k(t-t_i))^2 + (y_k(t) - y_k(t-t_i))^2}}{t_i} \quad (\text{IV})$$

where $[\cdot]$ denotes the floor function i.e., in this case the highest possible integer lower than or equal to t_{tot}/t_i .

$$S_{t_i} = \frac{1}{N} \cdot \frac{1}{t_{tot}/\tau - t_i/\tau + 1} \sum_{k=1}^N \sum_{t=t_i \text{ by } \tau}^{t \leq t_{tot}} \frac{\sqrt{(x_k(t) - x_k(t-t_i))^2 + (y_k(t) - y_k(t-t_i))^2}}{t_i} \quad (\text{V})$$

For a given time interval, equation V thus gives the mean-speed of a sample of a population of cells, for which the average speed of the individual cells has been calculated using the method of complex, overlapping intervals. In the following, cell speed calculated according to equation V is referred to as “mean-cell speed”.

2.3.3. Parameters Derived from Persistent Random Walk Models

The root-mean-square speed, S , and the persistence time in direction, P , are estimated after plotting the mean-squared displacement $\langle d^2 \rangle$ against time by subsequent curve fitting to the equation

$$\langle d^2 \rangle = 2S^2 P (t - P(1 - e^{(-t/P)})) \tag{VI}$$

The curve fit simultaneously permits an estimate of the rate of diffusion, $R = S^2P$ (I2).

Likewise, the two components of an Langevin equation, α and β , are estimated by curve fitting to the equation:

$$\langle d^2 \rangle = 2 \frac{\alpha}{\beta^3} (t\beta - 1 + e^{(-t\beta)}) \tag{VII}$$

α represents the magnitude of random fluctuations (i.e., the variance of the “white noise” contributing to the cell displacement), and β is the velocity decay rate (i.e., the magnitude of the resistance to the cellular velocity) (14-16).

Alternatively, S and P can be estimated by linear regression according to the equation,

$$\frac{1}{\sqrt{\langle d^2 \rangle}} = \frac{1}{S} \left(\frac{1}{t} + \frac{1}{6P} \right) \tag{VIII}$$

which is an approximation of equation VI modified to provide a linear relationship between time and dispersion. By plotting $1/\sqrt{\langle d^2 \rangle}$ against $1/t$ the data should produce a straight line with the slope $1/S$ and an intercept with the x -axis $-1/(6P)$ (I2).

2.3.4. Additional Calculations

The mean-path-length, $\langle L \rangle$, for a sample of a population of cells at a given time of observation, t_{obs} , is calculated as:

$$\langle L \rangle = \frac{1}{N} \sum_{k=1}^N \sum_{t=\tau \text{ by } \tau}^{t_{obs}} \sqrt{(x_k(t) - x_k(t - \tau))^2 + (y_k(t) - y_k(t - \tau))^2} \tag{IX}$$

The chemotactic index, CI , is calculated as the simple relationship

$$CI = \langle d^2 \rangle / \langle L \rangle \tag{X}$$

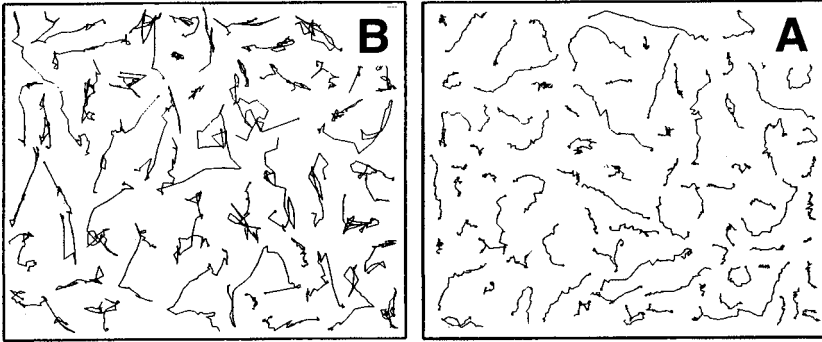


Fig. 2. Tracks of BT4Cn-cells (A) and L929-cells (B) were generated from recordings performed for 10 h with a time interval between observations, τ , of 15 min.

which for any value of t_{obs} , using the simple method of calculation, can be determined from estimates of $\langle d \rangle$ and $\langle L \rangle$ (see equations II and IX, respectively).

3. Methods (see Notes 6 and 7)

From data files containing information of the positions of individual cells at various time-points it is possible to create tracks describing the motile behavior of the individual cells (Fig. 2A, B). The visual representations of cell tracks reflect the basic information utilized for subsequent quantitative studies of the motile behavior of the cells, and they give a simple impression of the behavior of the cell lines under investigation. From Fig. 2 it is apparent that one of the two shown cell lines, BT4Cn, (Fig. 2A) changes direction relatively often, whereas the other cell line, L929, (Fig. 2B) in general moves in approximately the same direction for longer periods of time.

3.1. Motility Parameters Derived from the Persistent Random Walk Model

According to the persistent random walk model the motile behavior of cells may be described by their rate of diffusion, R , which can be dissected into the two parameters: persistence time (in direction), P , and root-mean-square speed, S , the relationship being $R = 2S^2P$ (12). By plotting the mean-squared displacement, $\langle d^2 \rangle$, against the time, t , one obtains a curve which after some time ($t \gg P$) approximates a straight line. S , P and R are best estimated by performing nonlinear curve fits of the plotted data. However, approximate values of the parameters may also be estimated directly from the plot, since R corresponds to the slope of the linear part of the curve and P corresponds to the intercept of this (extrapolated) straight line at the x -axis (12,25) (Fig. 3).

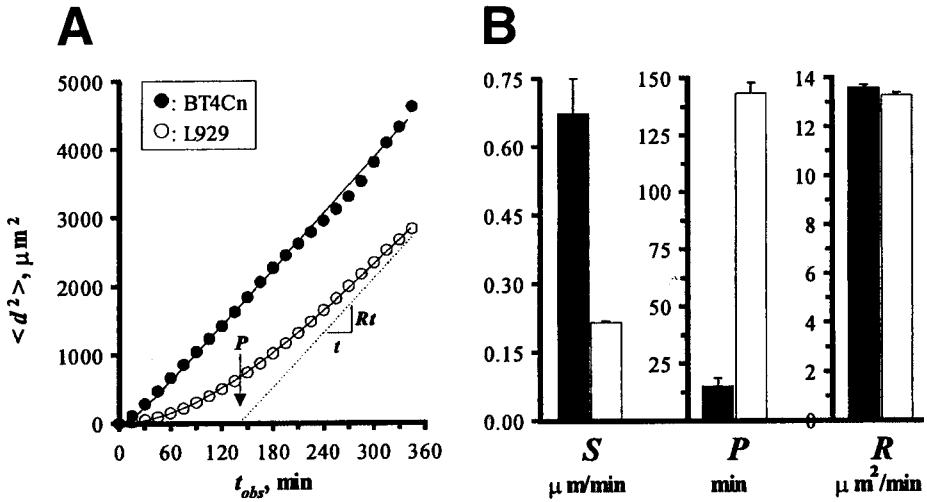


Fig. 3. Estimates of S , P and R on the basis of recordings of BT4Cn and L929-cells. The number of cells constituting the individual measurements was 50 and 71 for BT4Cn and L929, respectively. (A) Plots of the mean-squared displacement, $\langle d^2 \rangle$ of the cells vs the time of observation (calculated according to the “simple” procedure). Lines indicate curve fits according to equation VI (Subheading 2.3.3.). In addition it is indicated how the persistence time in direction, P , and the rate of diffusion, R , may be estimated from visual inspection of the plots. (B) Bar graphs showing the estimated values of S , P , and R based on the curve fittings presented in a. Error bars indicate SEM calculated on the basis of goodness of fit for the curve fittings with 24 data points $-2 = 22$ degrees of freedom (df). The data utilized for the estimates correspond to the data presented in Fig. 2.

Figure 3A presents nonlinear curve fits for data derived from two recordings of L929- and BT4Cn-cells, respectively. As estimated from curve fits, the L929-cells have a long persistence time in direction (143 min) and a root-mean-square speed of $0.22 \mu\text{m}/\text{min}$ whereas the BT4Cn-cells have a much shorter value of P (15 min), but a higher value of S ($0.67 \mu\text{m}/\text{min}$). Noticeably, the diffusion rates of the two cell lines are not significantly different from each other, both being approximately $13.5 \mu\text{m}^2/\text{min}$ (Fig. 3B).

An alternative to the determination of S and P is to estimate the parameters α and β . α represents the variation in the purely random behavior (the “white noise”) contributing to cellular displacement. β is the decay rate constant of the velocity of the cells (i.e., a low value of β indicates that there is little resistance to cellular motion, and thus the cells will move at the same speed for long periods of time. A high value of β , on the other hand, indicates a strong resistance to the cellular motion, and consequently the cells will move in short

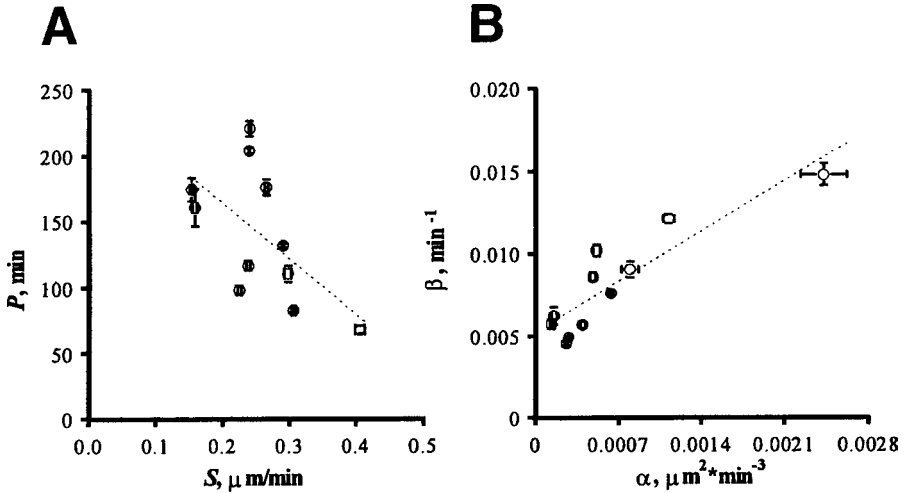


Fig. 4. Day-to-day variation in cell motility of L929-cells. 11 independent recordings each of 10 h were performed on different days. The values of P , S were estimated as in Fig. 3, and α , and β were determined using equation VII (Subheading 2.3.3.). (A) P plotted against S . The parameters exhibit a statistically significant inverse linear correlation ($r = 0.607371$, $df = 9$, $p < 0.05$, two-sided). (B) β plotted against α . The parameters exhibit a statistically significant linear correlation ($r = 0.889878$, $df = 9$, $p < 0.001$).

cycles of rapidly decreasing velocity. Although based on different mathematical assumptions the two pairs of parameters are interrelated. Thus, $S = \sqrt{\alpha/\beta}$ and $P = 1/\beta$. It should be noticed that this mathematical relationship predicts that a factor affecting persistence time should also affect speed, whereas the opposite needs not be the case.

The day-to-day variation of measurements of the same cell line is pronounced. Figure 4 demonstrates the variations in S , P , α and β measured on 11 different days at identical condition for L929-cells. The values for S range from 0.15 to 0.41 $\mu\text{m}/\text{min}$ and P range from 68 to 220 min. Calculations of the mean-cell speed, S_{15} , and the chemotactic index, CI , for $t_{obs} = 210$ min produce values ranging from 0.19 to 0.47 $\mu\text{m}/\text{min}$ (mean-cell speed) and from 0.40 to 0.70 (chemotactic index). This corresponds to a coefficient of variation of 28%, 36%, 27% and 17% for S , P , S_{15} and CI , respectively, emphasizing the importance of internal controls for all quantitative determinations of cell motility. The fact that the root-mean-square speed and the mean-cell speed have approximately the same coefficient of variation demonstrates that the two ways of calculating speed is equally sensitive to day-to-day variations.

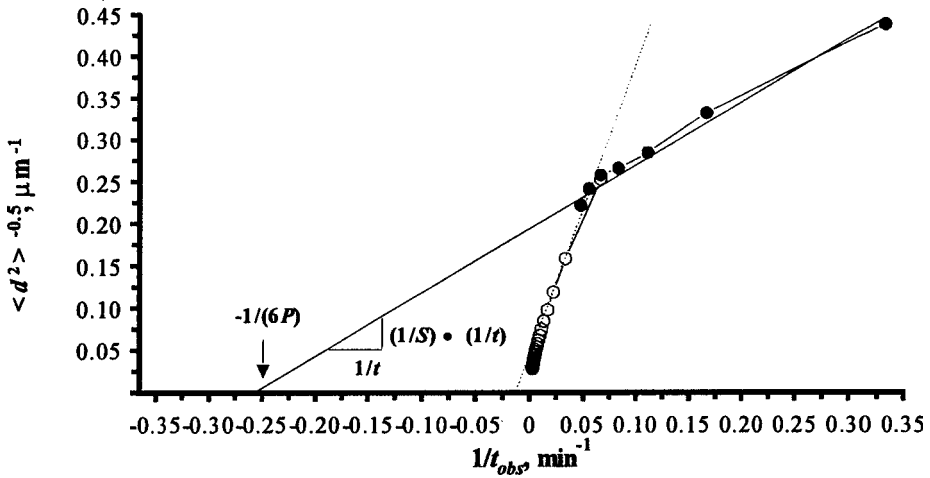


Fig. 5. Alternative procedure for estimation of P and S . The figure shows a plot of $1/\sqrt{\langle d^2 \rangle}$ against $1/t$ for a recording of 1321N1 cells. Open circles indicate data derived from a 10 h long recording, $t_{\text{tot}} = 10$ hours, performed with a time interval between observations, τ , of 15 min, solid circles indicate data derived from a simultaneously performed 21 min long recording performed with $\tau = 3$ min. The solid and dotted lines indicate regression lines obtained from the short ($t_{\text{tot}} = 21$ min) and long ($t_{\text{tot}} = 10$ h) recording, respectively.

It is seen from **Fig. 4** that for this cell line α and β exhibit a direct linear correlation, whereas an inverse linear relationship exists for S and P . A similar inverse relationship between speed and directional persistence has previously been observed between different cell lines (3).

Both the comparison of L929 and BT4Cn-cells and the day-to-day variation between measurements of the L929-cells serve to highlight the importance of using more than one parameter when describing the motile behavior of different populations of cells. For example, measurement of the diffusion rates of L929 and BT4Cn-cells (e.g., by measuring the area covered by a group of cells scattering from a single spot) would not have revealed any differences in the motile behavior of the two cell lines. Likewise, estimates of cellular diffusion may mask day-to-day variations in S and P , since the two parameters are likely to be inversely correlated.

In order to obtain reliable estimates of S , P , and R using non-linear curve fits as described above it is necessary for the curve to have reached its approximate linear part (see **Fig. 3**), and this requires a total recording time that is at least three to five times longer than the persistence time of the cells. This is a serious disadvantage of the procedure, since such long recording times require a high biological and physical stability of the system.

In 1983 Dunn (12) proposed an alternative procedure for estimating S and P , which by transformation of the original equation allows the parameters to be estimated on the basis of linear regression rather than a nonlinear curve fit. Thus, when plotting $1/\sqrt{\langle d^2 \rangle}$ against $1/t$, one should ideally obtain a straight line with a slope corresponding to $1/S$ and an intercept with the horizontal axis of $-1/(6P)$ (see **Subheading 2.3.3.** and **Fig. 5**).

Figure 5 shows data derived from a recording of astrocytoma cells. During the same recording time images of cells were obtained for $t = 15$ min, $t_{tot} = 600$ min and $t = 3$ min, $t_{tot} = 21$ min, respectively. It is seen that a plot of $1/\sqrt{\langle d^2 \rangle}$ against $1/t$ including all data points from the recording produces a non-linear curve. However, data obtained for $\tau = 3$ min ($t_{tot} = 21$ min) or $\tau = 15$ min ($t_{tot} = 600$ min) (**Fig. 5**, solid and open points, respectively) both approximate straight lines when observed individually, although they exhibit very different slopes and axis intercepts. Using the short τ and t_{tot} , P and S were estimated to be 0.50 min and 1.65 $\mu\text{m}/\text{min}$, respectively, whereas values of 20.92 min and 0.26 $\mu\text{m}/\text{min}$ were found using the long τ and t_{tot} . The estimated values of S and P determined by this procedure are therefore clearly dependent of τ and t_{tot} . Furthermore, the procedure tends to underestimate the persistence time significantly when compared to estimates based on non-linear curve fits using equation VI, which in the present case gives values for S and P of 0.15 $\mu\text{m}/\text{min}$ and 97 min (see below and **Fig. 8**).

In contrast to the non-linear curve fits, the linear regression procedure should be performed on data-points derived from observation times not longer than approximately five times the persistence time of the cells, since the accuracy of the linear approximation decreases as the observation time increases (12). The choice of procedure can therefore be determined on the basis of the length of time with which actual recordings are performed. Thus, when non-linear curve fitting is not advisable (due to a too short recording time) the linear regression procedure can be regarded as an acceptable alternative, and indeed it has been employed in several studies (19–21).

3.2. Mean-Cell Speed

Theoretically the simplest way of estimating speed is to divide the displacement of an object with the time it takes for the displacement to occur. As explained in **Subheading 2.3.2.** determination of the mean-cell speed, S_{t_i} , is based on this simple approach, although the actual formula (V) from which the S_{t_i} is calculated may appear rather complex. **Figure 6** presents two series of S_{t_i} -determinations derived from the recordings presented in **Figs. 2** and **3**. From **Fig. 6A** it is seen that S_{t_i} of a sample of a population of cells is highly dependent on the size of the employed time interval of interest, t_i . Thus, S_{t_i} decreases as t_i increases, as it would be expected for particles exhibiting a ran-

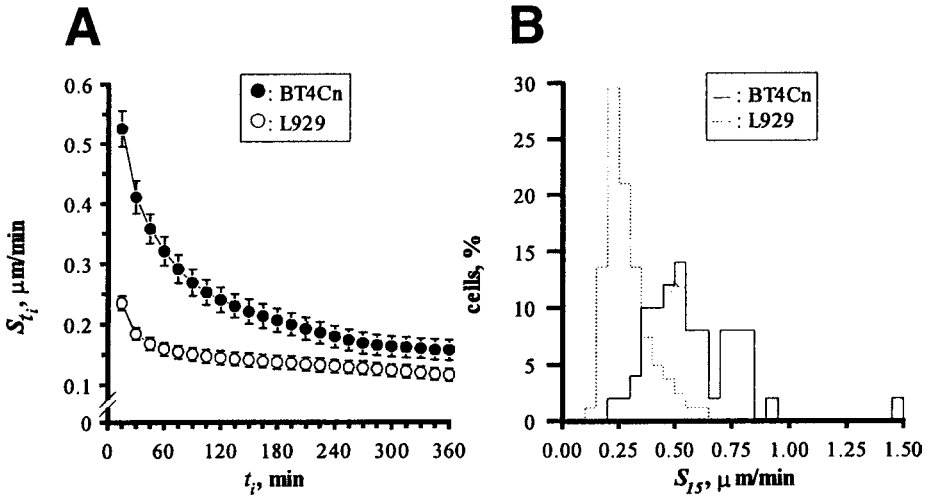


Fig. 6. Mean-cell speed of L929 and BT4Cn-cells (same recordings as presented in Figs. 2 and 3). (A) Mean-cell speed calculated at varying times of interest. (B) Distribution of the speed (calculated with a time of interest, t_i , of 15 min) of the individual cells from the recordings presented in (A).

dom walk (10). It can also be seen that BT4Cn has a higher speed than L929-cells for all values of t_i . Furthermore, the speed of BT4Cn-cells decreases more rapidly at increasing values of t_i than that of the L-cells, and thus the absolute difference in speed between the two cell lines is greatest at low values of t_i .

The time interval-dependent behavior of the S_{t_i} is in part related to the directional persistence of the cells. Thus, S_{t_i} of a cell line with a short persistence time in direction, such as BT4Cn, will decrease more rapidly at increasing values of t_i than a cell line with a long persistence time, such as the L929-cells. In addition, S_{t_i} is affected in a time interval-dependent manner by “noise”, which may be cell-morphology-dependent (e.g., due to an increasing effect of cell shape changes on the accuracy by which cell displacement is measured at shorter time intervals), and also mechanical inaccuracies, e.g., of the movable microscope stage will affect S_{t_i} in a time interval-dependent manner. The value of t_i employed for calculations of S_{t_i} of a given cell-line must therefore be relatively short in order for S_{t_i} to be largely unaffected by the directional persistence of the cells, although long enough to obtain a reasonable signal-to-noise-ratio.

Figure 6B presents the distributions of the cell speed (calculated for $t_i = 15$ min) for the individual cells in the investigated samples of L929 and BT4Cn-cells (the mean value of the distributions correspond to the first point of the graphs presented in Fig. 6A). It is apparent from the figure that cell speed is not

normally distributed. Therefore, the mode or the median rather than the mean may be preferred for the description of the speed of a cell population. In addition, the histograms give information about the uniformity of the cell sample. Thus, it is seen from both **Fig. 6A** and **6B** that the speed of BT4Cn-cells on average is higher than for L929-cells, but in addition **Fig. 6B** demonstrates that BT4Cn-cells exhibit larger intrapopulation variability than do the L929-cells.

In conclusion, when compared to the root-mean-square speed, S , the mean-cell speed suffers from being time interval dependent. On the other hand it can be estimated for individual cells, and it can be employed for studies in which the experimental conditions are modulated during the recording (*see also Sub-heading 3.5.*). Furthermore, simple calculations of cell speed can be used for even more detailed investigations by extending the study to include evaluations of the motile behavior of individual cells over time. For example, individual cells from several cell types have been demonstrated to cycle between periods of high and low speed (*see 18,22*).

3.3. Chemotactic Index

The chemotactic index, CI , for a sample of a population of cells is in its most simple form defined as $CI = \langle d \rangle / \langle L \rangle$ and therefore $0 < CI \leq 1$ (3). Thus, cells moving in perfectly straight lines will give a CI of one, whereas cells with a lower directional persistence will have lower CI -values. The index is traditionally utilized to describe the effect of a chemoattractant on the directional persistence of cells. However, in the absence of any chemotactic gradients the index can be used as an estimate of the directional persistence of randomly moving cells.

Figure 7A presents CI as a function of t_{obs} employed for the recordings of L929 and BT4Cn cells presented earlier (**Figs. 2, 3, and 6**). The value of CI is clearly time interval-dependent, demonstrating a decrease for increasing values of t_{obs} . When comparing the two cell lines it is seen, that all the values for CI are lower for BT4Cn-cells than for L929-cells (except for the value of the first point, which by definition must be 1), and the decrease at increasing time intervals is also more pronounced for BT4Cn-cells than for L929-cells. This indicates that BT4Cn has a lower directional persistence than L929. Although the chemotactic index reflects directional persistence, it cannot be used as an estimate of the actual persistence time, P , of the cells. However, in contrast to estimates of P the index has the advantage that it can be calculated for individual cells. Thus, it is possible to obtain estimates of the distribution of the directional persistence in a sample of a population of cells simply by calculating CI for the individual cells. **Figure 7B** presents the distributions of CI (calculated for $t_{obs} = 210$ min) for the individual cells in the

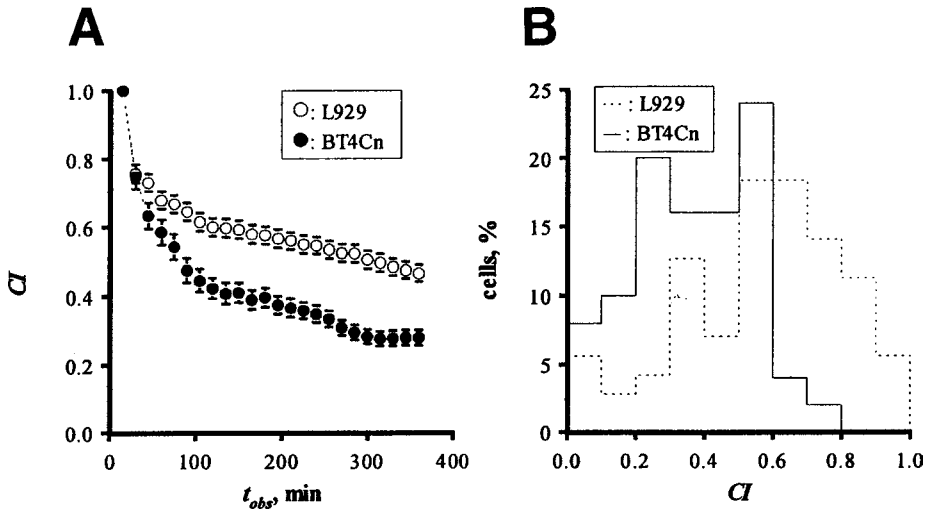


Fig. 7. Chemotactic index, $CI = \langle d \rangle / \langle L \rangle$ for L929 and BT4Cn-cells (same recordings as presented in Figs. 2, 3, and 6). (A) CI calculated at varying times of observation, t_{obs} . (B) Distribution of CI (calculated for $t_{obs} = 210$ min) of the individual cells from the recordings presented in a.

investigated samples of L929-cells and BT4Cn-cells. In the chosen example it is seen that the chemotactic indices of the individual cells from both cell lines range from near zero to near 1, and that the fraction of cells with a high chemotactic index is clearly larger for L929-cells than for BT4Cn-cells.

3.4. Correlation Analysis of Parameters

In order to evaluate and compare the various procedures and parameters described in the preceding sections we performed recordings of 7 different cell lines; 1321N1, BT4Cn, CHO, COS7, HeLa, L929 and Swiss 3T3. The individual recordings were performed with both $\tau = 15$ min and $\tau = 3$ min, simultaneously (for $t_{tot} = 5-10$ h and 21 min, respectively). In Fig. 8 the various parameters estimated and calculated from the recordings have been correlated. The correlations include the following parameters:

3.4.1. Cellular Velocity

1. Root-mean-square speed estimated from non-linear curve fits (eq. VI) of long recordings ($t_{tot} > 5$ h, $t = 15$ min), S , (see Fig. 3).
2. Root-mean-square speed estimated from linear regression (eq. VIII) of data from intermediate time intervals ($t_{tot} = 2$ h, $\tau = 15$ min), $S_{120/15}$, (see Fig. 5).
3. Root-mean-square speed estimated from linear regression (eq. VIII) of data from short time intervals ($t_{tot} = 21$ min, $\tau = 3$ min), $S_{21/3}$, (see Fig. 5).

4. Mean-cell speed (eq. V) ($t_i = 15$ min), S_{15} , (see **Fig. 6**).
5. Mean-cell speed (eq. V) ($t_i = 3$ min), S_3 , (see **Fig. 6**).

3.4.2. Cellular Persistence in Direction

1. Persistence time in direction estimated from non-linear curve fits (eq. VI) of long recordings ($t_{tot} > 5$ h, $\tau = 15$ min), P , (see **Fig. 3**).
2. Persistence time in direction estimated from linear regression (eq. VIII) of data from intermediate time intervals ($t_{tot} = 2$ h, $\tau = 15$ min), $P_{120/15}$, (see **Fig. 5**).
3. Persistence time in direction estimated from linear regression (eq. VIII) of data from short time intervals ($t_{tot} = 21$ min, $\tau = 3$ min), $P_{21/3}$, (see **Fig. 5**).
4. Chemotactic Index (eq. X) for $t_{obs} = 210$ min, $\tau = 15$ min, CI , (see **Fig. 7**).

From **Fig. 8** it is seen that root-mean-square speed estimated from nonlinear curve fitting, S , and from linear regression of data points from intermediate t_i -values, $S_{120/15}$, and mean-cell speed calculated for $t_i = 15$ min, S_{15} , all correlate in a highly significant, linear manner ($p < 0.001$). The remaining two speed estimates seem to be relatively poorly correlated to the others, indicating that the signal-to-noise-ratio at these short time intervals is too low. The same conclusions can be drawn from the estimated persistence times, where persistence time in direction estimated from nonlinear curve fitting, P , correlates well with $P_{120/15}$ ($p < 0.01$), but not with $P_{21/3}$. Interestingly, CI exhibits a statistically significant correlation to P , $P_{120/15}$ and $P_{21/3}$ ($p < 0.05$, 0.001 and 0.05, respectively).

The multi-correlation analysis demonstrates that in situations where parameters independent of τ and t_i (such as S and P) cannot be obtained (e.g., because the experimental conditions do not allow t_{tot} to be sufficiently long for reliable non-linear curve fits), estimates of the mean-cell speed, S_{t_i} (as in **Fig. 6**), the chemotactic index, CI (as in **Fig. 5**), and S and P based on linear regression analysis (as in **Fig. 5**) can serve as acceptable alternatives. As regards determinations of S_{t_i} and S estimated by linear regression, the results show that the use of a relatively long t_i , *in casu* 15 min rather than shorter intervals (3 min) yields results correlating with S determined by nonlinear curve fitting, and it is therefore advisable not to use too low t_i -values. Concerning determinations of directional persistence our data show that CI can be recommended as a simple and robust parameter.

3.5. Test of Data Reliability

Stable physical and biological conditions are obviously required for reliable quantitative estimates of cellular motility. Accurate estimates of S , P and R demand total recording times of many hours (5–10 or more). Clearly, conditions cannot be kept stable during these long recording times, since cells divide, secrete growth factors and extracellular matrix components and so on. The stability of some parameters (e.g., pH and temperature) can be monitored dur-

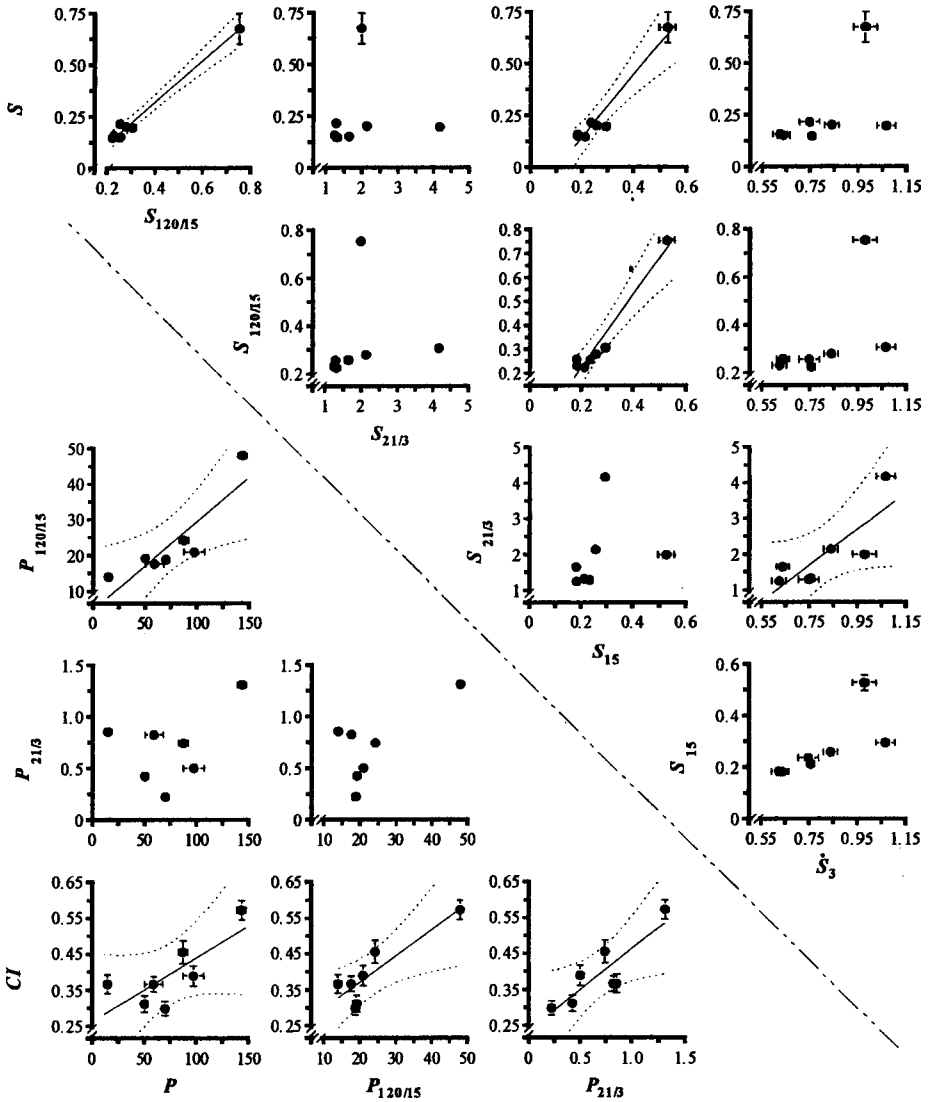


Fig. 8. Correlations between various estimates of cellular velocity and directional persistence (see text for details). Plots presenting parameters that demonstrate a statistically significant linear correlation ($p < 0.05$, two-sided) include regression lines (solid lines) with 95% confidence limits indicated (dotted lines).

ing recording, but whether significant changes in the motility of cells have taken place during a recording can only be detected by evaluating the actual motility data.

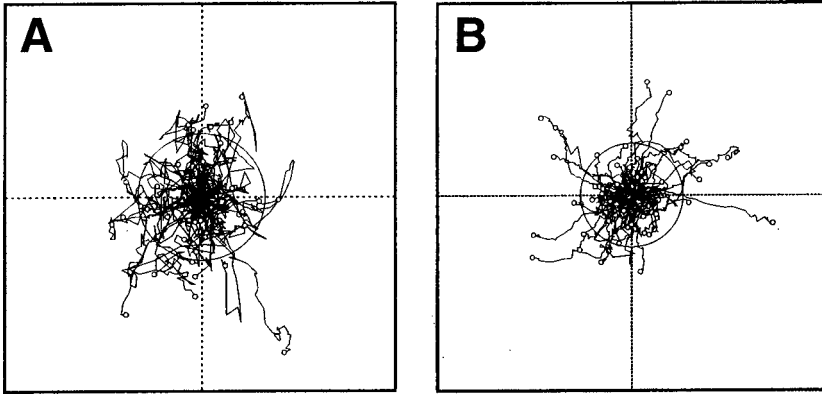


Fig. 9. Windrose plots (A, B) of BT4Cn-cells (A) and L929-cells (B) recorded for 10 h (same recordings as presented in Figs. 2, 3, 6, and 7). The circles in A and B indicate $\sqrt{\langle d^2 \rangle}$ of the traced cells. Performing a Rayleigh test (23) it was found that none of the two recordings exhibits any statistically significant deviation from uniformity with respect to directional distribution of the cellular movements.

For recordings performed in the absence of any chemotactic gradient the motile behavior of cells should be random with respect to directionality. If anything in the experimental set up (e.g., temperature or light gradients) has caused any directional bias, this can be evaluated by the use of “windrose” plots, in which the starting points of the individual cell-tracks have been superimposed (Fig. 9A, B, compare with Fig. 2), and statistically significant deviations from circular uniformity may be assessed using a Rayleigh test (23).

Figure 10 shows plots, which can be utilized to evaluate whether the system (physically as well as biologically) was stable during recording. The figure

Fig. 10. (*opposite page*) Test of systematic instabilities during a recording. The figure present two different recordings of L929-cells performed on different days. Figure A, C, E, G show one and B, D, F, H the other recording. All data have been calculated according to the “simple” procedure (see Subheading 2.3.1). A, B: Mean-path-length, $\langle L \rangle$, vs time of observation, t_{obs} . C, D: Mean-path-length/min vs t_{obs} . Under stable conditions the plots in A and B should produce straight lines with varying slopes, whereas the plots in C and D should produce straight lines with slopes not significantly different from zero. E, F: Mean-cell speed, S_{15} , vs t_{obs} . Under stable conditions the plot should produce straight lines with slopes not significantly different from zero. G, H: Plots of the mean-squared displacement, $\langle d^2 \rangle$ vs t_{obs} . Open symbols: normal plot. Solid symbols: displacements calculated from the endpoints of the recording and back to time zero. Error bars indicate SEM calculated on the basis of cell number (85 and 72 cells for the experiments presented in A, C, E, G and B, D, F, H, respectively).

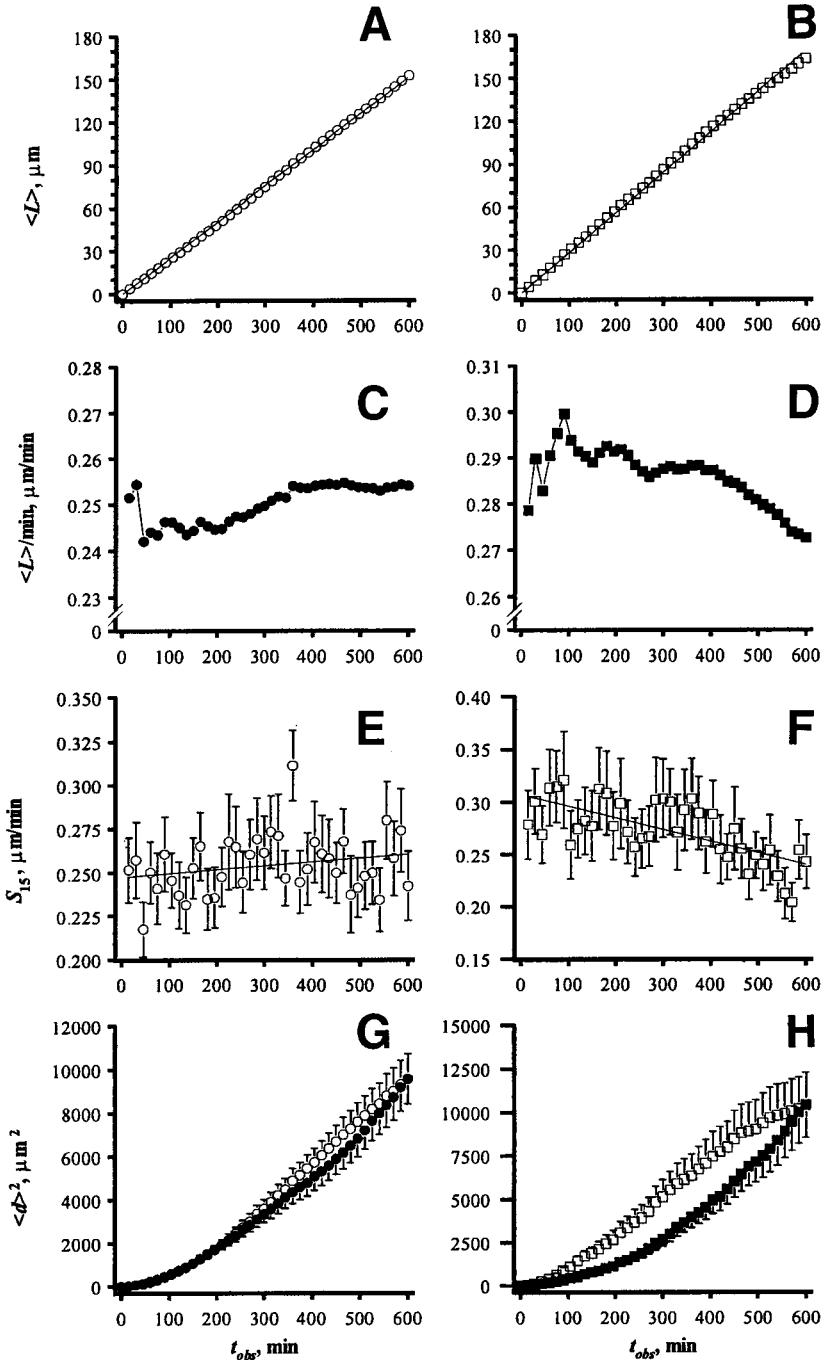


Fig. 10

presents data from two different recordings of L929-cells (**Fig. 10A, C, E, G** and **10B, D, F, H**, respectively). The plots presented in **Fig. 10A–F** can be used for the detection of any acceleration or deceleration of the cellular speed during the time of recording. Plots similar to those presented in **Fig. 10G** and **H** will in addition allow detection of alterations in P . **Figure 10A, B** presents plots of the mean-path-length, $\langle L \rangle$, against increasing values of t_{obs} . Under stable recording conditions these plots should ideally produce completely straight lines. However, since plots of $\langle L \rangle$ are based on cumulative data, evidently instabilities are difficult to detect. By dividing all values of $\langle L \rangle$ with the corresponding values of t_{obs} (the mean-path-length migrated by a sample of a population of cells during a given time of observation expressed as path-length/time) the sensitivity of the procedure increases considerably. Under stable conditions, these plots will produce straight lines with a slope not significantly different from zero (**Fig. 10C, D**). However, due to the interrelationship of the data points it is not statistically acceptable to perform a linear regression analysis on either of the plots presented in **Fig. 10A–D**.

Plots of S_t against t_{obs} (in which each data point is independent of the previous and subsequent points) are clearly more efficient at detecting instabilities. In case the system has been stable during recording, these plots should also produce straight lines with a slope not significantly different from zero, and since the points are not interrelated it is allowed to evaluate these plots statistically by simple linear regression analysis (**Fig. 10E, F**). Of the two recordings presented in the figure one (**Fig. 10E**) has been performed under apparently stable conditions, since the slope is not statistically significantly different from zero ($2.232 \cdot 10^{-5} \pm 1.490 \cdot 10^{-5}$ (mean \pm S.D.), $p > 0.05$, two-sided). As regards the other recording the slope is significantly different from zero indicating that it has been performed under unstable conditions ($-1.120 \cdot 10^{-4} \pm 1.922 \cdot 10^{-5}$, $p < 0.001$, two-sided, **Fig. 10F**).

Another sensitive method for the detection of changes in motile behavior of cells during a recording is the plotting of $\langle d^2 \rangle$ vs t_{obs} conventionally as well as “reversed” (i.e., a plot of $\langle d^2 \rangle$ using the final position of the cells as their starting point, calculating the displacement backwards in time (**Fig. 10G, H**). Any alterations in the overall motile behavior of the cells during the time of recording will prevent the two plots from being superimposed. Thus, it can be seen from **Fig. 10**, that for the recording performed under unstable conditions some of the data points calculated “normally” and “reversely” for the same time of observation have significantly different values (**Fig. 10H**), whereas this is not the case for the data points obtained from the recording performed under stable conditions (**Fig. 10G**).

An often-neglected problem in time-lapse video microscopy studies of cell motility is the number of cells necessary for obtaining representative estimates of the true motile behavior of the cell population. To elucidate the problem S_t

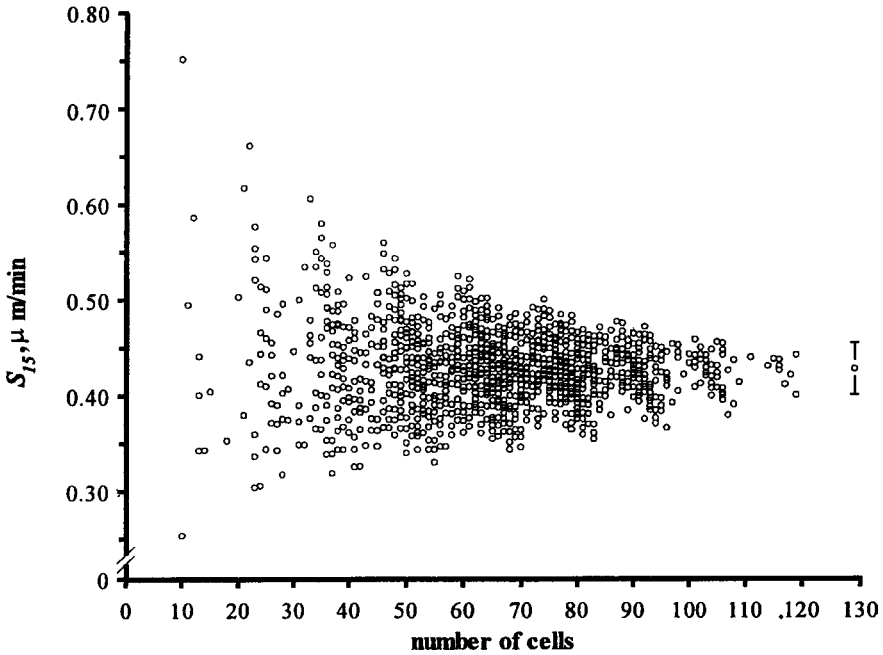


Fig. 11. Intra-assay variation of mean-cell speed. The presented data constitute a single recording ($t_{tot} = 10$ h, $\tau = 15$ min) of a total of 129 cells derived from 10 different microscopic fields (image frames). The mean-cell speed for $t_i = 15$ min is plotted against the cell number for all possible combinations $\binom{10}{k} = \frac{10!}{k!(10-k)!}$ of k fields ($k = 1$ to 10) out of the 10 fields. Error bars indicate \pm SEM for the mean-cell speed calculated for all 129 cells.

of cells from a single recording has been plotted against the cell number, N (**Fig. 11**). The recording includes a total of 129 cells derived from 10 different microscopic fields each containing from 10 to 18 cells. The figure shows the calculated values for S_{t_i} for all possible combinations of the 10 fields (*see* legend of **Fig. 11**). It is seen that the difference between the calculated values of S_{t_i} decreases as the number of cells constituting the estimates increases. S_{t_i} of the individual cells ranges from 0.09 to 1.3 $\mu\text{m}/\text{min}$ (data not shown), whereas S_{t_i} of the 10-18 cells measured in the individual frames ranges from 0.25 to 0.75 $\mu\text{m}/\text{min}$. S_{t_i} of all 129 cells was 0.427 $\mu\text{m}/\text{min}$ with an SEM of 0.027 $\mu\text{m}/\text{min}$ corresponding to 6% of the mean. This indicates that a considerable number of cells (preferably more than 100) have to be tracked to yield reliable estimates. Unfortunately, such high cell numbers are so far rarely reported in quantitative studies of individual-cell motility.

4. Notes

1. Theoretically any moving particle has a persistence time in direction (otherwise it could not move anywhere). Thus, whether a moving particle displays any persistence in direction is a question of scaling.
2. There are various mathematical alternatives to the “persistent random walk”-model (24–26) including the quantification of individual-cell motility on the basis of a Markov Chain-model (27–30).
3. The cellular outline and the position of the nucleus are not easily recognized automatically, especially not in cell types like fibroblasts. One way of improving the automatic recognition of the positions of the individual cells is to perform recordings using fluorescence microscopy after having labeled the cells with a fluorescent dye or protein. The fluorescent dye DiI has been used in several studies (31,32) but should be used with caution, since it has been shown to affect proliferation, adhesion and migration of several different cell lines (33). Alternatively cells may be transfected with green fluorescent protein, GFP (34). GFP can be introduced into cells in an unmodified form, which will produce a uniform staining of the cytoplasm, or after addition of a nuclear localization signal or a farnesylation signal, which will produce cells with fluorescent nuclei or fluorescent membranes, respectively. Cells transiently transfected with GFP retain fluorescent properties for several days, and can thus with advantage be used for long-term recordings.
4. The use of a HEPES-containing medium is only necessary in the absence of a CO₂-supplied incubator surrounding the microscope. An alternative to a HEPES-containing medium is a commercially available “CO₂-independent medium” (Gibco-BRL, USA). However, we have found that the motile behavior of cells differs substantially in these two media.
5. In general, the *x-y*-positions of individual cells are defined either as the position of their nuclei, or their geometrical centers (centroids). In general, the latter procedure causes more irregular tracks, as the shape-changes of cells within a time interval of observation often exceed their displacement (35).
6. The accuracy of the estimated motility parameters derived from non-linear curve fittings will only depend on the number of investigated cells if the determinations statistically are based on e.g., the so-called “jack-knife”-procedure (12). Conventional nonlinear curve fits will provide estimates based on the goodness-of-fit of the data to the curve, where the degrees of freedom are determined from the number of data-points and not the number of cells.
7. The chemotactic index, *CI*, is also termed the “locomotive index” (36,37), the “chemotactic ratio” (38), “degree of chemotactic motion”, *C*, (30) and the “chemotropism index”, *CI* (30,39), and the chemotactic index is almost identical to the chemotropism-parameter used by Dixon and McCutcheon (8). However, the term “chemotactic index” is also being used for a distinctly different phenomenon (the distance traveled by a population of cells towards a well containing a chemoattractant divided by the distance traveled towards a well without any chemoattractant, [30]).

Appendix

α	“magnitude of random fluctuations” ($\mu\text{m}^2/\text{min}^{-3}$)
β	“velocity decay rate” (min^{-1})
t	time interval between observations (min)
CI	chemotactic index
d	displacement (μm)
L	path-length (μm)
n	dimensions
N	total number of cells measured
P	persistence time in direction (min)
R	rate of diffusion ($\mu\text{m}^2/\text{min}$)
S	root-mean-square speed ($\mu\text{m}/\text{min}$)
S_{t_i}	mean-cell speed ($\mu\text{m}/\text{min}$)
t_i	time interval of interest (min)
t_{obs}	time of observation (min)
t_{tot}	total time of recording (min)
$x_k(\cdot)$	x -coordinates of cell k at a given time
$y_k(\cdot)$	y -coordinates of cell k at a given time

References

1. Hendrix, M. J. C., Seftor, E. A., Chu, Y.-W., Trevor, K. T., and Seftor, R. E. B. (1996) Role of intermediate filaments in migration, invasion and metastasis. *Cancer Metastasis Rev.* **15**, 507–525.
2. Waterman-Storer, C. M. and Salmod, E. D. (1999) Positive feedback interactions between microtubules and actin dynamics during cell motility. *Curr. Opin. Cell Biol.* **11**, 61–67.
3. Lauffenburger, D. A. and Linderman, J. J. (1993) Chapter 6. Receptor-mediated cell behavioral responses, in *Receptors. Models of binding, trafficking, and signaling*. Oxford University Press, New York, Oxford. pp. 236–344.
4. Boyden, S. (1962) The chemotactic effect of mixtures of antibody and antigen on polymorphonuclear leucocytes. *J. Exp. Med.* **115**, 453–466.
5. Tran, P. O. T., Hinman, L. E., Unger, G. M., and Sammak, P. J. (1999) A would-induced $[\text{Ca}^{2+}]_i$ increase and its transcriptional activation of immediate early genes is important in the regulation of motility. *Exp. Cell Res.* **246**, 319–326.
6. McCutcheon, M. (1924) Studies on the locomotion of leukocytes. III. The rate of locomotion of human symphocytes in vitro. *Amer. J. Physiol.* **69**, 279–282.
7. Lewis, W. H. (1934) On the locomotion of the polymorphonuclear neutrophiles of the rat in autoplasm cultures. *Bull. Johns Hopkins Hosp.* **55**, 273–279.
8. Dixon, H. M. and McCutcheon, M. (1936) Chemotropism of leucocytes in relation to their rate of locomotion. *Proc. Soc. Exp. Biol. Med.* **34**, 173–176.
9. Abercrombie, M. and Heaysman, J. E. M. (1953) Observations on the social behaviour of cells in tissue culture. 1. Speed of movement of chick heart fibroblasts in relation to their mutual contacts. *Exp. Cell Res.* **5**, 111–131.

10. Berg, H. C. (1983) *Random walks in biology*. Princeton University Press, Princeton, New Jersey.
11. Gail, M. H. and Boone, C. W. (1970) The locomotion of mouse fibroblasts in tissue culture. *Biophys. J.* **10**, 980–993.
12. Dunn, G. A. (1983) Characterising a kinesis response: Time averaged measures of cell speed and directional persistence. *Agents Actions Suppl.* **12**, 14–33.
13. Doob, J. L. (1942) The Brownian movement and stochastic equations. *Ann Math.* **43**, 351–369.
14. Dunn, G. A. and Brown, A. F. (1987) A unified approach to analysing cell motility. *J. Cell Sci. Suppl.* **8**, 81–102.
15. Stokes, C. L. and Lauffenburger, D. A. (1991) Analysis of the roles of microvessel endothelial cell random motility and chemotaxis in angiogenesis. *J. Theor. Biol.* **152**, 377–403.
16. Stokes, C. L., Lauffenburger, D. A., and Williams, S. K. (1991) Migration of individual microvessel endothelial cells: stochastic model and parameter measurement. *J. Cell Sci.* **99**, 419–430.
17. Soll, D. R. (1995) The use of computers in understanding how animal cells crawl. *I. Rev. Cytology* **163**, 43–104.
18. Soll, D. R. and Voss, E. (1998) Chapter 2. Two- and three-dimensional computer systems for analyzing how animal cells crawl, in *Motion analysis of living cells*. (Soll, D. R. and Wessels, D., eds.). Wiley-Liss, New York. pp. 25–52.
19. Glasgow, J. E. and Daniele, R. P. (1994) Role of microtubules in random cell migration: stabilization of cell polarity. *Cell Motil. Cytoskeleton.* **27**, 88–96.
20. Glasgow, J. E., Farrell, B. E., Fisher, E. S., Lauffenburger, D. A., and Daniele, R. P. (1989) The motile response of alveolar macrophages. An experimental study using single-cell and cell populations approaches. *Am Rev. Respir. Dis.* **139**, 320–329.
21. Tranquillo, R. T., Fisher, E. S., Farrell, B. E., and Lauffenburger, D. A. (1988) A stochastic model for chemosensory cell movement: application to neutrophil and macrophage persistence and orientation. *Math. Biosci.* **90**, 287–303.
22. Shenderov, A. D. and Sheetz, M. P. (1997) Inversely correlated cycles in speed and turning in an ameba: an oscillatory model of cell locomotion. *Biophys. J.* **72**, 2382–2389.
23. Fisher, N. I. (1995) Chapter 4. Analysis of a single sample of data, in *Statistical analysis of circular data*. Cambridge University Press. pp. 59–103.
24. Germain, F., Doise, A., Ronot, X., and Tracqui, P. (1999) Characterization of cell deformation and migration using a parametric estimation of image motion. *IEEE Transactions Biomed. Eng.* **46**, 584–600.
25. Otmer, G. H., Dunbar, S. R., and Alt, W. (1988) Models of dispersal in biological systems. *J. Math. Biol.* **26**, 263–298.
26. Tourtellot, M. K., Collins, R. D., and Bell, W.J. (1991) The problem of movelength and turn definition in analysis of orientation data. *J. Ther. Biol.* **150**, 287–297.
27. Boyarsky, A. (1975) A Markov chain model for human granulocyte movement. *J. Math. Biol.* **2**, 69–78.

28. Boyarsky, A. and Noble, P. B. (1977) A Markov chain characterization of human neutrophil locomotion under neutral and chemotactic conditions. *Can. J. Physiol. Pharmacol.* **55**, 1–6.
29. Lee, Y., Markenscoff, P. A., McIntire, L. V., and Zygorakis, K. (1995) Characterization of endothelial cell locomotion using a Markov chain model. *Biochem. Cell Biol.* **73**, 461–472.
30. Noble, P. B. and Levine, M. D. (1986) *Computer-assisted analysis of cell locomotion and chemotaxis*. CRC Press, Inc., Boca Raton, Florida.
31. Chon, J. H., Vizena, D. A., Rock, B. M., and Chaikof, E. L. (1997) Characterization of single-cell migration using a computer-aided fluorescence time-lapse videomicroscopy system. *Anal. Biochem.* **252**, 246–254.
32. Chon, J. H., Netzels, R., Rock, B. M., and Chaikof, E. L. (1998) a4b1 and a5b1 control cell migration on fibronectin by differentially regulating cell speed and motile cell phenotype. *Ann. Biomed. Eng.* **26**, 1091–1101.
33. Goldbrunner, R. H., Bouterfa, H., Vince, G. H., Bernstein, J. J., Roosen, K., and Tonn, J.-C. (1997) Transfection and dye premarking of human and rat glioma cell lines affects adhesion, migration and proliferation. *Anticancer Res.* **17**, 4467–4472.
34. Farina, K. L., Wyckoff, J. B., Rivera, J., Lee, H., Segall, J. E., Condeelis, J. S., and Jones, J. G. (1998) Cell motility of tumor cells visualized in living intact primary tumors using green fluorescent protein. *Cancer Res.* **58**, 2528–2532.
35. Giuliano, K. A. (1996) Dissecting the individuality of cancer cells: The morphological and molecular dynamics of single human glioma cells. *Cell Motil. Cytoskeleton* **35**, 237–253.
36. Rydgren, L., Norberg, B., Hakansson, C. H., and v Mecklenburg Soderstrom, N. (1976) Lymphocyte locomotion. I. The initiation, velocity, pattern, and path of locomotion in vitro. *Lymphology* **9**, 89–96.
37. Rydgren, L., Brodin, H., Håkansson, C.-H., Norberg, A., Norberg, B., and Westrup, C. (1980) The computer leucocyte. Analysis of the random movement of leucocytes in a visual field by means of computer simulation. *Scand. J. Haematol.* **25**, 45–50.
38. Allan, R. B. and Wilkinson, P. C. (1978) A visual analysis of chemotactic and chemokinetic locomotion of human neutrophil leucocytes. *Exp. Cell Res.* **111**, 191–203.
39. Tranquillo, R. T. and Lauffenburger, D. A. (1987) Stochastic model of leukocyte chemosensory movement. *J. Math. Biol.* **25**, 229–262.

Evaluation of Cell Morphology

**Eugene A. Lepekhn, Peter S. Walmod, Anton Berezin,
Vladimir Berezin, and Elisabeth Bock**

1. Introduction

The shape of a cell reflects cell-substratum and cell-cell attachment and organization of the cytoskeleton (*1-4*). Many studies on cell morphology have until recently been purely qualitative for the simple reason that morphological changes resulting from e.g., modulation of cell attachment or perturbation of cytoskeletal components often are so pronounced that quantification may seem unnecessary. However, quantitative determination of cellular morphology greatly expands the possibility of characterizing the role and regulation of macromolecules involved, e.g., in cytoskeletal functions and cellular differentiation.

In recent years, large-scale determination of cellular morphology has been made possible by the rapid development in time-lapse video microscopy and computer-assisted image analysis. Quantification of cell morphology can be performed statically or dynamically. A typical example of the first would be a comparison of morphological features of different cell lines or of a single cell line subjected to different treatments. Such investigations may be relatively simple to perform, since the cells can be studied after fixation and staining, simplifying the subsequent determination of cell morphology. Determination of morphological changes of living cells may give important information about the dynamics of cell attachment and cytoskeletal organization, but is much more complicated to perform since it demands observation of the living cells under controlled conditions and the recognition of morphological features of unstained cells.

A number of parameters for evaluation of cell morphology have been developed. Some are based on the contour of a cell, yielding parameters such as area

and perimeter. Others are calculated using the convex hull of a cell as well as its contour, e.g., process index and process domain. Other approaches for quantification of cellular morphology are based on stereological principles or binary image thinning transformations. Additionally, the brightness (gray levels) of the cells observed by means of phase-contrast optics may be used as a measure of cellular attachment/detachment.

This chapter summarizes and evaluates parameters suitable for quantification of the two-dimensional morphology of cultured cells based on images derived from digital video microscopy. The presentation includes methods for evaluation of single cell morphology as well as morphometric evaluation of populations of cells.

2. Materials

2.1. Cell Cultures

1. Cell culture conditions affect cellular morphology and should therefore be carefully selected and kept constant during the experimentation (5). Fixation of cells may be recommended in order to preserve cell morphology and both stained and unstained cultures can be used for microscopy and video-recording.
2. For the experiments presented in this chapter, cultures of L929 (mouse fibroblasts) and BT4Cn (rat glioma) cell lines and primary cultures of rat hippocampal neurons were used. Fibroblasts and glioma cells were grown in Dulbecco's modified Eagle's medium (DMEM) supplemented with 10% fetal calf serum, penicillin (100 U/mL), streptomycin (100 μ g/mL) and fungizone (2.5 μ g/mL) at a density of 3,000 cells/cm² in order to exclude the possible influence of cell-cell interactions on cell morphology. Hippocampal cells were obtained by means of dissociation of whole hippocampi isolated from rat embryos at gestational days 17–19 (6). Isolated hippocampal cells were seeded in 35 mm diameter tissue culture dishes coated with fibronectin (1 μ g/cm²) at a density of 7,000 cells/cm² and maintained at 37°C, 5% CO₂ in a DMEM/F12 cell culture medium with N2 supplement (Gibco BRL, Denmark). After careful removal of the medium, cultured hippocampal cells were fixed for 30 min in a medium containing 2.5% glutaraldehyde, washed with phosphate buffered saline and stained with Coomassie Brilliant Blue R250 (2.5 g/L in 50% v/v ethanol, 10% v/v acetic acid) for 30 min.

2.2. Microscopy and Video Recording

1. Microscopy and video-recording of cells can be performed using either an inverted or upright microscope equipped with a video camera connected to a computer. Time-lapse video microscopy may also be applied to follow the kinetics of morphological changes of living cells. Depending upon the experimental conditions and the contrast of the image, transmitted light, phase contrast, differential interference contrast (Nomarski), Hoffmann optics or interference micros-

copy with automatic phase-shifting can be used with a magnification giving the desired resolution of the morphological features to be quantified (1,3,7,8).

2. We used a Nikon Diaphot 300 inverted microscope equipped with phase-contrast optics (20× magnification; Nikon, Denmark). Images were grabbed with a black and white CCD video camera (Burle, Lancaster, USA) using PRIMA software (Protein Laboratory, Copenhagen, Denmark) and stored as 512 × 512 pixel images. Images from 20 to 30 microscopic fields per cell culture were recorded and only single cells were evaluated.

2.3. Object Recognition and Outlining of Cells

1. Identification of cell contours is necessary in order to evaluate cellular morphology. Initially, the image containing the relevant objects has to be transformed to its binary form. At this stage, simple binary thresholding is sufficient in most cases. If the simple binary thresholding does not yield a satisfactory binary image of the cells, a variety of image processing methods for edge detection and feature recognition may be applied (9–11). Most available image analysis software provide suitable edge detection procedures and may thus be successfully used for recognition of selected morphological features (1,12).
2. A thresholding value may be selected arbitrarily or determined after analysis of the distribution of the gray values of the image pixels, e.g., assuming that the total area of all cells within the image constitutes a significant part of the whole image area (15–20%), the thresholding value may be selected as the gray value corresponding to the gap (minimum) between two distribution peaks representing the cell image pixels and the background pixels, respectively.
3. Subsequently, connected components corresponding to either cells or background are labeled by an automatic procedure based on an appropriate algorithm. Finally, a contour following algorithm is applied to obtain a representation of cell contours as a list of coordinate pairs, or as a chain code representation (13).
4. Alternatively, cell contours can be drawn manually by means of a computer pointing device, e.g., a mouse.
5. In the experiments presented, contours of living or stained cells were outlined either manually or recognized automatically by means of thresholding and binary transformation.

3. Methods

3.1. Parameters for Evaluation of Cell Shape (see Notes 1–4)

In order to facilitate measurement of cellular shape, a variety of morphometric parameters has been proposed (8,12,14–17). A selection of valuable parameters is listed in **Table 1**. They may be divided into three groups based on:

1. Contour.
2. Convex hull.
3. Brightness (gray value) of the object.

Table 1
Morphometric Parameters

Parameter	Description	Mathematical definition
Object Area		$\left \frac{1}{2} \sum_{i=0}^{n-1} (x_i \cdot y_{i+1} - x_{i+1} \cdot y_i) \right $, (see text for x , y and n)
Object Perimeter		$\sum_{i=0}^{n-1} \sqrt{(x_i - x_{i+1})^2 + (y_i - y_{i+1})^2}$, (see text for x , y and n)
Object Breadth	Shortest distance between extreme points of an object	
Object Length	Longest distance between extreme points of an object	
Object Width		$4 \cdot \text{Area} / \pi \cdot \text{Length}$
Object Form Factor		$4 \pi \cdot \text{Area} / \text{Perimeter}^2$
Bipolarity Index		Object Length/Object Breadth
Convex Hull Area	Total area of the convex hull	(see object area)
Convex Hull Perimeter	Perimeter of the convex hull	(see object perimeter)
Convex Hull Form Factor	Form factor of the convex hull	(see object form factor)
Spreading Index		$\pi (\text{Convex hull length})^2 / 4 (\text{Convex hull area})$
Process Index	Number of domains created by subtracting the object area from the convex hull area	
Process Domain	The area of domains created by subtracting the object area from the convex hull area	
Brightness	The average brightness of cell image pixels	

3.1.1. Morphometric Parameters Based on the Contour of the Object

A closed contour is described as a sequence of n points with corresponding coordinates pairs $P_0 = (x_0, y_0)$, $P_1 = (x_1, y_1)$, ..., $P_n = (x_n, y_n) \equiv P_0$, i.e. the final coordinate pair is equal to the first pair. To draw the closed contour, one should connect P_i and P_{i+1} with a straight line, where $i=0, 1, 2, \dots, n-1$ (**Fig. 1A**).

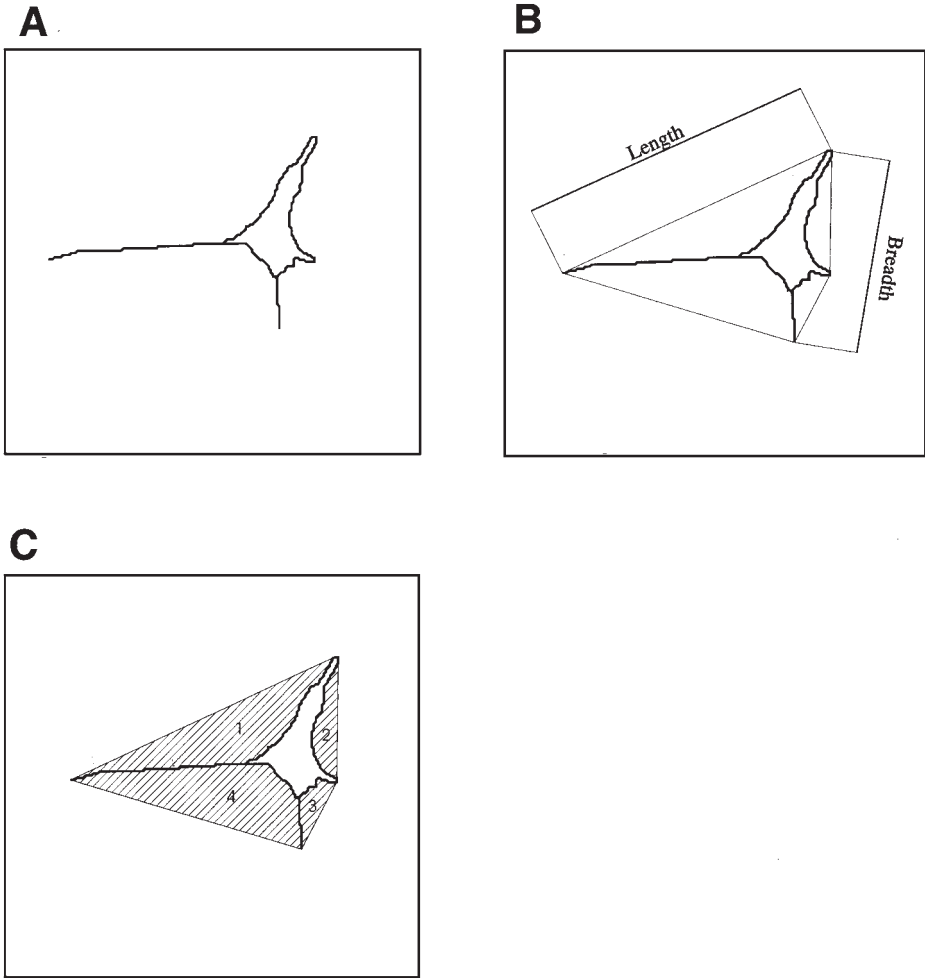


Fig. 1. Schematic presentation of cell contour, length and breadth, and convex hull. (A) Contour of the cell. (B) Length and breadth of the same cell. (C) The convex hull of the cell with numbered areas obtained after superimposing the contour on the convex hull. The number of areas represents the process index, the total area obtained by subtracting cell area from convex hull area represents the process domain (hatched in the figure).

The *perimeter* of the contour of an object, *in casu* a cell, is merely the sum of the individual distances between adjacent points of the contour,

$$\sum_{i=0}^{n-1} \sqrt{(x_i - x_{i+1})^2 + (y_i - y_{i+1})^2}$$

and the area of the region surrounded by the closed contour thus represents the *cell area*

$$\left| \frac{1}{2} \sum_{i=0}^{n-1} (x_i \cdot y_{i+1} - x_{i+1} \cdot y_i) \right|$$

The *length* of the cell is the longest distance between two extreme points of the cell contour, and the *breadth* is the smallest distance between two parallel lines touching the cell contour at extreme points (**Fig.1B**). Evidently, the breadth of bent or concave cells, is not a particularly good measure of how wide the cell is. One may in that case use the *cell width*, which is defined as the width of an ellipse having the same area and length as the cell. The *bipolarity index* reflects the degree of the cellular elongation and is defined as the ratio of the cell length to the cell breadth. The *form factor* is defined as

$$4 \pi \cdot \text{Area} / \text{Perimeter}^2$$

and it is a measure of the degree of cellular roundness. Thus, a perfectly round cell has a form factor of 1, whereas more elongated or stellate cells have lower form factors (**8**).

3.1.2. Morphometric Parameters Based on Cell Contour and Convex Hull

1. The convex hull of the object is obtained by rotation of the coordinate system finding the extreme left and right points of the object. By rotating the coordinate system in a reasonably large number of different angles (100–150), the coordinates of the extreme points form a polygon that closely approximates the convex hull boundary (**Fig. 1C**, [**18**]). Parameters such as the *perimeter*, *area*, *form factor* and *width* of the convex hull can be calculated in the same way as those for the contour of the cell. Note, that the *length* and *breadth* of the convex hull are the same as the length and breadth of the object/cell.
2. By subtracting the area occupied by an object from the area of its convex hull, a set of minor areas is obtained (**Fig. 1C**). Areas which are smaller than a chosen lower value (e.g. smaller than 5% of the object area) may be excluded. The number of the remaining areas, in the following termed the *process index*, and the total area of these areas termed the *process domain* correlate with the number and length of cellular processes (**19**). Another parameter of interest is the *spreading index* which measures the degree of roundness of the convex hull and thus reflects cellular spreading.

3.1.3. Cellular Brightness

Cells that display a strong attachment to the substratum usually appear darker in phase-contrast optics than more weakly attached cells. Thus, the

brightness of one or more objects, determined as an average gray level value of pixels inside the cell contour(s), may serve as a measure of cellular attachment. Brightness is of course a relative value and strongly depends on the illumination conditions, the type of culture chamber used, substratum, video camera characteristics, etc. Nevertheless, cellular brightness has been used successfully to study the dynamics of cell attachment (5,20).

3.1.4. Examples 1 and 2

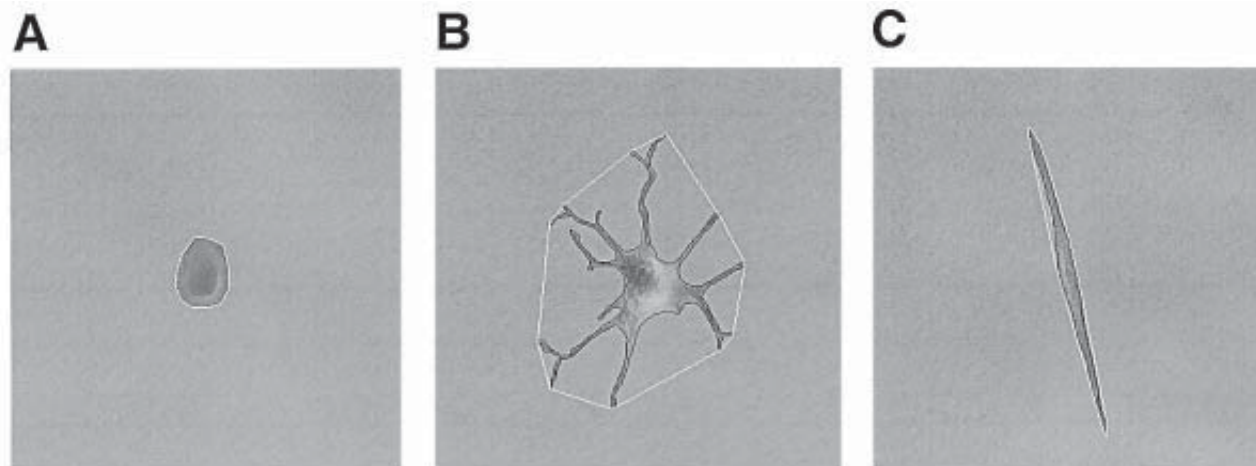
1. In **Fig. 2**, the images of three different morphological cell types, a rounded, a stellate and an elongated cell, are presented and the values of selected parameters are given below. These include cell length, breadth, area, form factor, bipolarity index, spreading index, process index and process domain. It can be seen that form factor is an appropriate measure of cellular roundness, bipolarity index and spreading index reflect the elongation of a cell whereas process index and process domain successfully can be used for estimation of the number and length of cellular processes, respectively.
2. An example of the use of cellular brightness is shown in **Fig. 3**, which presents the kinetics of the detachment of mouse fibroblasts (L929 cell) and rat glioma cells (BT4C cells) from a fibronectin substratum after addition of:
 - a. Cytochalasin D, which disrupts actin filaments
 - b. Nocodazole, which depolymerizes microtubules
 - c. An RGD-containing peptide, GRGDSP, which influences cell adhesion mediated by RGD-recognizing integrins.
3. L929 cells treated with cytochalasin D, nocodazole or the RGD-peptide gradually became rounded and thereby achieved a higher degree of brightness due to detachment from the substratum accompanied by a decrease in cellular area. With regard to BT4C-cells, cellular attachment was affected when actin filaments were depolymerized by cytochalasin D treatment, whereas BT4Cn attachment was unaffected by perturbation of the microtubules by nocodazole treatment, and evidently these cells were not attached to fibronectin via an RGD-recognizing integrins since the RGD-peptide had no effect.

3.2. Parameters for Evaluation of Cellular Processes

Quantitative analysis of long cellular processes, e.g., neuronal axons and dendrites is currently a laborious and time-consuming task since processes often are drawn manually. However, new quantitative procedures are currently being developed for measurement of cellular processes.

3.2.1. Manual Determination of the Number and Length of Cell Processes

Long cellular processes (e.g., neurites) can simply be analyzed using a manual tracing (drawing) procedure, where processes including their branches are traced by the investigator on a computer monitor by means of computer



Cell A

Cell B

Cell C

Cell length	58.34 μm	212.18 μm	243.69 μm
Cell breadth	52.50 μm	140.60 μm	19.15 μm
Cell area	2177.44 μm^2	4021.76 μm^2	2105.27 μm^2
Form factor	0.82	0.028	0.09
Bipolarity index	1.111	1.509	12.725
Spreading index	1.184	1.660	15.012
Process index	0	8.0	3.0
Process domain	0 μm^2	16806.77 μm^2	887.11 μm^2

Fig. 2. Morphological description of three different cells (A, B, and C). The values of following parameters are indicated: cell length, breadth, area, form factor, bipolarity index, spreading index, process index and process domain.

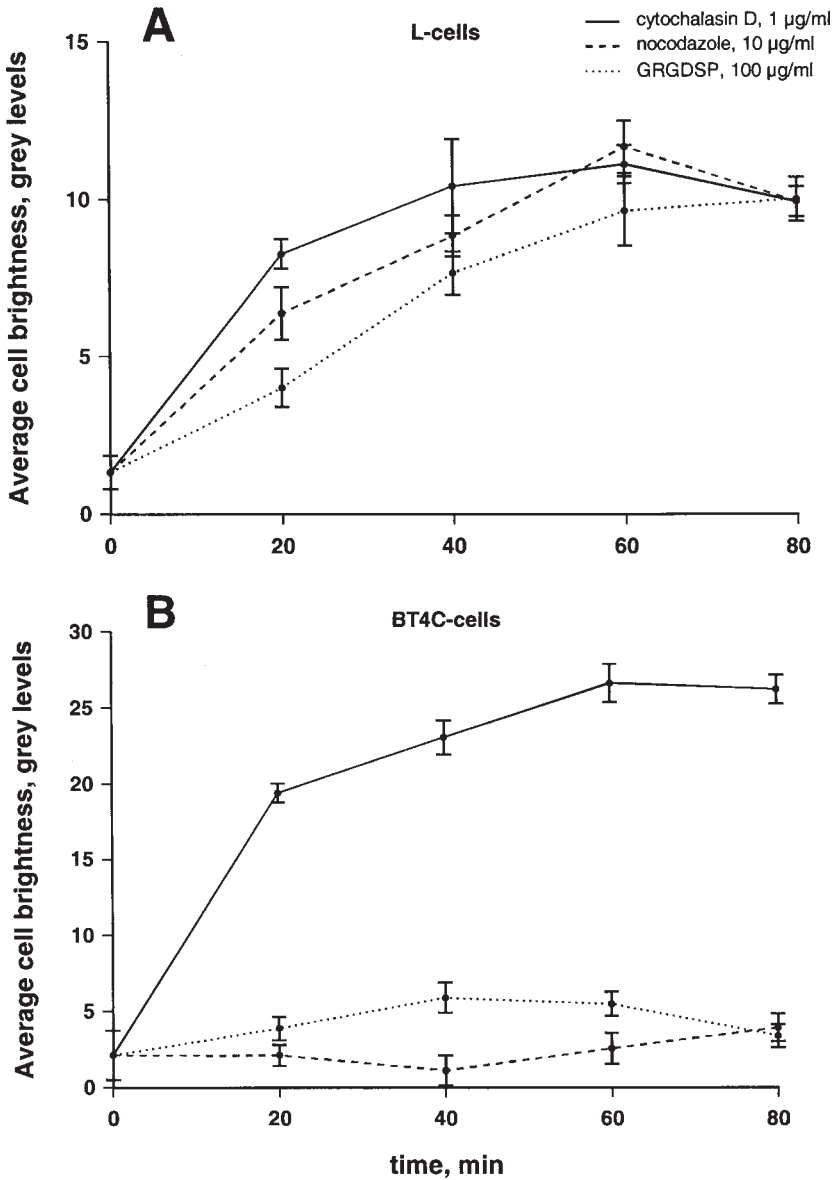


Fig. 3. Kinetics of detachment of L929 cells (A) and BT4Cn cells (B) from fibronectin ($1.2 \mu\text{g}/\text{cm}^2$) after addition at time 0 of cytochalasin D ($1 \mu\text{g}/\text{mL}$), nocodazole ($10 \mu\text{g}/\text{mL}$), or the GRGDSP peptide ($100 \mu\text{g}/\text{mL}$), evaluated by measurement of average cell brightness (Evaluation of cell morphology by video recording and computer-assisted image analysis. V. Berezin, G. Skladchikova and E. Bock. *Cytometry*, 27:106–116. Copyright 1997, John Wiley & Sons, Inc. Reprinted by permission of Wiley-Liss, Inc., a division of John Wiley & Sons, Inc.).

mouse. The *process number* and the *process length per cell* or the *average length per process* can thereby be calculated.

3.2.2. Convex Hull-Derived Parameters for Evaluation of Process Length

As mentioned above, the convex hull-derived parameters, process index and process domain are well suited for the estimation of the number of cellular processes and the process length per cell, respectively. And both process index and process domain determined for populations of cells have been shown to correlate statistically significantly with manually determined parameters of process number and length (19).

3.2.3. Morphological Binary Thinning of the Cell Contour

1. Given that most cellular processes are relatively thin, a procedure of process length determination based on methods of mathematical morphology (21) may be used. Morphological image thinning is a transformation in which an object without holes (Fig. 4A) is eroded to a minimally connected stroke located equidistantly from the nearest outer boundaries of the object (9). By applying a thinning algorithm to a binary image of a cell an image of a cellular “skeleton” is produced (Fig. 4B). In order to obtain an accurate image of the cellular processes, it is necessary to remove the parts of the “skeleton” residing inside the cell body. Images of cell bodies can be produced from the original binary image by means of morphological binary erosions, followed by dilations (9). The number of erosion transformations necessary to achieve this depends on the thickness of the cellular processes; three erosions followed by three dilations are typically enough to remove all processes from a binary image (Fig. 4C). The image of the cell body is then used to mask out the parts of the thinned image residing inside the cell (Fig. 4D). Optionally, process-like features with length less than a certain value (spurious processes) may be removed to yield an accurate image of the cell processes.
2. In this way the length and number of processes per cell can be determined automatically without manual tracing (see Fig. 6). Moreover, the degree of process branching can also be estimated.

3.2.4. Stereological Determination of Process Length

If automatic delineation of cell contours is not possible, the average process length per cell can be estimated using stereological principles (22). An unbiased counting frame containing a grid with a certain number of test lines is superimposed on an image (Fig. 5). The number of intersections of test lines by cellular processes are counted and related to the number of cell bodies. This ratio gives a simple estimate of the average process length per cell

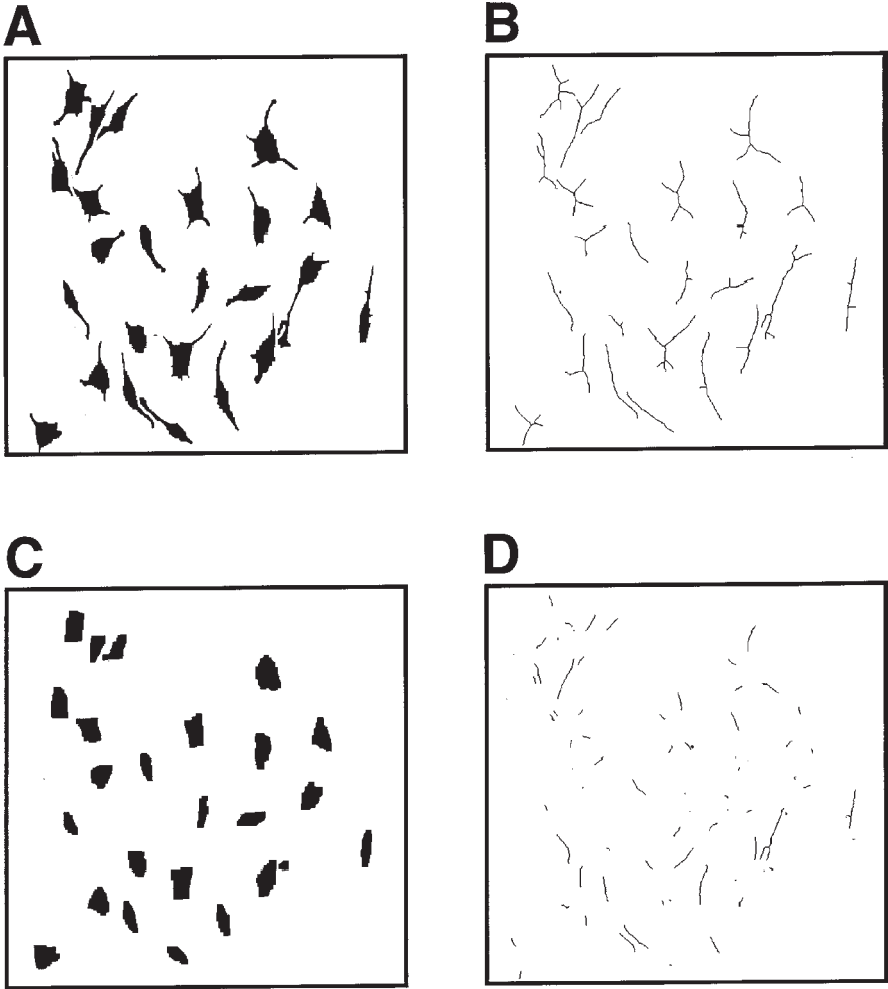


Fig. 4. Automatic identification of cellular processes by binary thinning transformation. (A) A binary image of cells. (B) The result of binary thinning of the image (the cell “skeleton”). (C) The result of three erosions followed by three dilations (cell bodies). (D) Parts of the thinned image masked out by cell bodies.

measured in arbitrary units. The absolute length of the process can be estimated according to the equation

$$L = \pi/2 \cdot d \cdot I,$$

where L is the process length, d is the vertical distance between two neighboring test lines and I is the number of intersections between test lines and cellular

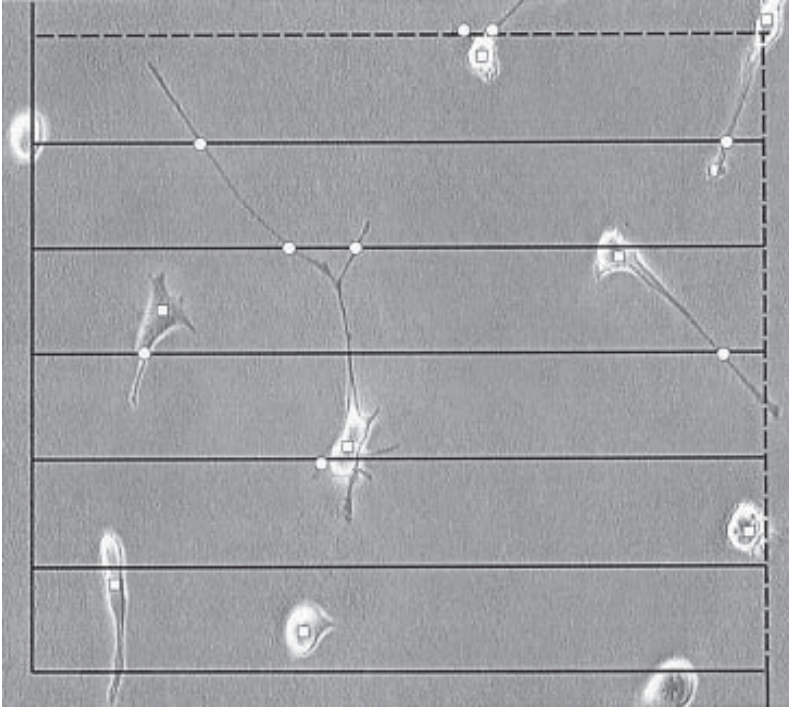


Fig. 5. Stereological determination of process length. A counting frame is superimposed onto an image of a cell culture. Objects within the frame or in contact with the hatched inclusion lines are considered, whereas objects outside the frame or in contact with the solid exclusion lines of the frame are omitted. By means of a computer mouse, the intersections of the horizontal lines by cell processes (white circles) and the cell bodies (white squares) are marked. The ratio between the number of intersections and the number of cells is subsequently calculated.

processes (23). The procedure is easy and rapid to perform and therefore suitable as a screening assay.

3.2.5. Example 3

In Fig. 6 the results of the quantification of neurite outgrowth from hippocampal cell culture by means of the above described four methods is shown. Neurite outgrowth from hippocampal neurons at various times of development in vitro was estimated. The correlation coefficients between values determined by mean of manual tracing and the three other methods were in all cases higher than 0.99 ($p < 0.05$). This indicates that all methods are suitable for evaluation of process length.

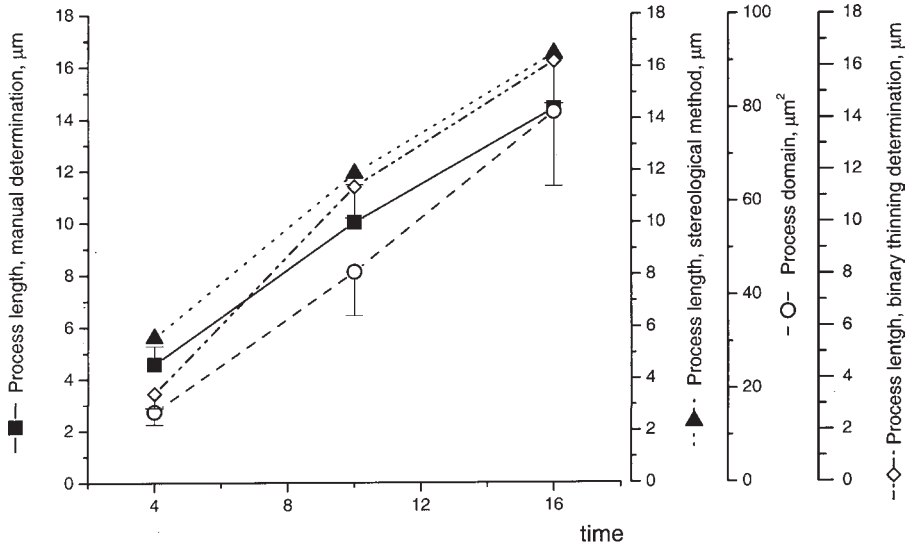


Fig. 6. Morphometric analysis of hippocampal neurons at various times of development in vitro. The average process length determined by means of stereology (\blacktriangle), binary thinning transformation (\diamond) or by calculation of process domain (\circ) was compared to the average process length determined manually (\blacksquare).

4. Notes

1. The terminology used for description of morphometric parameters is not standardized and somewhat confusing. In the literature one often finds different names for the same parameters or different parameters with the same names. For example, the term "object width" has in some studies been applied to the distance obtained by dividing cellular area by cellular length (8,24), and form factor is also described as a factor of "roundness" or "circularity" (8,24) or expressed reciprocally (1,12).
2. The sampling process is important when only a part of a cell population is evaluated. Generally, the sampling from each culture dish should have a random starting point followed by regular sampling intervals. If a microscope with a computer-controlled movable stage is available, a starting point can be determined by picking random numbers corresponding to the first X- and Y-sampling coordinates. The steps in the X and Y directions can be defined to yield a desired number of images per culture. If the sampling is performed manually, a randomization procedure is advised.
3. Contour determination (or cell outlining) is difficult to achieve automatically. To assure recognition, cells on images should have a high contrast against the background. Generally, staining cells with cytoplasm- or membrane-specific dyes helps to increase the contrast. Recognition of the contour of living cells is espe-

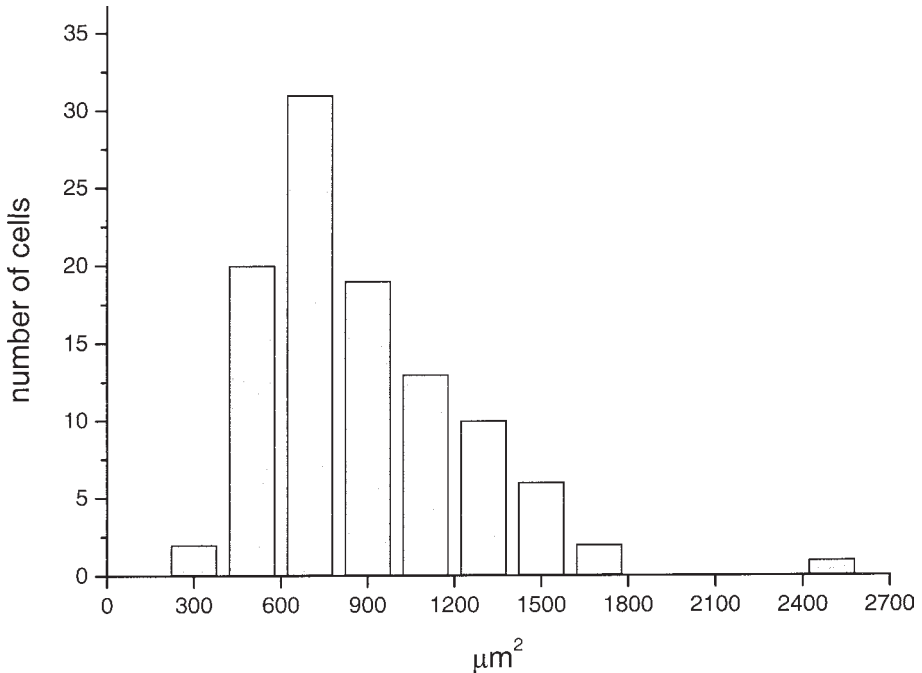


Fig. 7. Asymmetric distribution of cell area values in a sample of rat glioma BT4Cn cells (104 cells).

cially difficult when using phase-contrast optics, due to the small difference in gray level values between cells and background, especially in very thin cellular regions such as the lamellipodia. Moreover, the presence of a distinctive halo in phase contrast images limits the applicability of cell recognition algorithms to images obtained with this type of optics.

- The distribution of a chosen parameter in a population may in some cases differ from the normal distribution. In case of a significantly asymmetric distribution, the arithmetical mean value may therefore be substituted by the median or the mode. **Fig. 7** shows the distribution of cell area values for a sample of cells from the rat glioblastoma cell line BT4Cn. The skewness and kurtosis of the distribution are 1.29 ± 0.24 and 2.38 ± 0.47 , respectively, and the distribution differs statistically significantly from a normal distribution, $p < 0.001$. The arithmetical mean value for the sample is $878.1 \mu\text{m}^2$ and the median is $792.5 \mu\text{m}^2$.

References

- Moustafa, Y., Chancel, J., Rosetti, F., Montmasson, M.-P., and Idelman, S. (1992) Image analysis of lymphoid cell differentiation in rat thymus throughout development. *Thymus* **19**, 127–144.

2. Brown, A. F., Dugina, V., Dunn, G. A., and Vasiliev, J. M. (1989) A quantitative analysis of alterations in the shape of cultured fibroblasts induced by tumour-promoting phorbol ester. *Cell Biol. Internat. Report* **13**, 357–366.
3. Verschueren, H., Houben, B., Braekeleer, De, J., Wit, De, J., Roggen, D., and Baetselier, De, P. (1993) Methods for computer assisted analysis of lymphoid cell shape and motility, including Fourier analysis of cell outlines. *J. Immunol. Methods* **163**, 99–113.
4. Ingber, D. E., Dike, L., Hansen, L., Karp, S., Liley, H., Maniotis, A., et al. (1994) Cellular tensegrity: exploring how mechanical changes in the cytoskeleton regulate cell growth, migration, and tissue pattern formation during morphogenesis. *Int. Rev. Cytol.* **150**, 173–224.
5. Berezin, V., Skladchikova, G., and Bock, E. (1997) Evaluation of cell morphology by video recording and computer-assisted image analysis. *Cytometry* **27**, 106–116.
6. Schousboe, I., Larson O. M., and Schousboe, A. (1989) Development of homospecific activity of GABA-transaminase in the mouse cerebral cortex and cerebellum and in neurons cultured from these brain areas. *Int. J. Dev. Neurosci.* **7**, 115–121.
7. Dunn, G. A., Zicha, D., and Fraylich, P. E. (1997) Rapid, microtubule-dependent fluctuation of the cell margin. *J. Cell Sci.* **110**, 3091–3098.
8. Soll, D. R., Voss, E., Varnum-Finney, B., and Wessels, D. (1988) “Dynamic morphology system”: a method for quantitating changes in shape, pseudopod formation, and motion in normal and mutant amoebae of *Dictyostelium discoideum*. *J. Cell. Biochem.* **37**, 177–192.
9. Pratt, W. K. (1991) *Digital image processing*. 2nd ed. Wiley, NY.
10. Klette, R. and Zamperoni, P. (1996) *Handbook of image processing operators*. John Wiley, NY.
11. Gonzalez, R. C. and Woods, R. E. (1992) *Digital image processing*. Addison-Wesley, 1992.
12. Barret, L., Soubeyran, A., Usson, Y., Eysseric, H., and Saxod, R. (1996) Characterization of the morphological variations of astrocytes in culture following ethanol exposure. *Neurotoxicology* **17**, 497–508.
13. Pavlidis, T. (1982) *Algorithms for graphics and image processing*. Computer Science Press, Rockville, MD.
14. Giuliano, K. A. (1996) Dissecting the individuality of cancer cells: the morphological and molecular dynamics of single human glioma cells. *Cell Motil. Cytoskeleton* **35**, 237–253.
15. Doughty, M. J. (1989) Towards a quantitative analysis of corneal endothelial cell morphology: a review of techniques and their application. *Optom. Vis. Sci.* **66**, 626–642.
16. Noble, P. B. and Levine, M. D. (1986) *Computer-assisted analyses of cell locomotion and chemotaxis*. CRC Press, Boca Raton.
17. Masseroli, M., Bollea, A., and Forloni, G. (1993) Quantitative morphology and shape classification on neurons by computerized image analysis. *Comput. Methods Programs Biomed.* **41**, 89–99.

18. Russ, J. C. (1990) *Computer-assisted microscopy: the measurement and analysis of images*. Plenum Press, N. Y.
19. Kawa, A., Stahlhut, M., Berezin, A., Bock, E., and Berezin, V. (1998) A simple procedure for morphometric analysis of processes and growth cones of neurons in culture using parameters derived from the contour and convex hull of the object. *J. Neurosci. Methods* **79**, 53–64.
20. Walmod, P. S., Skladchikova, G., Kawa, A., Berezin, V., and Bock, E. (1999) Antiepileptic teratogen valproic acid (VPA) modulates organization and dynamics of the actin cytoskeleton. *Cell Motil. Cytoskeleton* **42**, 241–255.
21. Serra, J. (1982) *Image Analysis and Mathematical Morphology*. Academic Press, London.
22. Gundersen, H. J. G., Bendtsen, T. F., Korbo, L., Marcussen, N., Moller, A., Nielsen, K., et al. (1988) Some new, simple and efficient stereological methods and their use in pathological research and diagnosis. *APMIS* **96**, 379–394.
23. Rønn, L. C., Ralets, I., Hartz, B., Bech, M., Berezin, A., Berezin, V., et al. (1999) A simple procedure for quantification of neurite outgrowth based on stereological principles. *Manuscript in preparation*.
24. Soll, D. R. (1995) The use of computers in understanding how animal cells crawl. *Int. Rev. Cytol.* **163**, 43–104.

A Quantitative Assay for Measurement of Chemokinesis in *Tetrahymena*

Uffe Koppelhus, Per Hellung-Larsen, and Vagn Leick

1. Introduction

Rapidly swimming cells, like the ciliated protozoa, offer an interesting opportunity to study the chemosensory behaviour involved in chemoattraction/repulsion in response to external chemical stimuli. The membrane ultrastructure of ciliates resembles that of the chemosensory neurones and the olfactory epithelium in mammals (1). As in higher organisms, the cilia may have adapted a sensory role. Ciliates may therefore be viewed as “swimming receptors” where correlations between cellular behaviour, cell behaviour and molecular signal transduction events can be studied experimentally because many ciliates are easy to grow and handle in the laboratory.

Previous studies of the chemosensory behaviour of *Tetrahymena* have shown that this ciliate is chemoattracted to a range of different proteins, peptides, and amino acids (2). Using the so called two-phase assay (3) one can study the adaptative (temporal) element of the chemosensory response. Adaptation is a widespread feature of many chemotactic cells and is a temporal mechanism that represents a kind of short-term memory (4). Adaptation is here defined as a reversible elimination of the responsiveness of a cell caused by an adjustment of its sensitivity. This property reflects the ability of the cells to read and “remember” a certain concentration of a chemoattractant thereby repelling them from swimming towards lower concentrations (5). Adaptation might be studied using other experimental set-ups all based upon the cellular response of a chemotactic gradient established by diffusion (2). In the two-phase assay, a suspension of cells (the top phase) is gently placed on the top of a dense Metrizamide phase (4–5% w/v) containing the test substance (the lower phase). Subsequently, after establishment of the chemotactic gradient, the impact of the test

substance is measured quantitatively by the degree to which the cells swim into the lower Metrizamide phase. In our paper from 1986 (3) several high density agents were tested (e.g., gelatine, ficoll and sucrose) but for reasons discussed in the original paper, Metrizamide should be the first choice in this assay. Originally, the two-phase assay was only semiquantitative because of a marked day-to-day variation observed at that time. However, upon extensive studies of the physiological parameters affecting the growth and chemotactic behaviour of the cells, we were able to develop a highly sensitive and reproducible assay. It is important, however, to understand that success in this assay is dependent on strict control of the history of the cells, and that each step of the cell growth and preparation for the assay should be carried out precisely as stated in the following protocol. Although this protocol is complete for the set-up of the assay, carefully reading the two original papers concerning the development of the assay in its present form (6,7) is recommended.

2. Materials

1. Cells : *Tetrahymena thermophila* is available from American Type Culture Collection (ATCC) 12301 Parklawn Drive Rockville MD 20852 USA.
2. PY medium: 0.75% proteose peptone (Difco), 0.75% yeast extract (Difco), 1.5% glucose, 1 mM MgSO₄, 50 μM CaCl₂ and 100 μM ferric citrate (see Note 1).
3. The PY medium should be diluted in water to 1/3 prior to use. All materials and medium involved in the growth and starvation of the cells should be sterilized by pressure, heat sterilisation (2 atm, 120°C, 30 min).
4. Metrizamide (2-[3-acetamido-5-N-methylacetamido-2,4,6-triiodobenzamido]-2-deoxy-D-glucose) (Sigma).
5. Disposable plastic cuvetts (Plastibrand, Germany, Cat. No. 759015) Pasteur pipet.
6. Thermostated recording spectrophotometer with an automized multicuvette cassette. A thermostated spectrophotometer without recording might also be used for manual OD readings.

3. Methods

3.1. Growth (see Notes 2–4)

Inoculate the cultures to a concentration of approx 10⁴ cells mL⁻¹ (see Note 2).

3.2. Starvation of Cells

1. Collect the cells by centrifugation at 500g for 3 min using sterile centrifuge tubes.
2. Gently resuspend the cells in deionized water to a cell concentration of approx 1.5 × 10⁵ cells mL⁻¹ (see Note 5). Transfer the cell suspension to 500 mL Fernbach Flasks containing (at a maximum) 50 mL of cell suspension.
3. Incubate the cells for 40–50 h at 21°C.
4. Measure the OD₆₀₀ of the cell suspension.

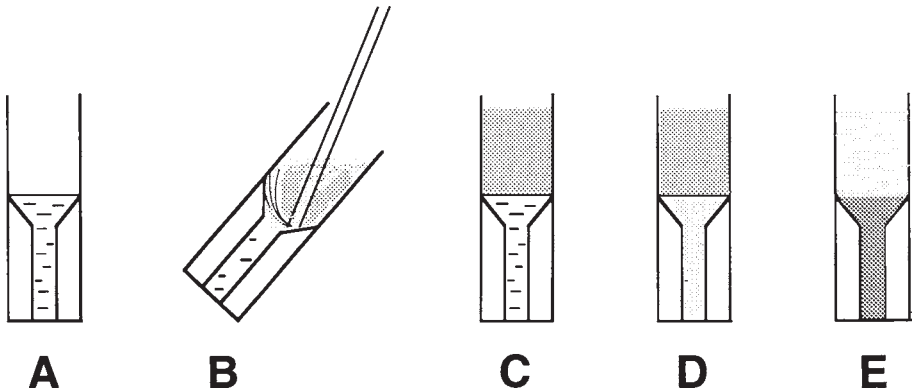


Fig. 1. Schematic representation of individual steps in the two-phase assay. One mL of the Metrizamide solution is filled into the microcuvettes and each cuvette is blanked (A). Using a Pasteur pipet, 1.5 mL of the cell suspension is carefully layered on the top of the Metrizamide-containing lower phase (B). Immediately after layering, the optical density of the lower phase must still be zero or close to zero (C). After 20–30 min, only few cells will have entered the lower phase in the control cuvet where no attractant is present (D) while approximately 80% of the cells are displaced by swimming into the lower phase if a strong chemoattractant such as proteose peptone is present (E).

3.3. Finding the Optimal Metrizamide Concentration

1. Make solutions of Metrizamide in water ranging from 2–5% w/v. The water should be sterilized and kept at 21°C for a period of at least one day. Water stored at, e.g., 4°C will have higher oxygen tension which can influence the background in the assay.
2. Use metrizamide concentrations of 2, 3, 4 and 5% respectively with or without proteose peptone at a concentration of 1 mg/mL to find the optimal metrizamide concentration for a particular cell suspension as described in **Subheading 3.4**. In general, we find a concentration of Metrizamide of 4% to be pertinent (*see Note 6*).

3.4. The Two-Phase Assay

1. Prepare solutions of the test substances in the Metrizamide solution and load 1 mL of each to plastic cuvetts. One cuvet is loaded with Metrizamide solution and used as a control.
2. Blank each cuvet in the spectrophotometer.
3. Fill the Pasteur pipet with 1.5 mL of the cell suspension using a pipet bulb or rubber tube adapted to the Pasteur pipet at one end and a mouthpiece at the other. Make a mark on the pipet corresponding to 1.5 mL. Then fill the pipet with somewhat more than 1.5 mL of cell suspension, quickly change the tube/pipet bulb for a fingertip and adjust the content of the pipet to 1.5 mL by gently allowing flow

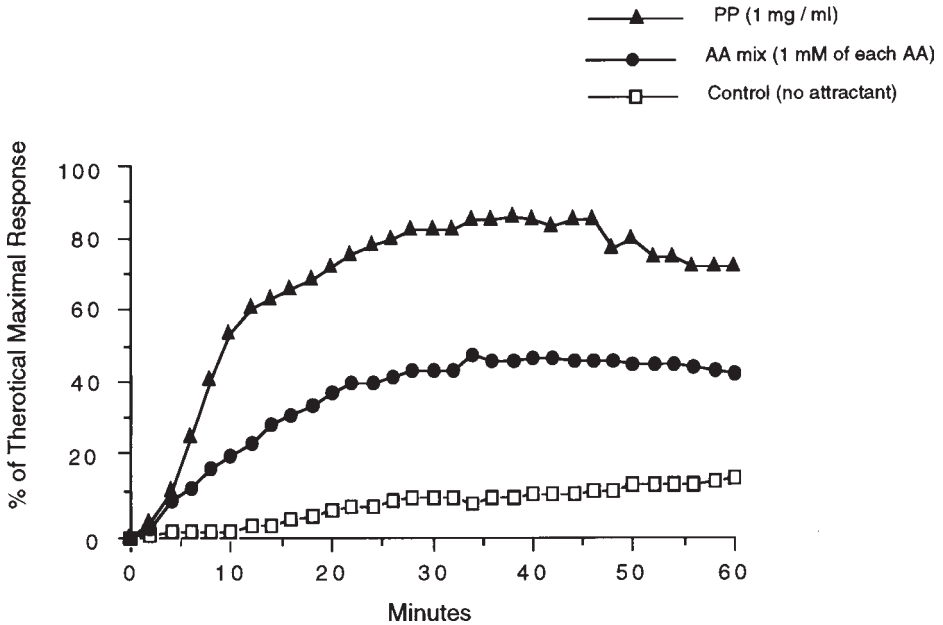


Fig. 2. Chemosensory response of *Tetrahymena thermophila* to two different attractants in the two-phase assay at 28°C. The optical density at 600 nm of the lower Metrizamide-containing phase was monitored every two minutes. The figure illustrates the chemosensory responses obtained using either proteose peptone at a concentration of 1 mg/mL (closed triangles) or a mixture of amino acids (1 mM of each [7]) in the Metrizamide phase (closed circles). Metrizamide solution containing no attractant was used as the control (open squares).

of the cell suspension out of the pipet. It may take a little practice, and a steady fingertip, to master the technique of gently releasing cell suspension from the pipet.

4. While tipping the microcuvette slightly, gently layer 1.5 mL of cell suspension on top of the Metrizamide solution (**Fig. 1**).
5. Check the optical density of the lower phase immediately after the layering process has been completed. If the optical density is not still zero, discard the sample because this indicates that the cell suspension has mixed with the metrizamide.
6. Transfer the microcuvettes to the multicuvette cassette thermostated at 25°C and measure the OD_{600} of the lower phase of each cuvette every 2–5 min for 60 min.

3.5. Calculations

1. Plot the results directly as measured, e.g., OD_{600} versus time.
2. As an alternative, calculate the response as follows:

$$\frac{OD_{600} \text{ of the lower phase}}{1.5 \times (OD_{600} \text{ of the original cell suspension used})} \times 100\%$$

and plot against time. The 100% response corresponds to the theoretical situation in which all cells from the upper phase (1.5 mL original cell suspension) are equally distributed throughout the lower phase (1 mL of Metrizamide), thus giving rise to an optical density 1.5 times that of the cell suspension (7)

The time-response curves offer three possibilities for quantitative analysis :

- a. Initial slope of the response versus time
- b. Maximal response within the time period of the measurements
- c. Signal-to-noise ratios (S/N) at a fixed time.

Based on our findings (7,8) we recommend to use S/N at the time corresponding to the response reaching the plateau typically seen with PP as attractant. Further, we recommend always to test PP as reference attractant. In the experiment shown in **Fig. 2**, S/N should be calculated after about 30 min.

4. Notes

1. *Tetrahymena* can be grown in both complex and defined medium. We recommend a complex medium such as PY for these experiments.
2. Most important for optimal growth is to culture the cells at a high surface-to-volume ratio of the culture medium to ensure sufficient/optimal oxygenation of the medium. We use, for example, 50 mL cultures grown in 500 mL Fernbach flasks (surface-to-volume ratio : 4.8 cm^{-1}). The high surface-to-volume ratio is necessary in order to avoid growth limitation due to low oxygen tension. If *Tetrahymena thermophila* is used, the cells should be grown at 35°C . After 40–50 h, the cell density will be approximately $1.3 \times 10^6 \text{ cells mL}^{-1}$ (corresponding to early stationary phase) and the cells can be transferred to starvation medium.
3. Shaking of the cultures with a lower surface-to-volume ratio than that recommended above will compensate only slightly with respect to oxygenation. Furthermore, shaking of cultures of *Tetrahymena* seems to stress the cells leading to higher doubling times (8).
4. The cultures should be inoculated from exponentially growing cells, and the cells should be collected for starvation at a cell concentration corresponding to early stationary phase as described in the protocol.
5. Concerning starvation, it seems evident that starvation does not induce chemokinesis in *Tetrahymena per se*. On the contrary, chemokinesis seems to be a permanent quality of the cells. Nevertheless, starvation is necessary to deplete the cells from competing attractants in the medium and also to increase the sensitivity and reproducibility in the assay. We recommend deionized water as starvation medium. However, a buffer such as 10 mM Hepes-KOH, pH 7.4 can be used. In any case, it is important to use the starvation medium as solvent for the test substances, as differences in ion composition or pH between the cell environment and the solvent can lead to false responses in the assay based on the influence of, e.g., K^+ on the swimming speed of the cells. We have found deionized water to give the best overall responses, and shown that the lack of buffer capacity in this medium is not a problem if the oxygen saturation is kept above 60% as will be the case when starvation takes place as described in the protocol. The period of star-

vation as well as the temperature during starvation should, as for the growth parameters, be maintained as described in the protocol.

6. For optimal sensitivity of the assay, no (or very few) cells should be swimming into the control Metrizamide while a quick and significant response to PP is observed with many cells swimming as a homogeneous suspension to the bottom of the cuvette. An example of this optimal situation is shown in **Fig. 1**.

References

1. Hufnagel, L. A. (1992) Cortical ultrastructure and chemoreception in ciliated protists (ciliophora). *Microcop. Res. and Technique*. **22**, 225–264.
2. Leick, V., Grave, M., and Hellung-Larsen, P. (1996) Signal peptide-induced chemosensory behaviour in free ciliates: Bioassays and cellular mechanisms. *Progress in molecular and subcellular biology*. Springer Verlag/Heidelberg (Editors Csaba, G. and Müller, W. E. G.) **17**, 61–66.
3. Hellung-Larsen, P., Leick, V., and Tommerup, N. (1986) Chemoattraction in *Tetrahymena*.: On the role of chemokinesis. *Biol Bull.* **170**, 357–367.
4. Morimoto, B. H. and Koshland, D. E., Jr. (1991) Short-term and long-term memory in single cells. *FASEB Journal* **5**, 2061–2067.
5. Leick, V., Koppelhus, U., and Rosenberg, J. (1995) Cilia-mediated oriented chemokinesis in *Tetrahymena thermophila*. *J. Euk. Microbiol.* **41**, 546–553.
6. Koppelhus, U., Hellung-Larsen, P., and Leick, V. (1994) Physiological parameters affecting the chemosensory response of *Tetrahymena*. *Biol. Bull.* **187**, 1–7.
7. Koppelhus, U., Hellung-Larsen, P., and Leick, V. (1994) An improved quantitative assay for chemokinesis in *Tetrahymena*. *Biol. Bull.* **187**, 8–15.
8. Hellung-Larsen, P. and Lyhne, I. (1992) Effect of the shaking on the growth of diluted cultures of *Tetrahymena*. *J. Protozool.* **39**, 345–349.

III

REAGENTS FOR STUDYING CYTOSKELETON PROTEIN FUNCTION

Jasplakinolide

An Actin-Specific Reagent that Promotes Actin Polymerization

Andreas Holzinger

1. Introduction

The actin system is involved in different cellular processes such as exo- and endocytosis, organelle motions, maintenance of organelle distribution, motility, cell division, and cytoplasmic streaming in plant cells. Several substances are known to influence these processes by altering intracellular actin organization and have been used extensively for cell biological research. Their mechanisms of action are mostly destructive on actin filaments (F-actin), either by inhibition of F-actin elongation as in the case of cytochalasins (**1**) or by interaction with actin monomers (G-actin) in order to avoid actin polymerization as described for latrunculins (**2**). In contrast, F-actin polymerizing and stabilizing capacities were found for jasplakinolide (**3–6**). Moreover jasplakinolide has the valuable advantage of being membrane permeable (**7**).

Originally jasplakinolide was isolated from the marine sponge *Jaspis* sp. collected at Fiji or the Palau islands (**8,9**). The sponge was authenticated as *Jaspis johnstoni* (**10**), however, taxonomic difficulties were pointed out (**11**), and the compound can also be isolated from other sponge genera (**11,12**). Detailed procedures for jasplakinolide extraction can be found in (**13**). Different approaches have been used to synthesize this substance (**14,15**) or generate nonpeptide mimetics (**16**); only recently has it become commercially available from Molecular Probes. Chemically, jasplakinolide is a cyclo-depsipeptide containing a tripeptide moiety linked to a polypeptide chain (**8,10**) (**Fig. 1**). Jasplakinolide is also called jaspamide (**9,10**), however, in the recent literature exploring this substance the name jasplakinolide is preferably used (**3,4,6,8,17,18**), occasionally abbreviated as JAS (**17**).

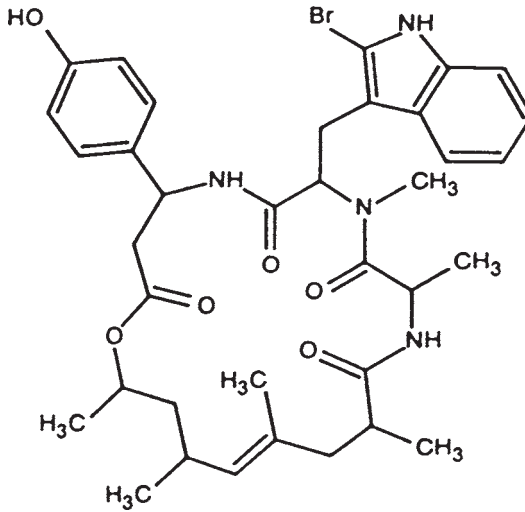


Fig. 1. Molecular structure of jasplakinolide, as reported by Scott et al. (19).

The biological activities of jasplakinolide are described as anthelmintic, antifungal, insecticidal, and selective antimicrobial (8,9,19). The basis of the general cytotoxic effect of jasplakinolide (3,15,20) was found in the selective action on the actin cytoskeleton. Specifically, *in vitro* investigations have elucidated the actin polymerizing- and stabilizing capacities of jasplakinolide (3). Cell biological experiments have been carried out in different carcinoma cell lines (12,21–24), neutrophils (5), MDCK cells (17), liver sinusoidal endothelial cells (LSEC) (25), lymphocytes (18), yeast (13), amoebae *Dictyostelium* (6), and the unicellular green alga *Micrasterias* (4). In the later organism the tremendous effect caused by this drug is already visible at the light microscopic level. As a consequence of drug treatment, inhibition or retardation of *Micrasterias* cell development occurs. During recovery from drug treatment, the cells develop a malformed pattern (4) (Fig. 2A). Changes in cell shapes are reported in different animal cells, where protrusions of the cell surface are formed (18,22). Moreover, when applied during mitosis, binucleated cells are generated as a consequence of jasplakinolide treatment (4,22) (Fig. 2B).

Visualization of the effect of this drug *in situ* was achieved by the use of fluorescently labeled phalloidin as F-actin targeting agent. After jasplakinolide treatment, an altered F-actin distribution was found, characterized by a patchy appearance of cortical actin (18), the formation of actin dots (25) or a disruption of the actin cytoskeleton (22).

As competitive binding inhibition of phalloidin to F-actin by jasplakinolide is described (3), and decreased FITC-phalloidin labeling is

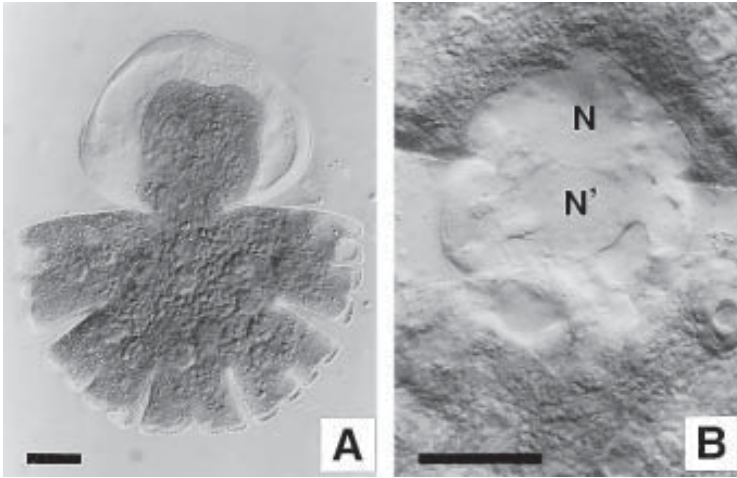


Fig. 2. Effect of jasplakinolide treatment on developing *Micrasterias denticulata* cells. (A) very young developmental stage treated with 3 μM jasplakinolide for 0.5 h and allowed to recover for 3 h in nutrient solution, young semi-cell exhibits complete loss of normal cell pattern (above) when compared to non-growing semi-cell (below). (B) treatment before septum formation with 10 μM jasplakinolide for 2 h, two nuclei (N, N') are visible in the isthmus region, septum is not formed. Bar = 20 μm . Reprinted from reference (4) with permission, Copyright[©] 1997, Wiley-Liss, Inc., a subsidiary of John Wiley and Sons, Inc.

noted as a consequence of jasplakinolide treatment in MDCK cells (17), the problems visualizing jasplakinolide effects by fluorescently labeled phalloidin are obvious. Moreover, phalloidin and jasplakinolide have the same effect when applied to living *Dictyostelium* cells, namely the formation of actin aggregates (6).

In order to avoid the difficulties mentioned, electron microscopy appears to be a sufficient technique for detection of jasplakinolide effects on F-actin (4). At electron microscope resolution, tangential sections of F-actin can easily be recognized by the filament diameter of about 4–5 nm. In organisms like *Micrasterias*, where normally almost no bundling of F-actin occurs, and thus F-actin is hardly found in electron microscopical images, alterations causing extensive bundling of actin are easily detected (4) (Fig. 3). Also immunodetection of the altered F-actin system after jasplakinolide treatment is successful (18) and allows a comprehensive picture to be drawn in combination with other techniques. As jasplakinolide specifically targets F-actin, other cytoskeletal components like desmin or β -tubulin were not influenced by jasplakinolide in carcinoma cells (22), microtubule dependent processes are

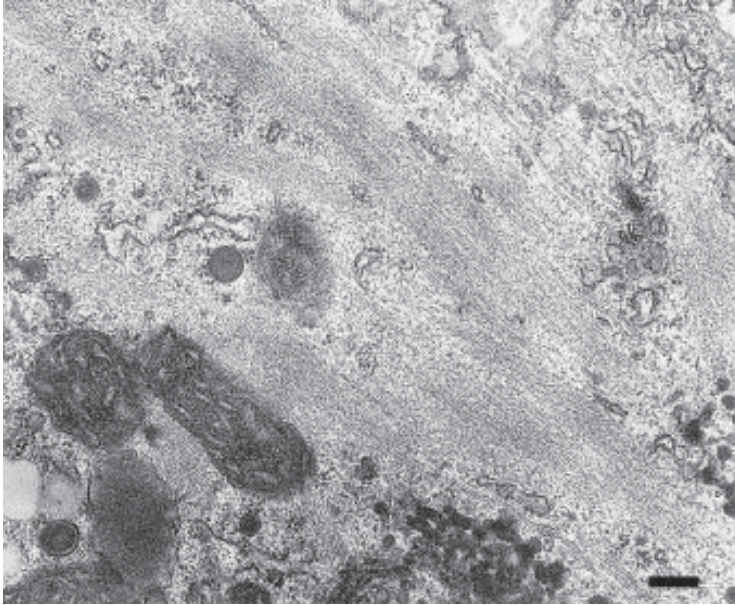


Fig. 3. Detail of the ultrastructure of a *Micrasterias denticulata* cell treated with 3 μ M jasplakinolide for 2 h and fixed for electron microscopy according to **Subheading 3.2.1.**, dense accumulations of F-actin are visible in the cytoplasm. Bar = 0.2 μ m. Reprinted from reference (4) with permission, Copyright© 1997, Wiley-Liss, Inc., a subsidiary of John Wiley and Sons, Inc.

not affected (26), and the distribution of microtubules and microtubule dependent processes were not altered in green algae (4).

Herein different procedures shall be described for the detection of actin filament aggregates generated by application of jasplakinolide. Due to the advantages of electron microscopy and/or immunomethods, these will be mentioned more in detail. However, different protocols for phalloidin stainings will be given as they have been used for some organisms in combination with jasplakinolide treatment (6,17,18).

2. Materials

2.1. Cell Cultures

The unicellular green alga *Micrasterias denticulata* Bréb., well established as a model system for morphogenetic processes (27), is used for light and electron microscopical investigations (see **Subheadings 3.2.1.–3.2.2.**) because alterations in cell shape caused by drug treatments are easily detected. More-

over, the natural distribution of F-actin in these cells has been characterized by different techniques (28).

1. Culture medium: 100 mg/L KNO_3 , 10 mg/L $(\text{NH}_4)_2\text{HPO}_4$, 10 mg/L $\text{MgSO}_4 \cdot 7\text{H}_2\text{O}$, 4 mg/L EDTA, 3.5 mg/L $\text{FeSO}_4 \cdot 7\text{H}_2\text{O}$, 50 $\mu\text{g/L}$ H_3BO_4 , 10 $\mu\text{g/L}$ $\text{MnSO}_4 \cdot 4\text{H}_2\text{O}$, 5 $\mu\text{g/L}$ $\text{ZnSO}_4 \cdot 7\text{H}_2\text{O}$, 5 $\mu\text{g/L}$ $\text{Co}(\text{NO}_3)_2 \cdot 6\text{H}_2\text{O}$, 5 $\mu\text{g/L}$ $\text{Na}_2\text{MoO}_4 \cdot 2\text{H}_2\text{O}$, 25 ng/L $\text{CuSO}_4 \cdot 5\text{H}_2\text{O}$, 10 mL/L of saturated CaSO_4 solution, 30 mL/L soil extract, for details *see* (29).
2. Culture conditions: Cells are grown in culture medium (under semisterile conditions) in a light/dark regime of 14/10 h at 20°C.

Fluorescence microscopy techniques (*see Subheadings 3.2.3.–3.2.5.*) have been adjusted for murine interleukin 2 dependent T cell line CTLL-20 (18), *Dictyostelium* cells NC4A2, AX4 (6) and MDCK cells, strain II (17).

1. cRPMI 1640 culture medium.
2. HL-5 culture medium.

2.2. Chemicals

2.2.1. Drug

1. Methanol reagent.
2. DMSO (dimethyl sulfoxide) reagent.
3. Jasplakinolide, Mol. Wt. 709.68, Molecular Probes (Eugene, Oregon, USA; Leiden, The Netherlands, ordering no. J-7473). 100 μg , diluted upon arrival in methanol or DMSO to achieve 10 mM stock solution and kept refrigerated at -20°C (*see Note 1*).

2.2.2. Electron Microscopy Fixation

1. Cacodylic buffer: 50 mM Cacodylic acid, Na-salt ($\text{C}_2\text{H}_6\text{AsO}_2\text{Na} \cdot 3\text{H}_2\text{O}$), pH 7.2.
2. Cacodylate-glutaraldehyde: 50 mM Cacodylic acid, 1% glutaraldehyde, pH 7.2.
3. Cacodylate-osmium: 50 mM Cacodylic acid, 1% OsO_4 , 0.8% $\text{K}_3[\text{Fe}(\text{CN})_6]$, pH 7.2.
4. 2% Aqueous uranyl acetate dihydrate ($(\text{CH}_2\text{COO})_2\text{UO}_2 \cdot 2\text{H}_2\text{O}$).
5. Ethanol solutions: 15%, 30%, 40%, 50%, 70%, 80%, 90%, 95%, 100%.
6. 1,2 Propylene oxide reagent.
7. Propylene oxide-ethanol mixture: 1,2- Propylene oxide and ethanol (1:1 v/v).
8. A suitable embedding resin: Embed-812, Araldite 502, or others.
9. Propylene oxide-embedding resin mixture: Mixture of 1,2- Propylene oxide and embedding resin (1:1 v/v).
10. Formvar 1595 E.
11. Lead citrate.

2.2.3. Chemicals for Immunoelectron Microscopy

1. 10% Lecithin dissolved in chloroform.
2. Acetone-tannic acid: acetone containing 0.1% tannic acid (v/v).

3. Acetone-osmium: acetone containing 2% OsO₄ and 0.05% uranyl acetate.
4. LR white resin (London resin company, medium grade).
5. TBS: 50 mM Tris buffered saline, pH 7.5.
6. Blocking Solution: TBS containing 1% BSA, 1% acetylated BSA, 0.1% Tween-20.
7. Modified Blocking Solution: TBS containing 1% BSA, 0.1% acetylated BSA, 0.01% Tween-20.
8. 10% bovine calf fetal serum.
9. Primary Antisera/Antibodies, e.g., antiactin monoclonal antibody N 350 (Amersham).
10. 10 nm colloidal gold-conjugated, secondary antibody appropriate for the primary antibody.

2.2.4. Chemicals for Fluorescence Microscopy

1. Paraformaldehyde fixative: 4% paraformaldehyde and cytospun (Cytospin 3 preparation system, Shandon Scientific Ltd., Cheshire, UK).
2. 50 μ M NH₄Cl.
3. PBS: 137 mM NaCl, 2.7 mM KCl, 4.3 mM Na₂HPO₄·7H₂O, 1.4 mM KH₂PO₄, pH 7.5.
4. Triton solution: 0.1% Triton X-100 in PBS.
5. 2% bovine serum albumin (BSA).
6. Anti actin monoclonal antibody N 350 (Amersham).
7. Phalloidin: 0.4 mg/mL FITC-conjugated phalloidin.
8. MCPB fixative: 10 mM Na₂HPO₄, 10 mM KH₂PO₄, 2 mM MgCl₂, 0.2 mM CaCl₂, pH 6.5) containing 2.5% formaldehyde, 0.1% glutaraldehyde, 0.01% Triton X-100 and 1 μ M fluorescent-phalloidin.
9. Jasplakinolide stock solution (*see Subheading 2.2.1.*).
10. Glycerol-gallate mounting medium: 50% glycerol/1% n-propyl gallate in PBS.
11. Texas red conjugated antimouse IgM antibody (Jackson ImmunoResearch).

3. Methods

3.1. Treatment and Recovery Experiments with Developing *Micrasterias* Cells

1. Collect *Micrasterias denticulata* cells of a defined developmental stage under a stereo microscope using a pulled glass Pasteur pipet.
2. Incubate cells in 1 mL of culture medium containing 1.5, 3, 10 μ M jasplakinolide for time periods of 0.5, 1, 2, 3, 4, 24, 48 h (*see Note 2*).
3. Incubate cells in 1 mL of culture medium containing 3 μ M jasplakinolide for 0.5 h, remove the jasplakinolide solution, wash several times with culture medium and allow to develop in culture medium for 3 h. This is regarded as "recovery experiment".
4. Investigate the cells treated as in **steps 2** and **3** under a regular light microscope or fix for electron microscopy (*see Subheadings 3.2.1. and 3.2.2.*).

3.2. Visualization of F-Actin Aggregates After Jasplakinolide Treatment

3.2.1. Chemical Fixation/Electron Microscopy

The procedure described herein was first used for *Micrasterias* cells by Meindl (30).

1. Fix all cells, both treated samples and controls, in cacodylate-glutaraldehyde for 15 min (see **Note 3**).
2. Wash cells 3 times 5 min each in cacodylate buffer.
3. Postfix cells in cacodylate-osmium for 2 h.
4. Wash cells, as in **step 2**, 3 times 5 min each with distilled water.
5. Incubate cells in uranyl acetate for 2 h (see **Note 4**).
6. Wash 3 times 5 min each with distilled water.
7. Dehydrate the cells in increasing concentrations of cold ethanol (see **Note 5**), 15 min per concentration: 15%, 30%, 40%, 50%, 70%, 80%, 90%, 95%, 100%. Keep in 100% for 30 min.
8. Transfer the cells to the propylene oxide-ethanol mixture and allow to equilibrate for 10 min, then transfer to propylene oxide.
9. Transfer the cells to the propylene oxide-embedding resin mixture (see **Note 6**).
10. Rotate the cells in this mixture for 48 h in order to allow the propylene oxide to evaporate and a sufficient penetration of the cells with the resin to be achieved.
11. Transfer the cells to freshly prepared resin in aluminum dishes and orientate them by the use of eyelashes connected to holders.
12. Incubate in an exsikkator for 4 d.
13. Allow the resin to polymerize for 24 h at 60°C.
14. Select cells and section at an ultramicrotome.
15. Collect sections on formvar coated copper grids (see **Note 7**).
16. Counterstain the sections with uranyl acetate and lead citrate (see **Note 8**).
17. Investigate and photograph at a transmission electron microscope at 60–80 kV.

3.2.2. Immunoelectron Microscopy

The following fixation technique has been carried out for *Micrasterias* for the first time by Meindl et al. (31). The recipe for actin detection by means of immunogold localization is based on (32).

1. Prepare gold or aluminum specimen holders with bed depths of 100–300 μm by dipping in lecithin dissolved in chloroform.
2. Collect treated cells to be transferred to specimen holders. Large cells like *Micrasterias* (200 μm in diameter) can be easily collected under a stereo microscope by wrapping with cotton fibers.
3. Fix treated cells by high pressure freeze fixation by the use of a Hyperbaric freeze device (Balzers HPM 010), for other methods (see **Note 9**).
4. Collect and store samples under liquid nitrogen.

5. Transfer samples to a freeze substitution device (Reichert-Jung, cs auto).
6. Substitute samples at -80°C for 24 h in acetone-tannic acid solution.
7. Wash several times with acetone.
8. Substitute samples at -80°C for 24 h in acetone-osmium solution (*see Note 10*).
9. Allow samples to reach -30°C within 5 h.
10. Continue substitution at -30°C for 10 h.
11. Allow samples to reach room temperature (20°C) within 5 h.
12. Remove acetone-osmium solution and rinse several times with acetone.
13. Exchange acetone for ethanol by several rinses.
14. Transfer samples to LR white in aluminum dishes and cover with cellophane foil.
15. Allow samples to infiltrate in an exsikkator for 24 h.
16. Polymerize under UV light at room temperature for 24 h.
17. Prepare sections for electron microscopy as described in **Subheading 3.2.1.**, and transfer to formvar coated gold or gilded copper grids.
18. Incubate in blocking solution for 30 min up to 1 h. A blocking step with 10% bovine calf fetal serum may be applied if blocking is not sufficient.
19. Transfer into primary antibody against actin. Purified antibody may be diluted in Modified Blocking Solution for 1.5 h at room temperature or for up to 24 h at 4°C .
20. Wash 4 times 15 min in TBS by transferring grids to 50 μL droplets of TBS.
21. Incubate in 10 nm-gold (*see Note 11*) labeled secondary antibody diluted in Modified Blocking Solution (*see Note 12*).
22. Wash by rinsing with TBS, followed by incubation in droplets of TBS for 2 min, followed by a brief rinse with distilled water.
23. Counterstain with uranyl acetate and lead citrate if necessary (compare **Subheading 3.2.1.**).
24. Investigate at a transmission electron microscope at 60-80 kV.

3.2.3. *ImmunoFluorescence Microscopy of Jasplakinolide Treated Lymphocytes After Posey and Bierer (18)*

1. Grow CTLL-20 cells in cRPMI 1640 medium.
2. Wash cells with cRPMI 1640-10% three times and resuspend at a final density of 2×10^5 cells/mL.
3. Transfer cells to cRPMI 1640-10% Medium containing jasplakinolide (final concentration of Me_2SO should not exceed 0.1%).
4. Fix cells (1×10^6 /sample) in the paraformaldehyde fixative on glass slides.
5. Incubate cells in NH_4Cl for 5 min.
6. Permeabilize cells with the Triton solution for 2.5 min.
7. Block with BSA.
8. Incubate with 30 $\mu\text{g}/\text{mL}$ anti actin monoclonal antibody for 30 to 45 min at room temperature.
9. Wash three times with PBS.
10. Incubate with 15 $\mu\text{g}/\text{mL}$ Texas red conjugated anti-Mouse IgM antibody for 30 min at room temperature.

11. Wash three times and mount samples in glycerol mounting medium.
12. View at a confocal laser scanning microscope.

3.2.4. FITC-Phalloidin Staining

of Jasplakinolide Treated Dictyostelium Cells After Lee et al. (6) (see **Note 13**)

1. Grow wild-type (NC4A2, AX4) *Dictyostelium* amoebae in 100 mm petri dishes at 22°C in HL-5 medium.
2. Plate the cells over night in a 35 mm dish and remove the cover slip to a Rose chamber.
3. Replace the medium with fresh HL-5 medium containing 3 μM jasplakinolide for 1–2 h.
4. Fix treated *Dictyostelium* cells in MCPB fixative.
5. Investigate at a confocal laser scanning microscope.

3.2.5. FITC-Phalloidin Staining

of Jasplakinolide Treated MDCK Cells After Shurety et al. (17)

1. Grow MDCK cells for 4 days at coverslips or semipermeable filters.
2. Treat cells with 1 μM jasplakinolide for 45 min.
3. Fix cells in paraformaldehyde for 5 min.
4. Permeabilize cells in triton solution.
5. Incubate in FITC-conjugated phalloidin.
6. Mount coverslips in glycerol-gallate mounting medium.
7. Examine at a light microscope fitted for epifluorescence.

4. Notes

1. Jasplakinolide is also dissolvable in DMSO (**19**).
2. For *Micrasterias denticulata* 1.5 μM of jasplakinolide was found to be the lowest effective concentration. Concentrations above 250 μM of jasplakinolide were lethal. The concentrations of jasplakinolide needed for other cells have to be found empirically. However they should be in the same range as described herein, since the effective concentrations correlate with data obtained from the literature (**6,17,19**). Lee et al. (**6**) remark that the effective concentration has varied with different batches and that therefore each lot should be titrated to find an effective concentration before usage.
3. The fixation procedure is performed in a "Balzers Fixomat"—a device not commercially available anymore—consisting of sintered glass suction filters connected via a valve to a pump station, allowing to remove solutions by underpressure while cells remain in the filter. Moreover the temperature can be adjusted via a cooling bath. Alternatively the cells can be fixed in glass dishes, ideally in the shape of a hemisphere. In this case it is best to remove only the solutions with a pipet and not to transfer the cells.

For other organisms more specialized methods might be necessary for example, embedding of the specimens in agarose prior to the fixation procedure.

4. During incubation in uranyl acetate solution it is necessary to keep the cells in darkness, by covering the filter or dish with aluminum foil.
5. During the whole procedure of dehydration the temperature should be kept at 6°C. At the steps 50% and 70% ethanol temperature might be lowered to 4°C. In case of fixation in round glass dishes they should be kept over ice. At the step of 100% ethanol the temperature should be increased to room temperature.
6. Very good results are obtained with a 1:1 mixture of glycid ether 100 (a substance equivalent to Epon 812) and MNA. Prior to use DMP must be added (5 droplets to 10 mL of resin). However, a mixture of Embed-812/Araldite 502/DDSA (DMP-30 or BDMA must be added prior to use) will also give adequate results.
7. Coating of grids with formvar may not be necessary for all objects. We use the following procedure: A light microscopic slide is cleaned with lens tissue, tipped into 0.3% formvar dissolved in chloroform. The resulting formvar film is cut at the edges of the slide and allowed to float on distilled water. Grids are placed on the film which is then removed with parafilm.
8. The time periods needed for counterstaining depend on the staining already achieved during the fixation/staining procedure and are typically 5–30 min for uranyl acetate and 1–5 min for Reynolds' lead citrate.
9. For large cells like *Micrasterias* (about 200 µm in diameter) high pressure freezing has been found the only appropriate technique for freeze fixation. However, for small and less vacuolated cells plunge freezing which might be achieved with a relative simple equipment, will also give reasonable results.
10. OsO₄ dissolves well in acetone. Uranyl acetate is best to be sonicated to dissolve it. For other organisms it might be appropriate to substitute without OsO₄ and uranyl acetate.
11. Gold particles with 10 nm diameter are used commonly. The usage of smaller gold particles might enhance the accuracy of the detected locus.
12. The actual dilution factor has to be found empirically for each system, but it should be in the range of 1:50–1:200.
13. As mentioned in the introduction, the use of phalloidin is problematic due to competitive binding with jasplakinolide. However, some authors were successful in detection of actin aggregates with the methods described in **Subheadings 3.2.4.** and **3.2.5.**

References

1. Brown, S. S. and Spudich, J. A. (1979) Cytochalasin inhibits the rate of elongation of actin filament fragments. *J. Cell Biol.* **83**, 657–662.
2. Cou, M., Brenner, S. L., Spector, I., and Korn, E. D. (1987) Inhibition of actin polymerization by latrunculin A. *FEBS Lett.* **213**, 316–318.
3. Bubb, M. R., Senderowicz, A. M. J., Sausville, E. A., Duncan, K. L. K., and Korn, E. D. (1994) Jasplakinolide, a cytotoxic natural product, induces actin polymerization and competitively inhibits the binding of phalloidin to F-actin. *J. Biol. Chem.* **269**, 14,869–14,871.

4. Holzinger, A. and Meindl, U. (1997) Jasplakinolide, a novel actin targeting peptide inhibits cell growth and induces actin filament polymerization in the green alga *Micrasterias*. *Cell Motil. Cytoskeleton* **38**, 367–372.
5. Sheikh, S., Gratzer, W. B., Pinder, J. C., and Nash, G. B. (1997) Actin polymerisation regulates integrin-mediated adhesion as well as rigidity of neutrophils. *Biochem. Biophys. Res. Comm.* **238**, 910–915.
6. Lee, E., Shelden, E. A., and Knecht, D. A. (1998) Formation of F-actin aggregates in cells treated with actin stabilizing drugs. *Cell Motil. Cytoskeleton* **39**, 122–133.
7. Matthews, J. B., Smith, J. A., and Hrnjez, B. J. (1997) Effects of F-actin stabilization or disassembly on epithelial Cl⁻ secretion and Na-K-2Cl cotransport. *Am. J. Physiol.* **272** (*Cell Physiol.* **41**), C254–C262.
8. Crews, P., Manes, L. V., and Boehler, M. (1986) Jasplakinolide, a cyclodepsipeptide from the marine sponge, *Jaspis* sp. *Tetrahedron Lett.* **27**, 2797–2800.
9. Zabriskie, M. T., Klocke, J. A., Ireland, C. M., Marcus, A. H., and Molinski, T. F. (1986) Jaspamide, a modified peptide from a *Jaspis* sponge, with insecticidal and antifungal activity. *J. Am. Chem. Soc.* **108**, 3123–3124.
10. Braekman, J. C., Daloz, D., and Moussiaux, B. (1987) Jaspamide from the marine sponge *Jaspis johnstoni*. *J. Nat. Prod.* **50**, 994–995.
11. Murray, L. M., Johnson, A., Diaz, M. C., and Crews, P. (1997) Geographic variation in the tropical marine sponge *Jaspis* cf. *johnstoni*: An unexpected source of new terpene-benzoides. *J. Org. Chem.* **62**, 5638–5641.
12. Fabian, I., Shur, I., Bleiberg, I., Rudi, A., Kashman, Y., and Lishner, M. (1995) Growth modulation and differentiation of acute myeloid leukemia cells by jaspamide. *Exp. Hematol.* **23**, 583–587.
13. Ayscough, K. R., Stryker, J., Pokala, N., Sanders, M., Crews, P., and Drubin, D. G. (1997) High rates of actin turnover in budding yeast and roles for actin in establishment and maintenance of cell polarity revealed using the actin inhibitor latrunculin A. *J. Cell Biol.* **137**, 399–416.
14. Chu, K. S., Negrete, G. R., and Konopelski, J. P. (1991) Asymmetric total synthesis of (+)-jasplakinolide. *J. Org. Chem.* **56**, 5196–5202.
15. Inman, W., Crews, P., and McDowell, R. (1989) Novel marine sponge derived amino acids. 9. Lithium complexation of Jasplakinolide. *J. Org. Chem.* **54**, 2523–2526.
16. Kahn, M., Nakanishi, H., Su, T., Lee, J. Y.-H., and Johnson, M. (1991) Design and synthesis of nonpeptide mimetics of jaspamide. *Int. J. Pept. Prot. Res.* **38**, 324–334.
17. Shurety, W., Steward, N. L., and Stow, J. L. (1998) Fluid-phase markers in the basolateral endocytic pathway accumulate in response to the actin assembly-promoting drug jasplakinolide. *Mol. Biol. Cell* **9**, 957–975.
18. Posey, S. C. and Bierer, B. E. (1999) Actin stabilization by jasplakinolide enhances apoptosis induced by cytokine deprivation. *J. Biol. Chem.* **274**, 4259–4265.
19. Scott, V. R., Boehme, R., and Matthews, T. R. (1988) New class of antifungal agents: jasplakinolide, a cyclodepsipeptide from the marine sponge *Jaspis* species. *Antimicrob. Agents Chemother.* **32**, 1154–1157.

20. Inman, W. and Crews, P. (1989) Novel marine sponge derived amino acids. 8. Conformational analysis of jasplakinolide. *J. Am. Chem. Soc.* **111**, 2822–2829.
21. Stingl, J., Andreson, R. J., and Emerman, J. (1992) In vitro screening of crude extracts and pure metabolites obtained from marine invertebrates for the treatment of breast cancer. *Cancer Chemother. Pharmacol.* **20**, 401–406.
22. Senderowicz, A. M. J., Kaur, G., Sainz, E., Laing, C., Inman, W. D., Rodriguez, J., et. al. (1995) Jasplakinolide's inhibition of the growth of prostate carcinoma cells *in vitro* with disruption of the actin cytoskeleton. *J. Nat. Canc. Inst.* **87**, 46–51.
23. Duncan, M. D., Harmon, J. W., and Duncan, K. L. K. (1996) Actin disruption inhibits bombesin stimulation of focal adhesion kinase (pp125^{FAK}) in prostate carcinoma. *J. Surg. Res.* **63**, 359–363.
24. Takeuchi, H., Ara, G., Sausville, E. A., and Teicher, B. (1998) Jasplakinolide: interaction with radiation and hypothermia in human prostate carcinoma and Lewis lung carcinoma. *Cancer Chemother. Pharmacol.* **42**, 491–496.
25. Braet, F., Spector, I., DeZanger, R., and Wisse, E. (1998) A novel structure involved in the formation of liver endothelial cell fenestrae revealed by using the actin inhibitor misakinolide. *Proc. Natl. Acad. Sci. USA* **95**, 13,635–13,640.
26. daCosta, S. R., Yarber, F. A., Zhang, L., Sonee, M., and Hamm, A. S. F. (1998) Microtubules facilitate the stimulated secretion of beta-hexosaminidase in lacrimal acinar cells. *J. Cell Sci.* **111**, 1267–1276.
27. Meindl, U. (1993) *Micrasterias* cells as a model system for research on morphogenesis. *Microbiol. Rev.* **57**, 415–433.
28. Meindl, U., Zhang, D., and Hepler, P. K. (1994) Actin microfilaments are associated with the migrating nucleus and the cell cortex in the green alga *Micrasterias*. *J. Cell Sci.* **107**, 1929–1934.
29. Schlösser, U. G. (1982) List of strains. *Ber. Dtsch. Bot. Ges.* **95**, 181–206.
30. Meindl, U. (1990) Effects of temperature on cytomorphogenesis and ultrastructure of *Micrasterias denticulata* Bréb. *Protoplasma* **157**, 3–18.
31. Meindl, U., Lancelle, S., and Hepler P. K. (1992) Vesicle production and fusion during lobe formation in *Micrasterias denticulata* visualized by high pressure freeze fixation. *Protoplasma* **170**, 104–114.
32. Holzinger, A., De Ruijter, N., Emons, A. M., and Lütz-Meindl, U. (1999) Spectrin-like proteins in green algae (Desmidiaceae). *Cell Biol. Int.* **23**, 335–344.

Site-Directed Antibodies as Tools for Investigating Structure and Function of Cytoskeleton Proteins

Walter Steffen and Julie L. Hodgkinson

1. Introduction

The cytoskeleton is a complex structure composed of three distinct filament systems, microfilaments (actin), intermediate filaments, and microtubules. Each filament system consists of filamentous polymers and their associated proteins. Some of the associated proteins are capable of interconnecting the different filaments systems. The function of the cytoskeleton is manifold; not only is the cytoskeleton responsible for maintaining cell integrity and cell shape; it is also involved in cell locomotion and intracellular transport.

Antibodies can now be used to visualize the location of components within cells and protein complexes and can also be used to study the structure – function relationships. To study a structure – function relationship one can distinguish between two important (active) sites; (a) sites important for protein – protein interaction and (b) sites critical for intramolecular, conformational changes. An example of (a) is the binding between cytoplasmic dynein and dynactin, which can be disrupted and/or blocked by an antibody specific for the N-terminal region of the dynein intermediate chain. Disrupting the dynein-dynactin interaction will then result in a dissociation of dynein from membranous organelles (1). An example of (b) would be antibodies binding to the hinge region of myosin which is involved in conformational changes during the power stroke of myosin (2,3). Therefore, it can be seen that obtaining probes capable of interfering with the active sites will provide a powerful tool to investigate the cellular function of cytoskeletal components and site-directed antibodies can provide such a tool.

In this chapter we will discuss some considerations when generating site directed antibodies, either polyclonal or monoclonal antibodies. We will also provide our protocols of raising polyclonal and monoclonal antibodies, as well as providing protocols for using these antibodies in structural studies and functional assays.

1.1. General Remarks About Strategies to Generate Antibodies, Monoclonal Versus Polyclonal Antibodies

Two strategies can be employed to obtain site-directed antibodies: (a) polyclonal antibodies specific for a certain polypeptide region of the component in question and (b) monoclonal antibodies (4) specific for a particular epitope of functional importance. There are advantages and disadvantages for both of these types of antibodies. While a monoclonal antibody is specific for a single epitope, generating a specific monoclonal can be very time consuming (one should estimate between 3 mon and 1 yr). On the other hand, polyclonal antibodies can be generated within 4 to 6 wk; however, obtaining the appropriate antigen can be quite difficult, because the antigen must be small, well defined, and highly purified. The usefulness of a polyclonal antibody will, therefore, depend on the availability of well characterized protein fragments or synthetic peptides.

The successful approach to generate site directed antibodies will largely be influenced by the current knowledge about a given component. If only limited information about the component is available (i.e., the component has not yet been isolated and no sequence information is available), one can employ a so-called “shot gun approach”. In this approach one attempts to raise a monoclonal antibody to a heterogeneous mix of proteins hoping to isolate the appropriate antibody producing cell line. A successful production of useful monoclonal antibodies to a heterogeneous mix of proteins will, however, be left up to chance and one can easily compare such a method with an attempt to win the lottery. In the following paragraph we will discuss our strategies to enhance the chances in generating sited-directed antibodies specific for the dynactin-dynein motor complex and their employment in structural and functional studies.

1.2. Strategies to Generate Specific Antibodies by Selecting the Appropriate Antigen

Based on what has been discussed above, it becomes apparent that a successful strategy to generate specific site-directed antibodies will be governed by the selection of the antigen. Furthermore, selecting the appropriate antigen will be influenced by the current knowledge in terms of protein–protein interaction and possible binding sites. Protein binding studies and sequence analysis

will be essential in selecting the appropriate region of a protein. Based on such studies one can generate synthetic peptides, bind them onto a carrier protein and use them as antigens. Alternatively or in addition, one can generate the appropriate cDNA truncation mutants, express them in bacteria, and use them as antigens. It will be beyond the scope of this chapter, however, to describe here the generation and expression of cDNA truncation mutants.

1.3. Screening Assay

To study the structure–function relationships by using site directed antibodies it is important that these antibodies fulfil some basic requirements and these requirements have to be considered when screening for the appropriate antibodies. Foremost, it is essential that the antibodies are capable of recognizing the native components. While the screening for antibodies recognizing native proteins can be carried out by ELISA or dot blot, these assays require a highly purified antigen because they do not distinguish between a specific reaction with the antigen in question or a contaminant. In terms of its specificity the SDS-PAGE immunoblot provides a screening assay with a very high reliability while still allowing the screening of a large number of antibody clones. We have used quite successfully a SDS-PAGE immunoblot assay as a primary screening assay for testing antibodies followed by a dot blot as secondary assay.

1.4. Establishing a Functional Assay

When producing monoclonal antibodies, a functional assay as primary screening assay to identify functional antibodies is normally not feasible because of the limited concentration of antibody in cell culture supernatant. A functional assay will, therefore, be used as secondary assay after an antibody has been identified as recognizing the native component. Functional studies can be carried out by microinjecting antibodies into cells and then analyzing their effect. However, microinjecting antibodies is time consuming and the results are not always easy to interpret. Therefore, whenever possible one should establish an *in vitro* functional assay that reflects a particular cellular process and that can easily be reproduced. We will describe here our ER network formation assay which can be used to study any of the components involved in microtubule-dependent membrane transport or ER network formation in general.

2. Materials

2.1. Production of Polyclonal Antibodies

1. 20G, and 21G hypodermic needle.
2. 3-way stopcock (Luer lock).
3. 50 mL conical centrifuge tubes.
4. 50 mM ammonium acetate, pH 8.0.

5. 70% ethanol.
6. Clinical centrifuge.
7. Freund's Adjuvant, complete.
8. Freund's Adjuvant, incomplete.
9. Rabbits "New Zealand White" about 3 mo old.
10. Razor blades.
11. Restraining box.
12. Two 5 mL glass syringes (Luer lock) (Do not mix plungers of different syringes).
13. Water bath.

2.2. Ammonium Sulfate Purification of Polyclonal Antibodies

1. 40 mL centrifuge tubes.
2. Dialysis tubing.
3. PBS: 20 mM sodium phosphate, 150 mM NaCl, pH 7.4.
4. Peristaltic pump.
5. Saturated ammonium sulfate, 2 mM EDTA, pH 8.0 (kept at 4°C).

2.3. Production of Monoclonal Antibodies

1. 21G and 23G hypodermic needle.
2. 48-well cell culture plates.
3. 96-well cell culture plates.
4. Clinical centrifuge.
5. Dulbecco's modified Eagle's Medium (DMEM).
6. DMEM-FCS: DMEM, 10% Fetal Calf Serum (FCS), 10 μ M mercapto ethanol.
7. ELISA plates.
8. Freund's Adjuvant, complete.
9. Freund's Adjuvant, incomplete.
10. Haematocytometer.
11. HAT medium: DMEM, 0.1 mM hypoxanthine, 40 μ M aminopterin, 1.6 μ M thymidine.
12. HT medium: DMEM, 0.1 mM hypoxanthine, 1.6 μ M thymidine.
13. Hybri-Max fusion medium: 50% polyethylene glycol (w/v), 10% DMSO (v/v) in PBS. This medium is marketed as PEG/DMSO solution from Sigma (cat. # P-7306).
14. Lysis buffer: (A): 0.83 g NH_4Cl /100 mL, pH 7.2 and (B): 2.06 g Tris/100 mL, pH 7.2. Mix 9 mL of lysis buffer A with 1 mL lysis buffer B prior use.
15. Mice, Balb/c, female, 8–12 wk of age.
16. Multichannel pipettor.
17. Myeloma cells, X63-Ag 8.653, non-secreting.
18. Nitrocellulose.
19. PBS: 10 mM sodium phosphate, 150 mM NaCl, pH 7.4.
20. Phosphatase substrate: NBT/BCIP.
21. Phosphatase-conjugated anti-mouse IgG.
22. Tryptophan Blue.

23. Sterile tools for cell fusion:
 - a. Sterile Petri dishes.
 - b. Sterile 15 mL conical tubes.
 - c. Sterile 50 mL conical tubes.
 - d. Sterile forceps.
 - e. Sterile scissors.
 - f. Sterile wire mesh screen (0.5 mm mesh size; can be obtained at a local metal store as Stainless steel, wire screen.)
 - g. Sterile Pasteur pipets.
 - h. Several sterile boats for the multichannel pipettor.
 - i. Sterile 3cc plastic syringe.

2.4. Antibody Isolation from Cell Culture Supernatant

See Chapter 12, this volume.

2.5. Immuno-Electron Microscopy of Protein Complexes

See Chapter 11, this volume.

2.6. ER Network Formation Assay

1. 1 mg/mL cycloheximide.
2. 2% cysteine.
3. 11 mm round cover glasses.
4. Acetate buffer: 100 mM K-acetate, 2.5 mM Mg-acetate, 5 mM EGTA, 10 mM HEPES, 50 mM sucrose, 1mM dithiothreitol, pH 7.2.
5. Double-sided sticky tape.
6. Energy mix: 150 mM creatine phosphate, 20 mM Mg-ATP, 2 mM EGTA.
7. Glass slides.
8. Ionophore A23187.
9. Liquid N₂.
10. MNR/4 buffer: 100 mM NaCl, 2 mM KCl, 1 mM MgSO₄, 2 mM CaCl₂, 5mM HEPES, 0.1 mM EDTA, pH 7.8.
11. VALAP: equal weight of vaseline, lanolin and paraffin melted at about 50°C.

3. Methods

3.1. Production of Polyclonal Antibodies

To produce polyclonal antibodies the rabbits should be 3–4 kg in weight and about 3 mo old. About a third of the rabbit have endogenous anti-keratin antibodies and immunoactivity for various other cellular components. This emphasizes the importance of collecting pre-immune serum from any given rabbit.

3.1.1. Bleeding Procedure

1. Place the rabbit securely in a restraining box leaving the ear accessible and keep the rabbit relatively calm. Up to 50 mL blood can easily be collected from the main artery running down the center of the dorsal surface of the ear.

2. Shave left ear around the vein with a fresh razor blade.
3. Swab ear with 70% ethanol or isopropanol.
4. Hold the tip of the ear (firmly) and the collection tube in one hand and with the free hand insert a 21G hypodermic needle into the dilated artery. The blood should begin to flow immediately into the collection tube. For best results use a portion of artery mid-way along the ear.
5. Apply pressure just anterior to point of entry of needle to stop bleeding.

3.1.2. Obtaining Serum

1. Swirl tube with collected blood to coat surface and to prevent clot attachment to the tube.
2. Incubate blood at 37°C for 1 h.
3. Centrifuge at 2500g for 10 min.
4. Remove clot and spin serum at 3000g for 10 min.
5. Serum should be stored frozen.

3.1.3. Immunization

1. Dissolve ~400–600 µg antigen (~100 µg per rabbit per injection) in 2.2 mL 50 mM ammonium acetate, pH 8.0 or other appropriate buffer. The amount of required antigen can vary depending on the antigenicity of the protein to be injected.
2. Using a 5 mL glass syringe connected with a 20G hypodermic needle draw up 1.1 mL of Freund's complete adjuvant, then draw up 1.1 mL of antigen solution.
3. Freeze remaining 1.1 mL for boost.
4. Keeping the plunger immobile, remove the needle and attach a sterile 3-way stopcock.
5. Mix the antigen with the adjuvant by attaching a second glass syringe to the stopcock and injecting back and forth. (Caution if using plastic syringes: some plastic syringes might react with the mineral oil from the Adjuvant.)
6. A complete emulsion will be formed after about 20 min indicated by a rather sudden increase in viscosity of the solution. **Caution:** be sure that the mounting is secure!
7. To ensure that mixing is complete wait about 20 min before injection. The oil will separate again, if mixing was incomplete.
8. Shave back of rabbit from shoulder blades to pelvis.
9. Clean back with 70% ethanol or isopropanol
10. Inject the antigen mixture under the skin into about 10–15 sites along the spine between shoulder blade and pelvis using a 21G hypodermic needle. (Note: The first injection should take place one week after last preimmune bleeding).
11. Wait one month and boost with a mixture of antigen and Freund's incomplete adjuvant but avoid scars from previous injection.
12. Bleed after one week to check for immune-response (dot-blot, ELISA, etc.). The boost can be repeated, if immune response was too weak; however, a different rabbit should be chosen, if rabbit did not react at all.

3.2. Ammonium Sulfate Purification of Polyclonal Antibodies

Ammonium sulfate precipitation of immunoglobulins is an easy and fast method to purify polyclonal antibodies from serum. The IgG fraction of an antiserum is of sufficient purity for many studies.

1. Pool serum from one rabbit. All steps should be carried out at 4°C.
2. Determine volume of serum: V_1 .
3. Add 2/3 of volume of V_1 saturated ammonium sulfate. Note: add ammonium sulfate very slowly, dropwise (use a peristaltic pump) while stirring.
4. Stir for 15 min.
5. Centrifuge at 12,000g (Beckman JA-20: 10,000 rpm) for 10 min.
6. Discard supernatant.
7. Resuspend pellet in PBS [1/2 vol of V_1].
8. Centrifuge at 12,000g for 10 min, discard pellet.
9. Collect supernatant in beaker, wash tube walls with PBS.
10. Determine volume: V_2 .
11. Add 2/3 vol. V_2 saturated ammonium sulfate dropwise, while stirring. Continue stirring for 15 min.
12. Transfer suspension to 40 mL centrifuge tubes.
13. Centrifuge at 12,000g for 10 min.
14. Discard supernatant.
15. Resuspend pellets in 1/4 V_1 PBS.
16. Dialyse against PBS, 3 times for 6 h each.
17. Measure volume of purified IgG fraction and bring up to 1/2 vol V_1 with PBS.
18. Determine protein concentration. 1 mg/mL IgG corresponds to about 1.5 OD_{280nm}.

3.3. Production of Monoclonal Antibodies (see Note 1)

3.3.1. Injection Protocol (4 Wk Protocol)

1. Day 0: 1st immunization: mix dissolved antigen with Freund's complete adjuvant at a ratio of 1:1; use about 100 µg antigen per mouse (see protocol for polyclonal antibodies).
2. Day 14: 2nd injection: for 2nd to 4th injection use antigen in Freund's incomplete adjuvant.
3. Day 21: 3rd injection
4. Day 28: 4th injection
5. Day 30: collect some blood from the tail vein; separate serum and use for immuno-test (e.g., ELISA, immunoblot, dot-blot).
6. The desired titer of antibodies should be better than 1:500 for immunoblot and better than 1:30 for immunofluorescence

3.3.2. Preparatory Steps for Cell Fusion

1. Start culturing mouse myeloma cells 2 wk prior to planned fusion.
2. Test myeloma cells for genetic defect of the main biosynthetic pathway of guanosine by culturing an aliquot of the myeloma cell in the presence aminopterin

(see below: culturing of hybridoma cells). Blocking this pathway with aminopterin will be used later to select fused hybridoma cells from unfused myeloma cells.

3. Proceed with steps described in **Subheadings 3.3.2.1.** and **3.3.2.2.** in parallel using the spleen of one mouse and X63-Ag8.653 mouse myeloma cells. Perform all steps in a laminar flow hood.

3.3.2.1. USE THE SPLEEN OF ONE MOUSE

1. Remove spleen under sterile conditions.
2. Remove fat tissue and wash 2 times with DMEM medium in Petri dish.
3. Mince spleen with scissors and press through a 0.5 mm wire screen using 3 cc syringe plunger.
4. Wash screen with 10 mL DMEM medium.
5. Transfer cells to 15 mL conical tube and allow chunks to settle for about 5 min.
6. Transfer supernatant to new 15 mL conical tube.
7. Spin at 330g for 5 min.
8. Discard supernatant.
9. Resuspend cell pellet in 10 mL lysis buffer (to lyse red blood cells); Mix 9 mL of lysis buffer A with 1 mL of lysis buffer B.
10. Allow to lyse for 10 min and spin at 330g for 5–10 min.
11. Resuspend cell pellet in 10 mL DMEM medium; take an aliquot and dilute it 1:50 for cell count; spin at 330g for 5 min.
12. Resuspend cell pellet in 20 mL DMEM medium.
13. Cell count: about 10^8 cell per mouse.

3.3.2.2. USE X63-AG 8.653 MOUSE MYELOMA CELLS

1. Judge the quality of the myeloma cells by light microscopy: A smooth, round shape is essential for a good fusion.
2. Centrifuge at 1200 rpm for 5 min. Resuspend cells in 20 mL DMEM and count cells.

3.3.3. Spleen Cells-Myeloma Cells Fusion

1. Combine spleen cells (20 mL) with myeloma cells at a ratio of 5:1, mix and centrifuge at 280g rpm for 5 min.
2. Discard supernatant and loosen pellet by rubbing the tube along the metal grid of the laminar flow cabinet. Add 2 mL Hybri-Max fusion medium, resuspend pellet gently and let stand for exactly 1 min (*see Notes 2 and 3*).
3. Add 10 mL DMEM medium dropwise while gently shaking. Add additional 10 mL DMEM medium slowly while mixing (*see Notes 2 and 3*).
4. Centrifuge at 280g for 5 min; discard supernatant.
5. Resuspend cells in HAT medium and dilute to 0.5×10^6 cell/mL based on previous cell count.
6. Plate into 96-well plates; 200 μ L per well using a multi-channel pipettor.
7. Leave cells undisturbed for at least one week.
8. After 10 d start checking 96-well plates for cell colonies.

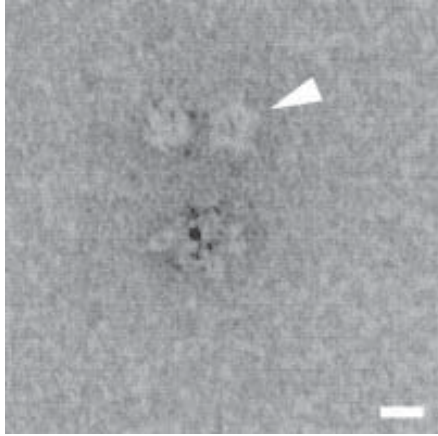


Fig. 1. Structural analysis: immunogold localization of a subunit within the complex of cytoplasmic dynein. A monoclonal antibody specific for the N-terminus of the dynein intermediate chain was conjugated with a 2–3 nm colloidal gold particle and used to identify the location of the intermediate chain at the base of the dynein complex (for a more detailed description of the labeling protocol *see* Chapter 11, this volume). Arrowhead indicates the globular heads of dynein. Magnification bar 10 nm.

9. Take 100 μ L cell culture supernatant for screening assay.
10. Transfer colony to a 48-well plate and add new culture medium (HT medium).
11. Keep all cell lines, which had been tested positive by screening assay, in culture.
12. Carry out “subcloning” as soon as possible (*see* **Subheading 3.3.4.**). One should also freeze cells from each positive cell line as back up.

3.3.4. Screening Procedures

The screening assay of choice depends on availability of antigen and on desired antibodies. For many applications the method of choice will be an ELISA test. The ELISA test is fast and in addition many clones can be tested at once. For an ELISA assay the antigen should have a high degree of purity. Before using an ELISA assay, one should determine the capacity of the plastic surface of the ELISA plates to bind the antigen.

Frequently, the antigen is not pure enough to avoid false positive clones in an ELISA assay. Furthermore, studies may require that the antibodies also recognize the components by SDS-PAGE immunoblot. Under these conditions a SDS-PAGE immunoblot should be used as primary screening assay. A nitrocellulose replica of a single minigel is sufficient to test more than 100 clones. We use plexiglass plates with milled in troughs, 3 cm long, 2 mm wide and 4 mm deep. 120 μ L cell culture supernatant per trough will be sufficient, if half-sized minigels (gel length 3 cm) are used to generate nitrocellulose repli-

cas. The SDS-PAGE immunoblot is nearly as fast as the ELISA assay and a few hundred clones can easily be tested at a given time, if an appropriate incubation tray is used.

3.3.5. Cloning and Expanding of Cell Lines

Cells have to be cultured under limited dilution (“subcloning”), to ensure that a given clone is derived from a single cell. The first subcloning should be carried out soon after a clone has been tested positive. The clones will be cultured at a concentration of 0.1, 0.2, and 0.5 cell/well (1 plate for each). It is also recommended that duplicate 96-well plates be prepared for each dilution. The subcloning should then be repeated a second time.

3.4. Protein G Affinity Purification of Antibodies

See Chapter 12, this volume.

3.5. Immunogold Electron Microscopy of Protein Complexes

See Chapter 11, this volume and Fig. 1.

3.6. Functional Assay:

ER-Network Formation as an Assay to Test Functional Antibodies (Modified According to Allen and Vale, [5])

3.6.1. Isolation of Cytoplasmic Extract of *Xenopus* Oocytes (see **Note 4**)

1. Wash eggs in MNR/4 buffer.
2. Wash eggs with freshly prepared 2% cysteine, pH 7.8 to remove jelly coat.
3. Wash eggs again 3 times with MNR/4 buffer each.
4. To obtain interphase extract activate with 0.4 $\mu\text{g}/\text{mL}$ ionophore A23187 for 5 min.
5. Wash eggs in MNR/4 containing 100 $\mu\text{g}/\text{mL}$ cycloheximide and incubate at room temperature for 20 min.
6. Wash eggs twice with ice cold acetate buffer.
7. Settle eggs by centrifugation at 150g for 1 min followed by centrifugation at 600g for 30 s.
8. After removing excess buffer crush eggs by centrifugation at 10,000g in a swing out rotor (e.g., Beckman SW60 at 10,000 rpm) for 20 min.
9. Collect the cytosol, add 0.05 volume of energy mix and protease inhibitors, snap-freeze as 50 to 100 μL aliquots in liquid N_2 , and store at -80°C .

3.6.2. ER-Network Formation

1. To construct a small microscope flow chamber place two strips of double-sided sticky tape (3M) at a spacing of about 2–3 mm onto a glass slide and stick down an 11 mm circular cover glass (6).
2. Dilute extract with acetate buffer and supplement cytoplasmic extract with 1 mM ATP and the appropriate concentration of antibody (usually about 10 to 500 $\mu\text{g}/\text{mL}$

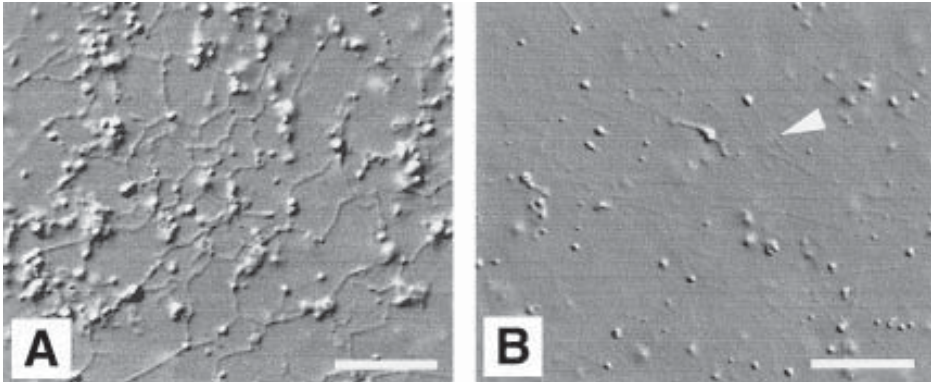


Fig. 2. Functional assay: inhibition of the function of cytoplasmic dynein during ER network formation using an epitope-specific antibody. **(A)** Cytoplasmic extract of *Xenopus* oocytes supplemented with control antibody, placed in a microscope flow chamber and incubated for 30 min at room temperature. **(B)** The same as in **(A)** but in the presence of 100 $\mu\text{g}/\text{mL}$ monoclonal antibody specific for dynein intermediate chain. The arrowhead in **(B)** points towards microtubules. Note there is no ER-network formed in the presence of the dynein-specific antibody. Bar represents 10 μm .

final concentration) and incubate on ice for 10 min. The final dilution of the extract should be between 1:3 and 1:5.

3. Place extract into the flow chamber and seal with VALAP.
4. Incubate for 30 min at room temperature and analyze for development of an ER-network by video enhanced differential interference contrast microscopy (see Fig. 2).

4. Notes

1. Our protocols rely on the use of animals to raise site specific antibodies. The successful generation of such antibodies will largely depend on the selection of appropriate antigens. A major problem with the standard protocol to raise monoclonal antibodies lies in the rather low cell fusion rate between spleen cells and myeloma cells and in the rather low survival rate of hybridoma cells. More recently molecular genetics techniques have been established to produce epitope-specific antibodies. These techniques rely on the fact that antibodies contain highly conserved regions, which can be utilized in PCR technology. Two systems are currently available; a bacteriophage lambda vector system (7) and the phage display system developed by the laboratory of Greg Winter (8). Employing these techniques will avoid the loss of antibodies due to an unsuccessful cell fusion or a failure of the survival of hybridoma cells. It can therefore be expected that future antibody production will involve more molecular genetics techniques.

2. It is critical for the success of this part of the protocol that the fusion pellet be resuspended gently and stand for exactly 1 min prior to adding DMEM medium.
3. It is critical that the DMEM medium is added slowly while mixing (*see Note 2*).
4. Additional details for preparation of *Xenopus* extracts can be found in Chapter 18, this volume.

References

1. Steffen, W., Karki, S., Vaughan, K. T., Vallee, R. B., Holzbaur, L. E., Weiss, D. G., and Kuznetsov, S. A. (1997) The 74-kD intermediate chain of cytoplasmic dynein is involved in binding the motor to membranous organelles. *Molec. Biol. Cell* **8**, 2077–2088.
2. Flicker, P. F., Peltz, G., Sheetz, M. P., Parham, P., and Spudich, J. A. (1985) Site-specific inhibition of myosin-mediated motility in vitro by monoclonal antibodies. *J. Cell Biol.* **100**, 1024–1030.
3. Peltz, G., Spudich, J. A., and Parham, P. (1985) Monoclonal antibodies against seven sites on the head and tail of *Dictyostelium* myosin. *J. Cell Biol.* **100**, 1016–1023.
4. Köhler, G. and Milstein, C. (1975) Continuous cultures of fused cells secreting antibody of predefined specificity. *Nature* **256**, 495–497
5. Allen, V. and Vale, R. (1994) Movement of membrane tubules along microtubules in vitro: evidence for specialized sites of motor attachment. *J. Cell Sci.* **107**, 1885–1897.
6. Weiss, D. G., Maile, W., Wick, R. A., and Steffen, W. (1999) Video microscopy. In: *Light Microscopy in Biology. A practical approach.* (ed.) A. J. Lacey, Oxford University Press, pp. 73–149.
7. Huse, W. D., Sastry, L., Iverson, S. A., Kang, A. S., Alting-Mees, M., Burton, D. R., Benkovic, S. J., and Lerner, R. A. (1989) Generation of a large combinatorial library of the immunoglobulin repertoire in phage lambda. *Science* **246**, 1275–1281.
8. Winter, G., Griffiths, A. D., Hawkins, R. E., and Hoogenboom, H. R. (1994) Making antibodies by phage display technology. *Annu. Rev. Immunol.* **12**, 433–455.

Direct Labeling of Components in Protein Complexes by Immuno-Electron Microscopy

Julie L. Hodgkinson and Walter Steffen

1. Introduction

Immunogold labeling has been used extensively to study the localization and distribution of antigens within cells and tissue. Gold-antibody complexes are generated by charge interaction of the colloidal gold with the antibody, although the exact nature of this interaction is not fully understood. Colloidal gold can be prepared in sizes ranging from 1 nm to over 30 nm allowing a simultaneous detection of several antigens within the same electron microscope preparation. Colloidal gold conjugated antibodies can be employed to label whole cells for light microscopy and to stain ultrathin sections for electron microscopy. In addition colloidal gold probes can also be used to identify the position of subunits within isolated protein complexes. We will present here our methods of preparing colloidal gold-conjugated primary antibodies. In combination with a modified technique of negative staining these primary antibodies can then be employed to identify subunits within protein complexes.

2. Materials

2.1. Preparation of Holey Formvar Film

1. 0.5% (w/v) Formvar in chloroform (freshly prepared).
2. 1,2 dichlorethane.
3. 400-mesh copper grids.
4. 50 mL Schott bottle (wide neck).
5. 50% glycerol in dH₂O.
6. Glass dish spray-painted black of 7 cm depth and 12 cm width (or larger).

From: *Methods in Molecular Biology*, vol. 161: *Cytoskeleton Methods and Protocols*
Edited by: R. H. Gavin © Humana Press Inc., Totowa, NJ

7. Glass Petri dishes.
8. Lens paper, lint-free.
9. Magnetic stirrer.
10. Methanol.
11. Microprobe sonicator.
12. Microscope slides.
13. Razor blades.
14. Staining jar.
15. Whatman filter paper #4.

2.2. Preparation of Carbon-Coated Mica Sheets

1. Carbon evaporator unit.
2. Carbon rods, spectrographically pure (e.g., Agar Scientific).
3. Mica sheets 3×1 inch, e.g., Agar Scientific G250-1 (*see Note 1*).

2.3. Preparation of 2–3 nm Colloidal Gold

1. 0.2M K_2CO_3 , 0.22 μm filtered.
2. 1% $HAuCl_4$ in dH_2O .
3. 1.0M NaSCN, 0.22 μm filtered.
4. 200 mL siliconized Erlenmeyer flask

2.4. Labeling of Antibody with 2–3 nm Colloidal Gold

1. 10 mg/mL Bacitracin, 0.22 μm filtered.
2. 10 mg/mL BSA (bovine serum albumin), 0.22 μm filtered.
3. 10% NaCl.
4. 10% NaN_3 (kept in dark bottle).
5. 10% sucrose in PBS.
6. 10X TBS: 100 mM Tris-HCl, 1.5M NaCl, pH 7.4.
7. 10 mL centrifuge tubes (Nalgene, Oak Ridge Centrifuge Tubes).
8. 2 mM borax.
9. Centricon-30 Microconcentrator (Amicon).
10. Spectrophotometer.
11. Ultracentrifuge.

2.5. Negative Staining of Immunogold-Labeled Protein Complexes

1. 1% (w/v) uranyl acetate in dH_2O (kept in the dark).
2. 1.5 mL Eppendorf reaction vials, painted black.
3. Carbon-coated mica.
4. Forceps (several pairs of self-closing fine-tipped forceps).
5. Grids with holey carbon film or holey Formvar film.
6. Razor blades.
7. Small, adjustable angled lamp.
8. Whatman filter paper #4.

3. Methods

3.1. Preparation of Holey Formvar Film and Holey Carbon Film (see Note 2)

1. Prepare fresh Formvar solution. Stir with magnetic stirrer for about 15–20 min.
2. Prepare fresh glycerol solution.
3. Add 15–20 drops of glycerol solution to dissolved Formvar.
4. Shake vigorously for 30 s.
5. Sonicate for 2 min at full power using a microprobe sonicator. Probe 1/3 from bottom of solution in a 50 mL Schott bottle (see Note 3).
6. Transfer solution into a staining jar.
7. Clean several microscope slides with lint-free lens paper.
8. Dip slides one at a time into the Formvar solution, remove rapidly and vertically to ensure an even film, stand on their ends on filter paper, and let dry completely. (Note: prepare all of the slides at one time, because the dispersion is unstable and the droplets slowly coalesce).
9. Test of film quality: As soon as a slide is dry, float off the film, pick up a couple of test grids, dry briefly, and check in EM for hole size, number and distribution. The holes should be larger than the viewing field at the desired working magnification.
10. Fill glass dish to the brim with clean dH₂O.
11. Wipe surface with sheet of lint-free lens tissue.
12. Score edges of slide with clean razor.
13. Breath lightly onto the slide.
14. Carefully float off the film on to the water surface by slowly sliding the slide into the water at a 45° angle (see Note 4).
15. Place grids on film, rough (dull) surface down. (**Caution:** do not overload film with grids, otherwise it will sink! As a rough guide no more than 25–30 grids per slide-sized piece of Formvar).
16. Pick grids and film up with #4 Whatman filter paper by gently touching the paper horizontally to floating Formvar film.
17. After grids are dry, place filter paper / grids / Formvar on a bed of filter paper saturated with methanol in a glass Petri dish for 10 min. This “etching” procedure removes glycerol/water droplets and dissolves any very thin plastic.
18. After the grids are dry, check a grid in the scope to ensure the quality and size of holes.
19. Place filter paper with grids in a glass Petri dish and store in refrigerator.
20. To obtain more stable carrier films, the Formvar film can be replaced by a carbon film, although this is not always necessary:
 - a. Coat grid heavily with carbon.
 - b. Place filter paper / grids / Formvar / carbon on a bed of filter paper saturated with 1,2 dichloroethane in a glass Petri dish for 2 h. This removes the Formvar, leaving the holey carbon.
 - c. Remove and dry in a glass Petri dish.
 - d. Store grids in a grid box.

3.2. Prepare Carbon-Coated Mica Sheets

1. Freshly cleave mica sheets. Keep cleaved side clean, do not touch with fingers at any time!
2. In a carbon evaporator expose mica sheets with new surface towards the carbon source.
3. Coat mica sheets at a vacuum better than 1×10^{-6} with thin (about 10 nm) carbon film (Note: gradual deposition over several evaporations produces stronger and better quality carbon film).
4. Remove coated mica sheets from carbon evaporator, cover, and store in refrigerator (careful, very delicate).

3.3. Preparation of 2–3 nm Colloidal Gold, Modified According to Baschong et al. (1)

1. Add 0.5 mL of 1% HAuCl₄ to 100 mL dH₂O in a siliconized Erlenmeyer flask
2. Add 0.75 mL of 0.2M K₂CO₃ to gold solution while stirring.
3. Add 0.3 mL of 1M NaSCN while stirring (note that the solution will become yellowish).
4. Leave solution in a dark place overnight and use it the following day for binding to antibodies.

3.4. Labeling of Primary Antibody with 2–3 nm Colloidal Gold (see Notes 5 and 6)

1. Dialyse antibody into 2 mM Borax or use Centricon filter for buffer exchange.
2. Adjust colloidal gold solution to pH 8.0.
3. Determine the minimum amount of antibody needed to stabilize the gold:
 - a. Prepare a serial dilution of antibody from 100 µg to 5 µg IgG per 100 µL dH₂O.
 - b. Add 0.5 mL colloidal gold solution and incubate for 2 min.
 - c. Add 0.5 mL of 10% NaCl and incubate for 30 min.
 - d. Measure the turbidity (formation of aggregates) using a Spectrophotometer at OD_{550nm}. (An increase in turbidity will mark the minimal concentration to stabilize gold particles).
4. Add antibody at the determined minimal concentration (usually about 20 µg/mL) to colloidal gold solution while stirring and incubate on ice for 15 min.
5. Add 100 µg/mL bacitracin or BSA to cover free surface of gold particles and incubate on ice for 60 min.
6. Add 1/10th of volume of 10X TBS.
7. Centrifuge through a 1mL 10% sucrose cushion in a Beckman 80Ti rotor at 47,000 rpm (150,000g_{ave}) for 30 min.
8. Aspirate supernatant and resuspend soft pellet in about 200 µL TBS containing 0.02% NaN₃ and store in refrigerator.

3.5. Negative Staining of Immunogold-Labeled Protein Complexes (2) (see Note 7)

1. Mix gold-conjugated primary antibody with isolated purified protein complex and incubate at room temperature for 10 min.

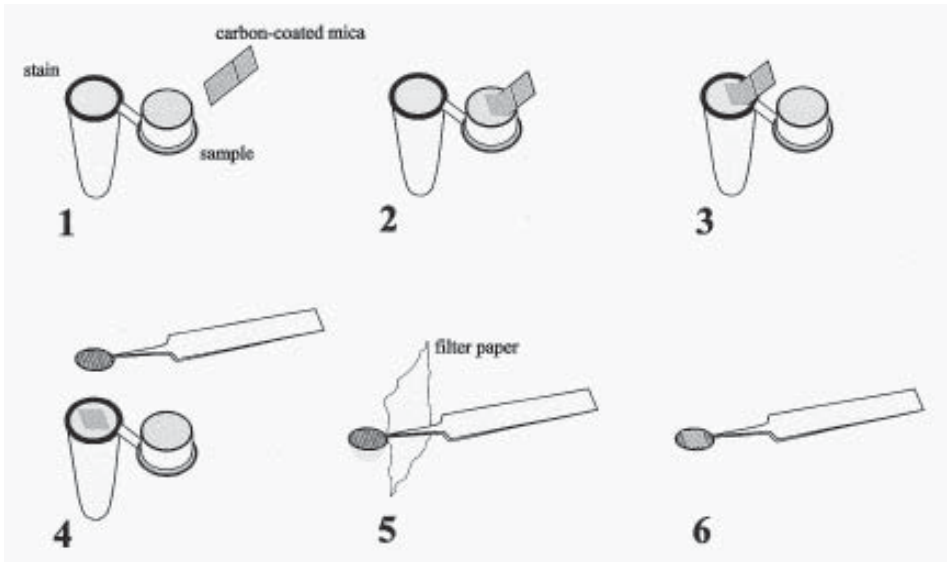


Fig. 1. Flow chart for negative staining of protein complexes. For an explanation of diagram see **Subheading 3.5**.

2. Dilute protein complex–antibody mixture to about 10 to 20 $\mu\text{g}/\text{mL}$ and place about 250 μL of the mixture into the cap of an 1.5 mL Eppendorf reaction vial (**Fig. 1, step 1**).
3. Fill the reaction vial with freshly filtered 1% uranyl acetate. Note that the meniscus of the staining solution should be slightly above the rim of the reaction vial (**Fig. 1, step 1**).
4. Cut a thin carbon-coated mica sheet into about 3×5 mm pieces and score the carbon film with a clean razor blade about 2 mm from one side of the small mica sheet.
5. Using a pair of self-closing fine tipped forceps partially float off the thin carbon film from the supporting mica sheet onto the surface of the protein solution (**Fig. 1, step 2**).
6. Withdraw the carbon film after 2–3 s and float the carbon film completely free of the mica onto the surface of the staining solution (**Fig. 1, step 3**).
7. Pick up the carbon film immediately with a 400-mesh grid coated with a holey carbon or holey Formvar film. (Note: use a small adjustable angle light source to help visualise the thin carbon by reflection) (**Fig. 1, step 4**).
8. Remove excess of uranyl acetate staining solution with filter paper (**Fig. 1, step 5**).
9. For optimal resolution take electron micrographs under low electron dose. An example is shown in **Fig. 1** in Chapter 10, this volume.

4. Notes

1. For some mica brands, carbon may not float off easily.
2. High-resolution electron microscopy of biological samples requires very thin and stable carrier films. These two features are almost incompatible; when reducing the thickness, the film becomes less stable. A higher stability of the carrier film can be produced when using holey Formvar and holey carbon film with a hole size slightly bigger than the viewing area at the required magnification.
3. The amount of glycerol and sonication time will vary depending on size and density of holes needed.
4. Reflected light from a lamp, and/or a dark surface underneath the glass dish will help clearly observe films.
5. When whole cells or ultrathin sections are stained by an indirect method (primary and gold-conjugated secondary antibody), the distance between the colloidal gold and the epitope is normally below the level of resolution of these techniques. However, when protein complexes are labeled and visualized by negative stain electron microscopy, the distance between gold and antigen-binding site can be of great significance. The size of an antibody is about 15 nm. So, if an antigen is detected by indirect means, the distance of a gold particle (center of the particle) from the epitope will be about 30 nm, even though a small gold particle such as 1 nm gold is used. For example, cytoplasmic dynein is a protein complex of about 40 to 50 nm. To identify a subunit within a complex of that size, it is therefore necessary to bring the gold particle much closer to the epitope. A gold conjugated primary antibody will bring the gold particle within a range of about 15 nm. Further improvement in resolution can be achieved when the colloidal gold is bound to a Fab fragment. Such fragments can easily be obtained by a papain digest of IgGs (3).
6. While colloidal gold can easily be prepared in different sizes, binding a single gold particle per IgG or Fab fragment might present a challenge. By varying the protein colloidal gold ratio and by the addition of an unspecific protein, e.g., BSA (4) it will, however, be possible to obtain a 1:1 ratio of antibody to gold particle. More effectively, one can use one of the newly developed gold probes from Nanoprobes (Stony Brook, NY). Nanoprobes has developed a 1.4 nm colloidal gold within an organic shell which allows the coupling of the gold probe covalently to an antibody. Summarizing, the negative staining of direct labeling with gold-conjugated antibodies (IgGs or Fab fragments) provides a powerful tool to identify subunits within a larger protein complex.
7. For most applications uranyl acetate is used as negative stain. A factor, which is critical in achieving a high quality staining, is the hydrophilic property of the carbon film. Unfortunately, the hydrophilic property of the carbon film changes over time, when exposed to air, and the carbon film has to be exposed to ionized gas (glow discharge) to revitalize the hydrophilic property of the carbon. In our method the negative staining is carried out on a carbon surface, which had never been exposed to air, by floating the carbon film first onto the protein solution and then onto the uranyl acetate.

References

1. Baschong, W., Lucocq, J. J., and Roth, J. (1985) "Thiocyanate gold" small (2-3 nm) colloidal gold for affinity cytochemical labelling in electron microscopy. *Histochem.* **83**, 409-411.
2. Steffen, W., Hodgkinson, J. L., and Wiche, G. (1996) Immunogold-localisation of the intermediate chain within the protein complex of cytoplasmic dynein. *J. Struct. Biol.* **117**, 227-235.
3. Mage, M. G. (1980) Preparation of Fab fragments from IgGs of different animal species. *Meth. Cell Biol.* **47**, 177-182.
4. Baschong, W. and Wrigley, N. G. (1990) Small colloidal gold conjugated to Fab fragments or to immunoglobulin G as high-resolution labels for electron microscopy. *J. Electron Microsc. Technol.* **14**, 313-323.

Tat-Mediated Delivery of Antibodies into Cultured Cells

Walter Steffen

1. Introduction

Many questions concerning the function of the cytoskeleton can be addressed using functional antibodies either in *in vitro* assays or in whole cell systems. Ultimately, the function of a component has to be studied within intact cell systems. A problem, which one has to overcome, is the delivery of the antibody into the cells. The delivery of antibodies can be a particular problem either, if large numbers of cells will be analyzed or if one wants to study adhesive as well as non-adhesive cells. Several approaches to introduce proteins and other components into cells have been published, such as electroporation (1), scrape loading (2), or delivery via liposomes (3). Among these the most widespread are microinjection and electroporation. While microinjection is routinely used for adhesive cells, this method will be very time consuming when large numbers of cells have to be studied. Also, it is not feasible to employ this technique for small cells in suspension. Electroporation, on the other hand, has been employed successfully to introduce various components into cells in suspension. Chang (4,5) has also developed an electroporation method for adhesive cells using an oscillating electric field; still a fair number of cells die during this procedure.

A very gentle and efficient method to introduce components into cells is the Tat-mediated delivery method (6). In contrast to microinjection and electroporation, this method does not cause any physical stress and is applicable to adhesive (6) as well as non-adhesive cells (Killisch, Mechtler, Beug, and Steffen, unpublished data). Tat is a polypeptide of the human HIV-1 virus, which can enter cultured cells efficiently when added to the culture medium (7). More recently it has been demonstrated that the cellular uptake is mediated

by residues aa37 to aa72 of the Tat peptide (6). If this polypeptide is coupled to a protein and added to the culture medium, such a protein will be taken up into the cytoplasm. The mechanism of cellular uptake is not yet solved; however, the internalization does not involve the endocytic pathway as no inhibition was observed at 4°C (8).

2. Materials

2.1. Antibody Purification

1. 0.02% (w/v) NaN₃ in dH₂O (kept in dark).
2. 0.45 µm Millipore bottle filter.
3. 200 mM glycine, pH 2.3.
4. 1.0M Tris (unbuffered).
5. Centricon-30 Microconcentrator (Amicon).
6. PBS: 20 mM sodium phosphate, 150 mM NaCl, pH 7.4.
7. Peristaltic pump.
8. Protein G Sephadex, 5 mL column.
9. Spectrophotometer.
10. Stirred Cell (Amicon, Millipore).
11. UV_{280nm} detector.

2.2. Synthetic Peptide

1. C FITKALGISY GRKKRRQRRR PPQGSQTHQV SLSKQ (piCHEM, Graz, Austria).
2. PBS: 20 mM sodium phosphate, 150 mM NaCl, pH 7.4.

2.3. Chemical Cross-Linking of Peptide to Antibody

1. 1.0M glycerol.
2. 1.5 mL reaction vials.
3. 100 mM sodium periodate, prepared fresh and kept in dark.
4. 5 mg/mL rabbit IgG.
5. 5 mg/mL mouse anti dynein intermediate chain (9).
6. Centricon-30 Microconcentrator (Amicon).
7. Coupling buffer: 100 mM sodium acetate buffer, pH 5.5.
8. DMSO (dimethylsulfoxide).
9. PBS: 20 mM sodium phosphate, 150 mM NaCl, pH 7.4.
10. PDP-Hydrazide, bi-functional crosslinker (Pierce).

2.4. Cell Culture

1. 10 mg/mL Hoechst 33258.
2. 24-well cell culture plates.
3. 4% formaldehyde.
4. 50% H₂SO₄.
5. Adhesion slides (BioRad).

6. Chinese hamster ovary (CHO) cells.
7. DMEM: Dulbecco's modified Eagle's medium, high glucose.
8. FCS: fetal calf serum.
9. FITC conjugated goat antimouse.
10. Methanol (-20°C).
11. PBS: 20 mM sodium phosphate, 150 mM NaCl, pH 7.4.
12. Penicillin / Streptomycin.
13. Poly-L-lysine solution (Sigma).
14. Porcelain rack (Thomas Scientific).
15. Sterile 10 mm round cover glasses.
16. Texas red conjugated goat-antirabbit.
17. Trypsin solution: 0.05% Trypsin Type III, 0.1% glucose, 0.25 mM EDTA, 5 $\mu\text{g}/\text{mL}$ Phenol Red, pH adjusted to 7.8 with NaHCO_3 .

3. Methods

3.1. Protein G Affinity Purification of Antibodies (see Note 1)

1. Grow cells either in serum-free culture medium or in culture medium containing IgG-depleted FCS (IgG can be depleted from the FCS using a protein G column).
2. Remove cells by centrifugation: 780g in clinical tabletop centrifuge for 5 min.
3. Filter culture supernatant through a 0.45 μm Millipore filter. (Culture supernatant can be stored in freezer; avoid, however, repeated freezing)
4. If available, use a serum concentrator (Stirred Cell) to reduce volume of the culture supernatant.
5. Add up to 0.02% NaN_3 to supernatant.
6. Bring column to room temperature (avoid the formation of air bubbles, by using degassed solutions).
7. If column is stored in 50% ethanol, equilibrate column with PBS.
8. Run culture supernatant through column at 0.5 to 1.0 mL/min (up to 1.5 L can be used for a 5 mL protein G column).
9. Wash column with PBS at a flow rate of 1 to 1.5 mL/min; use peristaltic pump and monitor wash with UV_{280} detector, about 20 mL PBS should be sufficient.
10. Elute IgG fraction with 200 mM glycine, pH 2.3 at a flow rate of 1 to 1.5 mL/min; use peristaltic pump and monitor effluent with UV_{280} detector. Note that the pH of glycine used will depend on the particular antibody.
11. Collect 1 mL fractions. Neutralize each fraction with unbuffered 1 M Tris-Base immediately (about 140 μL unbuffered Tris per 1 mL glycine).
12. Determine protein concentration by $\text{OD}_{280\text{nm}}$. ($\text{OD}_{280\text{nm}} \times 0.667 = 1 \text{ mg}/\text{mL}$ protein concentration).
13. Dialyze against PBS at 4°C (3 changes).
14. Concentrate antibody in Centricon filters by centrifugation at 6000 rpm (about 3000 g_{av}) in a SS34 or JA-21 rotor.
15. Aim at a final concentration of 5 to 10 mg/mL IgG.

16. Snap freeze antibody as 50 to 100 μL aliquots in liquid N_2 and store them at -80°C .
17. Most antibodies can be freeze dried in a Speed Vac (Savant) for prolonged storage.

3.2. Synthetic Peptide (see Notes 2 and 3)

1. Dissolve peptide at 1 mg/mL in PBS.
2. Snap freeze as aliquots in liquid N_2 .

3.3. Tat-Antibody Coupling (Chemical Cross-Linking) (see Note 4)

1. Dialyze antibody into coupling buffer or use a Centricon-30 Microconcentrator to exchange buffer.
2. Adjust antibody concentration to 3 mg/mL
3. Freshly prepare 100 mM sodium periodate and keep on ice in the dark.
4. Add 0.1 mL sodium periodate to 1 mL of purified antibody (3 mg total) and incubate on ice for 20 min in the dark.
5. Stop oxidation by adding 20 μL of 1M glycerol and incubate on ice for 5 min.
6. Dialyze overnight against coupling buffer.
7. Determine volume and transfer sample to a 1.5 mL reaction vial.
8. Freshly prepare 100 mM PDP-hydrazide in DMSO.
9. Add 5 mM PDP-hydrazide.
10. Incubate for 2 h at room temperature while gently rocking.
11. Remove unbound cross-linker and exchange buffer to PBS using Centricon-30 Microconcentrator.
12. Bring to 1 mL with PBS.
13. Add 0.2 mg peptide and incubate over night at room temperature while gently rocking.
14. Remove unbound peptide using a Centricon-30 Microconcentrator.
15. Adjust protein concentration to 5 mg/mL with PBS and snap freeze in liquid N_2 as 50 μL aliquots.

3.4. Uptake of Tat-Coupled Antibody

3.4.1. Preparation of Poly-L-Lysine Coated Cover Glasses

1. Place cover glasses in a porcelain rack.
2. Gently immerse rack with cover glasses in a beaker with 50% H_2SO_4 and incubate for 1 h.
3. Transfer rack with cover glasses into a beaker with tap water.
4. Wash with running tap water for 30 min.
5. Rinse cover glasses in porcelain racks with 3 changes of dH_2O .
6. Transfer racks with cover glasses into a plastic beaker with 0.04% poly-L-lysine and incubate for 1 h at room temperature (Note: the poly-L-lysine solution can be reused).
7. Transfer racks with cover glasses into a beaker with tap water.
8. Wash with running tap water for 1 h.
9. Rinse cover glasses in porcelain racks with 3 changes of dH_2O .

10. Place cover glasses on filter paper in a dust-free area to dry.
11. Place cover glasses in cell culture dishes and sterilize them under UV light in a laminar flow chamber for at least 4 h or overnight.

3.4.2. Test of Coupling Efficiency

Before employing the Tat-conjugated antibody, one should determine the efficiency by which the Tat-conjugated antibody is taken up by the cells.

3.4.2.1. ADHESIVE CELLS

1. Place poly-L-lysine-coated, sterile 10 mm round cover glasses into 24-well plates, one cover glass per well.
2. From a semiconfluent to confluent culture detach cells from plastic surface by trypsin treatment.
3. Transfer appropriate volume of cell suspension into each well.
4. Culture adhesive cells over night in 0.5 mL DMEM medium.
5. Add antibody-Tat conjugates to cells at concentrations ranging from 0.01 to 0.2 mg/mL.
6. Incubate cells at 37°C for 30 min.
7. Remove cover glass and fix cells in -20°C methanol or 4% formaldehyde for 10 min.
8. Wash 3 times (5 min each) with PBS.
9. Incubate with fluorophore conjugated secondary antibody for 60 min at room temperature. Include a nuclear counter stain (1 µg/mL Hoechst 33258).
10. Wash with PBS, 3 times (10 min each).
11. Mount cover glasses with mounting medium.
12. Analyze by fluorescence microscopy.

3.4.2.2. CELLS IN SUSPENSION

1. From a culture at the beginning of the exponential growth phase place 0.5 mL cell suspension per well of a 24-well plate.
2. Add antibody-Tat conjugates to cells at concentrations ranging from 0.01 to 0.2 mg/mL.
3. Incubate cells at 37°C for 30 min.
4. Take an aliquot and place on an adhesion slide (BioRad Adhesion Slides, BioRad). Alternatively, if a cytospin centrifuge is available, centrifuge cells onto a microscope slide.
5. Fix cells in -20°C methanol or 4% formaldehyde in PBS for 10 min.
6. Wash 3 times (5 min each) with PBS.
7. Incubate with fluorophore conjugated secondary antibody for 60 min at room temperature. Include a nuclear counter stain (1 µg/mL Hoechst 33258).
8. Wash with PBS 3 times (10 min each).
9. Mount cover glasses with mounting medium.
10. Analyze by fluorescence microscopy.

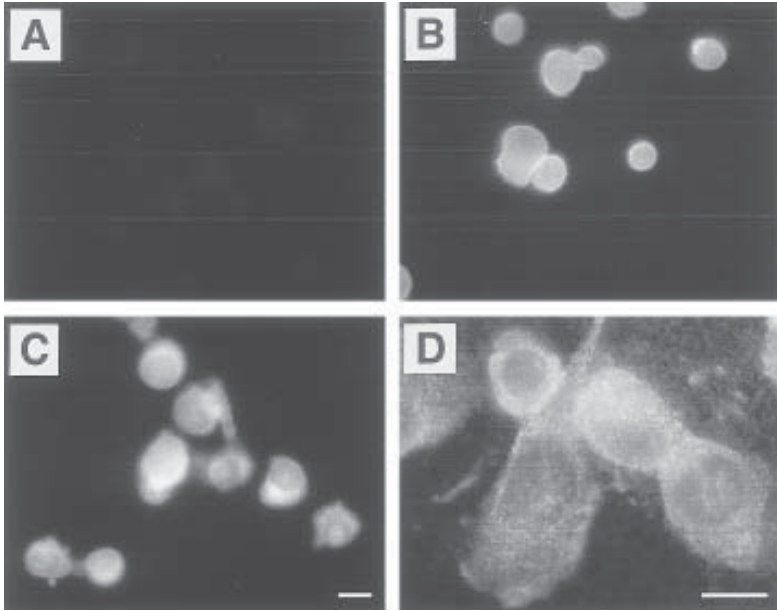


Fig. 1. Uptake of Tat-conjugated antibody by Chinese Hamster ovary cells. Cells were incubated with 50 $\mu\text{g}/\text{mL}$ of Tat-conjugated rabbit IgG (A–C) or Tat-conjugated monoclonal antibodies specific for dynein intermediate chain (D) and fixed in -20°C methanol; 0 min (A), 10 min (B), and 30 min (C and D) after the addition of the antibody to the culture medium. The rabbit IgG was detected using a Texas Red-conjugated goat anti-rabbit antibody and the mouse IgG was detected using a FITC-conjugated goat anti-mouse. The cellular uptake of the antibody increases over time and has reached a peak level about 10 to 20 min after the addition. A vesicular staining pattern can be observed with a Tat-conjugated antibody specific for cytoplasmic dynein complex (D). Bars represent 50 μm .

3.4.3. Time Course of Antibody-Tat Uptake

1. Repeat experiments described in **Subheading 3.4.2.** using optimal concentration of Tat-conjugated antibody and fix cells at various time points: 5 min, 10 min, 30 min and 60 min after the addition of the antibody (*see Fig. 1*).
2. Fix cells as described above.

4. Notes

1. Only highly purified antibodies should be employed for Tat-mediated delivery. An antigen affinity column has to be used for polyclonal antibodies. Monoclonal antibodies, on the other hand, can be isolated quite easily from cell culture supernatant using a recombinant protein G affinity column. The protocol in **Subheading 3.1.** describes the isolation and purification of monoclonal antibodies from cell culture supernatant and concentration using a Centricon filter.

2. Today, synthetic peptides can be obtained from many commercial companies. When designing a synthetic peptide, one should consider methods to covalently bind the peptide to the antibody. The SH-group of cysteine is frequently used to chemically cross-link proteins and polypeptides. When the Tat polypeptide was synthesized, a cysteine was included at the N-terminal end of the peptide.
3. Long synthetic peptides are rather expensive. Vives and co-worker have reported that shorter peptides, aa37-60, aa43-60, and aa48-60, also translocate through the plasma membrane (8). Alternatively, one could express the Tat-polypeptide in *E. coli* (10) and use the purified peptide to tag an antibody. An expression system will have the added benefit that one can also employ quite easily the Tat-mediated delivery of bacterially expressed cDNA clones into mammalian cell.
4. Several regions of an antibody can be used as possible attachment site for the Tat polypeptide, among those are the carbohydrate and the sulfhydryl group within the Fc portion of an antibody. Today's commercial, chemical cross-linkers will provide a whole range of possibilities to bind a synthetic peptide to a protein. Among the chemical cross-linker to select from are homobifunctional and heterobifunctional cross-linkers as well as cross-linkers which can be cleaved again. Before deciding on any particular cross-linker one should firstly consider possible binding sites for the Tat-polypeptide and secondly the binding conditions for cross-linking peptide and antibody. There are two specific binding sites the carbohydrate moiety and the disulfide bond of the Fc portion of the antibody. In any case, when cross-linking an antibody particular care should be taken to maintain immunoreactivity after the cross-linking. The protocol in **Subheading 3.3.** uses the heterobifunctional cross-linker PDPH to link the carbohydrate of the antibody to the sulfhydryl group of cysteine.

References

1. Chakrabarti, R., Wylie, D. E., and Schuster, S. M. (1989) Transfer of monoclonal antibodies into mammalian cells by electroporation. *J. Biol. Chem.* **264**, 15,494–15,500.
2. McNeil, P. L., Murphy, R. F., Lanni, F., and Taylor, D. (1984) A method for incorporating macromolecules into adherent cells. *J. Cell Biol.* **98**, 1556–1564.
3. Connor, J. and Huang, L. (1985) Efficient cytoplasmic delivery of a fluorescent dye by pH-sensitive immunoliposomes. *J. Cell Biol.* **101**, 582–589.
4. Chang, D. C. and Reese, T. S. (1990) Changes in membrane structure induced by electroporation as revealed by rapid-freezing electron microscopy. *Biophys. J.* **58**, 1–12.
5. Chang, D. C. (1997) Experimental strategies in efficient transfection of mammalian cells. Electroporation. *Meth. Mol. Biol.* **62**, 307–318.
6. Fawell, S., Seery, J., Daikh, Y., Moore, C., Chen, L. L., Pepinsky, B., and Barsoum, J. (1994) Tat-mediated delivery of heterologous proteins into cells. *Proc. Natl. Acad. Sci. USA* **91**, 664–668.
7. Frankel, A. D. and Pabo, C. O. (1988) Cellular uptake of the tat protein from human immunodeficiency virus. *Cell* **23**, 1189–1193.

8. Vives, E., Brodin, P., and Lebleun, B. (1997) A truncated HIV-1 tat protein basic domain rapidly translocates through the plasma membrane and accumulates in the cell nucleus. *J. Biol. Chem.* **272**, 16,010–16,017.
9. Steffen, W., Karki, S., Vaughan, K. T., Vallee, R. B., Holzbaur, L. E., Weiss, D. G., and Kuznetsov, S. A. (1997) The 74-kD intermediate chain of cytoplasmic dynein is involved in binding the motor to membranous organelles. *Molec. Biol. Cell* **8**, 2077–2088.
10. Kirsch, T., Boehm, M., Metzger, A. U., Willbold, D., Frank, R. W., and Rosch, P. (1996) Cloning, high-yield expression in *Escherichia coli*, and purification of biologically active HIV-1 Tat protein. *Protein Expr. Purif.* **8**, 75–84.

IV

CYTOSKELETON DYNAMICS

Studying Cytoskeletal Dynamics in Living Cells Using Green Fluorescent Protein

Yisang Yoon, Kelly R. Pitts, and Mark A. McNiven

1. Introduction

The cytoskeleton is a dynamic structure comprised of at least three distinct cellular filament systems: microfilaments, intermediate filaments, and microtubules. Microfilaments are composed of assembled globular actin monomers that form a filamentous system involved in the maintenance of cell shape and polarity. Intermediate filaments are made of fibrous proteins including vimentin, cytokeratin, nuclear lamins, and neurofilament proteins that assemble into fibers providing mechanical stability to animal cells. Microtubules are formed by the assembly of tubulin (α and β subunits) producing long, rigid polymers which govern the location of membrane-bounded organelles and other cellular components. While each filament system has specific cellular functions, an emerging view of the cytoskeleton is that actin, intermediate filaments and microtubule networks function in concert to provide the cell with stability, polarity and organization.

Mechanochemical enzymes work in conjunction with cytoskeletal systems to bring about changes in cell stability, polarity and organization. These enzymes, or “molecular motors”, are capable of translocating along a filament by converting chemical energy into mechanical force. This mechanical force is utilized to support a variety of different cellular processes including vesicle transport, cell migration, cell division, and the formation and maintenance of organelles. These conventional motor families include up to 14 different groups of actin-associated myosins and an expanding number of microtubule-dependent cytoplasmic dyneins and kinesins. Recently, the dynamin family of large GTPases has been demonstrated to perform a mechanochemical function

through their ability to constrict and sever membrane tubules during the formation of nascent secretory and endocytic vesicles.

Cytoskeletal and motor proteins participate in dynamic cellular processes that are optimally observed directly in living cells. Tagging these proteins with green fluorescent protein (GFP) allows direct visualization of these dynamic processes. In this chapter, we will discuss the strengths of using GFP as a vital protein tag compared to traditional methods of protein localization. Specifically, we will focus on how GFP has been applied to the study of the cytoskeletal filaments and associated motor enzymes, and how recent advances in GFP technology may help to further characterize many cellular processes.

1.1. Strengths of GFP

Traditional methods to localize proteins in cells employ polyclonal or monoclonal antibodies that recognize a protein of interest in fixed, permeabilized cells. The subsequent addition of chromophore-conjugated secondary antibodies permits the localization of the protein to be visualized by fluorescence microscopy. While this technique has been used extensively, it has several unavoidable disadvantages. First, because cells are fixed and permeabilized, a static localization of the protein is obtained. This is a significant disadvantage in the study of dynamic cellular functions. Second, visualizing spliced variants of the same gene product requires primary antibodies that efficiently and reliably distinguish subtle differences in spliceoform epitopes. For example, the number of kinesin variants now totals more than one hundred. Finding unique epitopes within such large and highly related groups of gene products is often not possible, as is the case for two spliced variants of dynamin 2, discussed later in this chapter.

Some concern has been raised regarding the use of GFP as a protein tag. Because of its substantial size (~30 kDa) compared to other epitope tags, many have argued that GFP may alter protein function. Indeed, proper controls need to be performed which include comparing protein localization when tagged at the N- and C-terminus and when it is tagged with another epitope (e.g., *myc*, FLAG). When possible, GFP localization can be compared to that of the untagged protein provided an antibody to the protein exists. This allows the localization of the expressed protein of interest to be compared to that of the endogenous population.

The popularity of GFP has led to the development of several variants with distinct spectral properties, including blue, cyan, and yellow emitting variants (BFP, CFP, and YFP, respectively; for an exhaustive review *see* (1); *see* also (2,3). With these new variants it is possible to simultaneously follow the movements of two or more tagged proteins in real time in the same cell. Most recently, subtypes of GFP have been developed that emit in distinct wave-

lengths. Hence, multiple GFP-tagged proteins can be resolved within the same living cell. Variants of GFP have been utilized in fluorescence resonance energy transfer (FRET) studies (4). In this approach, two distinct proteins tagged with GFP or BFP are transiently coexpressed in cells. When irradiated with the proper excitation wavelength, the blue light emitted from BFP is readily absorbed by the GFP chromophore and re-emitted as green light provided the two chromophores are in close proximity to one another. Visualizing and quantitating GFP fluorescence resulting from FRET can determine the extent to which the two proteins interact under a variety of conditions. GFP-based FRET has been used to demonstrate many protein-protein interactions, including Pit-1/Ets-1 transcription factor interactions (5) and Bax/Bcl-2 interactions in mitochondria (6).

While FRET utilizes the close proximity of a GFP/BFP pair, GFP has been used to measure the interactions of a single protein with itself by proximity imaging (PRIM). When two GFP molecules are brought into close proximity, there is a change in the relative intensities of green fluorescence emitted upon excitation at 395 vs 475 nm. These spectral changes provide a sensitive ratiometric index of the extent of self-association that can be exploited to quantitatively image homo-oligomerization or clustering processes of GFP-tagged proteins *in vivo*. Most recently this technique has been successfully applied to a protein whose oligomerization is well characterized. The immunophilin FKBP, which binds the immunosuppressants FK506 and rapamycin, does not dimerize, but can be induced to do so by adding FK1012, a membrane-permeable synthetic dimer of FK506. When GFP-FKBP was incubated in the presence of FK1012, fluorescence intensity at 395 nm decreased, whereas the fluorescence intensity at 475 nm increased, demonstrating efficient dimerization of GFP-FKBP (7). PRIM has also been used to demonstrate the clustering of glycosylphosphatidylinositol-anchored GFP at the cell surface (7).

1.2. Use of GFP to Study Cytoskeletal Filaments

1.2.1. Actin

GFP-actin has been expressed in the eukaryotic microorganism *Dictyostelium discoideum*. *In vitro* studies demonstrated that purified GFP-actin was able to co-polymerize with native actin from *D. discoideum* to form filaments. These actin filaments were found to be competent substrates for myosin (an actin-based motor discussed later in this chapter) suggesting that GFP-actin does not compromise the functional integrity of actin filaments (8). Further, in living cells expressing GFP-actin, functional incorporation of GFP-actin was confirmed by demonstrating dynamic properties of actin filaments, and colocalization with fluorescent phalloidin in various cellular protrusions

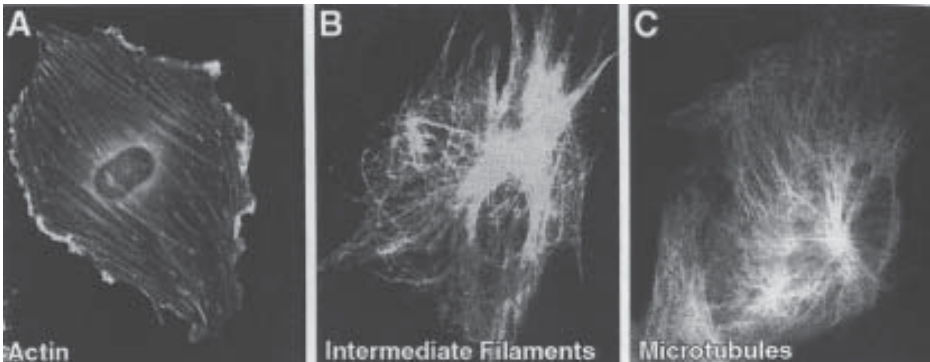


Fig. 1. Cytoskeletal systems visualized with GFP. GFP-tagged cytoskeletal proteins show actin dynamics in living melanoma cells (**A**; used with permission from Andrew Matus), intermediate filaments in living BHK cells (**B**; used with permission from Robert Goldman), and microtubule remodeling in living CHO cells (**C**; used with permission from Beat Imhof).

(8,9). GFP-actin has also been expressed in several other cell types including yeast (**10**), border cells in the *Drosophila* egg chamber (**11**), mammalian tissue culture cells (**9**), and hippocampal neurons (**12**), allowing actin dynamics in living cells to be visualized. One of the most striking images of actin cytoskeleton reorganization was obtained using GFP-fused β -actin in stationary and migrating mammalian cells (**13**). In stationary cells, GFP-actin incorporated into stress fibers (**Fig. 1A**) and into expanding ruffle-like structures found to be involved in the reorganization of the actin cytoskeleton as the cells underwent a shape change. In motile cells, redistribution of GFP-actin to lamellipodia was prominent while stress fibers disappeared. Heidemann and colleagues recently used GFP-tagged actin and microtubules to directly visualize the mechanical role of these polymers in cell shape determination (**14**). By applying physical manipulations with a glass needle to cells expressing GFP-actin, it was found that the actin cytoskeleton is highly elastic, exhibiting rapid recovery after deformation of actin bundles around the nuclear region or in spread regions of the cell. Unlike the actin cytoskeleton, the microtubule network showed more fluid behavior with less elasticity.

1.2.2. Intermediate Filaments

Vimentin, one of the intermediate filament-forming proteins, has been tagged with GFP (**Fig. 1B**) (**15**). Our understanding of the precise function of intermediate filaments is still superficial compared to what is known regarding microfilaments and microtubules mainly due to the lack of good *in vivo* probes.

However, using GFP-vimentin to elucidate intermediate filament function has revealed that intermediate filaments dynamically interact with the other cytoskeletal systems, and is itself dynamic. GFP-vimentin incorporates into endogenous intermediate filaments and has shown numerous motile phenotypes which can be observed in living cells using time-lapse imaging and fluorescence recovery after photobleaching (FRAP) analysis (15). In this study, GFP-vimentin incorporated into the endogenous intermediate filament network both in interphase and mitotic cells. Time-lapse observations of interphase arrays of vimentin fibers demonstrated that intermediate filaments undergo constant structural changes in the absence of alterations in cell shape. FRAP analysis showed that bleached zones rapidly recovered their fluorescence, also suggesting a highly dynamic system. Interestingly, treatment with nocodazole and cytochalasin B (two drugs that disrupt microtubule and actin networks, respectively) significantly reduced the motility of intermediate filaments, indicating that intermediate filament motile properties are mediated by microtubule and microfilament networks. The interaction of intermediate filaments and microtubules was shown more directly in studies using GFP-vimentin. Time-lapse observation of live spreading cells expressing GFP-vimentin showed that intermediate filament precursors (GFP-vimentin “dots”) move towards the cell periphery along microtubule tracks via a kinesin motor and are assembled into maturing intermediate filaments (16).

1.2.3. Microtubules

Tubulin subunits have been tagged with GFP and used for direct visualization of microtubule dynamics. GFP-tagged yeast α -tubulin incorporates normally into both cytoplasmic and spindle microtubules and exhibits intrinsic microtubule dynamic instability (17). The introduction of a dynein mutant in cells expressing GFP-tubulin interfered with spindle movement and orientation, and changed microtubule dynamics, suggesting that dynein mediates cortical interactions of microtubules that control spindle dynamics (17). In another study, yeast chromosomes and microtubules tagged with GFP allowed visualization of chromosomal and spindle movement during mitosis, demonstrating that chromosomes did not align during metaphase, and that centromeres separated before telomeres in anaphase (18). Visualization of GFP-tubulin in mammalian cells has been a difficult task due to the strong posttranscriptional inhibition of its overexpression (19). Recently, however, dynamic instability of microtubules was successfully visualized by expression of β -tubulin-GFP in CHO cells (Fig. 1C) (20). In subsequent studies with fibroblasts expressing GFP-tubulin, distinct behaviors of microtubules were observed in response to cellular manipulations. A cell fragment severed from a parent cell underwent rapid microtubule depolymerization and complete lysis while the cell body

maintained its integrity. Microtubule buckling was also observed in regions undergoing rapid retraction during EDTA treatment to induce rounding up of cells (14).

1.3. Use of GFP to Study Cytoskeletal Motors

1.3.1. Actin-Based Motors: The Myosins

Myosins comprise a large family of actin-based motor proteins found in all eukaryotic cells. To date, the myosin superfamily consists of at least 14 different subfamilies (myosin I–myosin XIV) that mediate diverse cellular processes, including cell contraction, migration, division, shape change, phagocytosis, and vesicle transport (21).

GFP-myosin has been expressed in *D. discoideum* to define new functions for myosin in living cells. *D. discoideum* cells expressing GFP-myosin display a transient increase of GFP-myosin in the tips of pseudopods, which was not detected by conventional immunological methods (22). Myosin light chain, which regulates myosin motor function, was tagged with GFP (MLC-GFP) and evaluated as a muscle-specific marker. The MLC-GFP construct was injected into zebrafish embryos and muscle-specific expression of MLC-GFP was observed. These transgenic fish expressed GFP within 24 h and continued to express high levels of MLC-GFP in skeletal muscle at 1.5 mo, demonstrating that MLC-GFP is an effective marker of muscle cells in vivo (23).

1.3.2. Microtubule-Based Motors: Kinesins and Dyneins

The kinesin family contains more than one hundred related proteins and continues to expand (24). There are three major types of kinesin molecules defined by the motor domain position within the primary structure of the protein: amino-terminal, middle, and carboxy-terminal (25). Although kinesins are generally considered microtubule plus-end directed motors, the kinesins with motor domains at the carboxy-terminus exhibit microtubule minus-end directed motor activities.

The yeast *Saccharomyces cerevisiae* kinesin-related proteins kip2p and kip3p have been fused to GFP. Kip2p-GFP was found to concentrate at the spindle poles suggesting a role in regulating microtubule numbers from the minus end (26). Unlike kip2p-GFP, GFP-kip3p localized to both spindle and cytoplasmic microtubules, functioning in their orientation (27). The combination of GFP fusion proteins and mutation analyses facilitated the real time observation of kip2p and kip3p during the cell cycle and provided insight into the role of kinesin-related proteins in changing microtubule stability and organization. The dynamics of a GFP fusion protein of the *Drosophila melanogaster* kinesin-related protein Ncd was examined during mitosis to elucidate its function. GFP-

Ncd was found to form filaments along spindle microtubules that extend across chromosomes during metaphase, suggesting that Ncd may interact functionally with chromosomes in metaphase (28).

Dyneins were the first microtubule-based motor enzymes identified and are classified into two distinct groups. The conventional flagellar dyneins have been shown to generate a motive force that drives the sliding of adjacent microtubules within motile cilia and flagella (29). In comparison, the more recently identified cytoplasmic forms of dynein (30) are believed to support the motility of numerous cytoplasmic organelles during endocytosis, secretion and cell division (31). Although highly related in sequence and structure, the two dynein classes have been shown to interact with an elaborate array of distinct accessory proteins believed to target dyneins to specific organelles or the flagellar matrix. The number of dynein members is small in comparison to the kinesins and myosins, although recent molecular studies have identified additional dynein heavy chain molecules (DHC2 and DHC3), (32,33).

In budding yeast, dynein-GFP was used to visualize spindle-pole body (SPB, equivalent to centrosomes) and astral microtubule dynamics throughout the cell cycle. The association of dynein with SPBs was found to vary during cell cycle progression with an unequal distribution subsequent to the separation of SPB, followed by an even distribution over several minutes. GFP-tagged astral microtubules exhibit dynamic instability, suggesting an essential role in nuclear migration to the bud (34). The dynamic properties of astral microtubules tagged with dynein-GFP in the yeast spindle were further observed by using time-lapse, three-dimensional fluorescence microscopy of living yeast (35). Astral microtubules revealed asynchronous dynamic instability throughout the cell cycle. Remarkably, the nucleus is pushed through the cytoplasm during interphase by dynamic astral microtubules then moved to the bud neck in S/G2 or G2/M via growing astral microtubules. This indicates that dynamic microtubules may act to probe the cytoplasm while pushing the nucleus into the developing bud.

1.4. Use of GFP to Study the Dynamins, Motor Enzymes That Constrict and Pinch Membranes

Secretory and endocytic vesicle formation requires a scission of membrane invaginations and tubules. The 100-kD GTPase dynamin is believed to be a molecular motor protein functioning in this process. Specifically, this motor constricts and severs the membrane while hydrolyzing GTP (36). To date, three dynamin isoforms (Dyn1, 2, and 3) have been identified and are expressed in a tissue-specific manner (37–43). Further, each isoform of dynamin is expressed as multiple alternatively spliced variants resulting in at least 25 different mRNAs produced from the three dynamin genes (37). Dynamin-GFP fusion

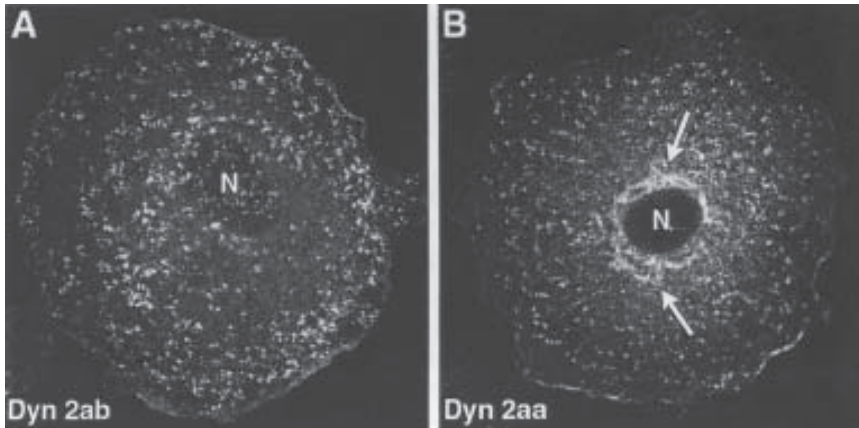


Fig. 2. GFP-tagged spliced variants of the membrane-associated GTPase dynamin reveal differential localizations. Expression of GFP-tagged spliced variants of dynamin 2 (Dyn2) in the normal rat hepatocyte cell line Clone 9. GFP-Dyn 2ab localizes to punctate clathrin structures at the plasma membrane (A), whereas GFP-Dyn 2aa associates with clathrin pits at both the plasma membrane and the Golgi (B, arrows). N, nucleus.

proteins have been utilized to demonstrate distinct cellular localizations of these multiple isoforms and spliced variants, specifically in the distribution of two spliced variants of Dyn2. The insertion of a modest four amino acids in the central region of Dyn2 changes the distribution of this enzyme from the plasma membrane to the Golgi apparatus (Fig. 2). Further, GFP fusion to other dynamins revealed that many of them associate with distinct membrane compartments, including clathrin coated pits at the plasma membrane, the Golgi apparatus, membrane ruffles, and several undefined vesicle populations (37).

1.5. Perspectives and New Directions

As discussed above, GFP technology permits the viewing of specific proteins in living cells and thus has significantly advanced our understanding of how cytoskeletal and motor proteins support cellular processes. In addition, GFP-tagged cargo proteins have also been useful in the study of cytoskeletal systems. For example, cells infected with vesicular stomatitis virus (VSV) synthesize the glycoprotein VSV-G in the rough endoplasmic reticulum that is transported to the plasma membrane via the Golgi apparatus where protein modifications and processing occur. The cellular secretory pathway was directly viewed in living cells using VSV-G tagged with GFP (VSVG-GFP). Time-lapse fluorescence microscopy of living cells expressing VSVG-GFP

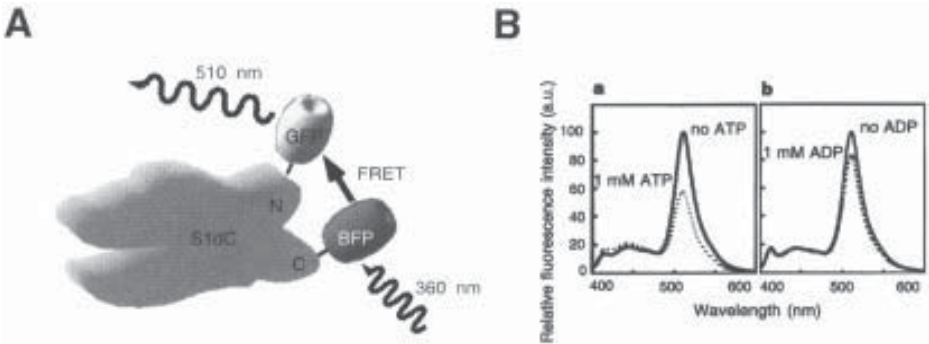


Fig. 3. Quantitative measurements of the predicted lever arm swing motion of *Dictyostelium discoideum* myosin II. The lever arm hypothesis for myosin motors predicts that during the working stroke the lever arm domain tilts against the motor domain, which is bound to actin in a fixed orientation. This working stroke can be detected and quantitated using a fusion protein consisting of the motor domain of *Dictyostelium discoideum* myosin II tagged with GFP at the N-terminus and BFP at the C-terminus (termed S1dC). When the molecule is irradiated with 360 nm light, only the BFP fluorophore absorbs and reemits. If GFP is within FRET distance it absorbs the light emitted by BFP and in turn emits light detectable at 510 nm (A). In the absence of ATP, excitation of BFP yields a strong GFP emission peak indicating that FRET has taken place (B, panel a, solid line). In the presence of 1 mM ATP, the GFP emission is reduced, suggesting that the fluorophores separate when ATP is bound (B, panel a, dotted line). However, GFP emission is unchanged in the presence of ADP, suggesting that the two fluorophores are brought within FRET distance upon phosphate release, demonstrating the reverse swing working stroke of myosin II (B, panel b, dotted line). Figures used with permission from Kazuo Sutoh.

allowed real time visualization of its transport along cytoplasmic microtubule tracks mediated by microtubule motors (44).

Recently, several in vitro applications using the GFP molecule have emerged as novel techniques for the quantitative characterization of motor proteins. Using the FRET analysis described in the previous section, the force-generating stroke of the myosin motor was quantitatively measured with the myosin motor domain fused to GFP and BFP at the amino- and carboxy-terminal ends (Fig. 3A). FRET analysis showed that the carboxy-terminal fluorophore swings back and forth to interact with the amino-terminal fluorophore during the ATP hydrolysis and release cycle, indicating the force-generating stroke is accompanied by a conformational change of the motor (Fig. 3B) (45). GFP-myosin was also used for in vitro studies to measure individual ATP turnovers by myosin using low background total internal reflection fluorescence microscopy

(46). Several GFP fusion constructs of kinesin with mutations in the neck coiled coil region have been expressed and purified for the characterization of the motor. Single GFP-kinesin molecules moving along a microtubule were visualized and the processivity of the motor was assayed using a specially equipped fluorescence microscope, elucidating the function of the kinesin neck region in motor processivity at the single molecule level (47). Therefore, the use of GFP in combination with specialized fluorescence microscopic techniques makes it possible to visualize and assay single molecule activity, providing useful techniques to analyze molecular function without producing large quantities of proteins.

While the study of molecular motors has benefited greatly from GFP technology, many important questions remain. Why do cells possess so many similar motor proteins? How do cells regulate multiple motors to differentially distribute and function in distinct cellular process? How do individual motors select their specific cargo? How are putative regulatory events for motor functions interconnected with intracellular signaling cascades? Certainly, the combination of conventional biochemistry, cell biology, and recent single molecular assay techniques with the GFP technologies discussed in this chapter will help provide valuable understanding regarding these important proteins.

References

1. Tsien, R. Y. (1998) The Green Fluorescent Protein. *Annu. Rev. Biochem.* **67**, 509–544.
2. Haseloff, J. (1999) GFP variants for multispectral imaging of living cells. *Methods Cell Biol.* **58**, 139–151.
3. Pepperkok, R., Squire, A., Geley, S., and Bastiaens, P. I. (1999) Simultaneous detection of multiple green fluorescent proteins in live cells by fluorescence lifetime imaging microscopy. *Curr. Biol.* **9**, 269–272.
4. Mitra, R. D., Silva, C. M., and Youvan, D. C. (1996) Fluorescence resonance energy transfer between blue-emitting and red-shifted excitation derivatives of the green fluorescent protein. *Gene* **173**, 13–17.
5. Day, R. N. (1998) Visualization of Pit-1 transcription factor interactions in the living cell nucleus by fluorescence resonance energy transfer microscopy. *Mol. Endocrin.* **12**, 1410–1419.
6. Mahajan, N. P., Linder, K., Berry, G., Gordon, G. W., Heim, R., and Herman, B. (1998) Bcl-2 and Bax interactions in mitochondria probed with green fluorescent protein and fluorescence resonance energy transfer. *Nat. Biotech.* **16**, 547–552.
7. DeAngelis, D. A., Miesenbock, G., Zemelman, B. V., and Rothman, J. E. (1998) PRIM: proximity imaging of green fluorescent protein-tagged polypeptides. *Proc. Nat. Acad. Sci.* **95**, 12,312–12,316.
8. Westphal, M., Jungbluth, A., Heidecker, M., Muhlbauer, B., Heizer, C., Schwartz, J., et al. (1997) Microfilament dynamics during cell movement and chemotaxis monitored using a GFP-actin fusion protein. *Curr. Biol.* **7**, 176–183.

9. Choidas, A., Jungbluth, A., Sechi, A., Murphy, J., Ullrich, A., and Marriotti, G. (1998) The suitability and application of a GFP-actin fusion protein for long-term imaging of the organization and dynamics of the cytoskeleton in mammalian cells. *Eur. J. Cell Biol.* **77**, 81–90.
10. Doyle, T. and Botstein, D. (1996) Movement of yeast cortical actin cytoskeleton visualized in vivo. *Proc. Natl. Acad. Sci. USA* **93**, 3886–3891.
11. Verkhusha, V., Tsukita, S., and Oda, H. (1999) Actin dynamics in lamellipodia of migrating border cells in the Drosophila ovary revealed by a GFP-actin fusion. *FEBS Letters.* **445**, 395–401.
12. Fischer, M., Kaech, S., Knutti, D., and Matus, A. (1998) Rapid actin-based plasticity in dendritic spines. *Neuron* **20**, 847–854.
13. Ballestrem, C., Wehrle-Haller, B., and Imhof, B. (1998) Actin dynamics in living mammalian cells. *J. Cell Sci.* **111**, 1649–1658.
14. Heidemann, S., Kaech, S., Buxbaum, R., and Matus, A. (1999) Direct observations of the mechanical behaviors of the cytoskeleton in living fibroblasts. *J. Cell Biol.* **145**, 109–122.
15. Yoon, M., Moir, R., Prahlad, V., and Goldman, R. (1998) Motile properties of vimentin intermediate filament networks in living cells. *J. Cell Biol.* **143**, 147–157.
16. Prahlad, V., Yoon, M., Moir, R., Vale, R., and Goldman, R. (1998) Rapid movements of vimentin on microtubule tracks: kinesin-dependent assembly of intermediate filament networks. *J. Cell Biol.* **143**, 159–170.
17. Carminati, J. and Stearns, T. (1997) Microtubules orient the mitotic spindle in yeast through dynein-dependent interactions with the cell cortex. *J. Cell Biol.* **138**, 629–641.
18. Straight, A., Marshall, W., Sedat, J., and Murray, A. (1997) Mitosis in living budding yeast: anaphase A but no metaphase plate. *Science* **277**, 574–578.
19. Cleveland, D. (1988) Autoregulated instability of tubulin mRNAs: a novel eukaryotic regulatory mechanism. *Trends. Biochem. Sci.* **13**, 339–343.
20. Ludin, B. and Matus, A. (1998) GFP illuminates the cytoskeleton. *Trends Cell Biol.* **8**, 72–77.
21. Mermall, V., Post, P., and Mooseker, M. (1998) Unconventional myosins in cell movement, membrane traffic, and signal transduction. *Science* **279**, 527–533.
22. Moores, S., Sabry, J., and Spudich, J. (1996) Myosin dynamics in live Dictyostelium cells. *Proc. Natl. Acad. Sci. USA* **93**, 443–446.
23. Moss, J., Price, A., Raz, E., Driever, W., and Rosenthal, N. (1996) Green fluorescent protein marks skeletal muscle in murine cell lines and zebrafish. *Gene* **173**, 89–98.
24. Hirokawa, N. (1998) Kinesin and dynein superfamily proteins and the mechanism of organelle transport. *Science* **279**, 519–526.
25. Hirokawa, N., Noda, Y., and Okada, Y. (1998) Kinesin and dynein superfamily proteins in organelle transport and cell division. *Curr. Opin. Cell Biol.* **10**, 60–73.
26. Huyett, A., Kahana, J., Silver, P., Zeng, X., and Saunders, W. (1998) The Kar3p and Kip2p motors function antagonistically at the spindle poles to influence cytoplasmic microtubule numbers. *J. Cell Sci.* **111**, 295–301.

27. Miller, R., Heller, K., Frisen, L., Wallack, D., Loayza, D., Gammie, A., and Rose, M. (1998) The kinesin-related proteins, Kip2p and Kip3p, function differently in nuclear migration in yeast. *Mol. Biol. Cell.* **9**, 2051–2068.
28. Endow, S. and Komma, D. (1996) Centrosome and spindle function of the *Drosophila* Ncd microtubule motor visualized in live embryos using Ncd-GFP fusion proteins. *J. Cell Sci.* **109**, 2429–2442.
29. Gibbons, I. (1981) Cilia and flagella of eukaryotes. *J. Cell Biol.* **91**, 107s–124s.
30. Vallee, R., Wall, J., Paschal, B., and Shpetner, H. (1988) Microtubule-associated protein 1C from brain is a two-headed cytosolic dynein. *Nature* **332**, 561–563.
31. Holzbaur, E. and Vallee, R. (1994) DYNEINS: molecular structure and cellular function. *Ann. Rev. Cell Biol.* **10**, 339–372.
32. Criswell, P., Ostrowski, L., and Asai, D. (1996) A novel cytoplasmic dynein heavy chain: expression of DHC1b in mammalian ciliated epithelial cells. *J. Cell Sci.* **109**, 1891–1898.
33. Vaisberg, E., Grisson, P., and McIntosh, J. (1996) Mammalian cells express three distinct dynein heavy chains that are localized to different cytoplasmic organelles. *J. Cell Biol.* **143**, 831–842.
34. Shaw, S., Yeh, E., Salmon, E., and Bloom, K. (1996) Digital time-lapsed DIC/Fluorescence imaging of dynein-GFP reveals dynamics of astral microtubules in *Saccharomyces cerevisiae* throughout the cell cycle. *Mol. Biol. Cell.* **7s**, 398a.
35. Shaw, S., Yeh, E., Maddox, P., Salmon, E., and Bloom, K. (1997) Astral microtubule dynamics in yeast: a microtubule-based searching mechanism for spindle orientation and nuclear migration into the bud. *J. Cell Biol.* **139**, 985–994.
36. McNiven, M. (1998) Dynammin: a molecular motor with pinchase action. *Cell* **94**, 151–154.
37. Cao, H., Garcia, F., and McNiven, M. (1998) Differential distribution of dynammin isoforms in mammalian cells. *Mol. Biol. Cell.* **9**, 2595–2609.
38. Cook, T. A., Mesa, K., and Urrutia, R. (1996) Three dynammin-encoding genes are differentially expressed in developing rat brain. *J. Neurochem.* **67**, 927–931.
39. Cook, T. A., Urrutia, R., and McNiven, M. A. (1994) Identification of dynammin 2, an isoform ubiquitously expressed in rat tissues. *Proc. Natl. Acad. Sci. USA* **91**, 644–648.
40. Nakata, T., Takemura, R., and Hirokawa, N. (1993) A novel member of the dynammin family of GTP-binding proteins is expressed specifically in the testis. *J. Cell Sci.* **105**, 1–5.
41. Obar, R. A., Collins, C. A., Hammarback, J. A., Shpetner, H. S., and Vallee, R. B. (1990) Molecular cloning of the microtubule-associated mechanochemical enzyme dynammin reveals homology with a new family of GTP-binding proteins. *Nature* **347**, 256–261.
42. Shpetner, H. and Vallee, R. (1989) Identification of dynammin, a novel mechanochemical enzyme that mediates interactions between microtubules. *Cell* **59**, 421–432.
43. Sontag, J.-M., Fykse, E. M., Ushkaryov, Y., Liu, J.-P., Robinson, P. J., and Südhof, T.C. (1994) Differential expression and regulation of multiple dynammins. *J. Biol. Chem.* **269**, 4547–4554.

44. Presley, J., Cole, N., Schroer, T., Hirschberg, K., Zaal, K., and Lippincott-Schwartz, J. (1997) ER-to-Golgi transport visualized in living cells. *Nature* **389**, 81–85.
45. Suzuki, Y., Yasunaga, T., Ohkura, R., Wakabayashi, T., and Sutoh, K. (1998) Swing of the lever arm of a myosin motor at the isomerization and phosphate-release steps. *Nature* **396**, 380–383.
46. Iwane, A., Funatsu, T., Harada, Y., Tokunaga, M., Ohara, O., Morimoto, S., and Yanagida, T. (1997) Single molecular assay of individual ATP turnover by a myosin-GFP fusion protein expressed in vitro. *FEBS Letters* **407**, 235–238.
47. Romberg, L., Pierce, D., and Vale, R. (1998) Role of the kinesin neck region in processive microtubule-based motility. *J. Cell Biol.* **140**, 1407–1416.

Use of Green Fluorescent Protein (GFP) to Study Cellular Dynamics

Constructing GFP-Tagged Motor Enzymes

**Hong Cao, Heather Thompson,
Eugene W. Krueger, and Mark McNiven**

1. Introduction

The green fluorescent protein (GFP) from the Pacific Northwest jellyfish *Aequorea victoria* is a member of a small but important class of proteins that exhibit strong visible fluorescence without the requirement of cofactors or other enzymes. In vivo, the photoprotein aequorin binds dimers of GFP allowing the blue light emitted by aequorin to be converted to green light (1). This visible fluorescence emitted by GFP is made possible by an internal *p*-hydroxybenzylideneimidazolinone chromophore formed post-translationally by cyclization of Ser65, Tyr66, and Gly67 and 1,2-dehydrogenation of the tyrosine. A number of mutations have been made in GFP, most of which result in a partial or complete loss of fluorescence without significant change in relative absorption or emission peaks. These mutations probably cause misfolding of the protein, failure of chromophore formation, or quenching of the fluorescence by insufficient shielding. A few mutations, however, have resulted in enhanced GFP spectra, increased brightness, a slower rate of photobleaching, or a spectral shift resulting in the emission of a different color, such as blue, yellow, or cyan. These GFP variants emitting new colors are thus called blue fluorescent protein (BFP), yellow fluorescent protein (YFP), and cyan fluorescent protein (CFP) (2).

The optimization of GFP spectral properties along with the new variants has provided for significant advances in optical microscopy of living cells (3). A major advantage of GFP is that it provides many experimental options that are not possible using other existing fluorescence techniques. Among these new

applications are the use of GFP as a real-time reporter gene in living systems, a dynamic marker for subcellular structures and organelles, and a tracer of intracellular protein trafficking. In addition, for proteins with a variety of splice forms that cannot be differentiated by antibodies, each splice form can be tagged with GFP and its localization in a cell viewed directly without the use of immunofluorescence.

To understand the change in properties of GFP upon mutation and to help in the tailoring of GFPs with altered characteristics, the three-dimensional structure of the Ser65Thr mutant of GFP was determined at a resolution of 1.9 Å. The main structural features of GFP are conserved in the mutants, even though they have quite dissimilar spectral properties. The most distinctive feature of the folding of GFP is an 11-stranded β barrel wrapped around a single central helix, where each strand consists of approx 9 to 13 residues. The barrel forms a nearly perfect cylinder 42 Å long and 24 Å in diameter. The *p*-hydroxybenzylideneimidazolinone chromophore is centrally located in the molecule where it is completely protected from bulk solvent. The total and presumably rigid encapsulation of the chromophore is probably responsible for the high quantum yield of fluorescence and inability of oxygen to quench the excited state of the molecule. The necessity of this total encapsulation also explains why mutations or deletions that affect GFP's folding and allow the chromophore to be exposed would result in a protein unable to fluoresce (*1*).

The following protocols provide a method for GFP-tagging of a protein of interest, starting with RNA isolation and ending with analysis and visualization of the protein. As an example, GFP-tagging of the large GTPase dynamin after RNA isolation from various rat tissues will be used. The dynamins are a family of large GTPases that have been implicated in the regulation of vesicular traffic (*4-7*). Multiple isoforms of dynamin have been identified and are encoded by at least three distinct genes (*8-11*). The existence of multiple dynamin isoforms suggests that dynamin function may be specialized in a cell- or tissue-specific manner. Studies which have overexpressed a mutant dynamin in cultured epithelial cells inhibit receptor-mediated endocytosis (*12*), while in vitro ultrastructural studies have clearly demonstrated the highly ordered localization of dynamin along clathrin-coated membrane invaginations (*13*). From these observations, dynamins are believed to play a general function in regulating the endocytic uptake of plasma membrane in all cells. Most recently, the dynamins have been implicated in diverse membrane functions in addition to traditional clathrin-mediated endocytosis. These newly identified functions include the scission of caveolae from the plasma membrane (*14,15*), trafficking of specific toxins from

endosomes to the Golgi apparatus (**16**), and formation of nascent secretory vesicles from the *trans*-Golgi network (**17,18**).

Mammalian cells express three distinct dynamin isoforms, dynamin 1 (Dyn 1) which is neuronal specific, dynamin 2 (Dyn 2) which is expressed in all tissues examined and is ~80% identical to dynamin 1, and dynamin 3 (Dyn 3) which is expressed in specific tissues such as testis, lung, and brain (**6,8,11**). It is known that the dynamin gene products exist as multiple spliced variants making at least 25 different forms expressed in mammalian tissues (**19**). The application of GFP technology is particularly useful toward understanding the distribution and function of this expanding enzyme family. See **Table 1** for overview of methodology.

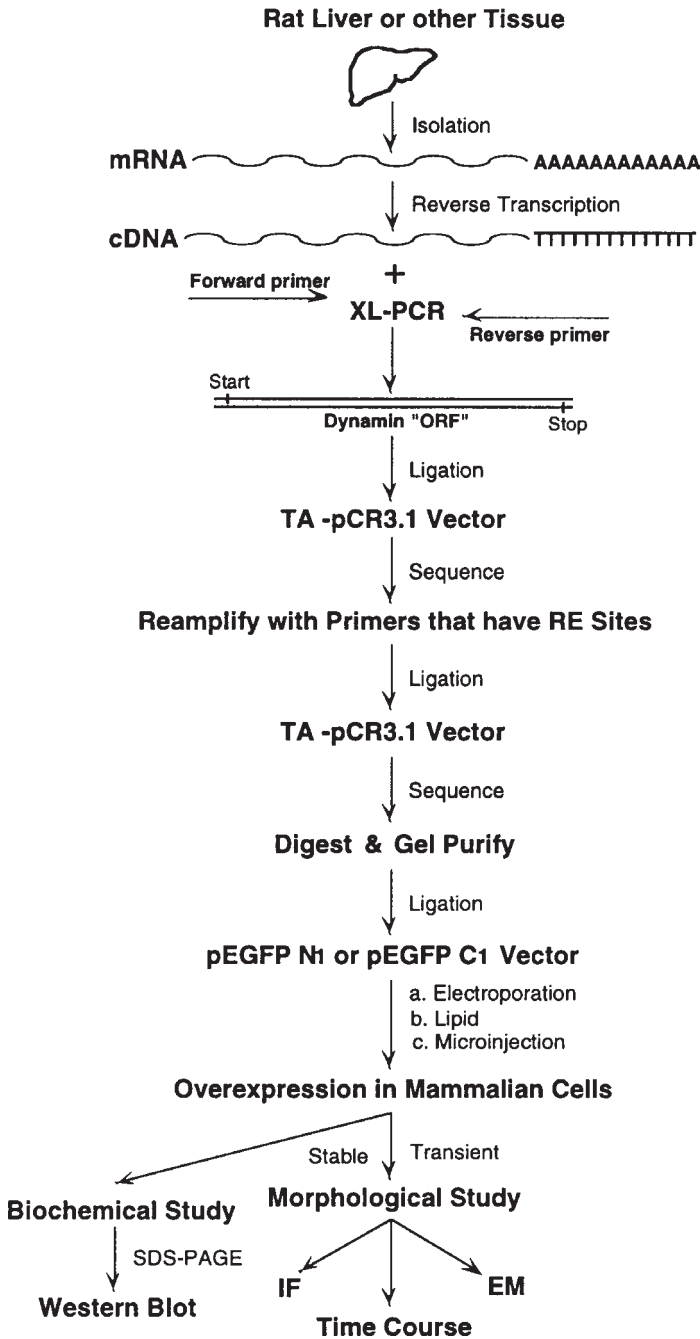
2. Materials

2.1. cDNA Synthesis

2.1.1. Isolation and Purification of RNA

1. Spectrophotometer.
2. Ultracentrifuge.
3. Clinical centrifuge.
4. Microfuge.
5. 26 gauge \times 1/2 in. needle.
6. To make DEPC-treated water:
 - a. Add diethyl pyrocarbonate (DEPC) to deionized water to a final concentration of 0.1%.
 - b. Incubate the water overnight at room temperature in a fume hood.
 - c. Autoclave the treated water for 20 min.
7. To make PBS use: 0.2 g KCl, 8.0 g NaCl, 0.2 g KH_2PO_4 , 1.15 g Na_2HPO_4
 - a. Add components one at a time to 900 mL of room temperature, deionized water and stir until completely dissolved.
 - b. Adjust the pH to 7.4 using 1N HCl or 1N NaOH if necessary.
 - c. Bring the final volume to 1 L with deionized water.
8. 70% ethanol: Add DEPC-treated water to 70 mL of 100% ethanol to a final volume of 100 mL.
9. GIT solution: 250 g (4M) guanidinium thiocyanate, 293 mL deionized water (65°C), 17.6 mL 0.75M sodium citrate (pH 7.0), 26.4 mL 10% sarcosyl.
10. 5.7M CsCl: 95.97 g CsCl, 20 mL 0.5M EDTA (pH 8.0); add DEPC-treated water to 100 mL.
11. 3M Na(OAc) solution: 40.83 g Na(OAc); add DEPC-treated water to 100 mL and adjust the pH to 6.0 using 1N HCl or 1N NaOH if necessary.
12. 2M Na(OAc) solution: 27.22 g Na(OAc); add DEPC water to 100 mL and adjust the pH to 4.0 using HCl.
13. Solution D: 50 mL GIT solution, 0.36 mL 2-mercaptoethanol.
14. Phenol: Nucleic acid grade, saturated with Tris pH 8.0.

Table 1
Protocol for Dynamin Overexpression in Mammalian Cells



15. Chloroform-alcohol: chloroform:isoamyl alcohol at a ratio of 24:1.
16. To make 10X Mops use: 41.9 g Mops, 4.1 g Na(OAc), 3.7 g EDTA (2 Na).
 - a. Dissolve the reagents in 900 mL of DEPC-treated water.
 - b. Adjust the pH to 7.0 then add DEPC-treated water to a final volume of 1 L.
 - c. Store the buffer in a brown bottle at 4°C.
17. To make an RNA gel solution use: 0.6 g Agarose, 6 mL 10X Mops, 51 mL dH₂O, 3.24 mL formaldehyde.
 - a. Dissolve the agarose in 10X Mops and dH₂O by heating.
 - b. Add the formaldehyde after heating.
18. Gel Loading buffer: 20 µL 10X Mops, 34 µL formaldehyde, 100 µL formamide.

2.1.2. Reverse Transcription (RT)

1. SUPERScript™ II RNase H⁻ Reverse Transcriptase kit (GIBCO).
2. 0.1M DTT (Dithiothreitol).
3. *E. coli* RNase H.
4. DEPC-treated water.

2.2. Constructing the Recombinant Protein

2.2.1. Extra-Long RT-PCR

1. Perkin Elmer XL PCR Kit (Perkin Elmer, Branchburg, NJ).
2. AmpliWax Gem 100 Beads (Perkin Elmer).
3. Thin-walled reaction tubes (Perkin Elmer).

2.2.2. cDNA Cloning

1. TA pCR 3.1 Cloning Kit (Invitrogen, Carlsbad, CA).
2. TOP 10F⁺ Ultracomp™ cells (Invitrogen).
3. 0.5M 2-mercaptoethanol.
4. LB-agar plate containing 50 µg/mL ampicillin.

2.2.3. Gel Extraction

1. 5X gel loading buffer.
2. 1X TAE buffer.
3. Sharp, clean, razor blades.
4. Microfuge spin columns.

2.2.4. Plasmid DNA Purification

1. 20 × 1 mL LB medium + antibiotic aliquots in small tubes.
2. Solution I: 10 mL 1.0M glucose, 10 mL 1M Tris-HCl, 4 mL 0.5M EDTA, 176 mL H₂O.
3. Solution II: 4 mL 10N NaOH, 2 mL 10% SDS, 194 mL H₂O.
4. Solution III: 60 mL 5.0M potassium acetate, 11.5 mL Glacial acetic acid, 28.5 mL H₂O.
5. Miniprep Express Matrix™ (BIO 101, Vista, CA).

6. 70% ethanol, 100% ethanol.
7. 1 mg/mL RNase.
8. Solid CsCl.
9. Beckman Quick-Seal centrifuge tubes.
10. TE buffer: 10 mL 1.0M Tris; 2 mL 0.5M EDTA; 988 mL H₂O.
11. Dialysis tubing (MWCO: 6000–8000) (Spectrum Medical Industries, Inc Houston, TX).

2.3. Overexpression of the Recombinant Protein in Mammalian Cells

1. Clone 9 cell, an epithelial cell line isolated from normal rat liver (ATCC CRL-1439, Rockville, MD).
2. Maintain Clone 9 cells in Ham's F-12K medium supplemented with 10% fetal bovine serum (Gibco-BRL), 100 U/mL penicillin, and 100 µg/mL streptomycin in 5% CO₂ / 95% air at 37°C, and use T-75 flasks (Fisher Scientific, Pittsburgh, PA).
3. 1X Trypsin-EDTA: 0.25% Trypsin, 1 mM EDTA-4Na (Gibco-BRL).
4. 15-mL Falcon tubes.
5. Gene Pulser II System (Bio-Rad, Hercules, CA).
6. Lipid transfection reagents: LIPOFECTAMINE and LIPOFECTAMINE PLUS™ Reagents (Life Technologies, Gaithersburg, MD).
7. OPTI-MEM media (Life Technologies, Gaithersburg, MD).
8. Hanks Balanced Salts (Sigma).
9. Geneticin-supplemented medium: medium described in **Subheading 2.3. (item 2)** is supplemented with Geneticin at a concentration of 400 µg/mL (Gibco-BRL).
10. Cloning cylinders (Bellco Glass, Inc. Vineland, NJ).

2.4. Immunofluorescence Reagents

1. Dulbecco's PBS (D-PBS): 8.1 mM Na₂HPO₄, 1.2 mM KH₂PO₄, 138 mM NaCl, 2.7 mM KCl, 0.9 mM CaCl₂, 0.5 mM MgCl₂.
2. Pipes Buffer: 0.1M Pipes (pH 6.95), 3 mM MgSO₄, 1 mM EGTA.
3. Blocking Buffer: 5% normal goat serum, 5% glycerol in D-PBS, 0.04% sodium azide.
4. Triton-DPBS: 0.1% Triton X-100 in D-PBS.
5. Formaldehyde-pipes fixative: 2.5% formaldehyde in Pipes buffer.
6. Antifade mounting reagent such as ProLong or Slow-Fade light (Molecular Probes, Inc., Eugene, OR).

2.5. Imaging

1. Fluorescence microscope. Cells can be viewed with any quality fluorescence microscope. We typically use an Axiovert 35 epifluorescence microscope (Carl Zeiss, Inc, Thornwood, NY) equipped with a 100-W Mercury lamp using Zeiss Plan-lenses. Images are captured with a 35mm camera loaded with film (Kodak T-Max, asa 3200) or a cooled charged coupled device (CCD) camera (Senys, Photometrics Inc., Tuscon, AZ) driven by the image capture and analysis

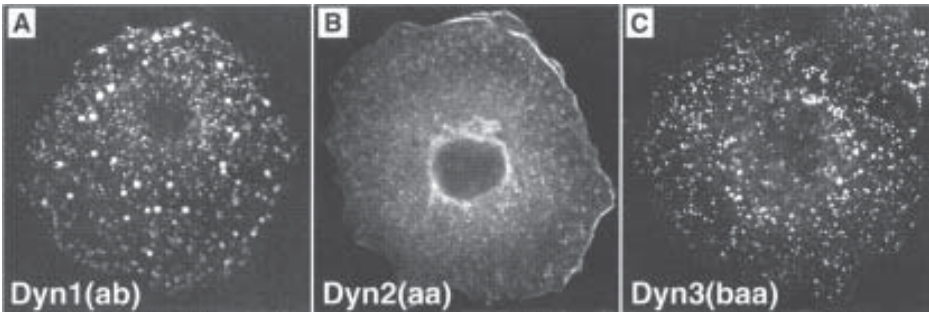


Fig. 1. Representative Confocal images of Clone 9 cells expressing GFP-Dynamin: a) Dyn1 (ab), b) Dyn2 (aa), and c) Dyn3 (baa). Note the differential distribution exhibited by the three isoforms.

program Metamorph (Universal imaging, West Chester, PA) using standard DAPI, FITC, and Texas Red filter sets (Omega Optical, Inc, and Chroma Technology Corp., both in Brattleboro, VT).

2. Confocal Microscope. LSM-310 (Carl Zeiss, Inc, Thornwood, NY) equipped with argon/krypton laser (excitations at 488 nm/568 nm), using standard DAPI, FITC and Texas Red filter sets. The confocal is attached to a dedicated PC which controls all acquisitions and saves images. An example of confocal images of GFP-tagged dynamin splice variants is shown in **Fig. 1**.
3. Fluorescence and Confocal microscopy on living cells. The GFP technology allows one to view the protein of interest in real time. This is a great improvement over the static images of the past. GFP imaging in living cells overcomes the old limitations of fixed and permeabilized cells, and is perfect for time-lapse video. Time-lapse video can be taken using any epi-fluorescence microscope that has a detector or a camera with sensitivity to low levels of light. A cooled CCD camera, a standard CCD camera with a photomultiplier tube attached, or a SIT camera is often used in conjunction with some sort of shuttering system to keep the cells from photobleaching or taking heat damage. A confocal microscope comes standard with detectors that are sensitive to low levels of light and can be set to take an image in any unit of time desired so a separate shutter is not necessary.
4. Different style setups for time lapse video.
 - a. Epi-fluorescence microscope equipped with:
 - 50 or 100 W arc lamp with excitation wavelengths appropriate for your fluorophores.
 - Appropriate filter sets, and a filter wheel if you want to do multi-fluorochrome imaging.
 - Cooled CCD camera or other detector.
 - Fast hard drive to allow rapid uninterrupted writes between acquisitions.
 - Computer controlled shutter.

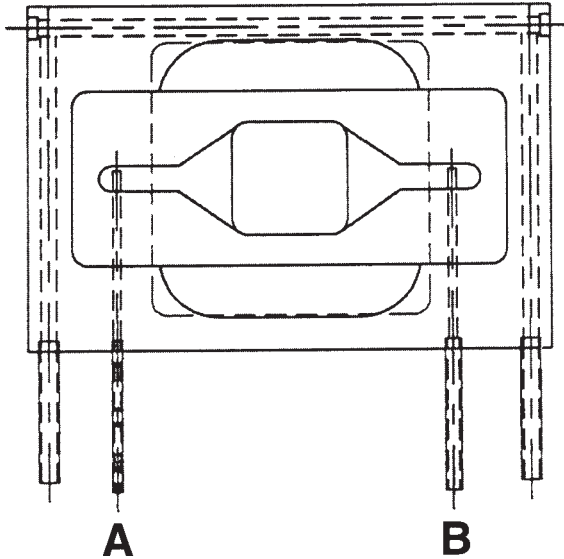


Fig. 2. Schematic of a perfusion chamber: A perfusion chamber is an invaluable tool for studying cells in a controlled environment. This sealed chamber allows media to go through tube A, across the imaging area, and out through tube B. The two outer tubes can be used to temperature control the chamber by pumping warm or cold fluid through them.

- b. Confocal microscope equipped with:
 - Argon/krypton laser excitations at 488 nm/ 568 nm.
 - Detector unit(s).
 - Fast hard drive to allow rapid uninterrupted writes between acquisitions.
5. Perfusion chambers and live cell imaging. The most important part of live cell imaging is keeping the cells as healthy and happy as possible. To accomplish this, we use a perfusion chamber (**Fig. 2**) to constantly supply the cells with fresh media and a heating/cooling stage to keep them at 37°C (or whatever temperature you need). The chamber is also useful for perfusing in different drugs, hormones, ligands, or anything else one might use to stimulate cells. The chamber and stage are both mounted to the microscope in a manner that minimizes vibration.
6. Acquiring the images
 - Representative settings for time-lapse videos taken on the Zeiss LSM 310:
 - Power = 10 (use lowest value possible to prevent heat/ laser damage to cells).
 - Pinhole = 35 (larger the pinhole, the thicker the optical section).
 - Excitation = 488 nm.
 - Time = 8 s, **No averaging**, shorter acquisition times are possible, but are dependant on intensity of the signal.
 - Resolution = 512 × 512 pixels.
 - Files are saved to disk, not a buffer or video memory.

3. Methods

3.1. cDNA Synthesis

3.1.1. Isolation and Purification of Total RNA from Tissues or Cells

The purity and integrity of isolated RNA is critical for its effective use in procedures such as cDNA synthesis, RT-PCR, Northern blotting, and translation *in vitro*. Subsequently, two methods of RNA isolation and purification are provided depending on whether tissue or cultured cells are used (*see Note 1*).

3.1.1.1. TISSUE

Total RNA can be extracted from a variety of tissues, such as brain, heart, kidney, liver, lung, muscle, pancreas, spleen, or testis. In the case of dynamin, various tissues were removed from an adult rat and quickly frozen in liquid nitrogen before storing at -80°C until use.

1. Thaw the tissue to be used and grind in 7 mL of GIT solution for each 2 g of tissue used in a tissue homogenizer.
2. Pass the homogenized mixture 5–6 times through a 26 gauge \times 1/2 in. syringe needle and centrifuge for 15 min at 12,580g at 20°C .
3. Collect the supernatant and layer it over a 4 mL cushion of 5.7M CsCl in a polyallomer tube then centrifuge the sample for 22 h at 35,000g at 20°C .
4. Resuspend the obtained RNA pellet on the bottom of the tube in 0.3M sodium acetate (pH 6.0) and transfer to a fresh RNase-free microcentrifuge tube.
5. Add 750 μL of 95% alcohol (DEPC-treated) to the resuspended RNA pellet and place at -80°C for 1 h to precipitate the RNA.
6. Centrifuge the RNA in a microcentrifuge at 15,000g at 4°C for 20 min.
7. Remove the supernatant and wash the pellet twice with 200 μL of 70% DEPC-treated alcohol.
8. Dry the pellet in a speed-vacuum for 3–5 min and dissolve in DEPC-treated water.
9. The obtained RNA is now ready to use.

3.1.1.2. CULTURED CELLS

Total RNA can also be extracted from cultured cells using the mRNA-single step method (**20**) as follows.

1. Collect 1×10^8 cells in a sterile 15 mL conical tube and centrifuge at 300g for 5 min at 4°C .
2. Wash the cell pellet with 10 mL of ice-cold PBS and centrifuge as before to collect the cells.
3. Decant the supernatant and freeze the cells in liquid nitrogen. Thaw the cells at room temperature then refreeze in liquid nitrogen. Repeat this 4 times.
4. Add 600 μL of solution D, 60 μL of 2M Na(OAc) (pH 4.0), 600 μL of saturated phenol, and 120 μL of chloroform:isoamyl alcohol with thorough mixing after the addition of each solution.

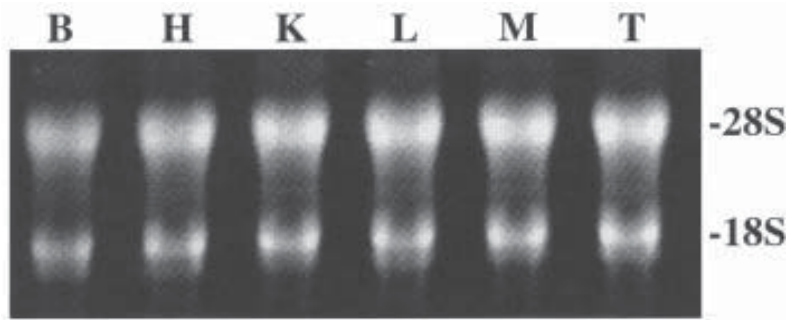


Fig. 3. Total RNA isolated and purified using the CsCl method. Lanes 1-6: Six replicates starting from 2g rat brain, heart, kidney, liver, muscle, and testis tissues. Consistent high yields and quality were obtained in each sample.

5. Shake the mixture vigorously and incubate the sample on ice for 10 min.
6. Centrifuge the sample at 10,000g for 20 min at 4°C then transfer the upper layer (aqueous phase) to a fresh RNase-free microcentrifuge tube.
7. Add an equal volume of isopropanol and incubate the sample at -80°C for 1 h to precipitate the RNA.
8. Centrifuge the sample at 15,000g for 20 min at 4°C then remove the supernatant.
9. Wash the pellet in 70% DEPC-treated alcohol twice and dry in a speed-vacuum for 3–5 min.
10. Dissolve the pellet in DEPC-treated water.
11. The obtained RNA is now ready to use.

3.1.1.3. DETERMINATION OF RNA CONCENTRATION

The concentration of isolated total RNA can be determined using an UV-spectrophotometer.

1. Make a known dilution (1:500) of the RNA sample and determine the absorbance at wavelengths of A_{260} and A_{280} .
2. Assume pure total RNA has an A_{260}/A_{280} absorbance ratio between 1.8 and 2.0.
3. Calculate total RNA concentration using $A_{260} \times \text{Dilution} \times 40 \mu\text{g/mL} = \text{Total RNA concentration}$ (see **Note 2**).

3.1.1.4. DETERMINATION OF RNA QUALITY

RNA quality can be analyzed using denaturing agarose gel electrophoresis.

1. Add 3.5× RNA loading buffer to 15–20 μg of total RNA to a final concentration of 1X and incubate at 55°C for 15 min.
2. Chill the RNA in loading buffer on ice immediately for 5 min.
3. Add 1 μL of ethidium bromide with 2 μL of RNA dye to the sample and load in a 1% agarose gel.

4. Run the gel in 1X Mops buffer for approximately 2 h at 55 V.
5. In order to analyze RNA degradation, assume that 28S and 18S eukaryotic ribosomal RNAs exhibit a near 2:1 ratio of EB staining (see **Fig. 3**).

3.1.2. Reverse Transcription (RT) (see **Note 3**)

1. Dilute 1–5 μg of total RNA in DEPC-treated water to a final volume of 11 μL .
2. Add 1 μL of 500 $\mu\text{g}/\text{mL}$ oligo(dT)₁₂₋₁₈ primer.
3. Heat the sample in a 70°C water bath for 10 min then quickly chill on ice.
4. Add 4 μL of 5X First Strand Buffer, 2 μL of DTT, and 1 μL of 10 mM dNTP mix to the sample and mix gently.
5. Incubate the sample at 42°C for 2 min then add 1 μL (200 units) of SUPER-SCRIPT™ II and pipet the mixture gently up and down.
6. Incubate the sample for 50 min at 42°C to allow for cDNA synthesis.
7. To inactivate the reaction, heat the sample in a 70°C water bath for 15 min.
8. To remove RNA complementary to the cDNA, add 1 μL (2 units) of *E. coli* RNase H and incubate the sample at 37°C for 20 min.
9. The obtained cDNA is ready to be used as template for amplification by polymerase chain reaction (PCR).

3.2. Constructing the Recombinant Protein

3.2.1. Extra-Long RT-PCR (see **Note 4**)

1. Design and synthesize 5' and 3' primers (see **Note 5**).
2. Prepare the lower layer reagent mix as indicated below for a 100 μL reaction in an autoclaved thin-walled reaction tube (Perkin Elmer):
Lower Layer
 - a. 11 μL H₂O.
 - b. 12 μL 3.3X XL Buffer II.
 - c. 8 μL dNTP Blend.
 - d. 4 μL Mg(OAc)₂.
 - e. 2.5 μL Primer 1 (1 $\mu\text{g}/\mu\text{L}$).
 - f. 2.5 μL Primer 2 (1 $\mu\text{g}/\mu\text{L}$).
3. Add an Ampliwax Gem 100 Bead to the lower layer reagent mix and spin the sample briefly.
4. Place the sample in a PCR machine for 5 min at 80°C and 2 min at 25°C for one cycle to melt the bead.
5. Add the upper layer reagent mix to the solidified wax as indicated below.
Upper Layer
 - a. 40 μL H₂O.
 - b. 18 μL 3.3X XL Buffer II.
 - c. 1 μL cDNA.
 - d. 1 μL r*Th* DNA Polymerase XL.
6. Place the sample in a PCR machine and set the cycle conditions. Generally, these must be experimentally determined and optimized following some basic guidelines (see **Note 6**).

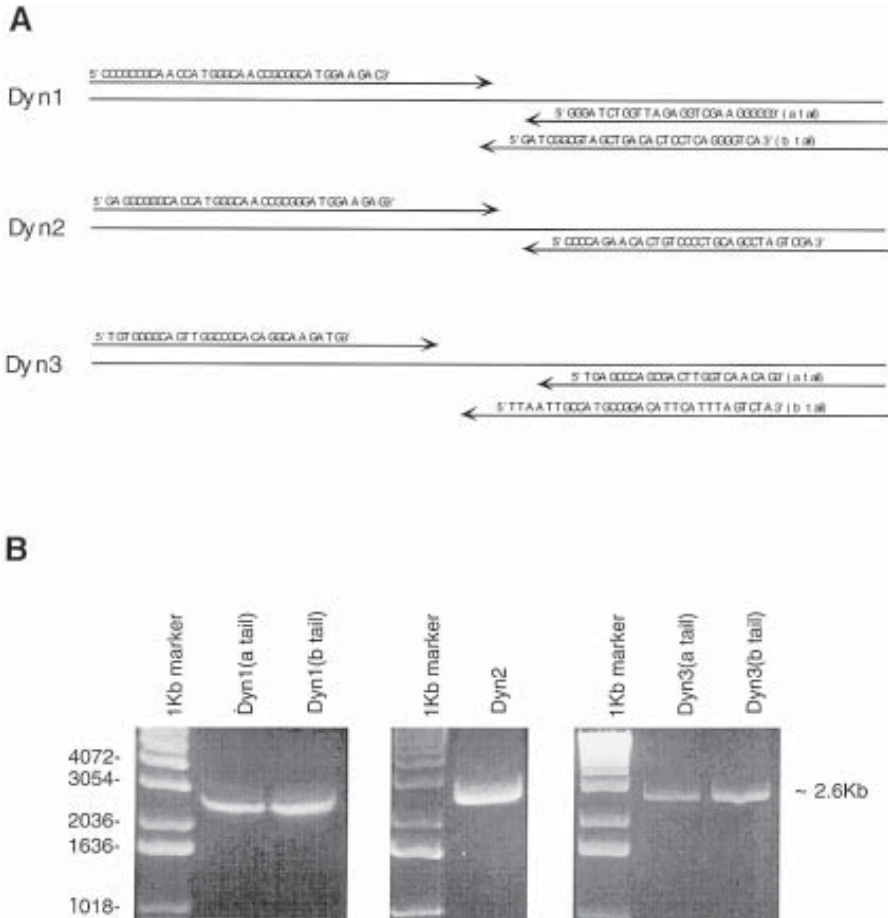


Fig. 4. Amplification of 3 different dynamin isoforms (Dyn 1, Dyn 2, and Dyn 3) from rat brain by long distance PCR. cDNA was synthesized from 10 μ g of total RNA from rat brain using an oligo (dT)_n primer. Amplification of the genes encoding full-length dynamin isoforms was performed using long distance PCR. Specific primers (A) were designed by software (MacVectorTM) using the dynamin cDNA sequence from Genebank. The 5' PCR primers were complementary to the initiation sequence. The 3' PCR primers included the corresponding stop codon for each dynamin coding region, thus discriminating between the two alternative C-termini of Dyn 1 and Dyn 3. After long distance PCR, the reaction products were analyzed by agarose gel electrophoresis (B). Approximately 2.6 Kb bands represent each dynamin isoform.

7. Use the following protocol for dynamin amplification: 28 cycles of 94°C for 1 min and 68°C (Dyn 1), 65°C (Dyn 2), 60°C (Dyn 3) for 5 min followed by a final 72°C extension time of 7 min at the end of cycle 28.
8. Analyze the reaction products by agarose gel electrophoresis (**Fig. 4B**).

3.2.2. cDNA Cloning and Construction of the Dynamin-GFP Expression Vector (see **Note 7**)

3.2.2.1. THE LIGATION REACTION

Combine the following reagents for the ligation reaction in a total volume of 10 μL :

1. Fresh PCR product 1.0 μL .
 2. 10X Ligation Buffer 1.0 μL .
 3. pCR 3.1 vector 0.5–1.0 μL .
 4. T4 DNA ligase 0.5–1.0 μL .
 5. Sterile H_2O 6–7 μL .
- Incubate the sample at 14°C overnight.

3.2.2.2. TRANSFORMATION

1. Use the ligation reaction to transform TOP 10F' Ultracomp™ cells (Invitrogen) using the heat shock method.
2. Quickly thaw a 50 μL aliquot of cells on ice.
3. Add 2 μL of ligation reaction mixture and 2 μL of 0.5M 2-mercaptoethanol to the cells without pipetting the cells up and down to mix (they are very fragile).
4. Gently tap the cells to mix and incubate them on ice for 30 min.
5. Heat shock the cells for exactly 30 s in a 42°C water bath.
6. Immediately place the cells on ice for 2 min.
7. Add 250 μL of warm SOC medium to the vial of cells and shake them at 37°C for 1 h at 225 rpm in a rotary-shaking incubator to allow the cells to recover.
8. From the 300 μL of transformed cells, plate 50 μL on an LB-agar plate containing 50 $\mu\text{g}/\text{mL}$ ampicillin and store the remaining cells at 4°C.
9. After all of the liquid is absorbed, invert the plate and place in a 37°C incubator overnight.
10. Screen positive clones for subcloning (*see* **Notes 8–10**).

3.2.2.3. RESTRICTION DIGESTS

1. 10 μg DNA.
2. 5 μL 10X digest buffer.
3. 30 U Restriction enzyme 1.
4. 30 U Restriction enzyme 2.
5. Sterile H_2O to a total volume of 50 μL .

3.2.2.4. GEL EXTRACTION

1. Add 5 μL of 5X loading buffer to the 50 μL restriction digest and load in a 1.2% agarose gel containing EB and made with 1X TAE buffer.
2. Run the gel at 75 V in 1X TAE buffer for an appropriate amount of time to separate the vector and insert. For dynamin in pCR3.1 a gel is run for 1 h 30 min to 2 h.
3. Check for the insert or vector band of interest using UV-light.

4. Cut out the band of interest with as little extra agarose as possible. Use a clean razor blade for each band to be excised.
5. Put the piece of gel in a spin column, such as Bio-Rad Freeze N'Squeeze columns and chop into small pieces.
6. Freeze the gel in the spin column at -20°C for 5 min.
7. Spin the column in a microcentrifuge for 3 min at 17,000 *g* (14,000 rpm).
8. The flow-through contains the DNA of interest and is ready to be used for ligation.

3.2.2.5. LIGATIONS (SEE NOTE 11)

Set up the following mixture for ligation with pEGFP vector and incubate overnight at 16°C :

1. 100 ng Vector.
2. 166 ng Insert.
3. 1 μL 10X Ligation Buffer.
4. 1 μL T4 DNA ligase.
5. Sterile H_2O to 10 μL .

3.2.2.6. PLASMID MINIPREP (SEE NOTE 12)

1. Grow overnight cultures by inoculating 20×1 mL LB medium + antibiotic aliquots in small tubes with 20 colonies obtained from plating transformed UltracomTM cells.
2. Incubate the cultures at 37°C for approximately 16 h in a rotary-shaker shaking at 300 rpm.
3. Centrifuge the 1 mL aliquots of bacteria containing the construct of interest in a desk top microcentrifuge for 5 min at 3000*g* (6000 rpm).
4. Aspirate the supernatant.
5. Add 50 μL of Solution I to each tube and resuspend the cells by vortexing briefly.
6. Add 100 μL of Solution II to each tube and invert 4–6 times to mix.
7. Add 75 μL of Solution III to each tube and vortex immediately for a few seconds then centrifuge at 17,000*g* (14,000 rpm) in a microcentrifuge for 5 min.
8. Transfer the supernatants to clean tubes and add 400 μL of Miniprep Express Matrix. Mix well by shaking vigorously.
9. Invert the samples 5–6 times to mix well and allow the plasmid DNA to bind the matrix.
10. Centrifuge the samples briefly and aspirate the supernatant.
11. Wash the matrix by resuspending it in 1.0 mL of 70% ethanol then briefly centrifuge again.
12. Aspirate the ethanol and then allow the matrix to dry completely at room temperature for about 20 min or speed-vacuum for 5–10 min.
13. Resuspend the matrix-bound DNA in 50 μL of H_2O by tapping to elute the DNA.
14. Spin the samples for 1 min at 17,000*g* (14,000 rpm) in a microcentrifuge and transfer the supernatant containing the DNA to a fresh tube.
15. The plasmid DNA is now ready to be used for restriction enzyme analysis and sequencing.

3.2.2.7. PLASMID MAXI-PREP

1. Grow overnight cultures of bacteria containing the construct of interest in 200 mL of LB medium + antibiotic.
2. Centrifuge the cultures at 6000g for 10 min at 4°C in 500 mL bottles (6000 rpm using a JA-14 rotor and Beckman centrifuge).
3. Aspirate the supernatant and resuspend the pellet in 5 mL of Solution I by thoroughly vortexing.
4. Add 10 mL of Solution II to each sample and incubate the samples at room temperature for 5 min.
5. Add 7.5 mL of Solution III to each sample and vortex to mix.
6. Transfer each sample, approximately 25 mL, to a 50 mL centrifuge tube and centrifuge at 20,000g for 10 min at 4°C (12,000 rpm using a JA-17 rotor and Beckman centrifuge).
7. Transfer the supernatant from each sample to a fresh tube and add an equal volume of 2-propanol, approximately 25 mL. Invert the samples a few times to mix and incubate them at -20°C for 1 h.
8. Centrifuge the samples at 20,000g for 10 min at 4°C (12,000 rpm using a JA-17 rotor and Beckman centrifuge).
9. Wash the resulting pellets twice with 70% ethanol and dry using a lyophilizer.
10. Add 10 mL of H₂O containing 16 µL of RNase to each pellet and incubate in a 37°C water bath for 2 h.
11. Add 11 g of solid CsCl, for a final concentration of 1.1 g CsCl/ mL, and 100 µL of a 10 mg/mL stock solution of EB in water to each sample for a solution with a final density between 1.55 and 1.60 g/mL.
12. Transfer the DNA/CsCl solutions to Beckman Quick-Seal centrifuge tubes (16 × 76 mm) and centrifuge at 245,000g (55,000 rpm) and 20°C for 22 h using a NVT 65 rotor (*see Note 13*).
13. After centrifugation, collect the lower band, which consists of closed circular plasmid DNA, by using a 21 gauge × 1 in. hypodermic needle inserted gently into the tube below the band and then moving the tip of the needle to the band of interest and drawing the band out (*see Note 14*) (*see Fig. 1.4 in [21]*).

3.2.2.8. REMOVAL OF ETHIDIUM BROMIDE FROM DNA

1. Add 100% ethanol to the collected DNA so that the ethanol concentration is between 70% and 80%, causing the DNA and part of the CsCl to precipitate.
2. Centrifuge the samples at 2200g (3,400rpm) for 10 min in an IEC clinical centrifuge.
3. Wash the resulting pellets twice with ethanol, first with 70% and next with 95%, and then dry using a lyophilizer.
4. Dissolve the DNA and small amount of CsCl left in 1 mL of H₂O for each sample.
5. Aliquot the samples in dialysis tubing and dialyze against TE buffer.
6. After 6 h of dialysis, change the TE buffer and further dialyze the samples for 6–8 h in fresh TE buffer.
7. Use an UV-spectrophotometer to check the concentration of plasmid DNA.
8. Check the DNA quality using restriction enzyme and sequence analysis (*see Note 15*).

3.3. Overexpression of the Recombinant Protein in Mammalian Cells (see Note 16)

3.3.1. Transfection by Electroporation (see Note 17)

1. Trypsinize a confluent flask of cells for approx 5 min or until the cells can be disrupted upon tapping the flask against the hand.
2. Resuspend the cells in 10 mL of cold PBS and transfer to a 15 mL Falcon tube.
3. Centrifuge for 5 min at 1100g (2260 rpm) in a swing centrifuge.
4. Resuspend the cells in fresh cold PBS to wash and centrifuge again at same speed.
5. Resuspend the cells in 400 μ L of cold PBS or approximately 3×10^6 cells/mL.
6. Transfer the cells to a sterile electroporation cuvet (0.4 cm) and add 20–50 μ g of plasmid DNA.
7. Incubate the cells on ice for 15 min.
8. Electroporate the cells at 0.3 kV and 300 μ F using a Gene Pulser II System (Bio-Rad, Hercules, CA).
9. Immediately place the cuvet with cells on ice again for 10 min.
10. Transfer the cells to a 100 mm tissue culture petri dish containing 10 mL media. For ease in transferring, add 0.5 mL of media first to the cuvet and resuspend the cells lightly then transfer to the petri dish.

3.3.2. Lipid Transfection (see Note 18)

1. The day before transfection, trypsinize cells and plate on acid-washed coverglasses in 35 mm petri dishes containing 2 mL media so that cells are 50% to 80% confluent on the day of transfection.
2. For each transfection, dilute 2–4 μ g of DNA in 100 μ L of serum-reduced OPTI-MEM media.
3. Add 6 μ L of LIPOFECTAMINE PLUS reagent per transfection to the diluted DNA, mix well, and incubate at room temperature for 15 min.
4. Dilute 4 μ L of LIPOFECTAMINE Reagent in 100 μ L of serum-reduced OPTI-MEM media, per transfection, in a separate tube.
5. Combine the pre-complexed DNA and diluted LIPOFECTAMINE Reagent and incubate at room temperature for 15 min.
6. During the last incubation, aspirate the media on the cells to be transfected and add 800 μ L of serum-reduced OPTI-MEM media.
7. Add the DNA-PLUS-LIPOFECTAMINE Reagent complexes to the dishes, 200 μ L per dish, and incubate the cells at 37°C at 5% CO₂.
8. After 3 h, add 1 mL of media containing serum to each dish and culture the cells overnight. If immunofluorescence is to be done the next day, it may be helpful to wash the cells with warm Hank's Balanced Salts before fixation to remove lipid from the surface of cells.

3.3.3. Creating a Stable Cell Line (see Note 19)

1. Transfect cells with the construct of interest using, for example, one of the methods described in **Subheadings 3.3.1.** and **3.3.2.** (see **Note 20**).

2. 24 h after transfection, place the cells under selective pressure by culturing them with medium containing the antibiotic to which the plasmid provides resistance (*see Note 21*).
3. Culture the transfected cells for 10–15 d then isolate resistant clones using cloning cylinders.
4. Transfer the isolated clones to fresh petri dishes for expansion and analysis.

3.4. Visualization (see Notes 22–28)

3.4.1. Immunofluorescence for Co-Localization Studies Using Antibodies

1. Grow cells on acid-washed coverglasses for 1–2 d. Perform transfections the day before the cells are fixed if necessary.
2. Aspirate the media from cells and rinse with D-PBS at room temperature or 37°C if the cells are sensitive to temperature changes.
3. Fix the cells for 20 min using approximately 2 mL per dish of formaldehyde-Pipes fixative at room temperature or 37°C.
4. Rinse the cells with D-PBS 3 times waiting 3 min between washes.
5. Permeabilize the cells using Triton-DPBS for 2 min.
6. After rinsing cells quickly 2–3 times with D-PBS to get rid of the Triton, rinse 3 times for 3 min with D-PBS.
7. Incubate the cells in blocking buffer for 1 h at 37°C. 1 mL of blocking buffer can be added to each dish, or coverglasses can be laid on top of a 150 µL drop of blocking buffer on Parafilm.
8. Incubate the cells in the chosen primary antibody (1–40 mg/mL in blocking buffer) for 2 h. To save antibody, lay the coverglass on a 60–100 µL drop of antibody solution on Parafilm. It is best to spin the diluted antibody briefly in a microcentrifuge before using.
9. Rinse the cells 2–3 times quickly with D-PBS to get rid of excess antibody, then rinse 3 times for 10 min each wash with D-PBS.
10. Incubate the cells in the appropriate fluorescently labeled secondary antibody (1–5 µg/mL) for 1 h. Again, it is best to spin the diluted antibody briefly in a microcentrifuge before using.
11. Rinse the cells 2–3 times quickly with D-PBS to get rid of excess antibody, then rinse 3–4 times for 5 min each wash with D-PBS.
12. Dip the coverglass briefly in distilled water, wick excess water away with a paper towel, then mount the coverglass on a glass slide using an antifade mounting reagent.

3.4.2. Digital Movie

Once you have acquired your images you will want to assemble them into a digital movie of some sort (e.g., QuickTime, mpeg, or avi) for further analysis. When using an epi-fluorescence microscope, use the image acquisition program to make movies which are then saved in an appropriate format. When images are taken on a confocal microscope (e.g., Zeiss LSM310) some manipulation of the data may be necessary. Use a program called ctc 1.4 (available at ftp://codon.nih.gov/pub/nih-image/programs/ctc_1.4.hqx) to convert the files from a

Zeiss file to a TIFF file that can be read in NIH Image 1.61 (available at <http://rsb.info.nih.gov/nih-image/index.html>) (Macintosh only). PC's can use Scion Image, which is a port of NIH Image over to the PC (available at Scioncorp.com). When collecting data with the confocal microscope, make sure that the computer gives each image a sequential file name.

3.4.3. Converting Zeiss Files to NIH Image files

1. Select all of your images for a specific series and drag them on top of the ctc 1.4 icon (this launches the script).
2. Enter `Imag` in the Creator dialog box, `TIFF` (all caps) in the file type box, and press enter. This will convert each image into an NIH Image TIFF file.
3. Now select all again, and double click. This will launch NIH Image and all of your files will open sequentially.
4. At the menu bar go to **Stacks ♦ Windows to Stack**. This will put all of your files into 1 stack.
5. Now that the stack is made, you can play, view, manipulate, or save as one of many different movie styles. There are many pre-made filters and macros available that facilitate taking measurements and logging data (available at <ftp://codon.nih.gov/pub/nih-image/macros/>).

3.4.4. Getting Your Video Out There

Once you have produced your time-lapse video you will want to show it to the world. This is easily accomplished using the internet, as many labs have their own web pages that contain GFP videos. This is not very useful if you are going to a conference or want to show it in conjunction with a poster. In these cases you will need to write your movie to a videotape and show it using a VCR and a television (less desirable), or use a computer with or without a video projector (most desirable). To output the video to videotape a specialized computer set-up is required. It generally requires a fast computer, fast hard drive(s), and usually a specialized video card that allows output to video or S-video (some even offer PAL or NTSC options). Showing the video using a projector is quite simple, just connect a projector to the monitor port of the computer and you are done, just load your video and hit play.

4. Notes

1. It is very important to use RNase free tips, tubes, and DEPC-treated water when isolating RNA.
2. Measure the A_{260} . A solution of RNA whose $A_{260}=1$ contains approximately 40 μg of RNA per mL.
3. First-strand cDNA synthesis by reverse transcription (RT) can be performed using kits from various companies with specific primers if only certain cDNAs are to be synthesized, with degenerate primers to synthesize a range of cDNAs, or with dT primers to amplify polyadenylated RNAs. In this case, cDNA synthesis

by reverse transcription was performed using the SUPERSCRIPT™ II RNase H⁻ Reverse Transcriptase kit (GIBCO).

4. Full-length cDNAs encoding the different dynamin isoforms were amplified using the Perkin Elmer XL PCR kit (Perkin Elmer, Branchburg, NJ), however, there are a variety of PCR kits available.
5. Specific oligonucleotide primers for the three dynamin isoforms were designed using MAC Vector™ software and the different dynamin isoform cDNA sequences from Genebank, accession numbers X54531, L25605, and D14076 for Dyn1, Dyn2, and Dyn3 respectively (**Fig. 4A**). The primers were synthesized on an Applied Biosystems model 394 DNA/RNA synthesizer. The 5' PCR primers were complementary to the initiation sequence and the 3' PCR primers included the corresponding stop codon for each dynamin, allowing discrimination between the two alternative C-termini of Dyn 1 and Dyn 3.
6. Start with a 1 min denaturing step at 94°C followed by a 1 to 5 min annealing step usually 5°C below the melting temperature of the primers used. When the primers have different melting temperatures, try to compromise with an in between temperature or use the lower melting temperature to determine the annealing temperature. Depending on the size of the PCR product, a 1 to 2 min extension time at 72°C can be added to each cycle after annealing or the annealing time can be extended and one final extension time can be used. After all cycles are complete, the PCR product should be held at 4°C until further use. Generally 25 to 30 cycles should result in an adequate amount of PCR product.
7. Dynamin PCR fragments were ligated into the TA pCR 3.1 (Invitrogen, Carlsbad, CA) eukaryotic expression vector. Use of the TA vector allows for optimal ligation efficiency, especially when dealing with a large insert size. In addition, the construct can be directly used to transform mammalian cells for overexpression as long as the insert is in the sense direction.
8. For subcloning of the full-length cDNAs corresponding to Dyn 1, Dyn 2, and Dyn 3, reamplification of the different isoforms was performed using PCR as before, however, with new 5' and 3' PCR primers. The 5' and 3' PCR primers for Dyn 1 and Dyn 2 were designed so that *Hind* III and *Eco*R I restriction sites were introduced, respectively. For Dyn 3 constructs, an *Eco*R I site was introduced at the 5' end and a *Bam*H I site at the 3' end. In addition to the restriction site, the 3' PCR primers were constructed to knock out the dynamin stop codon.
9. Before designing primers where an artificial restriction enzyme cut site is introduced, the restriction enzyme sites in the insert and the vector need to be analyzed. For example, first, a map of the dynamin nucleotide sequence was checked for restriction enzyme cut sites present and absent within the open reading frame (ORF). Second, the vector's multiple cloning site was analyzed to find enzyme cut sites not found in the dynamin ORF and that were far enough apart to allow for digestion of the vector and subsequent ligation with the dynamin insert. When possible, two unique restriction enzymes with efficient restriction digest activity should be chosen.

10. PCR products were ligated with the TA pCR3.1 vector, competent cells were transformed with this ligation product, and positive clones with restriction sites inserted were identified. Dynamin inserts from the pCR3.1 constructs were excised by digestion with the appropriate restriction enzymes, gel purified using Bio-Rad Freeze N' Squeeze™ spin columns, and ligated with pEGFP-N₁ and pEGFP-C₁ expression vectors (Clontech, Palo Alto, CA) digested with the same restriction enzymes as the dynamin insert and gel purified. Again, competent cells were transformed with the ligation product and positive clones were identified. All constructs were verified by restriction enzyme and sequence analysis (ABI PRISM 377 DNA sequencer, Perkin Elmer). Obtained sequences were analyzed using DNA analysis software (DNA star, Madison, WI).
11. Ligations can be performed at different vector: insert ratios: At first 1:1, 1:2, and 1:3 ratios can be tried and then the ratio optimized from here. As a general rule, 100 ng of vector is used and the amount of insert to use is calculated using the following equation: $(\text{vector amount in ng}) \times (\text{insert size}) \times (\text{ratio}) / (\text{vector size}) = \text{insert amount in ng}$. Using dynamin and the pEGFP-N₁ vector in a 1:3 ratio as an example, the calculation is as follows: $(100 \text{ ng})(2.6 \text{ kb})(3) / (4.7 \text{ kb}) = 166 \text{ ng}$ of dynamin insert.
12. Plasmid DNA purification is separation of the plasmid DNA of interest from the chromosomal DNA of the host, for which a number of methods have been developed. One method for purification of a small amount of plasmid (miniprep) and one method for purification of a large amount of plasmid (maxiprep) are provided.
13. Balancing of the tubes before centrifugation is important as a high speed spin is used. After centrifugation, two bands of DNA should be visible in ordinary light. The upper band, which usually contains less material, consists of linear bacterial DNA and nicked circular plasmid DNA, whereas the lower band consists of closed circular plasmid DNA and is the band to be collected.
14. It is important to insert a needle tip at the top of the tube before drawing the DNA out so air bubbles are not introduced thus disrupting the DNA bands. Generally approximately 2–3 mL of DNA are withdrawn.
15. This method allows very pure DNA to be obtained that is optimal for transfection, however, this method requires more time and work than commercially available kits.
16. The choice of cell type to be used for analysis of the protein of interest is an important part of an experiment and depends on the aim of the experiment. For example, if analysis of the protein in regards to cell morphology is of interest, the cell type used should be one that is large and well-spread. In addition, it is ideal when overexpressing a protein in mammalian cells when the cell type used is the same species as that which was used to obtain the sequence for the protein to be overexpressed. Another concern when overexpressing a protein in mammalian cells is that the protein is localizing and functioning properly. This is especially important when the cell type used does not express the protein endogenously.

17. Different cell types use different electroporation conditions (23), therefore, before electroporating cells it is necessary to research the optimal electroporation conditions for the cell type being used.
18. For lipid transfections there are many commercially available lipid transfection kits. The protocol here uses the LIPOFECTAMINE and LIPOFECTAMINE PLUS™ Reagents.
19. Stable cell lines can be useful when a large quantity of transfected cells is desired for biochemical studies. In addition, if it is necessary to overexpress more than one plasmid in a cell, creating a stable cell line with one of the plasmids allows subsequent transfections to be done with only a single plasmid.
20. It is preferable to transfect cells by electroporation when trying to establish a stable cell line so the cells can be plated thinly in petri dishes after transfection. This allows cells from a single clone to be easily isolated.
21. For example, Clone 9 cells transfected with a dynamin-pEGFP construct are cultured with media containing Geneticin at a concentration of 400 µg/mL.
22. The final products of all the molecular biology done in the earlier part of the chapter are cells expressing the GFP-tagged protein of interest. Now that you have the cells, you will surely want to get some images of the protein, and of other proteins that may or may not co-localize with it. As GFP is a 27 kDa protein, tagging another protein with GFP may alter its localization. Therefore, after tagging a protein with GFP and expressing it in cells, it is prudent to stain GFP-expressing cells for the endogenous protein in order to make sure the GFP-tagged protein and endogenous protein co-localize. Using a GFP-tagged protein in combination with immunofluorescence also allows one to look for co-localization of the protein of interest with other proteins while only having to stain for one of the proteins. Following is a standard fixation protocol for immunofluorescence microscopy and confocal microscopy. In this case, any fluorescent probes or ligands, such as endocytic markers (e.g., transferrin, toxins, or dextran), should be loaded prior to fixation.
23. It is important to use a medium that is low in cyclic hydrocarbons (e.g., Riboflavin) as they greatly increase the autofluorescence and consequently, lower your signal to noise ratio.
24. It is absolutely essential to optimize your imaging set-up. See how much you can attenuate your excitation source and still get good emission from your fluorophore. We have been able to attenuate a 100 W arc light over 95% with neutral density filters and still get a good signal when using a cooled CCD camera. See how much you can boost the gain of your detectors to improve your signal. Collect some sequences using frame averaging and some without. Examine for any noticeable differences. It is often better to do frame averaging after you have acquired the raw data, instead of during the acquisition process.
25. Make sure to use the appropriate microscopy set up for the type of data you want to collect. A standard epi-fluorescence microscope with a CCD camera might be perfect for imaging a flat cell type such as a fibroblast, but would be inadequate for the MDCK (Madin-Darby Canine Kidney) cell line which is thick and polarized. Only a confocal or 2-photon scope would give the required resolution to image the different domains.

26. It is critical that the hard drive being written to be attached locally (not across a network). Writing across a LAN can cause an interruption in your time-lapse acquisitions, giving you a series in which the times between frames are not equal.
27. When mounting shutter systems onto the microscope, it is often necessary to dampen the vibration from the shutter opening and closing. This is accomplished by putting rubber, felt, or something else between the microscope and the shutter unit. Putting a similar material onto the foot of the shutter unit (the piece it stands on) also helps reduce vibration. Alternatively the shutter can be attached not to the microscope, but to the table on which the microscope is sitting.
28. Tag both the N- and C-termini of your protein with GFP to see if the localization changes. Sometimes a peptide linker of 4 to 6 (or more) amino acids between GFP and the protein helps both function properly.

References

1. Ormo, M., Cubitt, A. B., Kallio, K., Gross, L. A., Tsien, R. Y., and Remington, S. J. (1996) Crystal Structure of the *Aequorea victoria* Green Fluorescent Protein. *Science* **273**, 1392–1395.
2. Cubitt, A. B., Heim, R., Adams, S. R., Boyd, A. E., Gross, L. A., and Tsien, R. Y. (1995) Understanding, improving and using green fluorescent protein. *Trends Biochem. Sci.* **20**, 448–455.
3. Chalfie, M., Tu, Y., Euskirchen, G., Ward, W. W., and Prasher, D. C. (1994) Green Fluorescent Protein as a Marker for Gene Expression. *Science* **263**, 802–805.
4. Baba, T., Damke, H., Hinshaw, J. E., Ideda, K., Schmid, S. L., and Warnock, D. E. (1995) Role of dynamin in clathrin-coated vesicle formation. *Cold Spring Harb. Symp. Quant. Biol.* **60**, 235–242.
5. McNiven, M. (1998) Dynamin: A molecular motor with pinchase action. *Cell.* **94**, 151–154.
6. Urrutia, R., Henley, J. R., Cook, T., and McNiven, M. A. (1997) The dynamins: redundant or distinct functions for an expanding family of related GTPases? *Proc. Natl. Acad. Sci. USA.* **94**, 377–384.
7. Warnock, D. E. and Schmid, S. L. (1996) Dynamin GTPase, a force-generating molecular switch. *BioEssays.* **18**, 885–893.
8. Cook, T. A., Urrutia, R., and McNiven, M. A. (1994) Identification of dynamin 2, an isoform ubiquitously expressed in rat tissues. *Proc. Natl. Acad. Sci. USA.* **91**, 644–648.
9. Nakata, T., Takemura, R., and Hirokawa, N. (1993) A novel member of the dynamin family of GTP-binding proteins is expressed specifically in the testis. *J. Cell Sci.* **105**, 1–5.
10. Obar, R. A., Collins, C. A., Hammarback, J. A., Shpetner, H. S., and Vallee, R. B. (1990) Molecular cloning of the microtubule-associated mechanochemical enzyme dynamin reveals homology with a new family of GTP-binding proteins. *Nature.* **347**, 256–261.

11. Sontag, J. M., Fykse, E. M., Ushkaryov, Y., Liu, J. P., Robinson, P. J., and Sudhof, T. C. (1994) Differential expression and regulation of multiple dynamins. *J. Biol. Chem.* **269**, 4547–4554.
12. Damke, H., Baba, T., Warnock, D. E., and Schmid, S. L. (1994) Induction of mutant dynamin specifically blocks endocytic coated vesicle formation. *J. Cell Biol.* **127**, 915–934.
13. Takei, K., McPherson, P. S., Schmid, S. L., and De Camilli, P. (1995) Tubular membrane invaginations coated by dynamin rings are induced by GTP- γ S in nerve terminals. *Nature.* **374**, 186–190.
14. Henley, J. R., Krueger, E. W., Oswald, B. J., and McNiven, M. A. (1998) Dynamin-mediated internalization of caveolae. *J. Cell Biol.* **141**, 85–99.
15. Oh, P., McIntosh, D. P., and Schnitzer, J. E. (1998) Dynamin at the neck of caveolae mediates their budding to form transport vesicles by GTP-driven fission from the plasma membrane of endothelium. *J. Cell Biol.* **141**, 101–114.
16. Llorente, A., Rapak, A., Schmid, S. L., van Deurs, B., and Sandvig, K. (1998) Expression of mutant dynamin inhibits toxicity and transport of endocytosed ricin to the Golgi apparatus. *J. Cell Biol.* **140**, 553–563.
17. Henley, J. R. and McNiven, M. A. (1996) Association of a dynamin-like protein with the Golgi apparatus in mammalian cells. *J. Cell Biol.* **133**, 761–775.
18. Jones, S. M., Howell, K. E., Henley, J. R., Cao, H., and McNiven, M. A. (1998) Role of dynamin in the formation of transport vesicles from the trans-Golgi network. *Science* **279**, 573–577.
19. Cao, H., Garcia, F., and McNiven, M. (1998) Differential distribution of dynamin isoforms in mammalian cells. *Mol. Biol. Cell.* **9**, 2595–2609.
20. Chomczynski, P. and Sacchi, N. (1987) “Single-step method of RNA isolation by acid guanidinium thiocyanate-phenol-chloroform extraction.” *Anal. Biochem.* **162**(1), 156–159.
21. Sambrook, J., Fritsch, E. F., and Maniatis, T. (1989) *Molecular Cloning a laboratory manual*, second edition, Figure 1.4.
22. *Methods in Electroporation* (1993) Bio-Rad Laboratories.

Transient Transfections and Heterokaryons as Tools for the Analysis of Keratin IF Dynamics

Jesús M. Paramio and José L. Jorcano

1. Introduction

All eukaryotic cells contain three distinct cytoskeletal networks: microtubules, microfilaments, and intermediate filaments (IF). In epithelial cells *in vivo*, the IF cytoskeleton is composed of heteropolymers of type I (acidic) and type II (neutral-basic) keratins, whose expression is carefully controlled in a cell type- and differentiation-specific manner (*1–3*). In addition, many epithelial cells in culture also induce the synthesis of the IF protein vimentin. In contrast to the other cytoskeletal proteins, which have been shown to be highly dynamic (*4–8*), IF in general, and keratins in particular, have long been considered the most stable and consequently the least dynamic components of the cell cytoskeleton (*9,10*). The majority of the dynamic studies on subcellular structures have been performed by microinjecting the proteins under study after their *in vitro* labeling. This approach, however, is very difficult with keratins due to the high insolubility shown by these proteins over a wide range of physiological conditions. In addition, this technique could lead to alteration in the dynamic process due to the large amount of protein injected into the cells (*11*) and because the incorporation of new molecules into IF structures also differs between preexisting and newly assembling filaments (*12*). As an alternative to microinjection, transfections can be used. However, in standard transient transfection experiments, expression of the transgene takes place during a broad range of time (12–96 h), and it is impossible to know the precise moment at which the expression started in any particular cell, thus making conventional transfection techniques unfavorable for dynamic studies. However, the standard transfection technique is very useful for investigating the behavior of mutated genes (*13–15*).

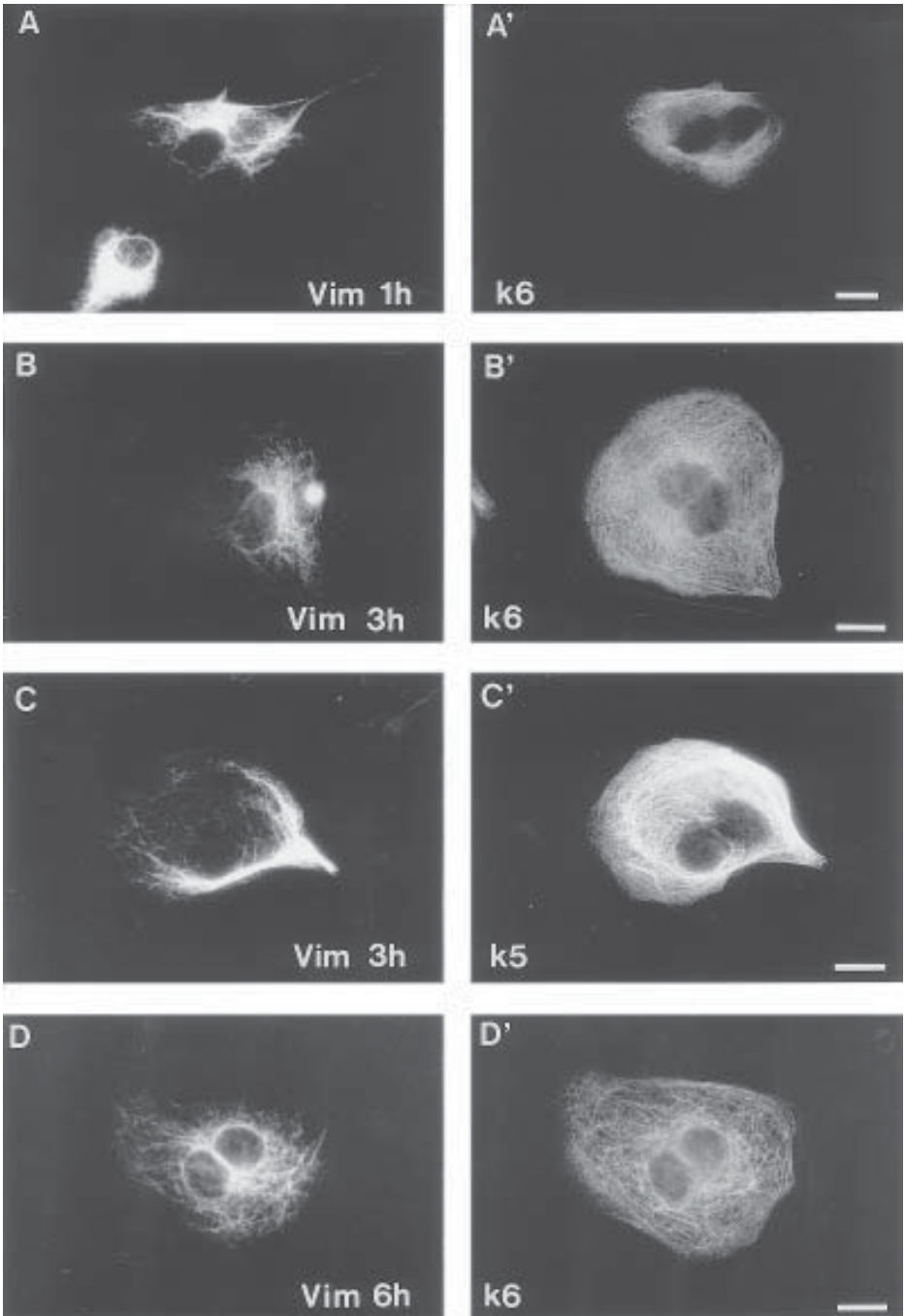


Fig. 1

Here we describe two alternative approaches to study the dynamics of IF proteins in general, and keratins in particular: the formation of cell hybrids and the transfection of keratin genes under synchronized expression conditions. In the first case, two different parental cell lines are chosen according to a different keratin (or other IF proteins) expression pattern. Upon their fusion, it is possible to study how the keratins from the parental cells recombine and copolymerize to form the heterokaryon cytoskeleton. In addition, the dynamics of different proteins during the process can be followed by immunofluorescence using specific antibodies. Therefore, the cell hybrids provide a tool for studying the dynamic properties of individual polypeptides *in vivo* without alterations in their endogenous amounts. The use of appropriate monospecific keratin antibodies allows the simultaneous observation of the temporal evolution of individual keratins and of the keratin cytoskeleton as a whole (**Fig. 1**), *see also (16)*. The second approach, transfections under synchronized expression conditions, is related to the dynamic incorporation of a newly synthesized keratin into the preexisting keratin cytoskeleton, and has been successfully used to analyze the precise mechanism of keratins K1 and K10 assembly into epithelial and non-epithelial cells (**Fig. 2**), *see also (17)*.

Finally, both approaches are suitable for analyzing the possible effects of other cellular processes, such as phosphorylation or dephosphorylation, on the dynamic behavior of keratins by adding drugs that inhibit or activate these processes during the temporal evolution of the experiments (**18**).

2. Materials

2.1. Cell Lines

In order to perform cell hybrid experiments, the different cells to be used should be selected according to their distinct keratin expression pattern, so they differ at least in the two polypeptides to be simultaneously analyzed. Usually a simple epithelium derived cell line can be used. However, other

Fig. 1. (*opposite page*) Example of the dynamics of vimentin (A, B, C,D) versus keratin K6 (A', B', D') or K5 (C') upon the fusion between PtK2 (simple epithelial cells, which also express vimentin) and MCA3D (non-transformed murine keratinocyte) cells. Note that keratins spread much faster than vimentin and by 3 h after fusion, K6 (B') and K5 (C') are distributed throughout the heterokaryon cytoplasm, while vimentin (B,C) appears restricted to filament bundles localized around the parental PtK2 nuclei. At 6 h postfusion, the process is completed for both vimentin (D) and keratins K6 (D') and K5 (not shown) which appear redistributed throughout the entire heterokaryon cytoplasm. Antibodies used were mouse mAb V9 against vimentin (Boehringer Mannheim) and rabbit polyclonals against K6 (A', B', D') or K5 (C'), both purchased from Babco. Bars represent 10 μ m.

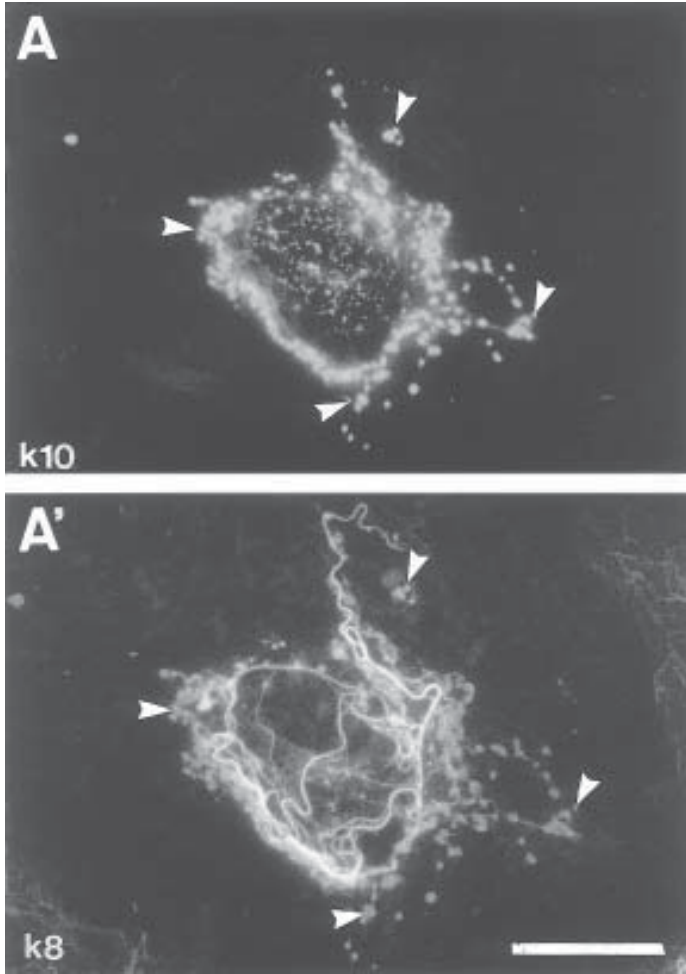


Fig. 2. Example of the interaction between keratin K10 (A) and endogenous keratin K8 (A') upon transfection of K10 gene under cytomegalovirus promoter (*17*) into PtK2 cells at early time upon synthesis and chase experiment (3 h). Note that at this early time, K10 (A) forms round aggregates that display an almost exclusive perinuclear localization and does not integrate into the endogenous keratin filaments. In addition, these aggregates led to the collapse of the endogenous keratins (A') and also tubulin, vimentin and actin cytoskeletal structures (*17*). The endogenous keratins remain in some perinuclear filaments and also appear colocalized in aggregates with transfected K10 (arrowheads). Later on in these experiments, the vast majority of the transfected cells displayed K10 forming a well developed and organized IF network together with the endogenous keratins (not shown, see also *17,18*). Antibodies used were mouse mAb K8.60 (Sigma) against K10, and rat mAb Troma 1 (kindly provided by Dr. R. Kemler) against K8. Bar represents 10 μ m.

possibilities are fibroblasts, that can be detected using anti vimentin antibodies, or different epithelial cells, which can be detected with species-specific keratin antibodies. Another important factor to take into account is the similarity of the different culture media for growing the parental cells. It is often advantageous to select cells that grow on similar types of media and at similar serum concentrations. It is important to note that immortalized human keratinocytes or Ha-ras transformed murine keratinocytes express keratins K8 and K18, thus making it very difficult to follow keratin dynamics upon their fusion with simple epithelial cells, which are normally followed using antibodies against these proteins.

For transfection studies, it is important to take into account transfection as a crucial parameter because under the modifications described here, there is a substantial decrease in the number of efficiently transfected cells. Another aspect, although less relevant, is the endogenous composition of the IF cytoskeleton, which must allow detection of the transfected protein. This possible problem can be partially alleviated using tagged constructs (*13,14*).

2.2. Chemical

1. To promote the cell fusion, we normally use polyethylenglycol (PEG) 1500 (Boehringer Mannheim), which can be purchased ready to use and stored at 4°C for several months.
2. Protein synthesis is inhibited by adding to the cultures 50 μ M cycloheximide (Sigma). Stocks (100X) can be made in 70% ethanol and stored at -20°C for at least one year.
3. PBS: 137 mM NaCl, 2.7 mM KCl, 4.3 mM Na₂HPO₄, 1.4 mM KH₂PO₄, pH 7.5.
4. PBS-T: PBS containing 0.1 % Tween 20.
5. BSA: bovine serum albumin.
6. Methanol fixative for immunofluorescence: cold methanol/acetone (2:1).
7. DAPI (4' 6-diamidino-2phenylindole).
8. Mowiol or similar aqueous mounting medium.

2.3. Other

For the immunofluorescence analysis, either after cell fusion or transfection, cells are grown onto glass coverslips that were previously washed with 70% ethanol and subsequently sterilized overnight. If the cells do not adhere properly, coverslips can be incubated for 30 min–1 h in fetal calf serum prior to seeding cells. The different antibodies against specific keratin polypeptides, can be purchased from different sources: Sigma, Boehringer Mannheim, Babco, and others. For a precise review describing the specificity of different keratin antibodies see (*19*). Secondary antibodies raised for multiple labeling purposes can also be obtained from different sources. We currently use those from Jackson Immunoresearch Labs.

3. Methods

3.1. Cell Fusion Protocol

1. The day before fusion, trypsinize parental cell cultures and plate an appropriate number of each cell type together onto glass coverslips. The critical aspect is that sufficient numbers of cells are plated. Plating too many cells will lead to confluent growth with polykaryon formation (*see Note 1*). Typically, $5 - 6 \times 10^4$ cells should be used for a 6 cm diameter petri dish, which can accommodate up to 11 glass coverslips (round 11 mm diameter).
2. Incubate cells in the appropriate medium containing serum at least 12–16 h at 37°C in 5% CO₂ atmosphere. Check to determine whether the cells are properly attached and in an appropriate number.
3. Wash the cells three times with prewarmed serum-free medium.
4. Aspirate the medium carefully and add PEG (1 mL per p60 petri dish).
5. Incubate at room temperature for 1 min gently rotating the plate to cover all the glass coverslips.
6. Wash the cells 3–4 times as in **step 3**.
7. Add normal medium containing serum and incubate for different periods of time, for example, a typical experiment must include: 0, 15 min, 30 min, 1 h, 2 h, 3 h, 6 h, 12 h, 24 h.
8. Collect coverslips for each period of time and process for conventional immunofluorescence analysis.

3.2. Transient Transfection

Under Synchronized Expression Conditions

1. The day before transfection, trypsinize parental cells and plate appropriate number onto glass coverslips. For a conventional calcium phosphate protocol, 5×10^5 cells per p60 petri dish.
2. Two hours before transfection change the medium to remove non attached cells and add 50 μ M cycloheximide to inhibit protein synthesis (*see Note 2*).
3. Incubate the cells in the presence of DNA-calcium phosphate precipitates for 12 h.
4. Wash the cells carefully with prewarmed PBS to remove the precipitates. Incubate the cells for 24 h in the presence of complete medium containing cycloheximide. This allows the transgene mRNA expression, but precludes its translation into protein.
5. Wash the cells 3–4 times with prewarmed serum-free medium to remove cycloheximide.
6. Incubate in complete medium for 12 h to allow the translation of the mRNA of the transfected gene.
7. Add cycloheximide again and incubate the cells for different periods of time (for example: 0, 3, 6, 9, 12 h). This procedure allows the analysis of the assembly of the protein translated during the period of culture in the absence of cycloheximide, without the effect of newly synthesized subunits.
8. At each time point, collect coverslips and process for immunofluorescence staining.

3.3. Indirect Immunofluorescence Analysis

1. Wash coverslips with PBS.
2. Fix the cells by incubation in cold methanol/acetone for 10 min at -20°C (alternative protocols for fixation can be followed).
3. Wash with PBS to rehydrate. Under these conditions the coverslips can be stored up to a week at 4°C . For longer storage do not rehydrate and store dry at -20°C (up to two months).
4. Wash the coverslips with PBS-T. Wipe out the excess of liquid.
5. Put the coverslips, cells face up, onto a parafilm foil in a humid chamber.
6. Add the appropriate dilution of primary antibodies. Be sure that they can be analyzed separately, i.e., they must come from different species. Normally, 10–13 μL of the mixture of primary antibodies is enough for a 11 mm diameter round coverslip. For initial tests, mouse or rat monoclonal supernatants can be diluted 1/5 to 1/20, ascites 1/100 to 1/500, rabbit, goat or sheep polyclonals 1/200 to 1/1000. Dilutions should be prepared in PBS-T (in some cases BSA can be added, up to 1%, to reduce background).
7. Incubate for 1 h at room temperature in a humid chamber.
8. Wash three times (10 min each) in PBS-T. Wipe out excess liquid.
9. Add the secondary antibodies diluted in PBS-T. Be sure that they are suited for multiple labeling purposes, i.e., raised in the same animal and preabsorbed against other animal serum proteins, and labeled with different fluorochromes. Usually manufacturers provide information to achieve appropriate dilution (*see Note 3*).
10. Incubate for 30 min to 1 h as in **step 7**.
11. Wash three times with PBS.
12. Mount with Mowiol or similar aqueous mounting media with the cells face down onto glass slides. If required, DAPI (Boehringer Mannheim) can be added to the mounting media to counterstain the nuclei.
13. Allow to dry for at least 2 h.
14. Analyze under epifluorescence microscope equipped with appropriate filters to avoid cross channel light contamination.

4. Notes

1. Sometimes in cell hybrid experiments a different number of each parental cell type fuse forming polykarions. In these, the speed of the dynamic process can be different because the distinct initial amounts of each polypeptide, which depends on the number of each parental type forming the polykaryon, and also on the volume of the cytoplasm in which the preexisting filaments or soluble proteins are spreading. The conditions of each experiment must be adjusted so the number of polykaryons is reduced as low as possible.
2. In cell fusion experiments, protein synthesis can be inhibited to follow the dynamics in absence of newly synthesized keratins (**16,18**). In this case, incubate the cells in the presence of 50 μM cycloheximide for at least 2 h before the fusion and afterwards. Other drugs that activate or inhibit different enzymes, which can

be involved in IF dynamics, must be adjusted for each requirement (18). Not all the cell lines can be efficiently transfected by conventional calcium phosphate protocols, and in some cases other methods should be followed. In these cases, the incubation times must be varied and adjusted for each precise requirement. The cycloheximide concentration provided here allows the transcription of transfected gene in PtK2 cells but precludes its translation into protein. In case of using a different cell line, check carefully the mRNA and protein expression at different drug concentrations.

3. Appropriate immunofluorescence controls must be performed by omitting primary antibodies, or/and by preincubation of the primary antibodies with the corresponding immunizing peptides if available. In addition, whenever possible, different antibodies against the same protein must be used to avoid the possible crossreactivity observed with certain antibodies when the antigens used in immunization are closely related, as in the case of keratins.

References

1. Moll, R., Franke, W. W., Schiller, D. L., Geiger, B., and Krepler, R. (1982) The catalog of human cytokeratin polypeptides: patterns of expression of specific cytokeratins in normal epithelia, tumors and cultured cells. *Cell* **31**, 11–24.
2. Quinlan, R., Hutchinson, C., and Lane, E. B. (1994) Intermediate filament proteins. *Prot. Profile* **1**, 779–911.
3. Fuchs, E. V. and Weber, K. (1994) Intermediate filaments: structure, dynamics, function and disease. *Ann. Rev. Biochem.* **63**, 345–382.
4. Gawlitta, W., Stocke, W., Wehland, J., and Weber, K. (1980) Organization and spatial arrangement of fluorescein-labeled native actin microinjected into normal locomoting and experimentally influenced amoeba proteus. *Cell Tissue Res.* **206**, 181–191.
5. Glacy, S. L. (1983) Pattern and time course of rhodamine-actin incorporation into cardiac myocytes. *J. Cell Biol.* **96**, 1162–1167.
6. Sammak, P. J., Gorbsky, G. J., and Borisy, G. G. (1987) Microtubule dynamics in vivo: a test of mechanisms turnover. *J. Cell Biol.* **104**, 395–405.
7. Shulze, E. and Kirschner, M. (1986) Microtubule dynamics in interphase cells. *J. Cell Biol.* **102**, 1020–1031.
8. Wadsworth, P. and Sloboda, R. D. (1983) Microinjection of fluorescent tubulin into dividing sea urchin cells. *J. Cell Biol.* **97**, 1249–1254.
9. Bloemendal, H. and Pieper, F. R. (1989) Intermediate filaments: known structure, unknown function. *Biochem. Biophys. Acta.* **1007**, 245–253.
10. Vikstrom, K. L., Miller, R. K., and Goldman, R. D. (1991) Analyzing dynamic properties of intermediate filaments. *Meth. Enzymol.* **176**, 506–525.
11. Miller, R. K., Khuon, S., and Goldman, R. D. (1993) Dynamics of keratin assembly: exogenous type I keratin rapidly associates with type II keratin in vivo. *J. Cell Biol.* **122**, 843–855.
12. Lu, X., Quinlan, R. A., Steel, J. B., and Lane, E. B. (1993) Network incorporation of intermediate filament molecules differs between preexisting and newly assembling filaments. *Exp. Cell Res.* **208**, 218–225.

13. Albers, K. and Fuchs, E. V. (1987) The expression of mutant epidermal keratin cDNAs transfected in simple epithelial and squamous cell carcinoma lines. *J. Cell Biol.* **105**, 791–806.
14. Albers, K. and Fuchs, E. V. (1989) Expression of mutant keratin cDNAs in epithelial cells reveals possible mechanisms for initiation and assembly of intermediate filaments. *J. Cell Biol.* **108**, 1477–1493.
15. Lu, X. and Lane, E. B. (1990) Retrovirus-mediated transgenic keratin expression in cultured fibroblasts: specific domain functions in keratin stabilization and filament formation. *Cell* **62**, 681–696.
16. Paramio, J. M., Casanova, M. L., Alonso, A., and Jorcano, J. L. (1998) Keratin intermediate filament dynamics in cell heterokaryons reveals diverse behaviour of different keratins. *J. Cell Sci.* **110**, 1099–1111.
17. Paramio, J. M. and Jorcano, J. L. (1994) Assembly dynamics of epidermal keratins K1 and K10 in transfected cells. *Exp. Cell Res.* **215**, 319–331.
18. Paramio, J. M. (1999) A role for phosphorylation in the dynamics of keratin intermediate filaments. *Eur. J. Cell Biol.* **78**, 33–43.
19. Lane, E. B. and Alexander, C. M. (1990) Use of keratin antibodies in tumor diagnosis. *Semin. Cancer Biol.* **1**, 165–179.

V

**CELLULAR SYSTEMS AS TOOLS
FOR INVESTIGATING CYTOSKELETON STRUCTURE AND FUNCTION**

Chromatophores as Tools for the Study of Organelle Transport

Bruce R. Telzer and Leah T. Haimo

1. Introduction

1.1. Chromatophores as a Model System to Study Organelle Transport

Chromatophores are pigmented cells found in a variety of animals. In lower vertebrates, i.e., fish and amphibia, chromatophores are present in the dermis, and in response to various stimuli, the pigment in these cells is transported to or from the cell center, conferring upon the cell a light or dark appearance, respectively. Changes in the distribution of pigment permit the animal to display variations in coloration which are used for territorial or sexual display and for camouflage. While color change is an important component of animal behavior, these cells have been exploited for cell biological studies, providing an excellent model system for examination of mechanisms generating and regulating organelle transport (*1*).

Chromatophores possess a number of attributes that make them particularly well suited to an analysis of organelle transport. These cells cyclically and coordinately transport hundreds of pigment granules; The entire population of these organelles either undergoes movement towards the cell center or towards the periphery, and accordingly, analysis of organelle transport in these cells is not confounded by simultaneous bidirectional movements as occurs in most other systems, including axonal transport. Moreover, the direction of transport of pigment granules in chromatophores can be externally controlled; Application of appropriate cell surface receptor agonists or membrane permeant signaling molecules induces pigment aggregation or dispersion. In addition, the pigment undergoes multiple rounds of transport to and from the cell center as the cells are cyclically stimulated with appropriate agents, permitting the

investigator multiple opportunities to interfere with transport. Chromatophores can be studied *in situ* (2,3) or in primary (4,5) or immortalized cultures (6); Transport of organelles can be reactivated in lysed cells (7–10) or in cell fragments (11); The cells can be transiently transfected (12–14), and the pigment granules can be isolated and analyzed biochemically or used in motility studies *in vitro* (15). Few other cell types possess so many amenable characteristics for the study of organelle transport.

Melanophores are the chromatophore type that has been most subject to analysis of pigment movements (2–4,6–9,11–15). Melanophores contain the pigment melanin which is packaged within membrane bound vesicles referred to as pigment granules or melanosomes. Melanophores are large, often 100–300 μm in diameter, flat, stellate or discoid shaped cells. In fish melanophores, the pigment granules aggregate or disperse at rates equivalent to those of fast axonal transport, about 1–2 μm per s. The pigment granules are readily visible by bright field microscopy. Moreover, melanin is extremely dense and the granules can be easily isolated through 80% Percoll (15).

1.2. The Cytoskeleton and Molecular Motors Driving Pigment Granule Transport

Melanophores contain a radial array of microtubules, and studies in live cells using drugs which depolymerize microtubules suggest that pigment granules aggregate and disperse along microtubules (2). Moreover, movement of the pigment granules, themselves, can organize microtubules into a radial array (11,16), and isolated granules from *Xenopus laevis* melanophores can move bidirectionally along microtubules *in vitro* (15), observations strongly supporting the hypothesis that pigment granules aggregate and disperse along microtubules. Further, purified granules contain the microtubule motors, cytoplasmic dynein and kinesin II (15). Microinjection of antibodies against microtubule motors into fish melanophores or transfection of *Xenopus laevis* melanophores with a dominant negative kinesin family member has implicated cytoplasmic dynein and kinesin or a member of the kinesin superfamily in generating aggregation and dispersion, respectively (14,17,18). Thus, microtubules and microtubule motors are implicated as the cytoskeletal system driving pigment granule transport in melanophores. However, the mechanism responsible for these movements may be more complex. Treatment with cytochalasin or with latrunculin A, which disrupt actin filaments, affects dispersion in fish and amphibian melanophores (19–21). Indeed, intact actin filaments appear to be essential for pigment dispersion in *Xenopus* melanophores. Moreover, myosin V has been localized on *Xenopus* pigment granules which can move along actin filaments *in vitro* (20). Thus, elucidation of the mechanisms generating movements of these organelles may provide a framework for understanding how the

two major motile systems, microtubules and actin filaments and their associated motors, interact to organize the distribution of organelles in cells, in general.

1.3. The Regulatory Pathway Controlling Direction of Pigment Granule Transport

Partial elucidation of the regulatory pathway controlling the direction of organelle transport has been obtained in studies on live, lysed and transfected melanophores. Analysis of the effect of various agonists and antagonists of cell surface receptors and of activators and inhibitors of signal transduction pathways using live melanophores and reactivation of transport in lysed melanophores has revealed that dispersion is activated by elevation of cAMP levels while aggregation of pigment occurs when cAMP levels are depressed (**1,3,8,9,23**). Protein kinase A and protein phosphatase 2B are the kinase and phosphatase, respectively, required for dispersion and aggregation in fish melanophores (**22,25,26**), while protein kinase C, in addition to protein kinase A, regulates dispersion (**12,13,24**), and protein phosphatase 2A is required for aggregation (**13**) in *Xenopus* melanophores.

In this chapter, we describe some of the methods utilized to work with melanophores. In addition to being an excellent model system for research, we use these cells in our undergraduate cell biology teaching labs. Aggregation or dispersion is induced in live cells. Then microtubules are depolymerized with nocodazole, and induction of aggregation or dispersion is again attempted. Finally, control and drug treated cells are prepared for immunofluorescence, using an antibody against tubulin. Control cells have a beautiful array of microtubules which never fails to impress undergraduates, particularly when it is they who have prepared the cells for immunofluorescence.

2. Materials

2.1. Source of Melanophores

2.1.1. Fish

Melanophores are present in the dermis of many fish and amphibia. The dermis grows onto the scales of fish, and it is this tissue from which melanophores are obtained. The most commonly used fish species as a source for melanophores are angelfish (*Pterophyllum scalare*) (**4**), black tetras (*Gymnocorymbus ternetzi*) (**11,17**), killifish (*Fundulus heteroclitus*) (**7**), Atlantic cod (*Gadus morhua*) (**16,18**) and African cichlids (*Tilapia mossambica*) (**3,8,22**). Angelfish and black tetras can be obtained from local fish and pet stores, *Fundulus heteroclitus* is available from Marine Resources Department at the Marine Biological Laboratory, Woods Hole, MA, Atlantic cod are available from commercial fisherman, and *Tilapia mossambica* is aquacultured in

California and is available from Aquafarms, Niland, CA. Any fish that contains numerous melanophores on its scales would be a suitable choice.

Scales are removed from the fish and placed into a Ringer's solution for use. After removal of the epidermis, the melanophores are then either examined *in situ* in the dermis still attached to the scale or the melanophores are dissociated from the dermis, adhered to and spread on microscope cover slips and maintained in primary culture.

2.1.2. *Xenopus*

Primary cultures of melanophores have also been obtained from the dermis of *Xenopus laevis* (24). Several years ago, however, Michael Lerner, (presently at the University of Texas) and colleagues generated an immortalized *Xenopus* melanophore cell line (6). These cells divide in culture but nevertheless retain their differentiated characteristics, producing pigment granules that undergo aggregation and dispersion upon appropriate stimulation. These melanophores can be transfected, and biochemical amounts of material can be obtained from this pure cell population (12–15).

2.2. Removal of the Epidermis from Fish Scales and Dissociating Melanophores from the Dermis

For working with melanophores from *Fundulus heteroclitus*, a small salt water fish, we remove the epidermis by shaking the scales in a marine Ringer's that contains EDTA. For removing the epidermis from the African cichlid, *Tilapia mossambica*, we use a fresh water Ringer's containing dispase, which enzymatically digests the matrix connecting the epidermis to the dermis. Once the epidermis has been removed from the scales, the scale with attached dermis is maintained in fresh water Ringer's. All Ringer's solutions can be made in advance and stored at room temperature or at 4°C.

1. Marine Ringer's: 134 mM NaCl, 2.5 mM KCl, 2 mM CaCl₂, 1 mM MgCl₂, 0.5 mM Na₂HPO₄, 15 mM NaHCO₃.
2. Marine Ringer's with EDTA: Marine Ringer's with addition of 10 mM EDTA and omission of CaCl₂.
3. Fresh water Ringer's: 103 mM NaCl, 1.8 mM KCl, 2 mM CaCl₂, 0.8 mM NaHCO₃, 5 mM Tris-HCl, pH 7.2.
4. Dispase solution: fresh water Ringer's containing 32 mg/mL dispase (Neutral Protease, Sigma) and 10 mg/mL bovine serum albumin (must be freshly prepared). In order to obtain primary cultures of fish melanophores, incubate the scales in a collagenase solution once the epidermis has been removed. The dermal cells dissociate from each other during this digestion, and the melanophores are released.
5. Collagenase solution: fresh water Ringer's containing 2 mg/mL collagenase (Type II, Sigma) and 5 mg/mL bovine serum albumin (must be freshly prepared).

2.3. Culturing Melanophores

2.3.1. Fish Melanophores

Fish melanophores in dermis attached to the scale remain viable in fresh water Ringer's for several hours after removal of the scale from the fish. Primary cultures of melanophores, liberated by collagenase from the dermis and spread on cover slips, can be maintained for several days in tissue culture medium.

1. Fish melanophore culture medium: Dulbecco's Modified Eagle's Medium (HEPES modification) containing 15% fetal bovine serum, 100 U/mL penicillin, 100 µg/mL streptomycin, 2 mM glutamine, 50 µg/mL gentamycin and 1:1000 dilution of Fungizone. All tissue culture reagents are obtained from Sigma with the exception of Fungizone which is obtained from Life Technologies. The complete medium can be stored for up to 30 d at 4°C.
2. Poly-lysine: 0.01% polylysine (70–150 kD)

2.3.2. *Xenopus* Melanophores

An immortalized cell line (β2 #7) of melanophores from *Xenopus laevis* is maintained in a tissue culture medium.

1. *Xenopus* melanophore culture medium: L-15 medium (Liebowitz Media with L-glutamine, obtained from Sigma) containing 15% fetal calf serum (heat inactivated; 56°C for 30 min), 100 U/mL penicillin, 100 µg/mL streptomycin and additional 2 mM glutamine. Medium with lower concentrations of serum but with the inclusion of insulin have also been used successfully to culture these cells (27).
2. Phosphate buffered saline solution (0.7X PBS): 95 mM NaCl, 1.9 mM KCl, 37.8 mM Na₂HPO₄, 14 mM NaH₂PO₄, 1.2 mM KH₂PO₄. Solution must be sterilized prior to use. PBS is used for washing cells prior to detaching them from plates for reseeded.
3. Trypsin solution: 1X trypsin in 0.7 X sterile PBS. (10X tissue culture trypsin obtained from Sigma). Aliquots of the 1X trypsin can be stored at -20°C. Brief exposure to the trypsin solution detaches the melanophores from the plates.

2.4. Inducing Aggregation and Dispersion in Melanophores

2.4.1. Aggregation

1. Fish: Induce aggregation by addition to the melanophores of 10⁻⁵–10⁻⁴ M epinephrine in fresh water Ringer's. A stock solution of epinephrine at 10⁻²M is prepared in DMSO and frozen. The solution will have a light yellow or pink tinge. Epinephrine is light sensitive and should be kept in the dark. Discard the stock when it gets visibly browner or redder. Prepare the working solution shortly before use and protect from light.
2. *Xenopus*: Induce aggregation by 10 nM melatonin, diluted into serum-free medium from a 10 µM stock in 95% ethanol. Melatonin is light sensitive. The stock can be stored for 6 mo at -20°C.

2.4.2. Dispersion

1. Fish: Induce dispersion by addition to the melanophores of 0.25–2.5 mM isobutyl methyl xanthine (IBMX) in fresh water Ringer's. A stock solution of 250 mM IBMX in DMSO can be stored for extended periods at room temperature. Dispersion can also be induced by addition to the melanophores of 10 μ M forskolin. A stock solution of 10 mM in DMSO is stored at -20°C .
2. *Xenopus*: Induce dispersion either by exposure of the melanophores to light or to 100 nM melanocyte stimulating hormone (MSH) in serum free medium. A 100 μ M stock of MSH in H₂O can be stored at -20°C for a year.
3. Reagents: Epinephrine, IBMX, melatonin, and MSH can be obtained from Sigma, forskolin from Calbiochem.

2.5 Lysing and Reactivating Melanophores

2.5.1. Fish Lysis and Reactivation

Fish melanophores can be lysed, and transport of pigment granules can then be reactivated by addition of ATP for aggregation or cAMP and ATP for dispersion.

1. Fish melanophore lysis solution: 0.0016% digitonin in 30 mM HEPES, pH 7.4, 33 mM potassium acetate, 2 mM EGTA, 1 mM MgSO₄, 2.5 % polyethylene glycol (MW: 20,000). The cells can then be reactivated in the same solution containing 1–3 mM ATP for aggregation or 1–3 mM ATP and 1 mM cAMP for dispersion.
2. Retain the detergent in the reactivation buffer so that the plasma membrane of the cells will not reseal.
3. Valap (1:1:1 Vaseline:lanolin:parafin).

2.5.2. *Xenopus* Lysis

We have not developed methods for reactivating pigment granule transport in *Xenopus* melanophores after lysis, but we have been able to obtain active microtubule motors from lysates of *Xenopus* melanophores. *Xenopus* lysis buffer: 40 mM Pipes, pH 6.9 (with NaOH), 1 mM EGTA, 1 mM MgCl₂ and a protease inhibitor cocktail containing 1 mM DTT and 10 μ g/mL each of aprotinin, leupeptin, AEBSF, benzamidine, and pepstatin (protease inhibitors are all available from Sigma).

3. Methods

3.1. Obtaining Melanophores from Fish Scales for Primary Culture

Several techniques have been reported for the culture of teleost melanophores (28,29) and erythrophores (5). We have adapted these procedures for the isolation and cultivation of melanophores from the killifish, *Fundulus heteroclitus*.

3.1.1. Removal of Scales

Remove individual scales from the back and sides of a fish by using a pair of fine, EM grade, forceps. For consistency, it is best to use the scales from a single fish to harvest cells for a set of experiments. The largest scales are typically found on the dorsal surface of the fish, directly behind the head. However, the melanophores and other cells of the dermis extend to the distal margins of these scales, and it is quite difficult to remove their epidermis. These scales are best avoided. The melanophores whose epidermis is easiest to remove contain a clear margin of epidermis at their edges.

3.1.2. Removal of the Epidermis

1. Transfer scales into a 35 mm Petri dish containing 3 mL of marine Ringer's with EDTA solution and incubate at 30°C for 30–40 min with occasional shaking. It is best to observe the scales against a black background with a dissecting microscope so that the clouding of the epidermis can be easily seen, indicating that it can be easily removed.
2. Hold down an edge of a scale with the forceps, and use a micropipettor to repeatedly squirt 200 μ L of solution across the surface of the scale. The epidermis should come off easily, but if it still adheres, it is preferable to incubate for a longer period of time than to attempt to force it off.
3. Transfer cleaned scales into a new Petri dish containing 3 mL fresh water Ringer's solution at room temperature until all are collected.

3.1.3. Dissociation of the Dermis (see **Note 1**)

1. Transfer scales, whose epidermis has been removed, into a 35 mm Petri dish containing 3 mL of a freshly prepared collagenase solution and incubate at 30°C for 10–30 min with occasional shaking.
2. Use a binocular microscope to observe the scales. A white background facilitates the visibility of scales.
3. Periodically, test the scales to determine whether melanophores can be easily dissociated from the dermis by squirting the enzyme solution across the dermis using a 20 μ L micropipettor tip. Initially, the dermis may come off the scale as an intact sheet, but it is difficult, if not impossible, to dissociate single cells from such a sheet, which tends to fold over and stick to itself.
4. After sufficient incubation, cells either come off a scale singly or in clusters. Dissociate any clusters into single cells by pipetting the clusters in and out of a micropipettor tip with the tips of a pair of fine forceps held across the opening of the tip.

3.1.4. Collection and Washing of Melanophores

1. After the release of single cells from the dermis, remove the denuded scales from the Petri dish, and swirl the dish so that cells gather in the center of the dish.
2. Collect as many well-spread melanophores as possible into a 20 μ L pipettor tip.

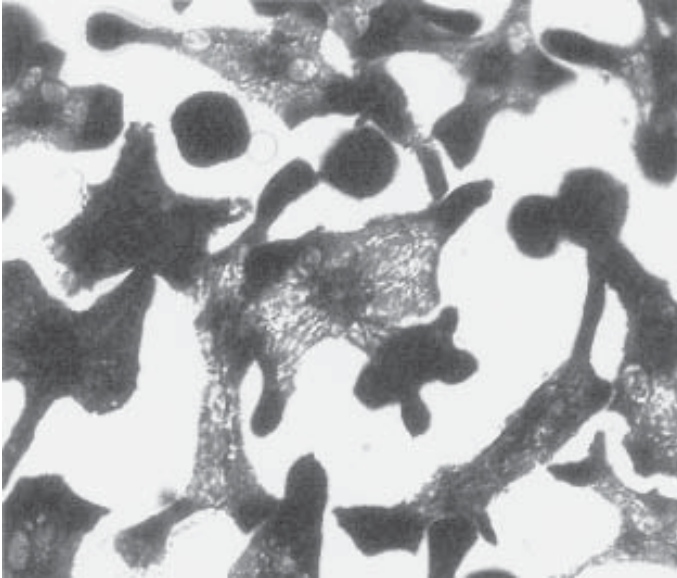



Fig. 1. Fish (*Fundulus heteroclitus*) melanophores after one day in culture. Most cells are attached and spread, but a few melanophores do not attach well or spread and appear as dark spheres.

3. Wash the melanophores from the enzyme solution by ejecting them from the pipettor tip into a new Petri dish containing fresh water Ringer's solution and allowing them to settle.
4. Immediately repeat this washing procedure at least three times using a new Petri dish and fresh Ringer's solution with each wash. It is critical to work quickly as cells will adhere to the surface of the dishes if allowed to settle for any period, and they then cannot be removed.
5. Use the pipettor tip to pick up the cells and deposit them onto an appropriate substrate for culture.

3.1.5. Preparation of Growth Substrate

1. Cut each of several 22 × 22 mm cover slips into four trapezoidal sections by using a diamond pen. The asymmetric shape will facilitate the identification of the top, coated surface of each trapezoidal piece.
appearance of cover slip after cutting into a trapezoidal shape: 
2. Clean cover slips by washing in detergent and sequentially rinsing with deionized water, 10 mM EDTA, deionized water, concentrated HCl, and 100% ethanol before flaming off residual ethanol.
3. Coat cover slips with polylysine to facilitate adhesion of cells.

4. Rinse with deionized water and dry before use.
5. Alternatively, coat cover slips with carbon in a vacuum evaporator.
6. Commercially available, fibronectin-coated cover slips (B-D Biosciences) also provide an excellent substrate for *Fundulus* melanophores.

3.1.6. Culturing of Melanophores

1. Deposit a drop of fresh water Ringer's containing washed melanophores on the surface of a coated coverslip in a 35 mm Petri dish.
2. Allow the cells to settle at 30°C. Attachment will typically occur within 10 min.
3. Carefully remove the Ringer's solution with a micropipet tip and immediately add a drop of culture medium, taking care not to disturb or dry out the cells.
4. Add three mL of culture medium and incubate the Petri dish at 30°C. Cells typically spread out within 6–12 h and can be maintained for 2–3 d in sterile conditions. The extension and spreading of arms from individual melanophores is highly variable within a cell culture and between different preparations of cells. **Figure 1** shows a field of cultured fish melanophores, most, but not all, of which have attached to the substratum and are well spread (*see Note 1*).

3.2. Culturing Immortalized *Xenopus* Melanophores

The immortalized cell line of *Xenopus* melanophores is cultured like that of any cell line except that the cells do not require CO₂ and grow well at room temperature. Thus, a tissue culture incubator is not necessary.

1. Maintain cells in continuous culture and split as they become confluent.
2. Pour off the culture medium and wash the cells twice with 0.7X PBS.
3. Detach the cells from the dishes by using a 1X trypsin solution.
4. Add 3 mL of trypsin to a 150 mM tissue culture plate and gently agitate the plate.
5. When the cells begin to dissociate, add 8 mL of *Xenopus* culture medium to quench the trypsin.
6. Collect the cells into a sterile conical 15 mL centrifuge tube and spin at 600g for 5 min.
7. Remove the supernatant, resuspend the cells in fresh medium and use to seed a number of tissue culture dishes. Generally, use one plate to seed 4 new plates of the same size.
8. Use cells for experiments within 2–3 d after plating.
9. Induce aggregation and dispersion in these cells by removing the medium from the culture dishes (*see Note 2*).
10. Wash the cells twice with 0.7X PBS and incubate overnight in serum free medium.
11. The following day, add melatonin or MSH to the cells in serum free medium. Aggregation or dispersion, respectively, should occur within 15 min but takes about 1 h to reach completion.
12. Scrape up aggregated or dispersed cells with a rubber policeman and place in *Xenopus* lysis buffer containing either melatonin or MSH.
13. Transfer the cells to a centrifuge tube and lyse by passage through a 25 gauge needle.
14. Clarify the lysate by centrifugation at 150,000g for 20 min. Use these lysates to examine the microtubule binding properties of the motors in the cells.

3.3. Perfusing or Microinjecting Melanophores

3.3.1. Cell Perfusion Studies

1. Construct a simple perfusion chamber by using a thin coat of Vaseline to adhere two 2 × 22 mm pieces of cover slip to the middle of a microscope slide parallel to its long axis, creating an 8–9 mm channel between the cover slips. Place another thin coat of Vaseline on the top surface of the cover slip “rails”.
2. Remove a cover slip containing melanophores from a culture dish and invert it onto the rails, taking care that a drop of culture medium on the cover slip fills the channel between the rails. It may be helpful to further immobilize the cover slip containing the cells with a drop of melted valap.
3. Remove culture medium from the top of the cover slip by drawing a piece of filter paper across its surface.
4. Clean the surface of the coverslip with a drop of deionized H₂O followed by blotting with filter paper. The slide is now ready for observation in a microscope. If using oil immersion objectives, care must be taken to insure that oil does not overflow the top and seep under the cover slip.
5. Add the appropriate perfusion fluid with a micropipettor on one side of the cover slip and allow it to be drawn under and past the cells by placing a piece of filter paper on the other side of the coverslip. Care must be taken to remove the filter paper before drying out the fluid under the cover slip. Typically, cells can be observed for 1–2 h with several changes of solution under these conditions.

3.3.2. Microinjection Studies

Melanophores may be microinjected by standard techniques, although success is complicated by the opacity and thinness of the pigmented cell (*see Note 3*).

1. Select regions of cells in which the pigment is sparse or induce aggregation with an agonist such as epinephrine. Otherwise, one cannot see the microneedle tip as one attempts to penetrate and then inject the cell.
2. Insert the microneedle tip near the base of an extended arm, in the region of the cell body, rather than near the distal tip of an arm, which has a marginal depth.
3. Place cover slips with attached melanophores into a small Petri dish from which the center of the base has been cut out and the missing plastic replaced by a thin cover slip which has been glued to the remaining plastic.
4. Place the cover slip with the cells onto the cover slip that now forms part of the base. The microneedle tip can be imaged much more clearly through the two cover slips (i.e., the cover slip on which the cells are grown and the cover slip which is part of the Petri dish) than it can be imaged through the plastic base of the Petri dish and the culture cover slip.
5. Fill the Petri dish with tissue culture medium or with Ringer’s containing epinephrine or IBMX or other test solutions.
6. Use an inverted microscope equipped with micromanipulators that approach the cell from above to microinject the cells.

3.4. Methods for Lysing Melanophores and Reactivating Transport In Vitro

We have recently published detailed methods for melanophore lysis and reactivation (26), and that paper should be referred to for these methods (see **Note 4**).

1. Perfuse scales (containing adhering dermis with melanophores) in lysis buffer or gently agitate the scales in the lysis buffer. Time of lysis needs to be empirically determined, but generally varies between 1 and 2 min.
2. Perfuse the melanophores with reactivation buffer containing ATP or cAMP and ATP.

4. Notes

1. In order to obtain primary cultures of fish melanophores, it is necessary to dissociate the melanophores from the dermis using collagenase. While we normally use type II collagenase (Sigma), we find that different lots of collagenase vary widely in their effectiveness for these studies. Once an effective batch of collagenase is found, it is wise to order sufficient enzyme to complete the anticipated experiments. In a few cases, the collagenase has been ineffective in disruption of the dermis, and melanophores are not liberated from the tissue. More frequently, the melanophores are dissociated and look quite nice, retaining a stellate conformation after detachment from the scale, but will not attach to the substratum (usually carbon-coated cover slips). In some other cases, the cells attach, but do not become well spread. If the melanophores attach and spread with axonal-like projections instead of pseudopodia-like projections, the melanophores then often cannot aggregate or disperse pigment. Most of these problems can be traced to the collagenase, and different lots from various companies that supply collagenase should be tested. Carbon-coated cover slips, although inconvenient to prepare, are the best substratum for primary culture of fish melanophores. However, if the carbon coat on a cover slip is too thick, the coat will often detach from the cover slip when submerged in tissue culture medium. In addition, the cells do not adhere and spread as well on a thick carbon coat as they do on a thin one.
2. We are currently examining the ability of microtubule motors in *Xenopus* melanophore extracts to bind to microtubules, comparing the behavior of motors derived from cells with aggregated pigment to those derived from cells with dispersed pigment. Highly variable results were obtained until we began using subconfluent cultures, those that had been plated for no more than 2 or 3 d. These cells respond most rapidly to melatonin and MSH, aggregating or dispersing pigment granules completely. Thus, when appropriate, *Xenopus* melanophores should be utilized when they are clearly in log phase. In addition, while the melanophores will often aggregate and disperse in complete medium upon stimulation with melatonin or MSH, serum may contain factors that affect this signaling pathway. One can therefore obtain much more uniform response of the cells to stimuli inducing aggregation or dispersion if the cells have been in serum free medium for some period.

3. Melanophores are somewhat more difficult than other cell types to inject as they are very flat, and moreover, the pigment, if dispersed, obscures visualization of the microneedle. These cells do, however, have the benefit of being quite large, thereby providing a big target for injection. The center of the cells is less flat than the periphery, and one usually has greater success microinjecting in this region. In addition, if the study permits, the pigment should be aggregated prior to microinjection. Then one can see the microneedle as one undertakes the injection.
4. It is relatively easy to reactivate transport of pigment in melanophores that are present in the dermis on the fish scale, although the time of lysis need be empirically determined. Factors required for transport can, however, be leached from the cells during lysis. For example, we found that too much agitation of *Tilapia mossambica* melanophores during lysis resulted in extraction of the phosphatase calcineurin (PP2B) from the cells, and aggregation could then only be reactivated upon addition of exogenous calcineurin (25). We have been unable to reactivate transport of pigment in lysed cultured melanophores, either those of fish or of *Xenopus*. We do not understand why cultured cells appear intractable to this approach, but these cells are extremely fragile and lyse much more thoroughly in lysis buffer than do fish melanophores in the dermis still attached to the scale.

Acknowledgments

This work was supported by a grant from the National Science Foundation (MCB9727728) and a grant from the Academic Senate of the University of California, Riverside.

References

1. Bagnara, J. T. and Hadley, M. E. (1973) Chromatophores and color change. *The Comparative Physiology of Animal Pigmentation*. Prentice-Hall, Englewood Cliffs.
2. Murphy, D. B. and Tilney, L. G. (1974) The role of microtubules in the movement of pigment granules in teleost melanophores. *J. Cell Biol.* **61**, 757–779.
3. Thaler, C. D. and Haimo, L. T. (1992) Control of organelle transport in melanophores: regulation of Ca²⁺ and cAMP levels. *Cell Motil. Cytoskel.* **22**, 175–184.
4. Schliwa, M., Weber, K., and Porter, K. R. (1981) Localization and organization of actin in melanophores. *J. Cell Biol.* **89**, 267–275.
5. Luby, K. J. and Porter, K. R. (1980) The control of pigment migration in isolated erythrophores of *Holocentrus ascensionis* (Osbeck). I. Energy requirements. *Cell* **21**, 13–23.
6. Daniolos, A., Lerner, A. B., and Lerner, M. R. (1990) Action of light on frog pigment cells in culture. *Pigment Cell Research* **3**, 38–43.
7. Clark, T. G. and Rosenbaum, J. L. (1982) Pigment particle translocation in detergent permeabilized melanophores of *Fundulus heteroclitus*. *Proc. Natl. Acad. Sci. USA* **79**, 4655–4659.

8. Rozdzial, M. M. and Haimo, L. T. (1986) Reactivated melanophore motility: Differential regulation and nucleotide requirements of bidirectional pigment granule transport. *J. Cell Biol.* **103**, 2755–2764.
9. Grumstrom, N., Karlsson, J. O. G., and Andersson, R. G. G. (1985) The control of granule movement in fish melanophores. *Acta Physiol. Scand.* **125**, 415–422.
10. Lynch, T. J., Wu, B., Taylor, J. D., and Tchen, T. T. (1986) Regulation of pigment organelle translocation. II. Participation of a cAMP-dependent protein kinase. *J. Biol. Chem.* **261**, 4212–4216.
11. Rodionov, V. I. and Borisy, G. G. (1997) Cell-centring activity of cytoplasm. *Nature* **386**, 170–173.
12. Graminski, G. F., Jayawickreme, C. K., Potenza, M. M., and Lerner, M. R. (1993) Pigment dispersion in frog melanophores can be induced by a phorbol ester or stimulation of a recombinant receptor that activates phospholipase C. *J. Biol. Chem.* **268**, 5957–5964.
13. Reinlein, A. R., Tint, I. S., Peunova, N. I., Enikolopov, G. N., and Gelfand, V. I. (1998) Regulation of organelle movement in melanophores by protein kinase A (PKA), protein kinase C (PKC), and protein phosphatase 2A (PP2A). *J. Cell Biol.* **142**, 803–813.
14. Tuma, M. C., Zill, A., Le Bot, N., Vernos, I., and Gelfand, V. (1998) Heterotrimeric kinesin II is the microtubule motor protein responsible for pigment dispersion in *Xenopus* melanophores. *J. Cell Biol.* **143**, 1547–1558.
15. Rogers, S. L., Tint, I. S., Fanapour, P. C., and Gelfand, V. I. (1997) Regulated bidirectional motility of melanophore pigment granules along microtubules in vitro. *Proc. Natl. Acad. Sci. USA* **94**, 3720–3725.
16. Nilsson, H. and Wallin, M. (1998) Microtubule aster formation by dynein-dependent organelle transport. *Cell Motil. Cytoskel.* **41**, 254–263.
17. Rodionov, V. I., Gyoeva, F. K., and Gelfand, V. I. (1991) Kinesin is responsible for centrifugal movement of pigment granules in melanophores. *Proc. Natl. Acad. Sci. USA* **88**, 4956–4960.
18. Nilsson, H. and Wallin, M. (1997) Evidence for several roles of dynein in pigment transport in melanophores. *Cell Motil. Cytoskel.* **38**, 397–409.
19. Malawista, S. E. (1971) Cytochalasin B reversibly inhibits melanin granule movement in melanocytes. *Nature (Lond)* **234**, 354–355.
20. Rogers, S. L. and Gelfand, V. I. (1998) Myosin cooperates with microtubule motors during organelle transport in melanophores. *Curr. Biol.* **8**, 161–164.
21. Rodionov, V. I., Hope, A. J., Svitkina, T. M., and Borisy, G. G. (1998) Functional coordination of microtubule-based and actin-based motility in melanophores. *Curr. Biol.* **8**, 165–168.
22. Rozdzial, M. M. and Haimo, L. T. (1986) Bidirectional pigment granule movements of melanophores are regulated by protein phosphorylation and dephosphorylation. *Cell* **47**, 1061–1070.
23. Sammack, P. J., Adams, S. R., Harootunian, A. T., Schliwa, M., and Tsien, R. Y. (1992) Intracellular cyclic AMP, not calcium, determine the direction of vesicle movement in melanophores: direct measurement by fluorescence ratio imaging. *J. Cell Biol.* **117**, 57–72.

24. Sugden, D. and Rowe, S. J. (1992) Protein kinase C activation antagonizes melatonin-induced pigment aggregation in *Xenopus laevis* melanophores. *J. Cell Biol.* **119**, 1515–1521.
25. Thaler, C. D. and Haimo, L. T. (1990) Regulation of organelle transport in melanophores by calcineurin. *J. Cell Biol.* **111**, 1939–1948.
26. Haimo, L. T. (1998) Reactivation of vesicle transport in lysed teleost melanophores. In: *Methods in Enzymology*, Vol. 298, (Vallee, R. B., ed.), Academic Press, San Diego, pp. 389–399.
27. Rogers, S. L., Tint, I. S., and Gelfand, V. I. (1998) In vitro motility assay for melanophore pigment organelles. In: *Methods in Enzymology*, Vol. 298, (Vallee, R. B., ed.), Academic Press, San Diego, pp. 361–372.
28. Gyoeva, F. K., Leonova, E. V., Rodionov, V. I., and Gelfand, V. I. (1987) Vimentin intermediate filaments in fish melanophores. *J. Cell Sci.* **88**, 649–655.
29. Rodionov, V. I., Lim, S., Gelfand, V. I., and Borisy, G. G. (1994) Microtubule dynamics in fish melanophores. *J. Cell Biol.* **126**, 1455–1464.

Centriole Duplication, Centrosome Maturation and Spindle Assembly in Lysates of *Spisula solidissima* Oocytes

Andrew W. Suddith, Eugeni A. Vaisberg, Sergei A. Kuznetsov, Walter Steffen, Conly L. Rieder, and Robert E. Palazzo

1. Introduction

Marine oocytes and embryos have long been favored systems for the study of cell division and the cytoskeletal dynamics that accompany karyokinesis and cytokinesis. Several characteristics make marine egg systems ideal for the study of cell replication including: 1) the clarity of the eggs, which allows excellent real-time visualization of cytoskeletal components; 2) the natural synchrony of the cells, because the oocytes are typically arrested at a specific phase of the cell cycle until fertilized or artificially activated; 3) the rapid and synchronous cell divisions that follow fertilization or activation; and perhaps most importantly, 4) the large quantities of oocytes that can be obtained. Here we describe an *in vitro* system that utilizes cytoplasmic extracts prepared from surf clam, *Spisula solidissima*, oocytes for the analysis of the microtubule cytoskeleton during meiosis I spindle assembly.

Spisula solidissima represent an abundant natural resource. These clams are commercially harvested off of the northeast coast of the United States. The availability of large numbers of organisms allows for the daily isolation of hundreds of grams of uniform oocytes. *Spisula* oocytes are naturally arrested in late prophase at the G₂/M transition of meiosis I, and contain a large germinal vesicle which houses partially condensed meiotic chromosomes. Importantly, a large population of isolated oocytes can be easily activated, either artificially by treatment with KCl or naturally by fertilization, to complete meiosis I and II.

Fertilization or artificial activation induces germinal vesicle breakdown (GVBD) and meiosis I spindle assembly within fifteen minutes at room temperature (**1**). Oocyte activation also induces the assembly of two maternal centrosomes which direct the organization of microtubules during meiosis. The origin of these maternal centrosomes is not clear since mature *Spisula* oocytes are thought to be acentrosomal. Neither centrosomes nor centrioles have been detected in unactivated oocytes by high resolution light microscopy (**1**), immunofluorescence analysis using tubulin antibodies (**2**), or electron microscopy (EM) (**3,4**). However, at room temperature, within 2–5 min after fertilization or artificial activation with KCl, oocytes assemble two maternally derived astral microtubule arrays (**2**). By 8–10 min after activation, the germinal vesicles break down, and by 15 min oocytes contain a meiosis I spindle (**1**). Analysis of serial thick-sections of isolated asters and spindles by high voltage electron microscopy (HVEM) revealed that four minutes after oocyte activation the centrosomes within asters contained a single centriole (**5,6**). However, asters isolated 15 min after oocyte activation contain two centrioles, indicating that oocyte activation induces the rapid assembly and duplication of centrioles during meiosis I (**5**). The unique features of the *Spisula* oocyte system makes it an attractive one for the study of centrosome assembly and duplication (**5**), nuclear envelope breakdown (**7**), and the cytoskeletal dynamics that lead to meiosis I spindle assembly (**8**).

2. Materials

2.1. Isolation of *Spisula solidissima* Oocytes

1. Gravid clams (Marine Resources Center of the Marine Biological Laboratory, Woods Hole, MA).
2. Clam knife (or flat blade spatula).
3. Filtered sea water containing 10 mM Tris-base, pH 8.0.
4. Cheesecloth.
5. Beakers: 250 mL and 1 L and, 2 or 3 L.
6. Dissection scissors.
7. Phase-contrast microscope.
8. Polarized light microscope.

2.2. Preparation of Activated *Spisula* Oocyte Lysate (A4-Lysate)

1. 20 mL of pelleted oocytes (1000g pellet).
2. Clinical centrifuge.
3. Disposable centrifuge tubes (50 mL).
4. Filtered natural sea water or artificial sea water (200 mL).
5. Graduated cylinders (200 and 50 mL).
6. 250 mL beaker.
7. Magnetic stir plate and stir bar.

8. 0.5M KCl (28 mL; store at room temperature).
9. Glycerol/phosphate buffer: (1M glycerol, 10 mM NaH₂PO₄, pH 8.0, [250 mL; store at room temperature]).
10. Aster buffer: 20 mM PIPES, 100 mM NaCl, 5 mM MgSO₄, pH 7.2, (200 mL; ice-cold).
11. p5000 Pipetman.
12. Polycarbonate centrifuge tubes (45 mL).
13. Hexylene glycol.
14. High-speed centrifuge (capable of generating 8000–39,000g forces).
15. Swinging bucket rotor (e.g., Beckman JS 13.1).
16. Polarized light microscope.
17. Phase-contrast microscope.

2.3. Preparation of Crude Spisula Oocyte Lysate (Unactivated Lysate)

1. 1-5 mL of pelleted oocytes (1000g pellet).
2. Clinical centrifuge.
3. Disposable centrifuge tubes (50 mL).
4. Filtered natural sea water or artificial sea water (200 mL).
5. Glycerol buffer: (1M glycerol [250 mL; store at room temperature]).
6. Glycerol/phosphate buffer: (1M glycerol, 10 mM NaH₂PO₄, pH 8.0, [250 mL; store at room temperature]).
7. Aster buffer: 20 mM PIPES, 100 mM NaCl, 5 mM MgSO₄, pH 7.2, (200 mL; store at room temperature).
8. Phase-contrast microscope.

2.4. Preparation of High Speed Activated Extracts (HSA-Extracts)

1. 2 mL of clarified lysate prepared from oocytes activated for 4 min (A4-lysate).
2. High-speed centrifuge (capable of generating 10,000–39,000g forces).
3. Hexylene glycol.
4. Polarized light microscope.

2.5. Centriole Assembly and Duplication

1. 100 μL Unactivated lysate.
2. 100 μL HSA-extract.
3. Spindle Isolation Buffer (SIB): 20 mM MES, 10 mM EGTA, 5 mM MgSO₄, 20% Glycerol (pH 6.5).
4. Spindle Isolation Buffer with Detergent (SIBD): SIB containing 1% Triton X-100 or NP-40.
5. 1% Glutaraldehyde in SIB.
6. Microfuge.
7. 1% osmium tetroxide in dH₂O.
8. 1% Uranyl acetate in dH₂O.
9. Ethanol.

10. Propylene oxide.
11. Epon 812.

2.6. Germinal Vesicle Breakdown and Spindle Assembly

1. 100 μ L unactivated lysate.
2. 100 μ L HSA-extract.
3. Spindle Isolation Buffer with Detergent (SIBD) (*see Subheading 2.5.*).
4. Spindle Isolation Buffer (SIB) (*see Subheading 2.5.*).
5. Fixative solution (FS: 0.5% glutaraldehyde in Phosphate Buffered Saline [PBS, pH 7.2] and 0.4% Triton X-100 or NP-40).
6. Spin Tubes (**13**).
7. Polylysine coated coverslips (12 mm round).
8. 30% glycerol in PBS.
9. -20°C Methanol.
10. High-speed centrifuge (capable of generating 12,000g forces).
11. Swinging bucket rotor (e.g., Beckman JS 13.1).
12. Microscope equipped with DIC and Epifluorescence optics.

2.7. Inhibition of Spindle Assembly by Dynein Inhibitors

1. Materials listed in **Subheading 2.6.**
2. Antibodies (dynein antibody, m74-1 [10 mg/mL] and dynactin antibody, m150-1 [10 mg/mL]).
3. 100 mM Vanadate in dH_2O .

2.8. Immunofluorescence of Asters and Centrosomes

1. Phosphate Buffered Saline (PBS): 10 mM NaH_2PO_4 , 150 mM NaCl, pH 7.4.
2. Blocking Buffer (BB): PBS with 5% nonfat dry milk.
3. Anti- α -tubulin or anti- β -tubulin antibody.
4. Anti- γ -tubulin antibody.
5. Secondary antibodies.
6. Hoechst 33342 (2 mg/mL in dH_2O).
7. Elvanol (**11**).
8. Epifluorescence microscope.

3. Methods

3.1. Isolation of *Spisula solidissima* Oocytes

The protocol described below is based on the procedures described by Allen (**1**), and Costello and Henley (**9**).

1. Open clams by inserting the clam knife between the siphon and the overlying shell. Cut the adductor muscles by running the blade along the inside of the shell and expose the meat of the clam.
2. Determine the sex of the animal by touching the gonad with a clean wet clam knife. Oocytes appear as tiny sandy particles, which can individually be distin-

guished. Sperm generally spreads as a creamy substance with no particulate nature. Alternatively, for identification, a small drop of gonadal fluid can be placed on a glass slide and observed with a microscope. Oocytes are 55 μm diameter spheres, which contain a large germinal vesicle. Sperm have phase dense heads associated with long flagella and swim rapidly through the medium.

3. Dissect out female gonads by trimming off the gill tissue and then excising the gonadal tissue from the remainder of the animal. Collect the gonads by snipping this tissue so that it drops into a 200 mL beaker. Combine the gonads of multiple females.
4. Mince dissected gonads into a slurry with scissors, and transfer to a 1 L beaker. Add filtered sea water to bring the total volume to 500–700 mL.
5. Stir the suspension vigorously by hand to release the oocytes from the gonadal tissue.
6. Collect released oocytes by decanting the suspension through several layers of cheesecloth that are pre-wetted with sea water. The oocytes will pass through the cheesecloth while the gonadal tissue is retained.
7. Allow oocytes to settle out of solution at 1g and wash by cycles of decanting, settling, and resuspending eggs in filtered sea water.
8. Repeat the wash cycle a minimum of three times (*1*).

3.2. Preparation of Activated *Spisula Oocyte Lysate (A4-Lysate)* (see Note 1)

1. Concentrate oocytes into pellets by centrifugation at 1000g for approx 30 s.
2. Resuspend 20 mL of oocyte pellet to a final volume of 172 mL by addition of filtered sea water or artificial sea water.
3. Transfer oocyte suspension to a 250 mL beaker and stir gently.
4. Activate oocytes by adding 28 mL of 0.5 M KCl and continue stirring for 4 min at 22°C.
5. Aliquot equal volumes of the suspension into four 50 mL centrifuge tubes and centrifuge at top speed in a clinical centrifuge for 30 s.
6. Immediately decant the supernatant and resuspend the pellet in 8–10 vol of glycerol/phosphate buffer. Incubate oocytes in the glycerol/phosphate buffer for a total of 1.0 min. Incubation of the oocytes in the phosphate buffered glycerol solution removes the tough outer vitelline membrane present on the oocyte which prevents egg lysis (*6,12*). Use phase-contrast microscopy to observe the removal of this membrane, which appears as a phase-dense material that progressively lifts from the oocyte surface.
7. Following incubation in the glycerol/phosphate buffer, centrifuge oocytes again at top speed for 30 s using a clinical centrifuge.
8. Decant the supernatant and resuspend the pellet in 8–10 vol of ice-cold Aster buffer.
9. Immediately pellet the oocytes out of Aster buffer for 30 s at top speed using the clinical centrifuge. Removal of the vitelline membrane makes the oocytes very delicate and they will lyse, if incubated in Aster buffer too long. Therefore, centrifuge them out of solution as quickly as possible.

10. Aspirate the supernatant leaving a dry oocyte pellet.
11. Lyse the oocytes by triturating the pellets vigorously on ice using a p5000 Pipetman. The p5000 should be set to ~3.5 mL to avoid aspirating the viscous oocyte/lysate pellet into the Pipetman. Approximately 50 rapid triturations are required to rupture the oocytes completely. Monitor oocyte lysis by taking a small amount of the suspension and observing with a phase-contrast microscope. Continue trituration until all the oocytes are lysed.
12. Pool lysed oocytes in a 45 mL polycarbonate centrifuge tube and mix the various batches thoroughly by trituration with the p5000 Pipetman. Centrifuge the combined lysates at 8000-10,000g for 15 min at 2–4°C in a swinging bucket rotor. Successful clarification of the lysate results in the formation of three layers following centrifugation; an upper lipid layer, a clarified middle layer, and a pellet.
13. Collect the upper lipid and middle layers and triturate on ice with the p5000 Pipetman to effect a thoroughly mixed suspension. Repeat the centrifugation and collect the clarified middle layer and keep it on ice. If separation is not achieved after the first centrifugation (**step 12** above), collect the top 75% of the lysate mixture on ice, thoroughly triturate, and centrifuge. This second centrifugation should separate the lysate into the desired three layers. Collect the clarified middle layer and keep it on ice. Typically, this preparation yields ~10 mL of clarified lysate from 20 mL of packed oocytes.
14. To assay the clarified lysate for aster formation add 1.5 μ L of hexylene glycol to 48.5 μ L of lysate, mix thoroughly by pipetting and warm to room temperature. A final concentration of 3% hexylene glycol promotes the polymerization of microtubules from microtubule organizing centers (centrosomes) present in the lysate. This results in the appearance of birefringent asters, which can be viewed by polarized light microscopy (**6**).
15. After mixing with hexylene glycol, immediately place a small aliquot of the sample on a glass slide, cover with a cover slip, and mount for viewing with a polarized light microscope. Within 5–7 min bright birefringent asters should be visible using a 10 \times or a 20 \times pol lens. Count the number of asters per unit volume of solution using a standard hemacytometer. Typically, the concentration of asters is in the range of 3–10 \times 10⁶ asters/mL of lysate.
16. Use clarified lysates immediately or aliquot, snap freeze in liquid nitrogen, and store at –80°C. Lysates can be stored at –80°C for more than 6 yr with no apparent loss in the ability to form asters upon thawing.

3.3. Preparation of Crude *Spisula* Oocyte Lysate (Unactivated Lysate) (see Note 2)

1. Concentrate oocytes into pellets by centrifugation at 1000g for approx 30 s as described in **Subheading 3.2**.
2. Aspirate to remove as much sea water as possible, ensuring that the pellets are as dry as possible.
3. Resuspend oocyte pellets in 1M glycerol to 10 times the vol of packed oocytes, immediately centrifuge at 1000g for 30 s, and discard the supernatant.

4. Resuspend the oocyte pellet in glycerol/phosphate buffer to 10 times vol of packed eggs. Incubate for 60 s and then pellet the oocytes at 1000g for 30 s.
5. Discard the supernatant and resuspend oocytes in room temperature Aster buffer. Centrifuge oocytes immediately at 1000g for 30 s and aspirate the supernatant leaving a dry pellet.
6. Lyse oocytes by “flicking” the tube sharply 10–12 times and immediately place on ice.
7. Assay for oocyte lysis using a phase-contrast microscope (*see Note 3*).

3.4. Preparation of High Speed Lysate (HSA-Extract) (see Note 4)

1. Prepare 2–3 mL of fresh A4-lysate, or remove stored aliquots of A4-lysate from the –80°C freezer and thaw on ice.
2. Centrifuge at 29,000g for 15 min at 4°C.
3. Collect the clarified middle cytosolic layer, taking care not to collect any particulate material, and keep on ice.
4. Determine the ability to form asters by taking an aliquot, adding hexylene glycol, and assaying for aster formation using the polarized light microscope as described in **step 12** of **Subheading 3.2**.
5. Repeat **steps 2–4** until few or no asters form in lysates when assayed as described above. The inability to form asters indicates that centrosomes have been depleted from the lysate (HSA-extract). Keep on ice until use.

3.5. Centriole Assembly and Duplication (see Notes 5 and 6)

1. Combine equal volumes of unactivated lysate (100 µL) and HSA-extract (100 µL) and warm to room temperature.
2. At the 4 min and 15 min time points take 100 µL and add 2 mL of SIBD.
3. Centrifuge at 1,000g for 10 min.
4. Aspirate the supernatant and resuspend the pellet in 2 mL of SIB and centrifuge as in **step 3**.
5. Fix pellets by resuspension in 400–600 µL of SIB containing 1% glutaraldehyde for 15 min.
6. Centrifuge in a microfuge to pellet. In all of the following steps, take care not to disturb the integrity of the pellet during changes of solutions.
7. Aspirate and wash the pellet by gently overlaying with 400 µL of dH₂O while keeping the pellet intact.
8. Remove the wash and overlay the pellet with 300 µL of 1% osmium tetroxide and incubate on ice for 60 min to postfix.
9. Carefully add 500 µL of dH₂O to dilute the osmium tetroxide and remove the supernatant, taking care that the pellet surface is never exposed to the atmosphere or allowed to dry during the following steps.
10. Add 500 µL of dH₂O and incubate on ice for 15 min to wash the pellet. Repeat this step 3–5 times.
11. Remove the last wash, add 1 mL of 1% uranyl acetate, and incubate overnight in the refrigerator.

12. Wash by overlaying the pellet with dH₂O. Repeat three times, with 60 min intervals between each wash.
13. Dehydrate by washing the pellet with an ethanol series (30, 50, 70, 90, and 100% ethanol) with three changes and 3–5 min incubations at each step.
14. Wash the pellet three times with 100% ethanol.
15. Wash the pellet with 50% ethanol/50% propylene oxide.
16. Wash the pellet with 100% propylene oxide.
17. Incubate in 50% propylene oxide/50% Epon overnight at room temperature.
18. Transfer the pellet to 100% Epon and bake in a 60°C oven until hard (>16 h).
19. Section, stain, and observe with the electron microscope.

3.6. Germinal Vesicle Breakdown and Spindle Assembly (see Note 7)

1. Combine equal volumes of unactivated lysate and HSA-extract and warm to room temperature.
2. At various time points (0, 4, 8, and 12 min), remove 10 µL and dilute with 100 µL of SIBD. View samples directly using DIC microscopy or prepare them for immunofluorescence as described below.
3. For immunofluorescence, immediately after dilution in SIBD, fix by the addition of 3 mL of fixative solution (FS). Incubate at room temperature for 3 min, followed by 10 min on ice.
4. Centrifuge samples onto polylysine coated glass coverslips (5,8) using specialized centrifuge tubes described by Mitchison and Kirschner (13). Assemble spin tubes by placing a drop of PBS on the mount to adhere the coverslip. Place the coverslip-mount assembly into the spin tube, and overlay the coverslip with 2 mL of 30% glycerol in PBS. Then, overlay 1.5 mL of fixed sample on top of the 30% glycerol cushion.
5. Centrifuge at 12,000g for 15 min at 22°C in a swinging bucket rotor.
6. Remove the coverslips from the spin tubes (13) and transfer them into –20°C methanol.
7. Incubate in –20°C methanol for a minimum of 5 min. Store coverslips in –20°C methanol for up to one week.
8. Process for IMF as described in **Subheading 3.8**.

3.7. Inhibition of Spindle Assembly by Dynein Inhibitors (see Note 8)

1. Add 1 µL of vanadate solution or 1 µL of antibody solution to 100 µL of unactivated lysate and 100 µL of HSA-extract (final concentrations of 10 mM and 100 µg/mL respectively).
2. Combine the treated unactivated lysate and HSA-extract and warm to room temperature for 20 min.
3. Remove 10 µL of sample and dilute with 100 µL of SIBD. View samples directly using DIC microscopy or prepare them for immunofluorescence as follows.

4. For immunofluorescence, fix the diluted samples immediately by the addition of 3 mL of FS. Incubate at room temperature for 3 min followed by 10 min on ice.
5. Continue the procedure beginning with **step 4** of **Subheading 3.6**.

3.8. Immunofluorescence of Asters and Centrosomes

1. Remove coverslips with attached asters or spindles (*see Subheading 3.6.*) from -20°C MeOH and wash 3 times in PBS. To stain the chromosomes, add Hoechst 33342 (1:200 dilution) to the final PBS wash.
2. Incubate coverslips in BB for 20 min at room temperature.
3. Dilute the primary antibodies (anti- α or β -tubulin to stain microtubules and anti- γ -tubulin to stain centrosomes) in BB as desired. Pipet 20 μL of diluted primary antibody onto a piece of parafilm in a humidified chamber. Invert a coverslip onto the drop of primary antibody solution, sample side down, and incubate for a minimum of 20 min at room temperature.
4. Wash the coverslips three times in PBS.
5. Dilute the secondary antibodies in BB. Incubate coverslips in secondary antibody solution, (as described above [**step 3**]) for 30 min at room temperature.
6. Wash the coverslips three times in PBS.
7. Mount the coverslips (sample side down) on a slide using elvanol and allow the elvanol to harden overnight at room temperature in the dark.
8. Observe with an epifluorescence microscope.

4. Notes

1. The procedure for the preparation of oocyte lysates is based on those described by Palazzo et al. (**5,6,8**), Vogel et al. (**10**), and Palazzo and Vogel (**11**). Lysates can be prepared from different time points during meiosis by simply varying the incubation time after KCl activation. The procedure described is based on the use of 20 mL of oocytes.
2. Since *Spisula* oocytes are arrested at the G_2/M border it is possible to prepare both interphase and meiotic lysates from unactivated or KCl activated oocytes, respectively (**5,8**).
3. Take a small aliquot of the crude lysate and mount on a glass slide for observation. Lysates should contain free germinal vesicles (GVs) floating in a cytoplasmic suspension (**8**). In a good preparation, the GVs should remain stable after warming the lysate to room temperature. If the GVs break down and disappear within 15–20 min after warming, the lysate was activated during the procedure. Therefore, a new preparation will need to be made. If the GVs do not break down, but remain intact, the procedure was successful, and one can proceed with confidence. The unactivated lysate is kept on ice until use.
4. Centrosome-free lysate can be prepared from KCl activated oocytes and used to induce GVBD, centriole assembly, and spindle formation when mixed with unactivated lysate. The centrosomes can be removed from activated lysates by centrifugation, yielding a centrosome free lysate/extract as described by Palazzo et al. (**5,8**).

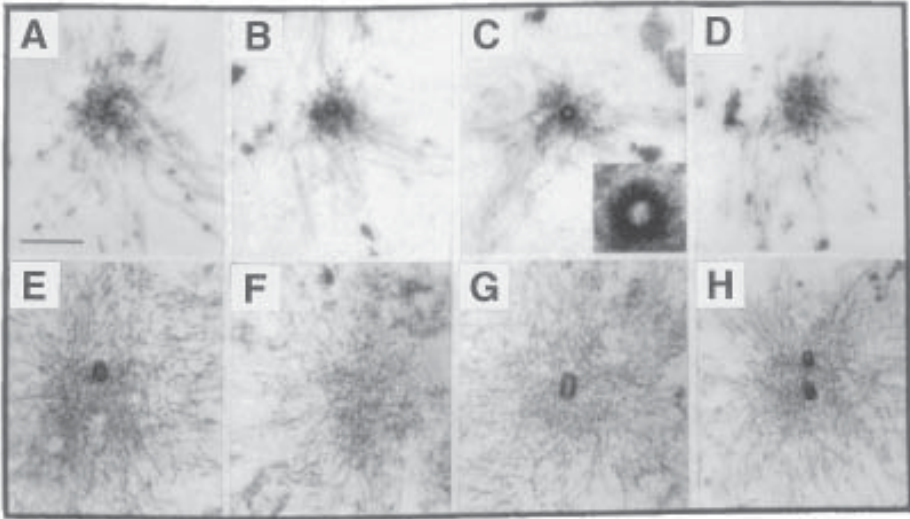


Fig. 1. High-voltage electron micrographs of serial 0.25 μm thick sections through asters formed in *Spisula* oocyte extracts. (A–D) Four serial sections through an aster formed 4 min after the addition of HSA-extract to unactivated lysate. A single centriole is visible in (B–D). The inset of figure (C) is high magnification of the sectioned centriole in (C) revealing the typical nine-triplet microtubule structure. (E–G) Three sections through an aster formed after 15 min. Two centrioles are visible in (E) and (G) which are separated by one section (F). (H) Two centrioles are visible in a single section through a second aster incubated for 15 min.

5. Many of the events that occur in live *Spisula* oocytes, can be replicated in vitro. For example, germinal vesicle breakdown (GVBD) can be induced in unactivated lysates made from quiescent oocytes by addition of the HSA-extracts (8). In addition, HSA-extract initiates centriole formation in unactivated lysates (5). Assembly of monopolar, bipolar, and multipolar aster-chromosome complexes, reflective of meiosis I spindles can also be induced to form in these lysate mixtures (8). Thus, this system enables experimentation aimed at the identification of the molecules and elucidation of the mechanisms responsible for these complex processes (8).
6. Surf clam oocytes are arrested at late prophase of meiosis I and do not contain centrioles, centrosomes, or asters. A cell-free system using lysates from *Spisula* oocytes has been developed that executes centriole formation and duplication (5). Treatment of crude unactivated lysate with HSA-extract results in the appearance of asters within 4 minutes of warming these lysate-extract mixtures to room temperature. HVEM of 0.25 μm thick serial sections of these asters revealed that 4 min after warming these mixtures to room temperature the centrosomes within asters contained a single centriole (5). Importantly, 15 min after

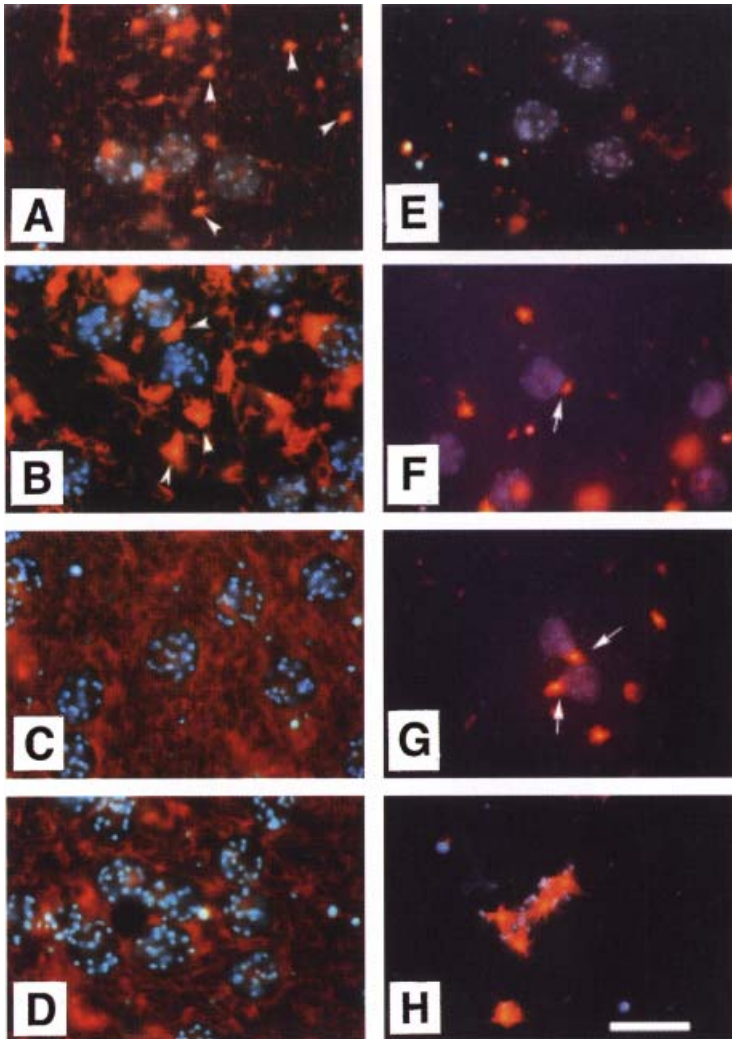


Fig. 2. Time course of in vitro spindle assembly. Unactivated lysate (**A–D**) and unactivated lysate treated with HSA-extract (**E–H**) were warmed to room temperature and processed for immunofluorescence microscopy (chromosomes, blue; microtubules, red) 0 min (**A, E**), 4 minutes (**B, F**), 8 min (**C, G**), and 16 min (**D, H**) after warming to room temperature. At 0 min, unactivated lysate (**A**) contains intact GV nuclei and small asters (arrowheads) which contain few microtubules. By 4 min (**B**) microtubules have elongated from these asters (arrowheads), and by 8 min (**C**) unactivated lysates have assembled a dense network of microtubules. GV nuclei remained intact in unactivated lysate throughout this period (**A–D**). Asters are present in lysate-extract mixtures 4 min after warming (**F**) and by 4–8 min asters are found associated with GV nuclei (arrows in **F** and **G**). Lysate-extract mixtures contain aster-chromosome complexes 16 min after warming (**H**), but no GV nuclei and no microtubule network.

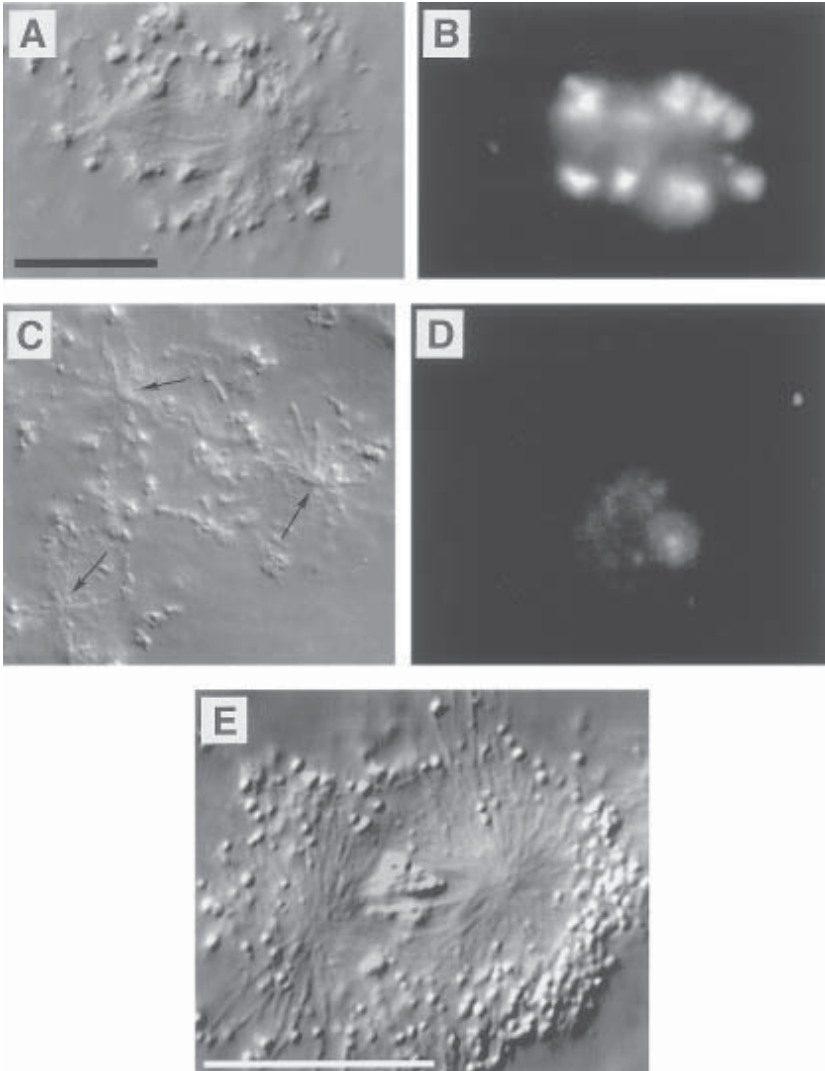


Fig. 3. Inhibition of spindle formation by dynein IC specific antibody m74-1 analyzed by DIC (**A**, **C**, and **E**) and fluorescence microscopy (**B**, **D**). Unactivated lysate was treated with HSA-extract and the mixture was warmed to room temperature for 15 to 20 min. Bipolar spindles with attached chromosomes form in these mixtures (**E**). Unactivated lysate and HSA-extract was supplemented with 0.5 mg/mL control antibody (**A**, **B**) or with 0.5 mg/mL dynein IC antibody m74-1 (**C**, **D**) prior to warming. (**B**, **D**) Fluorescent image of chromosomes found in the same field as the spindle and asters shown in **A** and **C**, respectively. (**A**) Bipolar spindle which contains a cluster of chromosomes (**B**) associated with asters formed in the presence of control antibody. In the presence of dynein IC antibody m74-1, asters formed (**C**), however, spindle assembly was inhibited and no aster-chromosome complexes were observed (**D**).

warming these lysate-extract mixtures, each centrosome contained two centrioles, replicating the events that occur *in vivo* (**Fig. 1**). Therefore, the addition of HSA-extracts to unactivated lysates induces centriole assembly and duplication and centrosome maturation.

7. Lysates prepared from unactivated *Spisula* oocytes contain intact GVs which house condensed chromosomes. The GVs will remain intact in these lysates for an indefinite period of time. However, GVBD can be induced by adding HSA-extracts to the unactivated lysate and warming to room temperature. Following the addition of the HSA-extracts, asters appear within 4 min, and many of these are associated with GV membranes. The GVs begin to break down within 8–10 min. Breakdown of the GVs releases the chromosomes which can then be captured by the microtubules that are associated with the maturing centrosomes that are assembling in the mixture at the same time. Chromosome capture results in the formation of various spindle types, including monopolar, bipolar, tripolar, and multipolar spindles (**8**) (**Fig. 2**). GVBD and spindle assembly can be observed by both DIC and immunofluorescence microscopy (**Figs. 2 and 3**) (**8**).
8. It has been demonstrated previously that in some systems chromatin can organize stabilized microtubules to form aastral spindles (**14**). In contrast, the spindles formed in the *Spisula* lysate system more closely resemble those in somatic mammalian cells, in that the spindles assemble as a result of chromosome capture by microtubules that are nucleated from centrosomes. The addition of agents that interfere with dynein function, such as antibodies or vanadate, to unactivated lysate/HSA-extract mixtures inhibits the formation of spindles but does not inhibit aster formation (**8**) (**Fig. 3**). These results suggest that dynein function is not required for centrosome assembly and maturation, but is required for the attachment of chromosomes to microtubules.

References

1. Allen, R. D. (1953) Fertilization and artificial activation in the egg of the surf clam *Spisula solidissima*. *Biol. Bull.* **105**, 213–239.
2. Kuriyama, R., Borisy, G. G., and Masui, Y. (1986) Microtubule cycles in oocytes of the surf clam, *Spisula solidissima*: an immunofluorescence study. *Dev. Biol.* **114**, 151–60.
3. Longo, F. J. and Anderson, E. (1970) An ultrastructural analysis of fertilization in the surf clam, *Spisula solidissima*. I. Polar body formation and development of the female pronucleus. *J. Ultrastruct. Res.* **33**, 495–514.
4. Sachs, M. I. (1971) A cytological analysis of artificial parthenogenesis in the surf clam *Spisula solidissima*. *J. Ultrastruct. Res.* **36**, 806–823.
5. Palazzo, R. E., Vaisberg, E., Cole, R. W., and Rieder, C. L. (1992) Centriole duplication in lysates of *Spisula solidissima* oocytes. *Science* **256**, 219–221.
6. Palazzo, R. E., Brawley, J. B., and Rebhun, L. I. (1988) Spontaneous aster formation in cytoplasmic extracts from eggs of the surf clam. *Zoological Science* **5**, 603–612.
7. Dessev, G., Palazzo, R., Rebhun, L., and Goldman, R. (1989) Disassembly of the nuclear envelope of *Spisula* oocytes in a cell-free system. *Dev. Biol.* **131**, 496–504.

8. Palazzo, R. E., Vaisberg, E. A., Weiss, D. G., Kuznetsov, S. A., and Steffen, W. (1999) Dynein is required for spindle assembly in cytoplasmic extracts of *Spisula solidissima* oocytes. *J. Cell Sci.* **112**, 1291–302.
9. Costello, D. P. and Henley C. (1971) *Methods for Obtaining and Handling Marine Eggs and Embryos*. Woods Hole, MA: Marine Biological Laboratory.
10. Vogel, J. M., Stearns, T., Rieder, C. L., and Palazzo, R. E. (1997) Centrosomes isolated from *Spisula solidissima* oocytes contain rings and an unusual stoichiometric ratio of alpha/beta tubulin. *J. Cell Biol.* **137**, 193–202.
11. Palazzo, R. E. and Vogel, J. M. (1999) Isolation of Centrosomes from *Spisula solidissima* Oocytes, in *Mitosis and Meiosis*, C.L. Rieder, (ed.) Academic Press: New York. p. 36–56.
12. Rebhun, L. I. and Sharpless, T. K. (1964) Isolation of spindles from the surf clam *Spisula solidissima*. *J. Cell Biol.* **22**, 488–491.
13. Mitchison, T. J. and Kirschner, M. W. (1986) Isolation of mammalian centrosomes., in *Methods Enzymol.* 261–268.
14. Heald, R., Tournebize, R., Blank, T., Sandaltzopoulos, R., Becker, P., Hyman, A., and Karsenti, E. (1996) Self-organization of microtubules into bipolar spindles around artificial chromosomes in *Xenopus* egg extracts. *Nature* **382**, 420–425.

***Xenopus* Egg Extracts as a Model System for Analysis of Microtubule, Actin Filament, and Intermediate Filament Interactions**

**Craig A. Mandato,* Kari L. Weber,* Anna J. Zandy,
Thomas J. Keating, and William M. Bement**

1. Introduction

It has long been apparent that the three cytoskeletal systems of eukaryotic cells, microtubules, f-actin, and intermediate filaments, act in a cooperative fashion, both to achieve their characteristic distributions within cells (1–3), and to execute a variety of complex cellular phenomena (4). However, defining the nature of interactions between the different systems has proven difficult. These difficulties stem from several different features of the three cytoskeletal systems. The filamentous nature of the systems makes it difficult to apply standard biochemical approaches, since most such approaches cannot distinguish between specific interactions and those that result from fortuitous entanglement. Similarly, because all three systems are very abundant in the typical cell, and because all three systems are to greater or lesser degrees dynamic, simultaneous imaging of the different systems in living cells may be less than informative. Further, in most cell types, it is difficult, if not impossible to adequately preserve all three systems in the same preparation using standard immunofluorescence approaches. For example, in *Xenopus* oocytes and eggs, entirely different fixation protocols are required for visualization of microtubules (5), f-actin (6), and intermediate filaments (7).

It has been our goal to develop simple model systems that allow in vivo assessment of the impact of the three systems on each other (8–9), and in vitro assessment of direct interactions between the three systems (10).

*These authors contributed equally to this work.

From: *Methods in Molecular Biology*, vol. 161: *Cytoskeleton Methods and Protocols*
Edited by: R. H. Gavin © Humana Press Inc., Totowa, NJ

For the latter, we have employed *Xenopus* egg extracts, the general utility of which for analysis of cellular and molecular processes has been discussed in detail by Murray (11). Here we describe three different applications of *Xenopus* egg extracts for analysis of different cytoskeletal networks and their interactions using fluorescence microscopy—fixation-free analysis in flow chambers, fixation-free analysis of samples sedimented through sucrose, and immunofluorescence analysis of thin, rapidly-frozen, specimens.

2. Materials

2.1. Animal Husbandry

Adult female frogs are purchased from either Nasco (Fort Atkinson, WI) or Xenopus I (Ann Arbor, MI) and housed in 3' × 3' × 2' polypropylene or metal tanks at a density of less than 25 frogs per tank. The tanks are filled to a depth of 12 inches with water that has passed through a commercial charcoal filtration system to remove chlorine and ammonia and to ensure the pH range is between 6–7. The tanks are scrubbed and the water replaced twice a week after the frogs have been fed Nasco frog brittle (*ad libitum*). The rooms where the frogs are kept are on a 12 h light/ 12 h dark cycle and remain at a constant 16°C. Adult males are housed in the same manner, but kept separate from the females, since frogs in general have no innate sense of propriety.

2.2. Egg Extraction

1. PMSG: Pregnant mare serum gonadotropin (Calbiochem; San Diego, CA). A 500 UI/mL stock is made in sterile water and stored at –20°C.
2. HGC: Human chorionic gonadotropin (ICN Biomedicals, Costa Mesa, CA). A 2500 UI/mL stock is made fresh in sterile water and stored on ice, until used.
3. Marc's Modified Ringer's Solution (1X MMR): 100 mM NaCl, 2 mM KCl, 1 mM MgCl₂, 2 mM CaCl₂, 0.1 mM EDTA, 5 mM HEPES, pH 7.8. Prepared as a 10X stock, and stored at 4°C.
4. Dejelling Solution: 2% w/v cysteine in 0.25% MMR, pH 7.8. This solution must be used within 1 h after making.
5. Egg Lysis Buffer (ELB): 250 mM Sucrose, 100 mM KCl, 0.1 mM CaCl₂, 1 mM MgCl₂, 1 mM DTT, 10 mM K-HEPES, pH 7.7.
6. Protease Inhibitors and Cycloheximide
 - a. 10 µg/mL aprotinin.
 - b. 10 µg/mL chymostatin.
 - c. 5 µg/mL leupeptin.
 - d. 10 µg/mL pepstatin.
 - e. 500 µg/mL Pefabloc.
 - f. 100 µg/mL cycloheximide.

All protease inhibitors and cycloheximide were purchased from Roche Molecular Biochemicals (Indianapolis, IN). Distilled water or DMSO were used as solvents for 1000X stocks.

2.3. Sperm Preparation

1. Modified Barth's Solution - High Salt (MBSH): 110 mM NaCl, 2 mM KCl, 1 mM MgSO₄, 2 mM NaHCO₃, 15 mM Tris-base, pH 7.6.
2. HSPPP: 250 mM sucrose, 1 mM EDTA, 0.5 mM spermidine, 0.2 mM spermine, 1 mM DTT, 15 mM HEPES, pH 7.4. Add protease inhibitors as listed in **Subheading 2.2**.
3. 10 mg/mL (w/v) aqueous Bovine Serum Albumin (BSA). Make a fresh stock solution.
4. HSPPP-BSA (3%): HSPPP, 3% BSA.
5. HSPPP-BSA (0.3%): HSPPP, 0.3% BSA.
6. HSPPP-BSA-Glycerol: HSPPP, 0.3% BSA, 30% glycerol.
7. 10 mg/mL aqueous L- α -lysophosphatidylcholine (Roche Molecular Biochemicals).
8. HSPPP-lysophosphatidylcholine: HSPPP, 500 μ g/mL L- α -lysophosphatidylcholine.

2.4. Flow Chamber

1. ATP regenerating system (**12**): 1.5 mg/mL creatine kinase, 100 mM creatine phosphate, 10 mM ATP, Store in 10 μ L aliquots at -80°C .
2. Microtubule Stabilization Buffer (TSB): 5 mM MgCl₂, 1 mM EGTA, 80 mM K-PIPES, pH 7.0.
3. 1 mg/mL Polylysine (Sigma).
4. TSB-BSA: TSB with 5 mg/mL BSA.
5. 10 mg/mL Fluorescent tubulin (Cytoskeleton; Denver, CO).
6. TSBT: TSB, 5 mg/mL BSA, 20 μ M taxol.
7. TSBT-phalloidin: TSBT, 5 mg/mL BSA, 1 U/mL fluorescent phalloidin (Oregon Green or Alexa 488 labeled; Molecular Probes; Eugene, OR).
8. Cy5: Cy5-labeled secondary antibody (Molecular Probes; Eugene, OR) diluted 1:100 in TSBT-BSA.
9. C11: Monoclonal anti-cytokeratin antibody (Sigma) diluted 1:250 in TSBT-BSA.
10. Glycerol mounting medium: 80% glycerol containing 20 mM *N*-propyl gallate.

2.5. Sucrose Sedimentation

1. 10 mg/mL rhodamine tubulin (Cytoskeleton; Denver, CO).
2. TSBT-phalloidin: TSBT (*see* **Subheading 2.4.**) and 10 μ M Alexa 488 labeled phalloidin (Molecular Probes; Eugene, OR).

2.6. Rapidly Frozen, Thin Prep

1. Phosphate Buffered Saline (PBS): 137 mM NaCl, 2.7 mM KCl, 4.3 mM Na₂HPO₄·7H₂O, 1.4 mM KH₂PO₄, pH \sim 7.3. Prepare a 10X stock solution.
2. PBSN: PBS, 0.1% Nonidet P-40.
3. PBSN-Borohydride: PBSN, 100 mM sodium borohydride.
4. PBSN-BSA: PBSN, 5 mg/mL bovine serum albumin.
5. Coverslips: This protocol requires 22 \times 50 mm and 22 \times 22 mm glass coverslips, which must be cleaned prior to the experiment. Separate 50 of each type of cover-

slip and drop individually into a beaker containing 200 mL distilled water and 5 mL Versa-Clean Liquid Concentrate (Fisher Scientific, Pittsburgh, PA). Sonicate at room temperature for 1 h. Rinse coverslips 20 times in distilled water, then cover with 6N HCl overnight. Again rinse coverslips 20 times in distilled water and store until use in 90% ethanol. Equal number of 22 × 50 mm and 22 × 22 mm coverslips are removed from 90% ethanol and allowed to air dry. After drying, 22 × 22 coverslips are covered with 150 µL 0.25% Casein (Sigma) and allowed to sit for 1–2 min. The excess casein is pipeted off and the remaining left to dry. 22 × 50 mm coverslips are treated with Rain-X (Unelko Corp. Scottsdale, AZ), a fluid repellent treatment generally used on windshields. Rain-X is applied with cotton swabs and repeatedly wiped until it is no longer visible on the coverslip.

2.7. Other Materials

1. Fixative: 80 mM K-PIPES, pH 6.8, 5 mM EGTA, 1 mM MgCl₂, 3.7% paraformaldehyde, 0.25% glutaraldehyde, 0.20% Triton X-100, 0.5 µM taxol. Add 1.85 g paraformaldehyde to ~10 mL fix buffer (80 mM K-PIPES, pH 6.8, 5 mM EGTA, 1 mM MgCl₂). Boil in water bath for 5 min, vortex, boil 5 min, add 1 drop 10N NaOH, vortex, boil for 5 min, vortex. At this point, the paraformaldehyde should be completely in solution. To the concentrated paraformaldehyde add 100 µL Triton X-100 (final concentration of 0.2%) and fix buffer to a final volume of 50 mL (final paraformaldehyde concentration is 3.7%). Mix until Triton is completely in solution. Immediately prior to experiment, add 250 µL 50% glutaraldehyde (for a final concentration of 0.25%) and taxol to 0.5–1.0 µM. Mix well.
2. 20 µM nocodazole (Calbiochem).
3. 10 µM Latrunculin B (Calbiochem).
4. 4.4 mg/mL Anti-pan cytokeratin antibody (Sigma).

3. Methods

3.1. Egg Extract Preparation

3.1.1. Collecting Eggs

Frogs are induced to ovulate by a series of injections of pregnant mare serum gonadotropin (PMSG) and human chorionic gonadotropin (HCG). The protocol we have had the most success with is a modified version of Murray's method (11).

1. Remove female frogs from the large housing tanks and place in smaller 20 L rectangular containers (2 or 3 per container) that contain 10 L of filtered water.
2. Throughout the priming protocol, ensure that the frogs remain in a quiet room at 16°C.
3. On d 1 of the priming, inject 50 UI (100 µL) of PMSG into the dorsal lymph sac using a 27-gauge needle. Make subsequent injections in the same manner.

4. During injection frogs will become agitated and spastic; to avoid this problem hold the frog down firmly on a bench top and completely cover the eyes with a wet paper towel. Once the frog is still, make the injection.
5. Administer a second dose of PMSG (25 UI) on d 3.
6. Induce ovulation in the frogs by injecting 500 UI of HCG on d 5. Ovulation can be induced on d 5 through d 10, but we find that inducing ovulation on the fifth d is most effective.
7. After the HCG injection, place frogs in separate containers containing 2 L of 1X MMR and store at 16°C. Ovulation should be induced by late in the evening; egg laying will begin anywhere from 10 to 16 h after injecting HCG.
8. Prior to collecting the layed eggs, hold the frog loosely in a prone position while separating the legs with fore and middle fingers of one hand; the other hand is used to tickle the frog's chin. This annoyance causes strain, which expels more eggs.
9. Collect and separate eggs from each frog.
10. Return frogs to MMR where they will continue to lay eggs.
11. Examine eggs from each frog for quality. Good eggs are uniformly pigmented, that is, the animal hemisphere is not mottled and has a distinct white spot at the animal pole.
12. Pool the high quality eggs, rinse thoroughly in MMR, and store at 16°C for 1–3 h until ready to use.

3.1.2. Making Egg Extracts

1. Remove MMR and dejelly eggs in the dejelling solution. This step will take between 5–10 min, gently stirring every 2–3 min. Dejelled eggs will be tightly spaced.
2. Remove dejelling solution and rinse 3 times in 0.25 MMR.
3. Rinse twice in ice cold ELB.
4. Rinse twice in ice cold ELB + protease inhibitors.
5. Transfer eggs into clear ultracentrifuge tubes and pack by a brief centrifugation in a clinical centrifuge. Remove the excess buffer.
6. Add protease inhibitors and cycloheximide to a final concentration (listed in **Sub-heading 2.2.**) relative to the packed egg volume.
7. Crush eggs by spinning at 4°C for 20 min at 20,000g in an SW41 rotor.
8. After centrifugation, the crushed eggs will have separated into three layers: a pale lipid layer at the top, a clear, yellowish cytoplasmic layer just below, and a dark greenish/black yolk layer at the bottom. Using a 3 mL syringe with an 18-gauge needle (bevel up) slowly and carefully remove the cytoplasmic layer by puncturing the centrifuge tube just above the bottom of the cytoplasmic layer. Avoid contaminating the cytoplasmic extract with either the lipid or yolk as this will adversely impact the quality of the extracts.
9. Divide extract into 50 µL aliquots, snap freeze in liquid nitrogen and store at –80°C until needed.

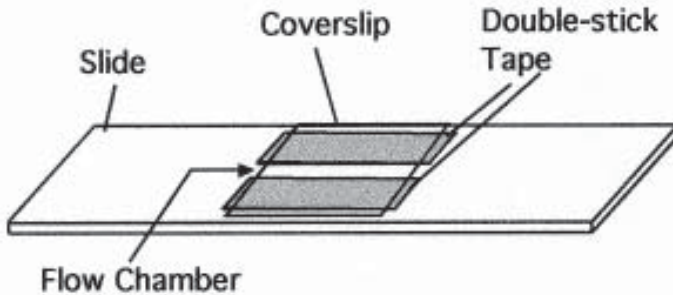


Fig. 1. Schematic diagram of flow chamber.

3.2. Demembrated Sperm Preparation

1. Three days prior to collecting sperm, prime male frogs by injecting with 25 UI (200 μ L) of PMSG.
2. On the day before collecting sperm, inject 200 UI (200 μ L) of HCG (*II*).
3. Remove the testes from decapitated frogs through an incision made in the lower abdomen. The testes are white, kidney bean-shaped organs located on either side of the spine.
4. Take precautions against tearing or puncturing the testes during this procedure.
5. Perform all of the following steps of the protocol on ice.
6. Rinse isolated testes three times in ice-cold MBSH.
7. Macerate testes in an ice-cold pyrex Petri plate in 4 mL of ice-cold HSPPP using the edge of four taped-together microscope slides.
8. Filter macerated testes through three layers of cheese cloth, to remove large pieces of connective tissue.
9. Pellet filtrate in a clinical centrifuge at 4°C at 2000g for 5 min.
10. Resuspend the pelleted sperm in HSPPP, re-pellet (as above) and resuspend in 1 mL of room temperature HSPPP-lysophosphatidylcholine.
11. Incubate for 5 min at room temperature.
12. Dilute sperm with 10 mL of HSPPP-BSA(3%) and pellet (as above).
13. Resuspend in 3 mL of HSPPP-BSA(0.3%) and pellet.
14. Resuspend in 2.5 mL of HSPPP-BSA-glycerol.
15. Divide sperm preparation into 50 mL aliquots, snap freeze in liquid nitrogen and store at -80°C until needed.

3.3. Fixation-Free Analysis in Flow Chambers (see Note 1)

1. Construct a flow chamber by inverting polylysine-coated coverslips over two pieces of parallel, double-stick tape adhered to a slide. Space the pieces of tape ~0.5 cm apart, so that flow chamber volumes will be ~10 μ L (**Fig. 1**).
2. Thaw 50 μ L of demembrated sperm; pipet 10 μ L into each flow chamber, and allow sperm to adhere for 10 min (*see Note 2*).
3. Wash chambers 5 times with TSB-BSA to remove unbound sperm and to mask remaining areas coated with polylysine.

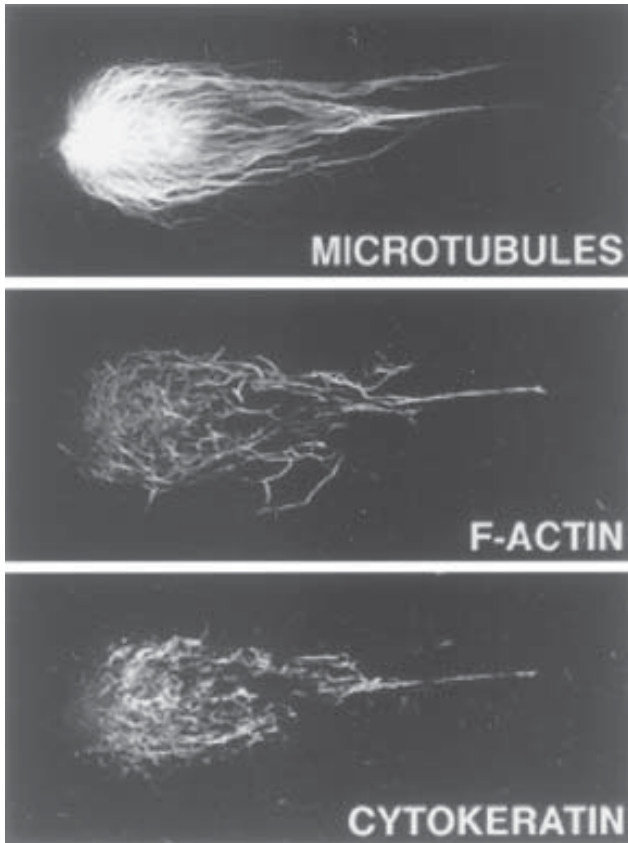


Fig. 2. Triple-label, confocal fluorescence micrograph of a *Xenopus* aster prepared in a flow chamber. No fixatives were used; microtubules were visualized using rhodamine-tubulin, f-actin using Alexa-488 phalloidin, and cyokeratin using anticyokeratin antibodies and a Cy5-labeled secondary.

4. Thaw 50 μL of egg extract and mix with 2 μL fluorescent tubulin and 2 μL ATP regenerating system (12). Let incubate on ice for two hours.
5. After the ice incubation, flow 10 μL of extract into sperm-coated chambers and incubate at room temperature for 15 min to allow tubulin, actin, and cyokeratin polymerization. The demembrated sperm are necessary to nucleate microtubule asters (14) while the adherence of sperm to the chamber permits subsequent washing of the samples.
6. Wash chambers 10 times with TSBT.
7. Incubate chambers for 15 min with TSBT-phalloidin. To visualize cyokeratin, use the C11 anticyokeratin antibody.
8. Wash 5 times with TSBT, then incubate in anti-Cy5 antibody.

9. Wash 5 times with TSBT and mount in glycerol mounting medium to extract membranes, stabilize protein-protein interactions, and prevent photobleaching. Refrigerate slides in darkness until viewed using a confocal fluorescence microscope. **Figure 2** shows one example of a washed, triple labeled aster, for other examples, see (10).

3.4. Fixation-Free Sucrose Sedimentation Analysis (see Note 3)

1. Thaw 50 μL of egg extract, combine with 2 μL of rhodamine tubulin, and incubate on ice for 2 h.
2. Add 1 μL of demembrated sperm and 2 μL ATP regenerating system, mix, and incubate the mixture at room temperature for 10 min.
3. Dilute the mixture fivefold with TSBT-fluorescent phalloidin.
4. Immediately centrifuge at 15000g for 5 min through a 30% sucrose cushion.
5. Resuspend the pellets in TSB, mount on standard microscope slides in glycerol mounting medium, coverslip, seal with nail polish, and examine by confocal fluorescence microscopy (as above). An example of the images produced by this approach can be seen in Sider et al. (10).

3.5. Analysis of Rapidly Frozen, Thin Specimens (see Note 4)

1. Thaw 50 μL aliquots of egg extracts and mix with 2 μL ATP regenerating system (12), 2 μL demembrated sperm and incubate on ice for 30 min (see Note 2).
2. Pipet 1–2 μL extract-sperm mixture onto large coverslips and small coverslips were inverted onto the extract such that it spread into a very thin sample.
3. Incubate at room temperature for 20 min.
4. Submerge coverslips into liquid nitrogen until thoroughly frozen.
5. Remove from liquid nitrogen, and place the coverslips on a ceramic plate, which is on a bed of dry ice to prevent thawing (see Note 5).
6. Quickly pry the small coverslip off the large coverslip and drop face up into a polystyrene well containing enough fix to cover the coverslip.
7. Unless otherwise specified, for all remaining steps use a 6-well polypropylene dish, with wells large enough to accommodate the 22 \times 22 mm coverslips.
8. Incubate samples in fix for 5 min while gently shaking.
9. Aspirate off the fix.
10. Immediately and gently wash samples 2 times in PBSN.
11. Quench the samples for 10 min using PBSN-Borohydride.
12. Wash the samples twice in PBSN-BSA. These and each subsequent wash consists of 5 min in the solution while gently shaking and should result in adequate blocking to prepare for antibody incubations.
13. Incubate in primary antibody (see Note 6) for 15 min at 37°C
14. Wash 4 times in PBSN-BSA.
15. Incubate in secondary antibody (see Note 6) for 15 min at 37°C, follow with four washes. If necessary, a tertiary antibody incubation and subsequent washes are performed in the same manner.

16. Pipet 5 μL glycerol mounting medium onto a slide and invert the coverslip containing the sample directly onto the mounting medium. The coverslip is then sealed onto the slide using nail polish and examined by confocal microscopy as previously described.

3.6. Further Study of Cytoskeletal Systems

Further study of cytoskeletal system interactions can be performed via disruption of one or more of three systems: microtubules, f-actin, and cytokeratin intermediate filaments. Microtubules can be disrupted by adding nocodazole to an extract prior to the ice-cold incubation. F-actin can be disrupted in the same manner using Latrunculin B. Cytokeratin intermediate filament assembly can be blocked by adding 3 μL of Anti-Pan Cytokeratin antibody to 25 μL of an extract prior to the ice-cold incubation.

4. Notes

1. For fixation-free analysis in flow chambers, microtubules are labeled by adding rhodamine-tubulin to *Xenopus* egg extracts, and microtubule asters are formed by incubation of extracts with demembrated *Xenopus* sperm adhered to coverslips that define the top of a flow chamber. After incubation, the flow chambers are washed with buffers containing taxol, to stabilize microtubules. F-actin is visualized by staining flow chambers with Alexa 488- or Oregon Green-phalloidin (**10**), while intermediate filaments are visualized by indirect immunofluorescence using antibodies that are applied to the flow chambers during sequential washes and incubations (**13**). After the final wash, chambers are flooded with a glycerol-based mounting medium, and viewed by confocal fluorescence microscopy.

The advantages of this approach are the absence of any fixation, which ensures the absence of fixation-induced artifacts. In addition, repeated washing of the chambers removes most of the material not bound to the aster microtubules, such as g-actin and unpolymerized tubulin, and consequently, the background is extremely low. Further, the opportunity to subject the chambers to washing also permits simple manipulations, for example, mild extraction with nonionic detergents.

The washing procedure, although it provides some of the strengths of this approach, is also responsible for the weaknesses. Washing distorts the overall organization of asters; instead of appearing circular, they are comet-shaped, with the plus ends of the microtubules and everything associated with them often being compacted together. Washing may also artificially increase the amount of material associated with asters, because it has the potential to push material into the asters. Conversely, it may also remove material that is normally associated with the asters.

2. Before adding demembrated sperm to any of the protocols listed, the glycerol must be removed. Thaw 50 μL aliquots of demembrated sperm and dilute with 200 μL TSB, microfuge at 14,000g for 2 min, and resuspend in 60 μL of TSB.

3. Sedimentation through 30% sucrose is a generally accepted approach to identify microtubule associated proteins, although it is typically employed for biochemical, rather than microscopy analyses. Here, sedimentation through sucrose is used as an alternative to washing in flow chambers to produce fluorescent microtubules and f-actin in the absence of fixation. Asters are assembled from demembranated sperm in extracts in the presence of rhodamine-tubulin, rapidly diluted in the presence of fluorescent phalloidin, and then sedimented through sucrose. Like washing in the flow chamber approach, sedimentation removes all “background” material. Unlike washing, the general morphology of the asters is preserved and the concern that material is being artificially pushed into asters is somewhat less than in the flow chamber protocol. On the other hand, it can be difficult to resuspend the pelleted asters without fragmenting them.
4. One of the strengths of *Xenopus* egg extracts is that they permit analysis of cytoskeletal dynamics (15–16). They can also be used for investigation of dynamic interactions between cytoskeletal systems. In both cases, detection of the polymer in question depends on the inclusion of a fluorescently labeled probe, such as rhodamine-tubulin or Alexa-488 phalloidin (see **Subheading 3.4.**). However, most proteins do not have such fluorescent probes readily available and are instead typically localized by immunofluorescence. As an alternative approach to the flow chambers (see **Subheading 3.3.**) which may not be suitable for immunolocalization of some proteins, it is possible to prepare and rapidly freeze very thin samples of extract, and then process those samples for immunofluorescence. This approach has the added advantage that it could, in principle, be used to first follow the dynamics of the sample and then immunolocalize specific proteins in the same area previously filmed.
5. In the flash freeze protocol, it is important to immerse the coverslip in fix immediately and not allow the sample to thaw first. The treatment of the coverslips discussed above should result in the frozen extract remaining adhered to the small coverslip. Solutions/washes are removed via aspiration and added back by gently dribbling solutions down the side of the well with a transfer pipette to avoid disturbing the sample.
6. Primary and secondary antibodies are applied as follows: Antibodies are appropriately diluted and then microfuged at 14,000g for 15 min. 110 μ L antibody solution per sample is pipetted onto parafilm that has been tightly pressed down against a glass plate. The sample containing coverslip is then inverted onto the antibody solution. A moist chamber is created by placing wet paper towels on the glass plate on either side of the parafilm such that another glass plate can be supported by the towels. This plate is then covered by another wet towel.

References

1. Gurland, G. and Gundersen, G. G. (1995) Stable, detyrosinated microtubules function to localize vimentin intermediate filaments in fibroblasts. *J. Cell Biol.* **131**, 1275–1290.
2. Waterman-Storer, C. M. and Salmon, E. D. (1997) Actomyosin-based retrograde flow of microtubules in the lamella of migrating epithelial cells influence micro-

- tubule dynamic instability and turnover and is associated with microtubule breakage and treadmilling. *J. Cell Biol.* **139**, 417–434.
3. Yoon, M., Moir, R. D., Prahlad, V., and Goldman, R. D. (1998) Motile properties of vimentin intermediate filament networks in living cells. *J. Cell Biol.* **143**, 147–157.
 4. Waterman-Storer, C. M. and Salmon, E. D. (1999) Positive feedback interactions between microtubule and actin dynamics during cell motility. *Curr. Opin. Cell Biol.* **11**, 61–67.
 5. Gard, D. L. (1991) Organization, nucleation, and acetylation of microtubules in *Xenopus laevis* oocytes: a study by confocal immunofluorescence microscopy. *Dev. Biol.* **143**, 346–362.
 6. Roeder, A. D. and Gard, D. L. (1994) Confocal microscopy of F-actin distribution in *Xenopus* oocytes. *Zygote* **2**, 111–124.
 7. Gard, D. L. (1997) The organization and animal-vegetal asymmetry of cytokeratin filaments in stage VI *Xenopus* oocytes is dependent upon f-actin and microtubules. *Dev. Biol.* **184**, 95–114.
 8. Canman, J. C. and Bement, W. M. (1997) Microtubules suppress actomyosin-based cortical flow in *Xenopus* oocytes. *J. Cell Sci.* **110**, 1907–1917.
 9. Bement, W. M., Mandato, C. A., and Kirsch, M. N. (1999) Wound-induced assembly and closure of an actomyosin purse string in *Xenopus* oocytes. In Press. *Curr. Biol.*
 10. Sider, J. R., Mandato, C. A., Weber, K. L., Zandy, A. J., Beach, D., Finst, R. J., Skobel, J., and Bement, W. M. (1999) Direct observation of microtubule-F-actin interaction in cell free lysates. *J. Cell Sci.* **112**, 1947–1956.
 11. Murray, A. W. (1991) Cell cycle extracts. *Methods Cell Biol.* **36**, 581–605.
 12. Leno, G. H. and Laskey, R. A. (1991) DNA replication in cell-free extracts from *Xenopus laevis*. *Methods Cell Biol.* **36**, 561–79.
 13. Weber, K. L. and Bement, W. M. (1998) Investigation of the interaction between cytoskeletal elements in cell-free *Xenopus* lysates. *Mol. Biol. Cell.* **9**, 39a.
 14. Stearns, T. and Kirschner, M. (1994) *In vitro* reconstitution of centrosome assembly and function: the central role of gamma-tubulin. *Cell* **76**, 623–637.
 15. Belmont, L. D., Hyman, A. A., Sawin, K. E., and Mitchison, T. J. (1990) Real time visualization of cell cycle-dependent changes in microtubule dynamics in cytoplasmic extracts. *Cell* **62**, 579–589.
 16. Theriot, J. A., Rosenblatt, J., Portnoy, D. A., Goldschmidt-Clermont, P. J., and Mitchison, T. J. (1994) Involvement of profilin in the actin-based motility of *L. monocytogenes* in cells and cell free extracts. *Cell* **76**, 505–517.

Detergent-Extracted Models for the Study of Cilia or Flagella

Charles B. Lindemann and Kathleen A. Schmitz

1. Introduction

The plasma membrane of the living cell is designed to regulate the internal composition of the cytosol and protect the interior of the cell from oxidative and enzymatic damage. It performs its role so well in these respects that it presents a major obstacle to the study of intracellular processes. Recognizing this problem, Szent-Gyorgyi (1) used high concentrations of glycerol to increase the permeability of the membrane. This allowed him to carry out his now famous studies of skeletal muscle physiology that demonstrated the central role of ATP and Ca^{2+} in muscle contraction. Adopting essentially the same approach, Hoffman-Berling and Bishop (2,3) applied the glycerination method to mammalian sperm cells and reported a limited success in inducing motion but not coordinated swimming. Applying the glycerination technique to sea urchin sperm, Brokaw and Benedict (4) successfully restored coordinated beating of the flagellum and progressive swimming. Using the nonionic detergent Triton X-100 Gibbons and Gibbons (5) showed that normal flagellar motility could be reactivated in the absence of the plasma membrane. This result made it clear that the flagellar axoneme is a self-contained machine, which only requires a suitable medium and a supply of Mg-ATP to function.

The adaptation and application of the detergent-extraction technique to a great diversity of cilia and flagella followed the initial development of a workable reactivation method by the Gibbons' laboratory. Tryptic digests of demembrated sea urchin sperm flagella provided the first dynamic observations of microtubule sliding (6). Subsequent application of the technique to *Tetrahymena* allowed the polarity of action of the dynein arms to be determined (7). The detergent-extraction technique was partially responsible

for identifying the cyclic AMP mediated control of the axoneme (8) and permitted the discovery of the role of Ca^{2+} in the symmetry of the flagellar beat (9).

The challenges that remain in the understanding of cilia and flagella are currently centered about two areas of exploration. The first involves the molecular construction of the axoneme. Modern molecular genetics provides the means to explore the function of individual components of the axoneme by targeted mutagenesis. In this endeavor *Chlamydomonas* is the leading model system, as an extensive library of mutations affecting flagellar proteins is readily available. Demembrated models represent the best hope for quantitatively documenting differences in functional performance of the flagellum under standardized assay conditions. Unless axonemal function is assayed under conditions where Mg-ATP, Ca^{2+} , cAMP and pH are rigidly controlled, too many confounding variables can obscure the true effect of a single mutation. For this reason, membrane permeabilized models are possibly the best assay for determination of gene function for flagellar proteins.

The second challenge is in the arena of theory development. Working hypotheses that are advanced on the basis of the available experimental data must be subjected to tests that confirm or reject their validity. Controlled experiments that test a specific hypothesis are often only possible without the interference of the membrane (10).

In the remainder of this report a general method will be presented for reactivation of detergent-extracted models. Variations that have been developed to facilitate working with specific systems will be considered, and the special problems inherent in working with demembrated cilia and flagella will be discussed.

2. Materials

2.1. Reagents and Solutions

Demembrated cells are extremely sensitive to contaminants that would be excluded from the cell interior in a live intact cell. For this reason it is very important to start with the highest purity ingredients when making solutions for reactivating membrane-extracted cilia and flagella.

1. Triton X-100 or Nonidet P-40: These are the most widely employed detergents for membrane extraction, although many available detergents can give a satisfactory result. Nonidet P-40 is no longer commercially available under that name but many companies still supply a chemically equivalent detergent. It is best to stay with a source that has worked in your own trials. We have had good results with Pierce's (Rockford, IL) Triton X-100 and ICN Biomedical's (Aurora, OH) Nonidet P-40 (Igepal CA-630).
2. Dithiothreitol (DTT) or Glutathione: These are excellent reducing agents and antioxidants. They must be stored dessicated and refrigerated and are critical

ingredients in a successful reactivation. It is good to stay with a supplier that has given good results. Our current supplier for DTT is Roche Molecular Biochemicals (Indianapolis, IN). The DTT should be made up as a stock solution and then stored frozen (-20°C) in small aliquots ($< 1\text{ mL}$) in sealed 1.5 mL microfuge tubes. Once a lot has proven itself in use, it is good to have fresh microfuge tubes of the same batch to work with. It is best in practice not to freeze and thaw the same microfuge tube more than 4 times. Keep the tube sealed and on ice during experiments. In its proper reduced form it is a smelly (skunky) compound; if it doesn't smell, don't use it. Glutathione will also give excellent results as an antioxidant. It can be treated much the same as DTT, and may be substituted if preferred. Glutathione is the natural antioxidant of the cell interior. Therefore, if your goal is to duplicate the natural interior condition of the cell, glutathione may be an attractive option.

3. Buffers: Tris, HEPES or PIPES. Tris (Tris[hydroxymethyl]aminomethane) is a suitable buffer for reactivating demembrated flagella at the more alkaline range of pH (7.4–8.0). HEPES (*N*-(2-Hydroxyethyl)-1-Piperazine-*N'*-ethansulfonic acid) and PIPES (piperazine-*N*, *N'*-bis[2-ethanesulfonic acid]) are more widely used for reactivation protocols in the pH range of 6.6 to 7.4. All are widely available. We have the most experience with Tris, preferring to work from the free base and titrating to neutral (pH 6.8–7.2) with HCl to make up the stock solution. We use Sigma (St. Louis, MO) or Fisher Scientific (Itasca, IL) as suppliers. Store refrigerated.
4. Organic Salts: Potassium glutamate or potassium acetate. Optimizing the reactivation of a flagellum or cilium depends to some extent on the ionic strength of the mixture. Potassium salts give better results than sodium salts and organic anions are greatly superior to inorganic anions. Bull sperm will not reactivate satisfactorily with Mg-ATP in a potassium chloride solution. Glutamate eliminates this problem when used as the predominant anion (**11**). Subsequent studies have confirmed that organic anions generally give superior results (**12**), acetate being particularly effective. We have had the best results titrating L-glutamic acid (supplied from Sigma) to neutral (pH 6.8–7.2) with KOH. These salts in solution grow bacteria extremely well. Store refrigerated and inspect for cloudiness before each use.
5. Nucleotides: Adenosine-5'-triphosphate (ATP) and adenosine-5'-diphosphate (ADP). When used in reactivations, these should always be the highest purity available and certified vanadate free. We currently use Fisher's ATP and Roche's ADP. Stock solutions should be titrated to the final working pH and frozen (-20°C) in small ($<1\text{ mL}$) aliquots in sealed microfuge tubes. ATP and ADP are strong buffers and can significantly change the working pH of the final reactivation solution if not pre-titrated to the working pH. Also, if they are left at their initial acid pH they hydrolyze rapidly, decreasing their storage time. ADP is the more unstable of the two compounds in storage; it is best to make up a fresh stock solution every 6 mo. Adenosine 3', 5'-cyclic monophosphate (cAMP): Stock solution should be stored frozen (-20°C) in small aliquots ($<1\text{ mL}$) in sealed

microfuge tubes. We currently use Sigma, but have had equally good results with other suppliers.

6. Chelator: EGTA. It is best made up as a stock solution titrated to neutral (pH 6.8–7.2) or slightly above using KOH. It should be remade every two weeks or less and stored refrigerated. Sigma has been a good source.
7. Inorganic salts: MgSO_4 , CaCl_2 : Use the best grades available of analyzed reagents. Store stock solutions refrigerated.
8. Water: The higher the purity of your water supply, the more likely reactivations will work consistently. If your water supply is rated ultrapure (18 megohm) and stored in a sterilized polycarbonate carboy, no longer than a month, it will be satisfactory. If you do not have access to ultrapure water, it will be necessary to use a deionizing column to pre-treat all the water for your reagent stock solutions.
9. Glassware: Clean glassware is critical to achieving a satisfactory experimental result when working with demembrated cells. We use Liqui-Nox detergent (Fisher) for soaking and washing our glassware. We achieve the best results when multiple (at least 4) small volume rinses in regular tap water are followed by multiple rinses in deionized or ultrapure water.
10. Stock Solutions: 10M, 5M, and 1M KOH; 5M and 1M HCl are used for titrating pH. Be sure to start with a high purity analyzed reagent-grade of KOH, as it will be used in many of the solutions. These stock solutions are stored refrigerated:
 - 0.6M potassium glutamate
 - 0.3M sucrose
 - 0.1M MgSO_4
 - 0.1M CaCl_2 (optional)
 - 0.1M EGTA
 - 0.1M fructose
 - 10% Triton X-100 (w/v). One gram weighed into nine grams of water. Mix with a magnetic stir bar to dissolve. Triton X-100 is available pre-diluted to 10% in 10 mL ampules from Pierce. These stock solutions are stored frozen:
 - 0.1M DTT
 - 0.1M ATP – Titrate to pH 7.8
 - 0.1M ADP – Titrate to pH 7.8
 - 0.001M cAMP.
11. Glutamate-Tris reactivation medium (GRM): Mix 6.0 mL of potassium glutamate stock with 70 mL of sucrose stock and 0.36 g of Trizma base. Stir to dissolve and then adjust pH to 7.8 with HCl. Adjust final volume to 100 mL with distilled water. This GRM mixture is isotonic to mammalian sperm. Sperm suspended in it will stay alive. This feature is occasionally very useful, so the final dilution to optimal reactivation ionic strength is deferred to the time of use. GRM is an excellent growth medium for bacteria, it must be remade at least every two weeks, and checked for cloudiness before each use. Store refrigerated and keep on ice during experiments.
12. Sodium citrate buffer: Dissolve 2.85 g of sodium citrate in 50 mL of distilled water; add 2 mL of fructose stock solution and 5 mL of MgSO_4 stock solution

and 1 mL CaCl_2 stock solution (optional). Mix and adjust pH to 7.4, then adjust final volume to 100 mL with distilled water. If you plan to explore the role of Ca^{2+} in the flagellar/ciliary reactivation, it is best to leave CaCl_2 out of the citrate buffer.

13. Hanks Balanced Salt Solution (HBSS).
14. Bull semen, diluted in a milk-based extender (approximately 7.5×10^7 cells per mL), from Genex Cooperative Inc. (Tiffin, OH).

2.2. Preparation of the Biological Sample

The main concern in the introduction of the biological sample into the membrane-extraction medium is the inadvertent introduction of contaminants that will interfere with reactivation of motility. In the case of bull sperm, three low speed centrifugations followed by resuspension in a well-defined medium rather easily resolves this problem. For this, we have used sodium citrate (0.105M) with 5 mM MgSO_4 , 1 mM CaCl_2 (optional) and 2 mM fructose. This is a good choice for our purposes as the sperm, and most other cells, tolerate it for short exposures (up to 4 h at room temperature and longer on ice). The citrate chelates heavy metals and is an organic anion. This simple mixture avoids addition of compounds that will effect the reactivation of the sperm. Unfortunately, every system will have somewhat different requirements to sustain the living cells prior to demembration. As a general guide, simple is better as long as the viability of the sample is not compromised. In addition, organic anions are better suited to be the principal ionic component. When attempting to reactivate a sample for the first time, plastic petri dishes are a better choice than glass slides or vessels. Glass and glass cleaning methods will sometimes foul a reactivation. Once the method is working on plastic it can usually be duplicated on clean glass especially if the glass has been used for this purpose repetitively.

2.3. Oxidation and Proteolysis

Oxidation and proteolysis were recognized as the main destroyers of axonal function since the detergent-extracted models were first produced in the Gibbons lab (5). DTT and EGTA, commonly used in most reactivation methods, are the ingredients that protect against these spoilers. DTT competes with protein as a sink for oxygen free radicals. EGTA chelates contaminating divalent cations to a level that interferes with calcium-dependent proteases. It also inhibits the creation of free radicals via the Fenton reactions (which require Fe^{3+} or Cu^{2+} ions). In this way, EGTA (and also EDTA) can mask a multitude of sins. If the reactivation method is clean, and the reagents and water are pure, good reactivations can be produced without EGTA or EDTA. We are in the habit of routinely including 0.5 mM EGTA. Hypothetically, if oxidation and enzymatic degradation could be stopped completely, then reactivated motility

should continue indefinitely. In practice this is not true. The average reactivation looks good for 20 to 30 min.

3. Methods

The following protocol is used in our laboratory for reactivating bull sperm samples. It works as well for sea urchin sperm and was easily adapted for a widely used laboratory exercise to reactivate *Tetrahymena* cilia. With some modification, it will also reactivate *Chlamydomonas* flagella (These variations are discussed in **Subheading 3.2.**).

3.1. Basic Protocol (see Notes 1–3)

1. Pre-warm, to room temperature, 20 mL of the citrate solution described above. If you are not using bull sperm you may need to substitute a suspension medium that is better suited to the specific cells you are using. For instance, rat and mouse sperm do better in HBSS.
2. Gently mix the starting sample of cells suspended in their own storage or growth medium. If using bull sperm, combine 4 mL of the semen solution with 6 mL of the citrate buffer.
3. Centrifuge the cells at 960g for 10 min. Decant the supernatant after the spin and add citrate buffer (or your substitute) to bring the total volume up to 10 mL.
4. Allow the pellet 2 min to “melt” before actively mixing the sample. Repeat the centrifugation process two additional times, resuspending the final pellet in 4 mL of citrate buffer. The purpose of this step is to transfer the living sample into a defined medium. Adapt this step to your sample density. Protozoa and algae will tend to be more dilute to begin with and may require a larger volume to be processed on the first washing (see **Subheading 3.2.** below). Solid tissues (e.g., Clam gill cilia) can be simply transferred instead of centrifuged. If centrifugation is used, you may need to determine the best speed and time needed to form a loose pellet.
5. Pipet 2 mL of the GRM mixture into a 60 mm plastic petri dish. For bull sperm and other mammalian tissues, add 1 mL of high purity water to the mixture. For algae and fresh water protozoa, it may be necessary to increase the ratio of water to GRM for optimal results (try 1.5:1.5 or 2:1).
6. Add the following solutions to the GRM-water mixture: 30 μ L of 0.1M DTT from a thawed microfuge tube stored on ice, 30 μ L of 0.1M MgSO_4 , 15 μ L of 0.1M EGTA and 30 μ L of 10% Triton X-100. Swirl to mix (see **Note 3**).
7. Add 20 μ L of the biological sample to the dish containing the GRM mixture. Trial and error will determine if the amount needs to be raised or lowered. Gently swirl.
8. Observe the cells in the dish at low power (10 \leftrightarrow or 20 \leftrightarrow) using phase contrast optics. There should be no motility, and if the washing procedure is suitable there should be intact flagella or cilia (see **Note 1**).
9. Add 3 μ L of the thawed 0.1M ATP stock solution from a microfuge tube stored on ice.

10. Observe again for motility. If the procedure has been successful, some motility of the cells should be obvious (*see Note 2*).
11. If **step 9** did not produce a positive result add 10 μL of 0.001M cAMP and observe the sample again for a minimum of ten minutes. Some cilia and flagella are inactive without cAMP.
12. If **steps 9** and **11** do not produce motility, repeat **steps 5–11** in a second dish but include 15 μL of 0.1M ADP at **step 9** in addition to ATP. All flagella will reactivate more easily if ADP is present with ATP. When reactivation can only be obtained with ADP present, it may be an indication of a contaminant problem.

3.2. Optimization of the Protocol

Once the general method has worked for you, even if marginally, it can then be optimized for your system. Virtually all cilia and flagella will do something at low ATP, especially if some ADP is also present (*see Note 2*). After reactivation has been achieved with an experimental system, try the following for optimization:

1. Work up to higher ATP concentrations in 10 μL increments to find an optimum concentration.
2. Explore the response to cAMP by leaving it out or adding more in 3 μL increments.
3. Try different dilutions of the stock GRM media with water, keeping the total volume at 3 mL so that you do not have to change the rest of the protocol (i.e., try ratios of 1.5:1.5 mL and 2:1 mL).
4. Vary the washing procedure to ensure that damage to the cilia or flagella is minimized.
5. Lower the pH. You may find that a lower pH works better for the cells you are using and you may want to vary the buffer accordingly.

Using this systematic approach, it is possible to customize the working conditions to your own needs.

3.3. Variations for Specific Systems

The basic protocol in **Subheading 3.1.** will reactivate bull sperm, mouse sperm, human sperm, rat sperm, sea urchin sperm, freshwater clam gill cilia, *Tetrahymena*, and *Chlamydomonas*. However, each system does require some fine-tuning to get the best results.

1. For rodent sperm, use HBSS instead of citrate. In our experience rodent sperm give good progressive motility only if the live sperm exhibits progressive motility before it is used for producing the models.
2. Do not use **step 2** of the basic protocol (**Subheading 3.1.**) for ciliates and alga because starting samples of ciliates and alga are more dilute than sperm samples. Therefore, **step 2** in the basic protocol will not be satisfactory for those types of cells.

3. For ciliates, use a method that has been developed for *Tetrahymena* cilia reactivation. One method is readily accessible as part of the “Exercises in Cell Biology for the Undergraduate Laboratory” manual, which is available from the American Society for Cell Biology via their website (<http://www.ascb.org/ascb/>). In addition, ciliated protozoa typically yield a better reactivation at a lower optimal pH (7.0–7.4) (7,13) than the various sperm cells (5,11). At pH lower than 7.4, Tris is not the optimal buffer for the job; HEPES or PIPES is preferable.
4. For *Chlamydomonas*, (see **Note 4**) make the following substitutions in the basic protocol described in **Subheading 3.1.**:
 - a. Centrifuge 10 mL of *Chlamydomonas* in TAP culture medium (described in [17]) at 960g for 10 min to form a loose pellet. Decant the supernatant and resuspend the cells in the small amount of residual fluid that remains.
 - b. Pipet 1.5 mL of the GRM mixture into a 60 mm plastic petri dish. Add 1.5 mL of high purity water to the mixture.
 - c. Add the following solutions to the GRM-water mixture: 30 μ L of 0.1M DTT from a thawed microfuge tube stored on ice, 60 μ L of 0.1M $MgSO_4$, 30 μ L of 0.1M EGTA, 3 μ L of cAMP and 30 μ L of 1.0% Nonidet P-40. Swirl to mix.
 - d. Add 20 μ L of the biological sample to the dish containing the GRM mixture.
 - e. After adding the cells to the dish, rapidly draw the sample into and out of a Pasteur pipet repetitively 10 times. This mechanically aids in the disruption of the membrane at the very low (0.01%) detergent concentration.
 - f. Follow **steps 8–12** in the basic protocol described in **Subheading 3.1.**

3.4. Capabilities and Limitations

There are two important advantages to demembrated-reactivated models. The first is that the investigator has almost complete control of the composition of the solution pervading the axoneme. The second is that a reactivated flagellum can be positioned, poked, probed, enzymatically digested or cut without the complications of a membrane. These advantages give the investigator fantastic control of the experimental conditions both mechanically and chemically.

The limitations of the reactivated state are largely related to the stability of the reactivated models. The working time is limited for most samples to less than 30 minutes before there is substantial loss of function and loss of structural integrity.

3.5. Removal of the Cytosol

The method as described in **Subheading 3.1.** must be modified if the endogenous cytosolic factors and the detergent are to be eliminated from the final reaction mixture. Rat sperm can be successfully separated from their cytosolic fraction by a slight modification of the basic protocol described in **Subheading 3.1.** The method described below works well for rat sperm and may be adapted to other samples as well. We found less than 0.01% carry over of the

original mixture into the final reactivation dish, using a tritium labeled cAMP tracer (**18**).

1. Nick rat sperm epididymides with a razor blade and gently express the sperm onto a plastic culture dish. Immediately cover with a few drops of HBSS at room temperature. The sperm are left to disperse into the medium for 5 to 10 min and then are gently pipetted to mix. The sample is diluted to 2 mL total volume with HBSS solution.
2. Place 200 μ L of the sperm suspension into 3 mL of the demembration mixture with 0.1% Triton X-100 as described in **step 4** of the basic protocol above.
3. Layer half (1.5 mL) of the total volume of demembrated sperm on top of 3 mL undiluted GRM solution in a 16 \times 100 mm test tube with the same ingredients as in **step 4** of the basic protocol (1 mM MgSO_4 , 1 mM DTT, and 0.5 mM EGTA) but without the Triton X-100. A visible meniscus should be present between the two layers. Immediately chill on ice.
4. Centrifuge the layered mixture in a swinging bucket rotor at 160g in a cold room for 10 min. The centrifuge must be regulated to spin up slowly and to slow down without braking. If successful, two layers separated by a visible meniscus should still be present at the end of the run.
5. Decant and discard the supernatant from the top down to the visible loose pellet of cells.
6. Use the re-suspended pellet as the stock suspension for a new reactivation as in **step 4** of the basic protocol described in **Subheading 3.1**. However, omit the Triton X-100.

4. Notes

1. The general utility of membrane extracted models often depends on being able to manipulate them or immobilize them; which in turn often depends on making them adhere or keeping them from sticking to various objects and surfaces. Once the flagellum is demembrated the exposed microtubules carry a net negative charge. It is sometimes possible to make use of this property to either enhance or reduce sticking. The sperm preparations used in our lab will stick readily to coated culture dishes (Falcon 3802, Becton Dickinson, Lincoln Park, NJ) but stay more mobile on uncoated plastic petri dishes. Some investigators have had good success promoting sticking with poly-lysine coated surfaces, which imparts a positive coating and attracts negatively charge proteins. We have had good results in preventing non-specific adhesion of sperm to glass microprobes by dipping the probe in a 1N HCl solution and drying it just prior to use. This may work by imparting a negative surface charge to the glass.
2. The most problematic aspect of working with demembrated models arises from the very thing that makes them attractive; the investigator is in complete control of the conditions. Complete control comes with a lot of headaches. The larger the number of ingredients that must be prepared and certified "safe" for use in an experiment, the greater the possibility for an error. In the case of reactivating

motility to flagella and cilia, the biological specimen lets you know you've made a mistake by refusing to do anything. This can be humbling and also very frustrating. The following are the most common headaches:

- a. The biological starting material is defective. If your "live" preparation is dead, or has been seriously injured, it is unreasonable to expect good reactivations. As an example, cold shock is a problem with mammalian sperm; inadvertently chilling them from 23°C to 5°C will render them useless. Check on the condition of the live material at the step before detergent extraction (**step 2** of the basic protocol).
 - b. The water is not an ultra-pure grade. "Bad" water can literally make it impossible to do any work with reactivated models. Be sure to rinse all of the glassware with "good" water before preparing solutions.
 - c. If the water and the starting material are in good shape, the antioxidant components of the mixture (DTT or glutathione and EGTA) are very often the culprits of a failed reactivation. Don't let the EGTA stock solution get old and make sure it has been properly titrated to neutral (pH 6.8–7.2) with a high quality KOH. DTT is the most erratic ingredient of the mixture because it tends to oxidize. When a lot is giving stable reactivations, stay with that lot using the suggestions given in the materials section. The telltale sign that oxidation is your problem is when the sample shows some or even good initial motility and rapidly loses it by degenerating to a jittering vibration-like residual motion.
 - d. Contamination contributed by a specific ingredient. This was once a major problem back in the days when some sources of ATP were contaminated with vanadate. It is less of a problem now, if the highest grades of nucleotides and salts are used, but it can still happen. It is informative to look at the manufacturer's analysis of the reagents. You will quickly see that some things you really don't want in a reactivation dish (e.g., Ni²⁺, Cu²⁺, Fe³⁺ and Hg²⁺) are common contaminants. Also things you may think you didn't have, like Ca²⁺, may actually be present at physiologically active concentrations.
 - e. The pH of the final mixture is in error. When everything else seems to be right, it is often useful to check the pH of the completed mixture.
3. Detergent extraction of sperm releases the acrosomal contents, including acrosin, a Ca²⁺-dependent serine protease. Most detergent extractions of other cell types will similarly mobilize lysosomal enzymes. To see if this problem could be minimized we have used organic solvents instead of detergent to permeabilize the membranes of bull and rat sperm. Acetone and the lower molecular weights of polyethylene glycol (PEG 400) will permeabilize cells allowing reactivation with exogenous Mg-ATP. These solvents must be used at much higher concentrations than detergent (0.7 mL GRM to 0.3 mL acetone or 0.5 mL GRM to 0.5 mL PEG 400) but we have observed the resulting reactivated motility last up to 2 h, rather than the usual 30 min. To extract the cells, 200 µL of the sperm stock suspension in citrate buffer (as in **step 2** of the basic protocol) is added to 1 mL of the acetone or PEG 400- extraction mixture with 1 mM DTT present. The sperm are incu-

bated in the extraction mixture for 10 min in acetone or 4 min in PEG 400. After extracting for the required amount of time, the treated cells are used as the starting material for a reactivation, as in the basic protocol although no detergent is required. Transmission electron microscopy revealed that the acrosomal contents had not dispersed in the acetone or PEG treated samples (unpublished results). Such alternate methods of permeablizing the membrane have not been extensively utilized. It has been recently reported that a bacterial pore-forming toxin, Streptolysin O, can be used to yield partially permeablized sperm cells (19). This is a very exciting alternative to detergent, as it may allow size-selective retention of some of the natural internal milieu.

4. The green alga *Chlamydomonas* is the dominant model system for the study of flagellar motility. This is owing to the genetic tractability of *Chlamydomonas* and the well-kept depository of mutant strains that is maintained for this organism at the *Chlamydomonas* Genetics Center, Duke University, Durham, NC (<http://www.botany.duke.edu/chlamy/>). The irony is that the *Chlamydomonas* flagellum is hardly the ideal choice to typify a “standard” flagellum. *Chlamydomonas* re-grows its flagellum daily and drops them at the slightest affront. Therefore, they are kind of Nature’s entry into the disposable organelle market. *Chlamydomonas* also use their flagellum for mating and gliding motility necessitating a sophisticated membrane-associated transport system. These adaptations make the organism interesting for a number of kinds of research. The downside is that a disposable flagellum is more fragile than one built to last. *Chlamydomonas* flagella are difficult to work with because the demembration conditions destabilize the axoneme, which then tends to fall apart or lose function. However, because of the intense interest in *Chlamydomonas* there are already good published methods available to use as a template to find a method that is suitable for a given experimental circumstance (14,15). There is also a cell wall defective strain (cw92) that allows the flagellar apparatus to be isolated in functional condition after detergent extraction (16). Nonidet P-40 is less disruptive to the axoneme of *Chlamydomonas* than Triton X-100.

Acknowledgments

Thanks to Dr. Anne Hitt and Dr. Sheldon Gordon for comments and suggestions on the manuscript. Thanks to Danial Oberski for testing the adaptation of the method to *Chlamydomonas*. Supported by N.S.F. grant MCB-9722822.

References

1. Szent-Györgyi, A. (1949) Free-energy relations and contraction of actomyosin. *Biol. Bull.* **96**, 140–161.
2. Hoffman-Berling, H. (1955) Geiselmoleküle und Adenosintriphosphat. *Biochim. Biophys. Acta.* **16**, 146–154.
3. Bishop, D. W. and Hoffman-Berling, H. (1959) Extracted mammalian sperm models. I. Preparation and reactivation with adenosine triphosphate. *J. Cell Comp. Physiol.* **53**, 445–466.

4. Brokaw, C. J. and Benedict, B. (1968) Mechanochemical coupling in flagella. I. Movement dependent dephosphorylation of ATP by glycerinated spermatozoa. *Arch. Biochem. Biophys.* **125**, 770–778.
5. Gibbons, B. H. and Gibbons, I. R. (1972) Flagellar movement and adenosine triphosphate activity in sea urchin sperm extracted with Triton X-100. *J. Cell Biol.* **54**, 75–97.
6. Summers, K. E. and Gibbons, I. R. (1973) Effects of trypsin digestion on flagellar structures and their relationship to cell motility. *J. Cell Biol.* **58**, 618–628.
7. Sale, W. S. and Satir, P. (1977) Direction of active sliding of microtubules in *Tetrahymena* cilia. *Proc. Nat. Acad. Sci. USA* **74**, 2045–2049.
8. Lindemann, C. B. (1978) A cAMP induced increase in the motility of demembrated bull sperm models. *Cell* **13**, 9–18.
9. Brokaw, C. J. (1979) Calcium-induced asymmetrical beating of Triton-demembrated sea urchin sperm flagella. *J. Cell Biol.* **82**, 401–411.
10. Lindemann, C. B. and Kanous, K. S. (1995) “Geometric Clutch” Hypothesis of axonemal function: Key issues and testable predictions. *Cell Motil. Cytoskeleton* **31**, 1–8.
11. Lindemann, C. B. and Gibbons, I. R. (1975) Adenosine triphosphate-induced motility and sliding of filaments in mammalian sperm extracted with Triton X-100. *J. Cell Biol.* **65**, 147–162.
12. Gibbons, I. R., Evans, J. A., and Gibbons, B. H. (1982) Acetate anions stabilize the latency of dynein 1 ATPase and increase the velocity of tubule sliding in reactivated sperm flagella. *Cell Motil.* **1**(Suppl.) 181–184.
13. Hamasaki, T., Murtaugh, T. J., Satir, B. H., and Satir, P. (1989) In vitro phosphorylation of *Paramecium* axonemes and permeabilized cells. *Cell Motil. Cytoskeleton* **12**, 1–11.
14. Goodenough, U. W. (1983) Motile detergent-extracted cells of *Tetrahymena* and *Chlamydomonas*. *J. Cell Biol.* **96**, 1610–1621.
15. Horst, C. J. and Witman, G. B. (1995) Reactivation of *Chlamydomonas* cell models. *Methods Cell Biol.* **47**, 207–210.
16. Hyams, J. S. and Borisy, G. G. (1978) Isolated flagellar apparatus of *Chlamydomonas*: Characterization of forward swimming and alteration of waveform and reversal of motion by calcium ions *in vitro*. *J. Cell Science* **33**, 235–253.
17. Harris, E. H. (1989) The *Chlamydomonas* sourcebook: A comprehensive guide to biology and laboratory use. Academic Press, San Diego, CA.
18. Lindemann, C. B., Gardner, T. K., Westbrook, E., and Kanous, K. S. (1991) The calcium-induced curvature reversal of rat sperm is potentiated by cAMP and inhibited by anti-calmodulin. *Cell Motil. Cytoskeleton* **20**, 316–324.
19. Johnson, L. R., Moss, S. B., and Gerton, G. L. (1999) Maintenance of motility in mouse sperm permeabilized with Streptolysin O. *Biol. of Reprod.* **60**, 683–690.

VI

GENETIC APPROACHES FOR STUDIES OF CYTOSKELETON PROTEIN FUNCTION

A Yeast Two-Hybrid Approach for Probing Cytoskeletal Protein Interactions

Jin-jun Meng and Wallace Ip

1. Introduction

Interactions among proteins are fundamental to biological processes. In recent years, molecular biological tools have made it possible to study not only interactions among native proteins, but also among recombinant proteins and protein domains. Such studies often yield considerable insight into the mechanisms by which the biological processes take place. In this chapter, we describe our experience with the yeast two-hybrid system, an approach that has significantly enhanced our laboratory's efforts to analyze protein-protein interactions that underpin the assembly of cytoskeletal structures. It is not our intention to present an extensive review on the principles and practice of the yeast two-hybrid system. Outstanding reviews already exist, e.g., (1). An excellent chapter on the practical aspects of the method recently appeared in Volume 88 of *Methods in Molecular Biology* (2). We strongly encourage the reader to take advantage of this resource. This document provides an excellent primer to the genetics behind the two-hybrid system and detailed information on yeast strains, vectors and other reagents. It is particularly helpful for investigators whose goal is to identify unknown interacting partners of a protein of interest by screening a two-hybrid library. Many vendors of two-hybrid system reagents also provide extensive manuals, both in printed format and on-line at their World Wide Web sites. For example, Clontech, Inc. has separate manuals for all of the two-hybrid systems for which they market kits (<http://www.clontech.com/clontech/manuals/>).

The yeast two-hybrid system exploits the fact that many transcriptional activators consist of two separate and essential domains—the DNA binding (DB) domain and the transcription activating (TA) domain—that must be in

proximity to one another to function (3–6). To analyze protein-protein interactions with this system, the cDNAs of two proteins of interest are cloned into separate vectors such that one is expressed as a fusion protein with the DB domain, and the other is expressed as a fusion protein with the TA domain, of a well-characterized transcriptional activator. The two most commonly used transcriptional activators are GAL4 (7) and LexA (8). Both plasmids are then introduced into yeast host cells. Interaction between the two proteins of interest brings the DB and TA domains into proximity and reconstitutes the activity of the transcriptional activator, leading to expression of a reporter gene.

Perhaps the widest application of the two-hybrid system is the isolation of binding partners for a given protein. In this application, the protein of interest (called the “bait”) is fused to the DB domain of GAL4 or LexA, and a cDNA library is subcloned into the TA vector. Interaction between the bait and any polypeptide expressed from the cDNA library is then identified by expression of the reporter gene. In our studies of cytoskeletal assembly (9,10), and more recently in an effort to elucidate the mechanism of action of a tumor suppressor molecule, we have found that a slightly simpler version of the yeast two-hybrid system is a very effective tool for characterizing putative binary interactions between two proteins and/or domains. This approach consists of expressing single fusion proteins from both the DB and TA vectors and assessing their interaction using a quantitative reporter gene assay. With certain limitations, it is possible to compare relative strengths of interactions involving, for instance, a series of *in vitro* mutants of the same protein. It is this application of the yeast two-hybrid system that we wish to focus upon in this chapter.

A distinct advantage of the yeast two-hybrid system, compared to other methods such as co-immunoprecipitation and chemical cross-linking, is that one can determine whether an interaction is a direct one between two proteins, or one mediated by additional components. However, it is important to point out that the utility of yeast two-hybrid assays is not restricted to binary interactions. As we will illustrate at the end of the chapter, it also can be used effectively to assess the effect of a third protein on a known binary interaction.

2. Materials

2.1. Media, Reagents, and Buffers

1. YEPD broth and YEPD agar (Becton Dickinson).
2. Yeast nitrogen base, without amino acids (Difco).
3. Amino acids (Sigma).
4. D(+) galactose (Sigma).
5. D-glucose (dextrose, Sigma or Fisher).

6. X-gal stock solution: 20 mg/mL 5-bromo-4-chloro-3-indolyl- β -D-galactopyranoside (GIBCO-BRL) dissolved in N,N-dimethylformamide. Store at -20°C in the dark.
7. ONPG test solution: 4 mg/mL o-nitrophenyl β -D-galactopyranoside (ONPG) (Sigma) in 0.1M potassium phosphate, pH 7.0.
8. 4-methylumbelliferyl-galactopyranoside (4-MUG) (Fluka, Sweden).
9. 50% polyethylene glycol, mol/wt 1500 (PEG1500), 4 mL/vial, sterile, fusion tested (Boehringer Mannheim, Germany). Add 1 mL LiOAc solution before using. Stable for 2 wk at 4°C .
10. Glass beads, acid-washed, 425–600 microns (Sigma).
11. Lithium acetate (LiOAc) (Sigma).
12. Dimethyl sulfoxide (DMSO) (Fisher).
13. LiOAc solution: 0.1M lithium acetate, 10 mM Tris-HCl, pH 7.5, 1 mM EDTA, 0.2 μm - filter sterilized.
14. LiOAc-glycerol solution: 15% glycerol in LiOAc solution, 0.2 μm -filter sterilized.
15. Z buffer: 0.1M phosphate buffer, pH 7.0, 10 mM KCl, 1 mM MgCl_2 , 50 mM β -mercaptoethanol.
16. Yeast lysis buffer: 20 mM Tris-HCl, pH 7.5, 50 mM KCl, 5 mM MgCl_2 , 0.1 mM EDTA, 0.5 mM dithiothreitol (DTT), 10 % (v/v) glycerol, 1 mM phenylmethylsulfonyl fluoride (PMSF), 2 μM pepstatin A, and 0.6 μM leupeptin.

2.2. General Use Media Formulations

1. YEPD medium for liquid culture (per 500 mL): 5.0 g yeast extract, 10 g peptone, 300 mL deionized distilled H_2O ; autoclave at 110°C for 20 min; cool to 55°C ; add 50 mL of 20% glucose; add H_2O to a final volume of 500 mL.
2. YEPD medium for plates (per 500 mL): same as for liquid YEPD medium except add 7.5 g of granulated agar before autoclaving.

2.3. Media Formulations for Yeast Selection

MinGal and MinGlu are media for yeast selection (*II*). Both media contain nitrogen base, a carbon source (galactose or glucose, respectively) and an amino acid drop-out mix containing all amino acids essential for growth except the ones used for selection (**Table 1**).

1. MinGal medium for liquid culture (per 500 mL): 3.5 g yeast nitrogen base without amino acids, 15 mL glycerol, 300 mL deionized distilled H_2O , autoclave at 110°C for 20 min; cool to 55°C ; add 50 mL amino acid drop-out mix solution; add 50 mL of 20% galactose; add H_2O to a final volume of 500 mL.
2. MinGal medium for plates (per 500 mL): 3.5 g yeast nitrogen base without amino acids, 7.5 g granulated agar, 15 mL glycerol, 300 mL deionized distilled H_2O , autoclave at 110°C for 20 min; cool to 55°C ; add 50 mL amino acid drop-out mix solution; add 50 mL 20% galactose; add 2.5 mL 20% glucose; add H_2O to a final volume of 500 mL.

Table 1
Stock Solutions for Amino Acid Drop-Out Mix

Amino acid	Stock solution (g/100 mL)	mL stock solution per liter medium
Adenine sulfate	0.4	5
L-glutamic acid	1.0	20
L-arginine	1.0	2
L-aspartic acid	1.0	20
L-histidine	1.0	2
L-leucine	1.0	3
L-isoleucine	1.0	3
L-lysine HCl	1.0	3
L-methionine	1.0	2
L-phenylalanine	1.0	5
L-serine	8.0	4
L-threonine	4.0	4
L-tryptophan	1.0	2
L-tyrosine	0.2	15
Uracil	0.2	10
L-valine	3.0	5

To make a drop-out mix solution, combine the appropriate volumes of all amino acid stock solutions except the one or more to be selected for. Substitute an equivalent volume of water to achieve the final volume.

3. MinGlu medium for broth (per 500 mL): 3.5 g yeast nitrogen base without amino acids, 15 mL glycerol, 300 mL deionized distilled H₂O, autoclave at 110°C for 20 min; cool to 55°C; add 50 mL amino acid drop-out mix solution, add 50 mL 20% glucose; add H₂O to a final volume of 500 mL.
4. MinGlu medium for plates (per 500 mL): same as for liquid MinGlu medium except add 7.5 g of granulated agar before autoclaving.

2.4. Yeast Strains

Yeast strains we use routinely in two-hybrid studies are listed in **Table 2**. It is generally advisable to use yeast strains recommended by the vendor from whom the vectors are obtained. We recommend that the reader consult the concise and thoughtful discussion on yeast vectors and strains by Bolger (2).

2.5. Plasmid Vectors

The two-hybrid vectors we use are listed in **Table 3**. Most of our work has been done using vectors kindly supplied by Drs. Pierre Chevray and Daniel Nathans at the Johns Hopkins University. Several commercial vendors of two-hybrid systems and their websites are: Clontech (www.clontech.com),

Table 2
Yeast (*S. cerevisiae*) Strains Commonly Used in the Two-Hybrid System

Name	Genotype
PCY2	<i>MATα Δgal4 Dgal80 URA3::GAL1-LacZ lys2-801^{amber} his3-Δ200 trp1-Δ63 leu2 ade2-101^{ochre}</i>
YRG2	<i>MATα ura3-52 his3-200 ade2-101 lys2-801 trp1-901 leu2-3 112 gal4-542 gal80-538 LYS2::GAL1_{UAS}GAL1-TATA^{HIS3} URA3::GAL4_{17mers(3x)}-CYC1_{TATA}-LacZ</i>
HF7c	<i>MATα ura3-52 his3-200 lys2-801 ade2-101 trp1-901 leu2-3 112 gal4-542 gal80-538 LYS2::GAL1_{UAS}GAL1-TATA^{HIS3} URA3::GAL4_{17mers(3x)}-CYC1_{TATA}-LacZ</i>
SFY526	<i>MATα ura3-52 his3-200 ade2-101 lys2-801 trp1-901 leu2-3 112 can^r gal4-542 gal80-538 URA3::GAL1-lacZ</i>

Table 3
Common Yeast Two-Hybrid Vectors

Name	Protein encoded	Source
pPC62	GAL4 DNA-binding (DB) domain	Nathans laboratory (ref. 17)
pPC86	GAL4 transcriptional activation (TA) domain	Life Technologies
pGAD	GAL4 DNA-binding (DB) domain	Stratagene
pAD	GAL4 transcriptional activation (TA) domain	Stratagene
PGBT9	GAL4 DNA-binding (DB) domain	Clontech
PGAD424	GAL4 transcriptional activation (TA) domain	Clontech
pSos	Human Sos gene product	Stratagene
pMyr	Src myristylation signal	Stratagene

Invitrogen (www.invitrogen.com), Life Technologies (www.lifetech.com), Promega (www.promega.com), and Stratagene (www.stratagene.com).

3. Methods

3.1. Construction of Yeast Two-Hybrid Vectors

Standard methods are used to clone cDNAs of interest into two-hybrid vectors. We routinely sequence our constructs to ensure that the cDNA insert is in-frame with the DB or TA domain such that a fusion protein is expressed. It is important to use caution when mixing plasmids from different two-hybrid systems. While many combinations of DB and TA domains will activate transcription (2), one must ensure that the two desired plasmids encode different selection markers.

3.2. Preparation of Competent Yeast Cells

1. From a freshly spread yeast (*Saccharomyces cerevisiae* strain) plate, pick out a single colony to inoculate 25 mL of YEPD medium and culture at 28°C overnight in a shaking incubator at 200 rpm until the cells reach mid-log phase ($A_{600} = 0.8\text{--}1.0$, or $0.5\text{--}1.0 \times 10^7$ cells/mL). (Also see **Note 1**).
2. Pellet the cells at low speed—typically 3500g in a bench-top centrifuge—for 2 min. Discard the supernatant.
3. Resuspend the pellet in 10 mL LiOAc solution and spin down the cells again. Repeat two more times.
4. Add 2 mL LiOAc-glycerol solution to the final pellet and gently shake by hand to resuspend the cells.
5. Aliquot the competent cells into 1.5-mL Eppendorf microcentrifuge tubes (50 μ L/tube). The competent cells can be either used immediately for transformation or stored frozen at -70°C or lower for future use. It is important to freeze competent cells slowly. A convenient way to do this is to wrap the microcentrifuge tubes containing cells in 8–10 layers of paper towel before placing in the freezer.

3.3. Yeast Co-Transformation and Culture

Either freshly prepared or previously frozen competent cells (thawed at room temperature) can be used in the following procedure (**12,13**):

1. Add 1–2 μ L of each vector (0.1–0.5 $\mu\text{g}/\mu\text{L}$ DNA) to 50 μ L of competent cells with gently mixing and incubate at room temperature for 5 min. (see **Note 2**).
2. Add 140 μ L PEG1500 solution and mix the content thoroughly by inverting the tube 4–5 times.
3. Place the cells in a 30°C incubator for 45 min or longer, then mix the contents by flicking with finger and heat shock the cells in a water bath at 42°C for 5 min.
4. Pellet the cells in a bench-top centrifuge at 3500g for 30 s. Wash the cells twice with 1 mL sterile distilled water, using a pipette to resuspend the cells. Discard the supernatant.
5. Resuspend the cells in 100 μ L of sterile distilled water. Spread the transformed cells onto a plate containing selective medium (**Subheading 2.3**). Invert the plate and incubate at 28°C for 34 d to allow growth of transformants.
6. When the yeast colonies reach 1–2 mm in diameter, use a single colony to inoculate 2 mL of MinGal medium supplemented with the appropriate amino acid drop-out mix. Incubate at 28–30°C with shaking for 48–72 h. This culture can now be used to assay for β -galactosidase activity.

3.4. β -Galactosidase Assays

The most common reporter gene used in two-hybrid studies is probably β -galactosidase. There are many available assays for β -galactosidase activity; the ones described below are used routinely in our laboratory and each has its own advantages and disadvantages. (see **Note 3**).

3.4.1. X-Gal Assay

This is a rapid, but qualitative assay for β -galactosidase (**14**). Two disadvantages of this method are that it is not possible to obtain numerical data and that when the blue coloration is faint the decision as to whether a yeast colony is positive often becomes subjective.

1. Grow transformed yeast on MinGal plates supplement with the appropriate amino acid drop-out mix at 28°C for 2 to 3 d. When colonies reach 1–2 mm in diameter, carefully lay an autoclaved nitrocellulose membrane on top of the plate as the membrane wets. Leave the membrane on the plate in a 30°C incubator for 30 min.
2. Using blunt forceps, carefully peel the membrane away from the agar surface. Immerse the membrane, colony side up, in an ice bucket containing liquid nitrogen for 5 s to permeabilize the cells.
3. Thaw the nitrocellulose membrane at room temperature and place onto a disk of Whatman 3MM filter paper soaked with 2 mL of Z buffer containing 1 mg/mL of X-gal in a 100-mm Petri dish. Cover the dish and incubate at 37°C for 10–60 min to develop the blue color.

3.4.2. ONPG Assay

This colorimetric method is quantitative and uses o-nitrophenyl β -D-galactopyranoside (ONPG) as substrate (**11**). Enzymatic cleavage of the substrate releases a bright yellow reaction product that can be read at 420 nm in a standard spectrophotometer.

1. Assays should be carried out in triplicate.
2. Use a single colony of yeast transformants grown on a MinGal plate supplement with the appropriate amino acid drop-out mix to inoculate 2 mL of liquid medium. Incubate at 28°C with shaking for 2 to 3 d until the cells reach mid-log phase ($A_{600} = 0.8$ – 1.0).
3. Pipet 0.1 mL of yeast culture in a 1.5-mL microcentrifuge tube. Add 0.8 mL of Z buffer, 0.1 mL chloroform and 50 μ L of 0.1% SDS, and vortex for 30 s.
4. Add 0.15 mL of ONPG test solution and vortex well.
5. Incubate at 30°C for 60 min or until the yellow color is developed. Add 0.3 mL of 1M Na_2CO_3 to stop the reaction.
6. Centrifuge at 14,000g in a microcentrifuge to clear cell debris.
7. Carefully remove the supernatant to a fresh tube. Read the absorbance at 420 nm.
8. Calculate the β -galactosidase activity using the following equation:

$$\text{activity (units/min}\cdot\text{mL)} = \left(\frac{A_{420}}{tVA_{600}} \right) \times 1000$$

where A_{420} = absorbance at 420 nm

A_{600} = absorbance of yeast culture at 600 nm

t = time in min

V = volume of yeast culture in milliliters (mL)

3.4.3. Fluorescence Assay

This assay uses the fluorescent substrate, 4-methylumbelliferyl β -D-galactopyranoside (4-MUG) (**9**). Enzymatic cleavage produces a reaction product that emits at 450 nm when excited at 360 nm. In our experience this is the most sensitive method of detecting β -galactosidase activity and thus lends itself most readily to discriminating between weak interactions and non-interactions in two-hybrid transformations. (See **Note 3**).

1. Perform all assays in triplicate.
2. Use a single colony of yeast transformants grown on a MinGal plate supplement with the appropriate amino acid drop-out mix to inoculate 2 mL of liquid medium. Incubate at 28°C with shaking for 2 to 3 d until the cells reach mid-log phase ($A_{600} = 0.8$ – 1.0).
3. Shake the yeast culture well and pipet 0.1 mL into a 1.5-mL microcentrifuge tube. Pellet the cells at 14,000g for 30 s. Carefully remove and discard the supernatant.
4. Permeabilize the yeast cells by freezing in liquid nitrogen for 2 min, then thawing at room temperature, or by placing them in a -20°C or -70°C freezer for several hours, then adding 3/4 volume of acid-washed glass beads (425–600 microns) and vortex rigorously.
5. Add 350 μL of 4-MUG reaction buffer (10 mM phosphate, pH 7.5, 1 mM MgCl_2 , 0.1% [w/v] bovine serum and 0.1% NaN_3) and 50 μL of 1 mM 4-MUG in 10 mM phosphate buffer, pH 7.0, 1 mM MgCl_2 . Vortex and incubate at 37°C for 60 min. (See **Note 4**).
6. Add 400 μL of 4-MUG stop solution (0.1M glycine, pH 10.3) to terminate the reaction. Centrifuge the reaction tube at top speed in a microcentrifuge for 1 min and carefully remove the supernatant to a fresh tube for fluorescence reading.
7. In a fluorescence spectrophotometer set for excitation at 360 nm, record the emission of each sample at 450 nm. (See **Note 5**).
8. Calculate the β -galactosidase activity using the following equation:

$$\text{activity (units/mL)} = 1.62 \left(\frac{FM}{VA_{600}} \right)$$

where F = fluorescence emission at 450 nm, in arbitrary units
 M = no. of times the sample was diluted before reading
 V = the volume (in mL) of yeast sample used in assay
 A_{600} = absorbance of the yeast culture at 600 nm
 1.62 = relative coefficient

3.5. Controls

It is of great importance to include all necessary controls in two-hybrid assays. At a minimum, these should include the following:

1. A positive control. Commercially available two-hybrid kits often include control plasmids that encode a pair of proteins known to interact with one another. Posi-

tive reporter gene activity resulting from this transformation will serve to ensure that all the reagents are in working order.

2. Transformation with the cDNA insert omitted from one of the two-hybrid plasmids. No reporter gene activity should be detectable. If a significant signal is detected in a transformation with one insert-containing and one blank vector, the cDNA insert likely encodes a polypeptide that activates transcription, or is non-specifically sticky. In this case, trying a different set of two-hybrid vectors may be the most expedient solution. A more laborious but more systematic solution is to replace the full-length protein with increasingly truncated versions, in the hope that the truncation eventually removes the offending region of the protein. (*See Note 6*).
3. Transformation with the cDNA inserted into the other two-hybrid vector. Swapping cDNA inserts and vectors should not alter the reporter gene activity significantly. We have found that, in general, a 10–15% variation is tolerable. In cases where the variation exceeds this practical limit, the result may still be valid, but caution should be exercised and confirmation by other methods should be sought.
4. An effective way of confirming a positive interaction is to ascertain that the two fusion proteins do indeed bind one another. This can be accomplished by chemical cross-linking of a protein extract from transformed yeast and demonstrating by western blotting that a complex of the proper molecular size (the sum of the two proteins plus the DB and TA domains) does exist (*see Subheading 3.6*). Co-immunoprecipitation is another way of confirming a protein-protein interaction. If available, antibodies to the proteins of interest should be used. If not, antibodies to the DB and TA domains of GAL4, LexA and others are available commercially and may be used.

3.6. Isolating Proteins from Yeast Cells

Often it is useful to isolate the expressed fusion proteins from transformed yeast cells for further biochemical studies. For example, the complex formed by the two interacting proteins may be further characterized by chemical cross-linking followed by western blot analysis (*9*), or even further purified by chromatographic procedures. At the very least, having the isolated proteins allows one to confirm by western blotting that the fusion proteins are properly expressed. A simple method for isolating proteins from yeast is described below (*9*).

1. Use a single colony of yeast transformants grown on a minimal medium plate to inoculate 2 mL of liquid MinGal medium supplement with the appropriate amino acid drop-out mix. Incubate at 28°C with shaking for 2 to 3 d until the cells reach mid-log phase ($A_{600} = 0.8\text{--}1.0$).
2. Inoculate 50 mL of liquid medium with 1 mL of the above small culture. Culture the yeast cells at 28°C to stationary phase ($A_{600} = 1.2$ to 1.5.) For optimal aeration, we usually culture no more than 50 mL of yeast in a 250 mL flask.
3. Transfer the yeast culture to a 50 mL conical centrifuge tube and chill it on ice for 10 min. Pellet the yeast at 4°C at 3500g for 5 min. Remove the supernatant, wash

the cell pellet with ice-cold water, repeat, and finally resuspend the cell pellet in 1 mL pre-chilled yeast lysis buffer.

4. Transfer 0.5 mL of this cell suspension to a 1.5-mL Eppendorf microcentrifuge tube and freeze in liquid nitrogen for 3 min. Allow the cells to thaw on ice for 20 min. Add 3/4 volume of acid-washed glass beads (425–600 microns) and lyse the cells with eight 30-s bursts of a vortex mixer interspersed with equal periods of cooling on ice.
5. Centrifuge briefly to separate the cell lysate from the glass beads. Rinse the glass beads twice with 0.2 mL lysis buffer and combine all the recovered supernatants.
6. At this point, the yeast cell lysate can be saved for a number of different purposes, such as SDS-PAGE analysis with or without chemical cross-linking, or further purification.

3.7. Using the Two-Hybrid System to Probe Mechanisms

In some circumstances the two-hybrid system may be used to explore interactions involving more than two proteins. Specifically, it is often possible to ask if a binary interaction is modulated positively or negatively by the presence of a third protein, by using a “three-hybrid” strategy. An example of positive modulation is illustrated in a study of the interaction between intermediate filaments and desmosomes, intercellular adhesive junctions between epithelial cells (10). The proteins of epithelial intermediate filaments, keratins K8 and K18, are obligate partners in filament formation, and we wished to know how they bind to desmoplakin I (DPI), the major intracellular constituent of desmosomes. The key aspect of this strategy was the fusion of K8 and K18 to the TA domain and the fusion of DPI to the DB domain of GAL4. This ensured that the known binding between K8 and K18 would not activate transcription but any interaction between K8/K18 dimers and DPI would. Western blot analysis ensured that all proteins were expressed appropriately. We showed that standard two-hybrid transformations of either K18-TA or K8-TA fusion constructs with DPI-DB produced no reporter gene activity, whereas co-transformation with all three fusion constructs activated transcription of β -galactosidase. Thus, the simultaneous presence of K8 and K18 is necessary for binding of intermediate filaments to desmosomes in epithelial cells.

Recently we used a similar strategy to demonstrate the negative regulation of a two-protein interaction. We showed that the presence of one major isoform (isoform I) of merlin, the neurofibromatosis type II gene product, inhibited the interaction of the other major isoform (isoform II) with ezrin, an ERM protein, by more than 90% (Meng et al., submitted). The two isoforms of merlin dimerize, and both isoforms interact with ezrin independently, but in a three-hybrid transformation, one binary interaction—the heterodimerization of merlin isoforms I and II—predominates. As in the previous example, the key to the success of this experiment lies in the design of the fusion constructs and, in this

case, the use of distinct selection markers for each of the three plasmids to ensure all three fusion proteins are properly expressed.

3.8. Conclusion

Although our experience with the yeast two-hybrid system primarily involves cytoskeletal proteins, we have attempted to present this chapter in a general way so that investigators interested in binary interactions between other protein pairs may also find it useful. In most of our studies we have found yeast two-hybrid assays to be straightforward, effective and efficient. In cases of non-specific transcriptional activation, alternative strategies and/or vectors have been readily available and easily implemented. Modifications of the system may sometimes be used to study the regulation of a binary interaction by a third component. Though not without limitations, the yeast two-hybrid system has become an indispensable tool for those interested in interactions among proteins.

4. Notes

1. In making fresh competent cells or in regenerating strains, yeast cultures may be allowed to grow in YEPD medium overnight at 28–30°C with shaking at 220 rpm. The cultures reach an A_{600} of 0.8–1.0 under these conditions. Cultures grown in liquid MinGal medium need at least 48–72 h to reach to an A_{600} of 0.8–1.0. Growth on MinGal plates is even slower. The addition of 0.1% (w/v) glucose promotes cell growth but does not significantly repress expression of GAL4 fusion proteins. Alternatively, one could first grow transformants on MinGlu plates, then pick single colonies to inoculate liquid MinGal medium.
2. Transforming 50–100 μ L of competent yeast cells with 1–3 μ g of each DNA usually results in 30–100 well-separated colonies on a MinGal plate. For most studies we use strain PCY2, but with rare exceptions all of the strains listed in **Table 2** work equally well.
3. The X-gal (replica plating) assay for β -galactosidase activity is at best semi-quantitative and, as discussed above, involves an element of subjectivity. The ONPG colorimetric assay is quantitative with a detection limit of ~ 1 ng or 1×10^9 molecules. The fluorometric assay using 4-MUG as substrate is more sensitive, with a detection limit of 1 fg or 1×10^6 molecules. Although results from X-gal assays do not always correspond strictly with results from the fluorescence assay, we have found that for the vast majority of the time the following correlations are valid:

Coloration in X-gal assay	Fluorescence (arbitrary units)
white	< 500
very light blue	500
light blue	1000–3000
blue	3000–7000
dark blue	> 7000

How useful is the two-hybrid system for comparing strengths of protein-protein interactions? Estojak et al. (**15**) assayed interactions of known rate constants with the yeast two-hybrid system and compared the linearity of response of several reporters. They concluded that the strength of interaction as judged by quantitative reporter gene assays generally correlates with that determined *in vitro*, so that comparing relative strengths is acceptable. However, there was no single reporter for which the amount of gene expression linearly reflected affinity measured *in vitro*, so that absolute values of interaction strength are not very meaningful.

Our own experience echoes these conclusions. We have found that we can quite accurately compare relative strength of interaction between, say, protein X and a series of deletion mutants of protein Y, but extending the comparison to the interaction between protein X and a third, unrelated protein, Z, is not always meaningful.

4. 4-MUG substrate should be made fresh. It dissolves very slowly and we usually place the solution in a light-proof container and allow it to stir overnight, or at least 3–4 h before using.
5. Fluorescence is readily detectable after 5 min of incubation with 4-MUG and increases steadily with time. After termination of the reaction by adding stop solution, the fluorescence remains stable for at least 4 h. The total change in fluorescence after 16 h of storage is less than 10%.
6. Potential pitfalls and some suggestions for remedies:

The GAL4 two-hybrid system does have several limitations. First, since it relies on transcriptional activation by GAL4, it cannot be used if one of the proteins of interest is itself an activator of transcription. (This limitation also applies to the LexA system). A solution to this problem is to use a two-hybrid system that does not rely on transcriptional activation. One such system, called the Cytotrap, was introduced recently by Stratagene (www.stratagene.com/vectors/signal_trans/cytotrap.htm). In this system, one vector fuses a myristylation signal to the expressed protein so that it is targeted to the inner surface of the plasma membrane. The other vector encodes a fusion protein consisting of the other protein of interest and Sos, a GDP-GTP exchange factor. Interaction between the proteins of interest brings Sos to the membrane where it activates the Ras pathway and promotes cell growth (**16**). The yeast host is a strain that carries a temperature-sensitive mutation at the *cdc25* (the yeast homologue of Sos) locus; it grows at 25°C but not 37°C. Rescue of the Ras pathway by Sos restores its ability to grow at 37°C and serves as a qualitative readout for protein-protein interaction.

Another commonly encountered limitation of transcription-based two-hybrid systems is that the protein-protein interaction occurs in the nucleus. This presents a problem for protein-protein interactions that only occur after post-translational modification, e.g., phosphorylation. Using a two-hybrid system such as the Cytotrap, in which the interaction occurs in the cytoplasm, increases the probability, but does not assure, that the protein modification will occur, since the modifying mechanism (kinases, and the like) may or may not be present or active

in yeast. In these cases, corroboration from another method is the only prudent alternative. Finally, the question is sometimes raised as to whether the nuclear milieu can be taken as equivalent to a cytoplasmic environment for protein interactions. The Cytotrap provides a means to explore this question. We have compared the GAL4 system with the Cytotrap using dimerization of the ezrin-radixin-moesin (ERM) family of cytoskeleton-membrane linker proteins as a model system, and have found the two systems to corroborate one another closely.

Acknowledgments

Development of the two-hybrid assays, and some studies cited herein, were supported in part by grants from the National Institutes of Health (R01-AR35973 and -CA78524) and the Ruth Lyons Cancer Research Fund. We gratefully acknowledge these agencies for their generosity.

References

1. Fields, S. and Sternglanz, R. (1994) The two-hybrid system: an assay for protein-protein interactions. *Trends Genet.* **10**, 286–292.
2. Bolger, G. B. (1998) Molecular genetic approaches I: Two-hybrid systems. In: *Methods in Molecular Biology* Vol. 88 (Clegg, R.A., ed.), Humana Press, Totowa, NJ, pp. 101–131.
3. Keegan, L., Gill, G., and Ptashne, M. (1986) Separation of DNA-binding from the transcription-activating function of a eukaryotic regulatory protein. *Science* **231**, 699–704.
4. Hope, I. A. and Struhl, K. (1986) Functional dissection of a eukaryotic transcriptional activator protein, GCN4 of yeast. *Cell* **46**, 885–894.
5. Ma, J. and Ptashne, M. (1987) Deletion analysis of GAL4 defines two transcriptional activating segments. *Cell* **48**, 847–853.
6. Ma, J. and Ptashne, M. (1987) A new class of yeast transcriptional activators. *Cell* **51**, 113–119.
7. Fields, S. and Song, O. (1989) A novel genetic system to detect protein-protein interactions. *Nature* **340**, 245–246.
8. Zervos, A. S., Gyuris, J., and Brent, R. (1993) MxiI, a protein that specifically interacts with Max to bind Myc-Max recognition sites. *Cell* **72**, 223–232.
9. Meng, J.-J., Khan, S. A., and Ip, W. (1996) Intermediate filament protein domain interactions as revealed by two-hybrid screens. *J. Biol. Chem.* **271**, 1599–1604.
10. Meng, J.-J., Bornslaeger, E. A., Green, K. J., Steinert, P. M., and Ip, W. (1997) Two-hybrid analysis reveals fundamental differences in direct interactions between desmoplakin and cell type-specific intermediate filaments. *J. Biol. Chem.* **272**, 21,495–21,503.
11. Yocum, R. R., Hansley, S., West, R., and Ptashne, M. (1984) Use of LacZ fusions to delimit regulatory domains of the inducible divergent GAL1-GAL10 promoter in *Saccharomyces cerevisiae*. *Mol. Cell Biol.* **4**, 1985–1998.
12. Hill, J., Donald, K. A., and Griffiths, D. E. (1991) DMSO-enhanced whole cell yeast transformation. *Nucleic Acids Res.* **19**, 5791.

13. Gietz, R. D. and Schiestl, R. H. (1991) Applications of high efficiency lithium acetate transformation of intact yeast cells using single-stranded nucleic acids as carrier. *Yeast* **7**, 253–263.
14. Breeden, L. and Nasmyth, K. (1985) Regulation of the yeast HO gene. *Cold Spring Harbor Symposium on Quantitative Biology* **50**, 643–650.
15. Estojak, J., Brent, R., and Golemis, E. A. (1995) Correlation of two-hybrid affinity data with in vitro measurements. *Mol. Cell Biol.* **15**, 5820–5829.
16. Aronheim, A., Engelberg, D., Li, N., Al-Alawi, N., Schlessinger, J., and Karin, M. (1994) Membrane targeting of the nucleotide exchange factor Sos is sufficient for activating the Ras signaling pathway. *Cell* **78**, 949–961.
17. Chevray, P. M. and Nathans, D. (1992) Protein interaction cloning in yeast: identification of mammalian proteins that react with the leucine zipper of Jun. *Proc. Natl. Acad. Sci. USA* **89**, 5789–5793.

Manipulating Dynein Genes in *Tetrahymena*

David J. Asai, K. Mark DeWall, Leslie M. Lincoln,
and Renotta K. Smith

1. Introduction

In this chapter, we outline methods to modify targeted genes in *Tetrahymena*. Such a strategy could be utilized to deduce the function of individual dynein isoforms, as well as to dissect the functional domains within a single heavy chain.

How does one define the tasks performed by an individual dynein isoform in the complex milieu of the cell? Several strategies have been utilized. Antibodies can locate a dynein isoform and perturb function by introducing the antibody into a living cell or into a reconstituted cellular extract (1). This method requires that the antibody render the dynein inactive, and depends on the absolute specificity of the antibody. A second strategy is to over-express a dynein subunit or a fragment of dynein, thus generating a dominant phenotype (2–4). A drawback of this method is that the over-expressed protein may no longer be regulated in terms of its cellular location and may alter the biology of the cell by accumulating where it does not normally belong. A third strategy is to disrupt the dynein gene and to determine the consequences of the disruption on the biology of the cell. Random insertional mutagenesis of axonemal genes in *Chlamydomonas* has proved to be a powerful way to assign function and location to gene products (5–7). This method depends on the detection of a phenotype in order to identify the mutants.

The disruption of a targeted dynein gene by homologous gene replacement is a powerful strategy by which to dissect dynein isoform functions (8–10). In contrast to random insertional mutagenesis, targeted disruption need not produce a phenotype; the lack of a phenotype, in itself, can be informative. Targeted gene replacement can be achieved in several organisms, including budding yeast,

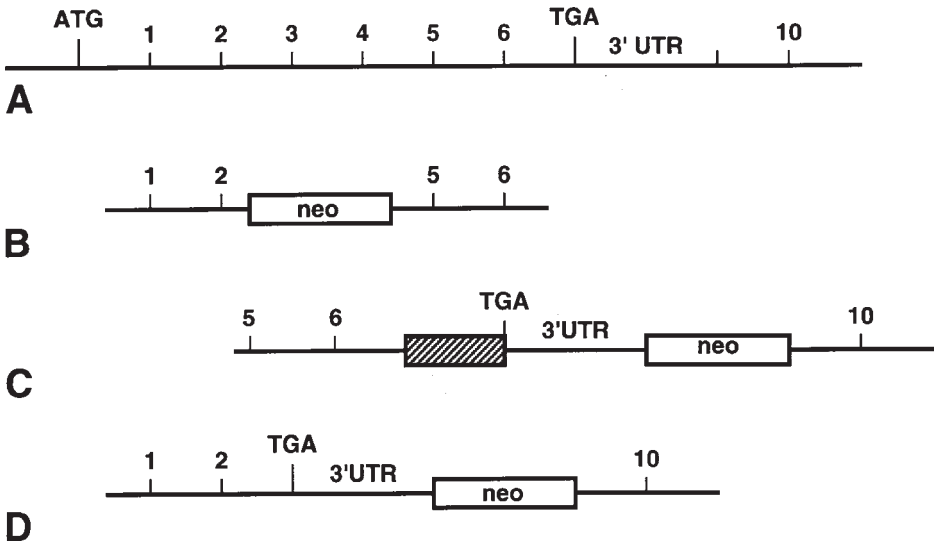


Fig. 1. Modifying genes by homologous replacement. Three different constructs (B,C,D) that will recombine with the targeted gene (A) are shown.

A: A diagram of the portion of the *Tetrahymena* chromosome encoding the wildtype version of the targeted gene. The initiation and termination codons, ATG and TGA, respectively, are shown. The 3' untranslated region (3'UTR) is indicated. The DNA is marked with evenly-spaced numbers to orient the various constructs shown in the figure.

B: Disruption construct. A portion of the coding region of the targeted gene has been replaced with the neomycin-resistance gene.

C: Tagging construct. A tag (shaded box)—e.g., epitope or GFP—has been added in-frame to the 3' end of the coding region of the targeted gene, immediately before the termination codon. Selection is with neomycin-resistance.

D: Truncation construct. A large portion of the coding region of the targeted gene has been deleted and the termination codon and 3'UTR fused to the remaining truncated gene. Selection is with neomycin-resistance.

filamentous fungi, and slime molds. However, these organisms do not express the array of dynein genes found in other organisms and little can be learned about dynein isoform functional specialization in these one-dynein systems.

The ciliated protozoan *Tetrahymena thermophila* presents numerous experimental advantages for the study of various cellular processes, including the analysis of dynein isoforms. A more complete overview of the biology and experimental accessibility of *Tetrahymena* has been recently published (11).

Like fungi, *Tetrahymena* genes can be disrupted or replaced exclusively by homologous recombination. However, unlike fungi, *Tetrahymena* expresses more than a dozen different dynein heavy chain genes. The number and sequences of the family of dynein heavy chains are conserved across a widely divergent array of organisms, including protozoa, green algae, and metazoan animals.

A key feature of *Tetrahymena* is that it, like other ciliates, possesses two functionally distinct nuclei within the same cytoplasm. The diploid micronucleus carries the germline and is transcriptionally silent. The macronucleus, which contains approximately 45 copies of each expressed gene, determines the phenotype of the cell. During vegetative growth, the micronucleus divides by mitosis but the macronucleus does not; instead, the macronucleus is partitioned at cytokinesis. The amitotic division of the macronucleus provides the basis for phenotypic assortment, in which an allele can be unequally segregated. At 30°C, *Tetrahymena* divides every 2.5–3 h. Thus, under the appropriate conditions, phenotypic assortment will rapidly lead to the accumulation of a high copy number of a selectable marker. If the selectable marker disrupts a non-essential somatic gene, the gene replacement can be complete, i.e., all 45 copies of the gene replaced. On the other hand, if the gene is essential, then a “balanced” genotype develops in which most, but not all, of the wildtype copies are replaced with the marker. Because even a partial knockout often produces a phenotype, it is possible to assess the contribution of any gene—essential or nonessential—in a living cell. Further, because *Tetrahymena* can be propagated without having to undergo conjugation, mutations in genes that render the mitotic spindle non-functional can be evaluated (12).

The general strategy for gene replacement is to transform cells with a DNA construct that includes 2–3 kb of chromosomal DNA on each side of a selectable marker (Fig. 1). The simplest construct is a “knockout” construct in which the selectable marker is inserted into the coding region of the targeted gene (Fig. 1B). Other variations of the strategy include tagging the gene with an epitope or other marker such as green fluorescent protein (Fig. 1C), and replacing the wildtype gene with a truncated version of the gene (Fig. 1D). Another application would be to replace the wildtype gene with a version containing specific modifications (e.g., changing one of the dynein P-loops) and to introduce the construct by co-transformation (13).

The replacement construct can be introduced into the macronucleus of vegetatively growing cells by microinjection, electroporation, or biolistic bombardment. A second strategy is to transform conjugating cells by electroporation or biolistic bombardment. Transformation during mating results in insertion of the construct either into the micronucleus or the macronucleus,

depending on when during conjugation the transformation takes place. These different methods have been developed by others (**13–16**).

In this chapter, we summarize the following protocols: (1) obtaining genomic clones of individual dynein heavy chain genes; and (2) macronuclear gene replacement by biolistic bombardment of vegetatively growing *Tetrahymena* cells. The genomic clone is utilized to make the replacement construct. The construct is used to transform *Tetrahymena* cells with the Bio-Rad PDS 1000/He biolistic gun.

2. Materials

2.1. Genomic Clones

1. Bgl II, reaction buffer provided by vendor.
2. Wizard DNA clean-up resin (Promega).
3. Lambda GEM-11 (Promega), predigested with BamHI, pre-phosphatased. Packagene System (Promega).
4. T4 DNA ligase (NEB), reaction buffer including ATP provided by vendor.
5. KW251 bacterial host cells (Promega).
6. Luria-Bertani (LB) medium (per 1 L): 10 g bacto-tryptone, 5 g bacto-yeast extract, 10 g NaCl, pH 7.0 with NaOH. For LB with tetracycline: add 15 µg/mL tetracycline (from a stock of 5 mg/mL dissolved in ethanol).
7. Agar plates: LB medium plus 15 g bacto-agar dissolved per 1 L medium.
8. Top agarose (100 mL): 1 g bacto-tryptone, 0.8 g NaCl, 0.6 g agarose.
9. Nitrocellulose circles (Micron Separations, Inc).
10. Phage denaturation solution: 1.5M NaCl, 0.5M NaOH.
11. Phage neutralization solution: 1.5M NaCl, 0.5M Tris-HCl, pH 8.0.
12. SSCP (20X): 2.4M NaCl (140.2 g/L), 0.3M sodium citrate (88.2 g/L), 0.25M KH₂PO₄ (35.4 g/L), 20 mM EDTA (40 mL of 0.5 M/L), pH 7.2 adjusted with NaOH.
13. [³²P]-labeled PCR-amplified dynein fragments, cloned into pUC118 (*see* Chapter 3).
14. SM: 50 mM Tris-HCl, pH 7.5, 100 mM NaCl, 8 mM MgSO₄, 0.01% gelatin.

2.2. Biolistic Bombardment

1. Neff's medium (1X): 0.25% proteose peptone, 0.25% yeast extract, 0.55% glucose, 33 µM FeCl₃; supplement medium with penicillin G and streptomycin sulfate (250 µg/mL each) and 1.25 µg/mL amphotericin B (Fungizone, Gibco).
2. Starvation medium: 10 mM Tris-HCl, pH 7.4.
3. Biolistic gun and accessories:
 - a. Bio-Rad PDS-1000/He biolistic gun
 - b. Autoclaved macrocarrier holder, stopping screens, rupture disk retaining cap, macrocarrier platform;
 - c. Rupture disks, 450 psi or 900 psi;
 - d. Whatman #1 filter paper 9.0 cm circles, autoclaved in large glass Petri dish.
4. Macrocarrier particles (Bio-Rad 0.6 µm gold particles, Cat. no. 165-2262), 60 mg/mL in sterile water or sterile 50% glycerol. Particle preparation:

- a. 60 mg 0.6 μm gold particles in a 1.5 mL Eppendorf tube.
 - b. Add 1 mL 70% ethanol; vortex 3–5 min.
 - c. Incubate 15 min at room temperature; collect by brief centrifugation; discard the supernatant.
 - d. Add 1 mL sterile water; vortex 1 min; allow gold particles to settle 1 min; collect by brief centrifugation; discard the supernatant.
 - e. Repeat **step (d)** twice.
 - f. Resuspend the gold particles to a final concentration of 60 mg/mL in sterile water for immediate use, or in 50% sterile glycerol for storage at -20°C (40 μL aliquots, enough for 4 shots).
5. 10 mM HEPES, pH 7.5, sterile, prewarmed to 30°C .
 6. Transforming vector DNA digested with the appropriate restriction enzymes to remove the insert DNA.
 7. Solutions pre-chilled on ice:
 - a. 70% ethanol.
 - b. 100% ethanol.
 - c. 0.1M spermidine (sterile), stored frozen.
 - d. 2.5M CaCl_2 (sterile).
 8. Recovery medium: 2X Neff's: 0.50% proteose peptone, 0.50% yeast extract, 1.1% glucose, 66 μM FeCl_3 , 250 $\mu\text{g}/\text{mL}$ penicillin G, 250 $\mu\text{g}/\text{mL}$ streptomycin sulfate, 1.25 $\mu\text{g}/\text{mL}$ amphotericin B.
 9. Selection drug: we use paromomycin (sterile stock solution of 100 mg/mL).
 10. Other hardware:
 - a. sterile Pasteur pipets.
 - b. 2 pairs of sterile forceps.
 - c. sterile plastic Petri dishes.
 - d. sterile 1-L flasks.
 - e. sterile 96-well microtiter dishes.
 - f. multiwell pipettor.

3. Methods

3.1. Isolation of Genomic Clones (see Note 1)

1. Partially digest 10 μg genomic DNA with BglIII. The goal is to obtain a partial digest in which >10 kb fragments hybridize with the PCR-amplified fragments. We found that the following conditions produced the desired partial digest: 2 μL BglIII (20 units), 60 min, 37°C .
2. After digestion, purify the DNA on the Wizard DNA clean-up resin. Wash the resin with 2 mL of 80% isopropanol and elute the DNA in TE preheated to 70°C . Determine the concentration of the eluted DNA by measuring its absorbance at 260 nm.
3. Ligate DNA with 0.5 μg of λ arms according to vendor's recommendations. It is usually important to try different ratios of DNA to λ arms. Ligation is performed in a total of 10 μL at 17°C , overnight.
4. Package the 10 μL ligation product with 50 μL Packagene extract as specified by the manufacturer.

5. Add 445 μL of phage buffer and 25 μL chloroform, mix gently, store at 4°C.
6. Infect KW251 host cells with diluted phage. Grow the bacterial cells in LB/tetracycline to an optical density measured at 600 nm of 0.6–0.8. Adsorb 100 μL of varying phage dilutions to 100 μL bacteria at 37°C, 30 min. Plate the infected bacteria in molten top agarose at 45°C onto LB agar plates prewarmed to 37°C. Incubate overnight at 37°C. Using this method, determine the titer of the phage library by infecting bacteria with different dilutions of the phage.
7. After determining the titer of the library, plate enough phage onto 150 mm LB plates to obtain approximately 3–5,000 plaques/plate. Grow for 8 h. The goal is to obtain pinpoint sized plaques.
8. Carefully lay nitrocellulose disc on plate, allow transfer for 1 min. Mark orientation with India ink.
9. Remove first filter, repeat transfer to a second filter, this time allow transfer for 3 min. Mark orientation.
10. Rinse filters in phage denaturation solution for 30 s.
11. Transfer filters to phage neutralization solution for 1 min.
12. Wash filters in 2X SSCP for 30 s, then air dry on Whatman paper.
13. Dry further in a 42°C oven overnight, or in a vacuum oven at 80°C for 1–2 h.
14. Process the filters for Southern blotting as described in previous chapter, using labeled dynein fragments as probes. We have performed this screening step by probing with a mixture of up to six different fragments and have subsequently recovered genomic clones for each of the six dynein genes.
15. Locate on the plates the positive plaques. Using the back of a sterile blue pipette tip (for P1000 micropipetter), remove a core of agar surrounding each positive plaque. Transfer each core to an eppendorf tube containing 500 μL SM and 25 μL chloroform. Store at 4°C.
16. Perform secondary screen by plating phage from the cores, repeating **steps 7–5**, except use tip of sterile Pasteur pipette to pick single plaque.
17. Perform tertiary screen, repeating **steps 7–15**. If successful, all of the plaques in the tertiary screen should hybridize with the probe.

3.2. Gene Replacement in Vegetative Cells by Biolistic Bombardment (see Note 2)

3.2.1. Cell Growth and Starvation

1. Day 1: Prepare starter culture by diluting 10 μL healthy stock of CU428.1 cells into 1 mL 1X Neff's (we use one well of a 6-well plate); 30°C overnight; no shaking.
2. Day 2: Expand the culture to 10 mL in 1X Neff's; 30°C overnight, shaking.
3. Day 3: Expand the culture to 100 mL in 1X Neff's on a shaking 30°C incubator; grow to mid-late log phase ($3 - 7 \times 10^5$ cells/mL). This typically takes 12 h.
4. Day 4: Collect the cells in oil tubes at 1100g for 3 min; decant the supernatant.
5. Wash the cells in a small volume of Starvation medium.

6. Resuspend the cells in a 2.8 L Fernbach flask in Starvation medium at a final concentration of 2×10^5 cells/mL. Starve cells 24 h, shake 100 rpm, 30°C.
7. Day 5: Count cells. Adjust concentration of cells to 2×10^5 cells/mL with Starvation medium. Return to 30°C shaker. 50 mL of cells per shot.

3.2.2. General Preparation

1. Sterilize the appropriate number of rupture disks and macrocarriers by soaking them in 95% ethanol in a Petri dish for 15 min with gentle agitation. Remove the disks and macrocarriers from the ethanol and allow them to air-dry on a sterile Petri dish lid in the laminar flow hood.
2. Thoroughly wipe down the exposed surfaces of the laminar flow hood and the biolistic gun, the gun inner chamber, and benchtops with ethanol.
3. Turn on the gun. Make sure that the helium pressure at the regulator valve is set at 200 psi over the pressure rating of the rupture disks being used.
4. Place a sterile macrocarrier in each macrocarrier holder. Ensure that the macrocarrier is completely inserted in each holder by using two sterile 1000 μ L pipet tips to press the macrocarrier under the lip of the holder.
5. Pre-chill on ice the 100% ethanol, 70% ethanol, and 2.5M CaCl₂. Thaw the prepared gold particles and 0.1M spermidine on ice.
6. For each shot: Transfer 50 mL 2X Neff's medium into a 500 mL Erlenmeyer flask (*see Note 3*).

3.2.3. Preparation of Transforming DNA

1. Purify the plasmid on a Qiagen column, following vendor's recommendations.
2. Release the insert from the plasmid by digestion with the appropriate restriction enzymes. It is critical that the two ends of the transforming DNA correspond to *Tetrahymena* chromosomal sequences.

3.2.4. Coat Gold Particles with DNA (*see Note 4*)

1. Add 20–30 μ g of prepared vector (1 μ g/ μ L) to 20 μ L of prepared gold particles, vortex 2–3 s.
2. Add 40 μ L of ice-cold 2.5M CaCl₂, vortex 2–3 s.
3. Add 16 μ L ice-cold spermidine, vortex gently for 10 min at 4°C.
4. Collect particles by brief centrifugation; carefully withdraw and discard supernatant.
5. Resuspend gently in 200 μ L ice-cold 70% ethanol, pulse in microcentrifuge, carefully withdraw and discard supernatant.
6. Repeat previous step with 100% ethanol.
7. Resuspend particles in 40 μ L 100% ethanol, vortex 2–3 s.
8. Pipet 10 μ L particles onto a macrocarrier; allow to air-dry.

3.2.5. Final Preparation of Starved Cells (*see Note 5*)

1. Transfer 100 mL cells (2×10^7 cells) into sterile oil tubes and collect by centrifugation at 1100g for 3 min; carefully remove all of the supernatant.

2. Resuspend cells in 25 mL of pre-warmed (30°C) 10 mM HEPES; wash in oil tubes and collect by centrifugation, discard supernatant.
3. Resuspend cells in 2 mL pre-warmed 10 mM HEPES.
4. Pre-wet a sterile 9 cm filter circle with 2 mL 10 mM HEPES; evenly spread 1 mL of concentrated cells over the surface of the filter paper.

3.2.6. Gun Assembly

Assemble the gun according to manufacturer's specifications. When the apparatus is assembled, the stopping screens should be 12 cm from the target cells.

3.2.7. Gun Shoot

Perform the gun shoot using a vacuum pressure of 27 psi.

3.2.8. Cell Recovery

1. Transfer the filter paper, and the solution in the Petri dish to a flask containing 2X Neff's medium.
2. Rinse the Petri dish with 1 mL 10 mM HEPES to retrieve remaining cells. If a second shot of the same vector is performed, combine the two sets of cells into one 1 L flask containing 100 mL 2X Neff's.
3. Allow the cells to recover at room temperature 2–6 h.

3.2.9. Selection (see **Note 6**)

1. After recovery, add paromomycin to the flask to a final concentration of 100 µg/mL.
2. Transfer the cells to the wells of 96-well microtiter dishes, 150 µL per well.
3. Incubate the cells in a humid container at 30°C. Resistant cells should be detectable 2–3 d after shooting. However, it may take 10 d for a resistant clone to emerge.
4. Transfer resistant cells to fresh growth medium containing selection drug. The objective over the next few weeks is to gradually increase the paromomycin concentration and to wean the cells from 2X Neff's to 1X Neff's.

4. Notes

1. These are standard methods (**17**).
2. This protocol is described by Bruns and Cassidy-Hanley (**16**) and is specifically for the BioRad 1000/He biolistic gun.
3. We often perform two shots with the same vector; in this case, use 100 mL 2X Neff's into a 1 L flask.
4. The protocol in **Subheading 3.2.4**, provides enough material for two shots.
5. The protocol in **Subheading 3.2.5**, provides enough material for two shots. Prepare cells in no more than 100 mL batches to minimize the time the cells are at high concentration.

Table 1
Summary of Vegetative Transformation by Biolistic Bombardment

Experiment	Plasmid	Form of DNA ^a	Micrograms DNA/experiment	Number of transformants	Efficiency ^b
1	pH1-Neo ^c	Circular	12.5	20	1.6
2	pH1-Neo	Linear	20	208	10.4
3	pH1-Neo	Linear	30	242	8.1
4	pDYH1 ^d	Linear	4	28	7.0
5	pDYH1	Linear	20	45	2.3
6	pβtail ^e	Circular	20	0	0
7	pβtail	Linear	30	2	<0.1
8	pβtail	Linear	30	6	0.2

^a circular, the uncut plasmid; linear, plasmid digested to free the insert

^b efficiency reported as number of transformants per μg of DNA

^c pH1-Neo, *Tetrahymena* histone H1 disruption construct¹⁸

^d pDYH1, *Tetrahymena* cytoplasmic DYH1 gene, tagged at the 3' end

^e pβtail, *Tetrahymena* beta DYH4 gene, truncated

6. **Table 1** summarizes the results of several separate vegetative shootings. Two things are clear. One, there is a significant variation from plasmid to plasmid. This presumably reflects differences in recombination efficiency depending on the location of the targeted gene. Two, linearized DNA is far more efficient at producing transformants than circular plasmids. Apparently, the recombination event requires a free end whose sequence matches that of the targeted chromosome.

Acknowledgments

We thank Marty Gorovsky, Peter Bruns, and Jim Forney for their advice in the many parts of these protocols. This work was supported by a grant from the National Science Foundation, MCB 9728207.

References

1. Vaisberg, E. A., Grissom, P. M., and McIntosh, J. R. (1996) Mammalian cells express three distinct dynein heavy chains that are localized to different cytoplasmic organelles. *J. Cell Biol.* **133**, 831–842.
2. Echeverri, C. J., Paschal, B. M., Vaughan, K. T., and Vallee, R. B. (1996) Molecular characterization of the 50-kD subunit of dynactin reveals function for the complex in chromosome alignment and spindle organization during mitosis. *J. Cell Biol.* **132**, 617–633.
3. Koonce, M. P. and Samsó, M. (1996) Overexpression of dynein's globular head causes a collapse of the interphase microtubule network in *Dictyostelium*. *Mol. Biol. Cell* **7**, 935–948.

4. Shaw, S. L., Yeh, E., Maddox, P., Salmon, E. D., and Bloom, K. (1997) Astral microtubule dynamics in yeast: a microtubule-based searching mechanism for spindle orientation and nuclear migration into the bud. *J. Cell Biol.* **139**, 985–994.
5. Myster, S. H., Knott, J. A., O'Toole, E., and Porter, M. E. (1997) The *Chlamydomonas Dhc1* gene encodes a dynein heavy chain subunit required for assembly of the II inner arm complex. *Mol. Biol. Cell* **8**, 607–620.
6. Smith, E. F. and Lefebvre, P. A. (1996) *PF16* encodes a protein with Armadillo repeats and localizes to a single microtubule of the central apparatus in *Chlamydomonas* flagella. *J. Cell Biol.* **132**, 359–370.
7. Pazour, G. J., Dickert, B. L., and Witman, G. B. (1999) The DHC1b (DHC2) isoform of cytoplasmic dynein is required for flagellar assembly. *J. Cell Biol.* **144**, 473–481.
8. Eshel, D., Urrestarazu, L. A., Vissers, S., Jauniaux, J.-C., van Vliet-Reedijk, J. C., Planta, R. J., and Gibbons, I. R. (1993) Cytoplasmic dynein is required for normal nuclear segregation in yeast. *Proc. Natl. Acad. Sci. USA* **90**, 11,172–11,176.
9. Li, Y.-Y., Yeh, E., Hays, T., and Bloom, K. (1993) Disruption of mitotic spindle orientation in a yeast dynein mutant. *Proc. Natl. Acad. Sci. USA* **90**, 10,096–10,100.
10. Koonce, M. P. and Knecht, D. A. (1998) Cytoplasmic dynein heavy chain is an essential gene product in *Dictyostelium*. *Cell Motil. Cytoskeleton* **39**, 63–72.
11. Asai, D. J. and Forney, J. D., editors (2000) *Tetrahymena thermophila*. Methods in Cell Biology volume 62. Academic Press, San Diego, CA.
12. Lee, S.-w., Wisniewski, J. C., Dentler, W. L., and Asai, D. J. (1999) Gene knockouts reveal separate functions for two cytoplasmic dyneins in *Tetrahymena thermophila*. *Mol. Biol. Cell* **10**, 771–784.
13. Cassidy-Hanley, D., Bowen, J., Lee, J. H., Cole, E., VerPlank, L. A., Gaertig, J., Gorovsky, M. A., and Bruns, P. J. (1997) Germline and somatic transformation of mating *Tetrahymena thermophila* by particle bombardment. *Genetics* **146**, 135–147.
14. Gaertig, J. and Gorovsky, M. (1992) Efficient mass transformation of *Tetrahymena thermophila* by electroporation of conjugants. *Proc. Natl. Acad. Sci. USA* **89**, 9196–9200.
15. Chalker, D. L., Ward, J. G., Randolph, C., and Yao, M.-C. (2000) Microinjection of *Tetrahymena thermophila*. *Meth. Cell Biol.* **62**, 469–484.
16. Bruns, P. J. and Cassidy-Hanley, D. (2000) Biolistic transformation of macro- and micronuclei. *Meth. Cell Biol.* **62**, 501–512.
17. Sambrook, J., Fritsch, E. F., and Maniatis, T. (1989) *Molecular Cloning: A Laboratory Manual, 2nd ed.* Cold Spring Harbor Laboratory Press, Cold Spring Harbor, NY.
18. Shen, X., Yu, L., Weir, J. W., and Gorovsky, M. A. (1995) Linker histones are not essential and affect chromatin condensation *in vivo*. *Cell* **82**, 47–56.

Functional Analysis of Cytoskeletal Components in the Developing Visual System of *Drosophila*

Qi He

1. Introduction

A central issue in neuroscience is to understand the mechanisms underlining the stereotyped patterns of neuronal connectivity. Studies of neuronal development in both vertebrates and invertebrates have established two distinct processes involved in neuronal patterning, reviewed in (1). At early stages, guidance mechanisms that are independent of neuronal synaptic activity establish connections that have a rather crude topographical accuracy. Later, activity-dependent mechanisms remodel these initial connections into the refined circuits of the mature nervous system.

Axonal navigation is led by the growth cone that senses guidance cues in the developing nervous system and makes directional locomotion. At the leading edge of the growth cone, surface guidance receptors encounter extracellular cues and subsequently initiate a chain of signaling events leading to the mobility of the growth cone.

Filopodia and lamellipodia are the specialized membrane structures of the growth cone that search the environment for guidance cues. These structures are supported by a network of cytoskeletal components, primarily actin and associated proteins, reviewed in (2). Thus, the actin cytoskeleton is the basic engine of crawling locomotion during growth cone navigation (3,4). As a result, characterizing the role of actin-associated proteins in axonal guidance is an essential part in revealing guidance mechanisms.

The *Drosophila* visual system provides a unique model for studying axon guidance and target recognition, and the highly stereotypic projection pattern of the retinal axons offers a high-resolution system for examining axonal connectivity, reviewed in (5).

This chapter describes methods for analyzing *Drosophila* actin-binding protein Profilin *chic^x* in the visual system development utilizing FLP/FRT generated mosaic animals and confocal microscopy. These analyses can be used to characterize other cytoskeletal components as well.

2. Materials

2.1. Equipment

1. Standard incubator for culturing *Drosophila*.
2. Dissecting microscope.
3. Confocal microscope.
4. Water bath.

2.2. Reagents

1. Geneticin (G418, Life Technologies, Gaithersburg, MD): Prepare 10 mg/ml stock solution and store at -20°C . Add to 0.7–1 mg/mL final concentration when preparing food for G418 selection in mosaic analysis.
2. Standard cornmeal medium: Mix 850 mL of water with 7.9 g of agar, 27.5 g of torula yeast, 52 g of cornmeal, and 110 g of dextrose. Heat to a boil and cool to 80°C . Add 2.4 g of tegosept dissolved in 92 mL ethanol and pour into culture vials and bottles.
3. G418 medium: Prepare standard cornmeal medium and cool it to 50°C . Add G418 and pour into culture vials.
4. 4% paraformaldehyde: To prepare 50 mL stock, weigh 2 g of paraformaldehyde powder and mix with 30 mL of water. Heat to 55°C with stirring and add a few drops of NaOH to facilitate dissolving. Cool to room temperature and add 5 mL of 10X phosphate-buffered saline (PBS). Add water to 50 mL, mix and store in aliquots at -20°C .
5. PBS (10X): Dissolve 80 g of NaCl, 21.6 g of $\text{Na}_2\text{HPO}_4 \cdot 7\text{H}_2\text{O}$, 2 g of KH_2PO_4 , and 2 g of KCl in 800 mL of H_2O , pH to 7.4 and add H_2O to 1000 mL.
6. PBT solution: Add 0.3% Triton X-100 to 1X PBS and mix.
7. Antibodies: Goat FITC-anti-HRP (ICN), rabbit anti- β -gal (ICN), Cy5 conjugated donkey antirabbit IgG (Jackson Lab).

2.2. *Drosophila* Strains and Culture

1. A fly Profilin mutant (later named as *chic^x*) was initially isolated from a P-element generated mutant collection (6) as a strain with retinal axon projection defects. Subsequent cDNA analysis revealed that it was a *Drosophila* Profilin mutant.
2. *P[ry⁻, FRT]40A/CyO* was obtained from M. Ashburner (Cambridge, UK), *w;{arm-lacZ24A, P[FRT]40A}/CyO* and *y,hsFLP¹²²;{arm-lacZ24A, P[FRT]40A}/CyO* originally from G. Struhl.

All strains should be grown on standard cornmeal medium.

3. Methods

3.1. Mosaic Analysis

3.1.1. Preparation of FRT and FLP Strains

1. P[ry⁻, FRT]40A strains in *w* background (*see Note 1*):

Set up the following cross:

+Y;P[ry⁻, FRT]40A/CyO X *yw/yw;Gla/y⁺CyO*

Select *Gla⁺* males and cross to *yw/yw;Gla/y⁺CyO*:

yw/Y;P[ry⁻, FRT]40A/y⁺CyO X *yw/yw;Gla/y⁺CyO*

Collect *yw/Y;P[ry⁻, FRT]40A* and *yw/yw;P[ry⁻, FRT]40A*, and establish a stock *yw;P[ry⁻, FRT]40A* referred to in the following text as *yw;P[FRT]40A*

2. Generation of the FLP strain:

Set up the cross:

w/Y;{arm-lacZ24A, P[FRT]40A}/CyO X *y,hsFLP¹²²;{arm-lacZ24A, P[FRT]40A}/CyO*

Collect *Cy* males and cross to *y,hsFLP¹²²;{arm-lacZ24A, P[FRT]40A}/CyO*:

y,hsFLP¹²²/Y;{arm-lacZ24A, P[FRT]40A}/CyO X *y,hsFLP¹²²;{arm-lacZ24A, P[FRT]40A}/CyO*

Select *Cy* and establish a stock. Due to the FLP enzyme activity of *hsFLP¹²²* at higher temperatures, all crosses should be cultured at 18°C.

3.1.2. Generation of Mosaic Animals

To generate somatic mosaic animals, the FLP/FRT method is used (*see Note 2*). This requires to first generate Profilin *chic^x/FRT* recombinants, where the Profilin mutation is distal to the FRT site (*see Note 3*).

1. Set up the following cross:

yw;chic^x26A/CyO X *yw/Y;P[FRT]40A*

2. Pick *CyO⁺* offsprings and mate to *yw/Y;Gla/y⁺CyO*:

yw;chic^x26A/ P[FRT]40A X *yw/Y;Gla/y⁺CyO*

3. Culture this cross in *neomycin* (G418) media (*see Note 4*), and select *w⁺* and cross to *yw/Y;Gla/y⁺CyO* (single animal cross):

yw/yw;{chic^x26A, P[FRT]40A}/y⁺CyO X *yw/Y;Gla/y⁺CyO*

4. Select *Gla⁺* offsprings and cross to the FLP strain:

yw/Y;{chic^x26A, P[FRT]40A}/y⁺CyO X *y, hsFLP¹²²;{arm-lacZ24A, P[FRT]40A}/y⁺CyO*

5. Collect eggs at 25°C and heat-shock for 60 min at 38°C in a water bath. Dissect third-instar larvae and stain with antibodies as described below.

3.2. Histology

3.2.1. Larval Eye Disc/Brain Specimen Preparation

Dissect the visual system of third instar larvae and fix in 4% paraformaldehyde at 4°C overnight (*see Note 5*).

3.2.2. Antibody Staining

1. Following fixation, wash specimens three times (5 min each) with PBT. Make sure all samples have sunk to the bottom of the tube.
2. Block nonspecific binding sites with 10% goat serum in PBT at 4°C overnight.
3. Incubate with a primary antibody. For visualizing photoreceptor cells and retinal axons, use mAb 24B10 supernatant (**9**) at 1:3 dilution (or FITC-anti-HRP, which labels all neurons) (**10**). For negatively marking mosaic clones, use rabbit anti- β -gal at 1:500 dilution (*see Note 6*). Dilution should be made with 10% goat serum in PBT. Leave overnight at 4°C.
4. Wash four times at room temperature with PBT for 15 min each.
5. Block as in **step 2**.
6. Incubate with fluorescently labeled secondary antibody. For mAb m 24B10, use FITC-conjugated goat antimouse IgG at 1:200 dilution. For anti- β -gal, use Cy5 conjugated donkey antirabbit IgG at 1:500 dilution. Incubate at 4°C overnight.
7. Wash as in **step 4**.
8. Go through 5-min serial washes of 25%, 50% and 75% of glycerol in PBS. Finally, resuspend samples in 75% glycerol/PBS with 0.1% p-phenylenediamine. Mount the samples onto slides (*see Note 7*) and examine under a confocal microscope.

4. Notes

1. Since *chic^x* is a P-element generated mutant with a mini-white gene carried by the P-element, the FRT strain should have a *w* eye phenotype.
2. Generating somatic mosaic animals has been instrumental in revealing later stage functions for genes whose homozygous mutation is lethal at early stages of development. In the case of *chic^x*, mosaic analysis will be critical to determine whether *chic^x* is required by the photoreceptor cells or by the target neurons in the brain or both. For instance, if mutant clones that includes photoreceptor cells produce axons with aberrant projection, it will implicate that *chic^x* is required in the photoreceptor cells.

The FLP/FRT system is most efficient in producing somatic mosaics at different stages of development (**7**). This method utilizes the recombination between two FRT target sites catalyzed by the yeast 2 μ m plasmid site-specific recombinase FLP. As a result, homologous chromosome arms harboring allelic FRT sites can be exchanged, generating one mutant daughter cell and one wild-type daughter cell (“twin spot cell”) following mitosis.

3. A collection of FRT strains is available where FRT sites have been inserted close to the centromere of the first, second and third chromosomes (**7**). For Profilin *chic^x* (26A), the FRT strain P[FRT]40A is chosen.
4. The structure P[FRT] carries two copies of the *neomycin* gene driven by a heat-shock promoter (*hs-neo*). When cultured at 25°C, animals with the *hs-neo* construct confers *neomycin*-resistance. Since the P-element contains a mini-white gene (*w⁺*), the *w⁺* selection confers the existence of the P-element. Also, to keep the

cross at 30°C during larval and pupal stages will increase the rate of recombination since spontaneous recombination is temperature-sensitive. Generally speaking, this is the speed-limit step and multiple crosses are recommended.

5. Care should be taken to ensure that all specimens have sunk to the bottom of the tube to have a sufficient fixation (8).
6. Due to the generation of “twin spot” cells in somatic recombination, homozygous *chic^x* mutant clones will not carry the transgene *arm-lacZ24A*, and thus appear negative with anti- β -gal staining.
7. The eye disc/brain specimens should be mounted onto a slide by cutting with a surgical knife at the middle of the two brain lobes. The two halves should then be allowed to rest on the surface generated by the cut so that the lateral perspective axis will be perpendicular to the slide.

Acknowledgments

I thank John Roote (M. Ashburner lab, Cambridge, UK) for providing FRT lines and Ray Gavin for reviewing the manuscript. This work was supported in part by a PSC-CUNY grant.

References

1. Goodman, C. S. and Shatz, C. J. (1993) Developmental mechanisms that generate precise patterns of neuronal connectivity. *Cell* **72/Neuron** **10** (Suppl.), 77–98.
2. Gavin, R. H. (1997) Microtubule-microfilament synergy in the cytoskeleton. *Int. Rev. Cytol.* **173**, 207–242.
3. Mitchison, T. J. and Cramer, L. P. (1996) Actin-based cell motility and cell locomotion. *Cell* **84**, 371–379.
4. Suter, D. M. and Forscher, P. (1998) An emerging link between cytoskeletal dynamics and cell adhesion molecules in growth cone guidance. *Curr. Opin. Neurobiol.* **8**, 106–116.
5. Kunes, S. and Steller, H. (1993) Topography in the *Drosophila* visual system. *Curr. Opin. Neurosci.* **3**, 53–59.
6. Torok, T., Tick, G., Alvarado, M., and Kiss, I. (1993) P-lacW insertional mutagenesis on the second chromosome of *Drosophila melanogaster*: Isolation of lethals with different overgrowth phenotypes. *Genetics* **135**, 71–80.
7. Xu, T. and Rubin, G. M. (1993) Analysis of genetic mosaics in developing and adult *Drosophila* tissues. *Development* **117**, 1223–1237.
8. Kunes, S., Wilson, C., and Steller, H. (1993) Independent guidance of retinal axons in the developing visual system of *Drosophila*. *J. Neurosci.* **13**, 752–767.
9. Fujita, S. C., Zipursky, S. L., Benzer, S., Ferrus, A., and Shotwell, S. (1982) Monoclonal antibodies against the *Drosophila* nervous system. *Proc. Natl. Acad. Sci. USA* **79**, 7929–7933.
10. Jan, L. Y. and Jan, Y. N. (1982) Antibodies to horseradish peroxidase as specific neuronal markers in *Drosophila* and in grasshopper embryos. *Proc. Natl. Acad. Sci. USA* **79**, 2700–2704.

Index

A

- Actin, 109–118, 153, 154, 229, 230, 231, 234–236
 - FITC-phalloidin labeling of, 114–117, 234–236
- Antibodies, 121–132, 133–138, 141–147
 - labeling with colloidal gold, 134–136
 - monoclonal, 122–132
 - materials for production, 124
 - production protocols, 127–130
 - protein G affinity purification, 142, 143, 144
 - polyclonal, 122–132
 - materials for production, 123, 124
 - production protocols, 125, 126
 - purification, 124, 127
 - Tat-mediated delivery, 141–147
 - Tat-antibody coupling, 142, 144
 - uptake of Tat-coupled antibody, 144–147

B

- Biolistic bombardment, 272–277
 - basic protocol, 273–277
 - materials, 272, 273

C

- Cell Demembration, 248, 249
- Cell Fusion, 127–129, 194
- Cell Morphology, 85–98
 - parameters, 87–98
- Cell Motility, 37–41, 45–57, 59–81, 101–106
 - assays, 37–41, 49–56, 60, 102–106
 - parameters, 49, 54, 55, 61, 70–72
 - chemotaxis, 72, 73, 101–106

Centriole, 215–227

- assembly and duplication, 217, 221, 222

Centrosome, *See* centriole.

Chemical cross-linking, 142, 144

Chemokinesis, *See* Cell motility.

Chlamydomonas, 242, 248

Chromatophores, 201, 202. *See also* Melanophores.

Cilia/Flagella, 241–251

- reactivation assays, 242–247

Colloidal gold, 134–137

- negative staining of immuno-labeled protein complexes, 136, 137
- preparation for direct labeling of primary antibody, 134, 136
- protocol for direct labeling of primary antibody, 136

See also Microscopy.

Confocal microscopy, *See* Microscopy.

Cytochalasin, 91, 93, 109

Cytoskeleton, 31, 32, 109–112, 121, 151, 152, 189–191, 202, 203, 229, 230

Cytokeratin, *See* Intermediate filaments.

D

Demembrated sperm, *See* Sperm.

Dictyostelium, 45–57, 111, 117, 156

DNA, 3–8, 17–27, 167–170, 173–179

- cDNA synthesis and purification, 19, 21, 167–169, 173–175
- circularizing DNA, 6
- cloning, 3–5, 19, 22, 177–179
- enzymatic digestion, *See* Restriction digests.

- ethidium bromide removal from, 179
 extraction from gels, *See* Gel extraction.
 genomic DNA isolation, 20, 23
 sequencing, 19, 22
Drosophila, 279–283
 culture, 280
 FRT and FLP strains, 281
 histology, 281
 mosaic analysis, 281
 Dynactin, 121
 Dynamin, 165–186
 overexpression, 168
 Dynein, 17–25, 121, 129, 156, 157, 269–277
 obtaining genomic clones, 272, 273, 274
- E**
- Electron microscopy, *See* Microscopy.
 Electrophoresis, 20, 174, 176
 Endoplasmic reticulum, 130, 131
 ER, *See* Endoplasmic reticulum.
 Ethidium bromide, *See* DNA.
- F**
- Fish, 203, 204
- G**
- β -Galactosidase assays, 260–262
 fluorescence, 262
 ONPG, 261
 X-Gal, 261
 Gel extraction, 169, 177, 178
 Gene replacement strategies, 269–272
 Germinal vesicle, 218, 222
 GFP, 32, 151–160, 165–186
 GFP-actin, 153, 154
 GFP-dynamin, 157, 158, 165–186
 GFP-dynein, 156, 157
 GFP-kinesin, 156, 157
 GFP-myosin, 156
 GFP-tubulin, 155, 156
 GFP-vimentin, 154, 155
- Golgi, 158
 Green fluorescent protein, *See* GFP.
- H**
- Heterokaryons, 189–196
- I**
- Intermediate filaments, 121, 151, 154, 155, 189–196, 229, 230, 234–236
 cytokeratin, 235
 keratin, 189–196
 vimentin, 154, 155, 189, 190
 Inverse PCR, *See* Polymerase chain reaction.
- J**
- Jasplakinolide, 109–118
 Jaspamide, *See* Jasplakinolide.
- K**
- Keratin, *See* Intermediate filaments.
 Kinesin, 156, 157
- L**
- Latrunculin B, 237
 Ligations, 178
 Lymphocytes, 116
- M**
- Melanophores, 202, 203–212
 aggregation and dispersion, 205, 206
 culturing, 205, 208, 209
 dissociating from fish dermis, 204, 206–208
 lysing and reactivating, 206, 211
 microinjecting, 210
 perfusing, 210
 source of, 203, 204
 MDCK cells, 117
Micrasterias, 112–116
 Microscopy, 31–43, 45–57, 59–81, 85–98, 113–118, 133–138, 170–172, 181, 182, 193, 195, 218, 221–223, 234–236, 246, 247, 280, 282
 confocal, 47, 55, 56, 171, 172, 231, 234–236, 280, 282

electron, 113–118, 221, 222
 carbon-coated grids, 135
 fixation, 113, 115
 formvar-coated grids, 135
 negative staining, 134, 136, 137
 reagents, 113
 FITC-phalloidin staining, 114, 117,
 234–236
 immunoelectron, 113–116, 130,
 133–138
 immunofluorescence, 116, 117, 170,
 181, 195, 218, 223, 234–236
 two-d and three-d image analysis,
 45–57
 basic protocols, 47–55
 equipment, 46, 47
 video-enhanced DIC, 31–43, 45–57,
 61, 86, 87, 130, 131, 171, 172
 basic protocols, 37–41
 equipment, 35–37
 theory, 33, 34
 Microsequencing, *See* Myosin.
 Microtubules, 31, 32, 121, 151, 202,
 203, 229, 230, 234–236
 Mosaic animals, 281
 Motility, *See* Cell motility.
 Myosin, 3, 9–15, 156
 isolation of peptides, 12
 microsequencing, 9–15
 peptide sequencing, 12, 13
 proteolytic digestion, 11, 12

N

Negative staining, *See* Colloidal gold;
 Microscopy.
 Nocodazole, 237

O

Oocytes, 216–221
 isolation, 216, 218
 lysates and extracts, 216, 217, 219–221
 Optical sectioning, 53, 54
 Overexpression, *See* Recombinant
 protein.

P

PCR, *See* Polymerase chain reaction.
 Phalloidin, 114, 117, 235
 Plasmid purification, 169, 170, 178, 179
 Polymerases, *See* Polymerase chain
 reaction.
 Polymerase chain reaction, 3–8, 9–15,
 19, 21, 22, 169, 175–177
 basic protocols, 6–8, 19, 21, 22
 cloning and sequencing products, 19,
 22, 169, 177
 extra-long reverse transcription (RT),
 169, 175, 176
 gel analysis of products, 6, 169,
 177, 178
 hot start approach, 8
 inverse, 6–8
 polymerases, 5, 19–21, 169
 primers, 5, 7, 21, 23, 24
 Primers, *See* Polymerase chain reaction.

R

Recombinant protein, 168–170, 175,
 176, 180, 181
 basic protocols, 168–170, 175, 176
 overexpression, 168–170, 180, 181
 Restriction Digests, 5, 177
 Reverse transcription (RT), 175. *See*
also Polymerase chain reaction.
 RNA isolation and purification, 18, 19,
 21, 167–169, 173–175

S

Saccharomyces cerevisiae, 255–267,
See also Yeast.
 competent cells, 260
 media formulations, 256–258
 transformation, 260
 Sperm, 231, 234, 248, 249. *See also*
 Cilia/Flagella; *Xenopus*.
 Spindle, 215–227
 assembly, 218
 inhibition of assembly, 218

Spisula, 215–227

Southern Blotting, 20, 23

 basic hybridization protocol, 23

 preparation of probes, 23

T

Tetrahymena, 3, 17–27, 101–106, 241,
 269–277

 culturing, 18

Transfection, 180, 181, 189–196

Transformation, 177

Tubulin, 155, 156

Two-hybrid system, 255–267

 basic protocol, 259–262

 controls, 262, 263

 vectors, 258, 259

V

Vimentin, See intermediate
 filaments

X

Xenopus, 229–238

 egg collection, 232–233

 egg extraction, 230, 232–233

 husbandry, 230

 sperm, 231, 234

Yeast, See *Saccharomyces*.

Series Editor: *John M. Walker*

Cytoskeleton Methods and Protocols

Edited by

Ray H. Gavin*Department of Biology, Brooklyn College, The City University of New York, NY*

Many recent advances in experimental instrumentation, reagents, and imaging technology have dramatically expanded the range of tools available for the study of the cytoskeleton. In *Cytoskeleton Methods and Protocols*, Ray Gavin brings together an international panel of experienced researchers to detail the readily reproducible methods that utilize biochemistry, immunology, genetics, microscopy, and image analysis for investigating cytoskeleton structure and function. Each protocol contains proven step-by-step instructions that enable both the novice and experienced researcher to achieve successful experimental results. The protocols utilize diverse model systems in a variety of organisms, including *Saccharomyces*, *Micrasterias*, *Tetrahymena*, *Drosophila*, *Spisula*, and *Xenopus*. Microscopy applications include digital-video microscopy and computer-assisted systems for the evaluation of cell motility and morphology. Help notes and tips accompany each protocol and provide additional, often unpublished, information that can make the difference between success and failure.

State-of-the-art and highly practical, *Cytoskeleton Methods and Protocols* makes available a diverse collection of powerful experimental systems and tools for successfully studying cytoskeleton structure and function.

FEATURES

- Offers many of techniques and model systems for the study of cytoskeleton structure and function
- Includes methods for computer-assisted analysis of cell motility and morphology
- Shows how to use antibodies and drugs that interact with specific cytoskeleton proteins
- Requires little previous experience to carry out the methods successfully

CONTENTS

Part I. Identification of Cytoskeleton Proteins. Using an Inverse PCR Strategy to Clone Large, Contiguous Genomic DNA Fragments. Microsequencing of Myosins for PCR Primer Design. Evaluating the Dynein Heavy Chain Gene Family in *Tetrahymena*. **Part II. Microscopy Applications.** Video-Enhanced Microscopy for Analysis of Cytoskeleton Structure and Function. Computer-Assisted Systems for the Analysis of Amoeboid Cell Motility. Evaluation of Individual-Cell Motility. Evaluation of Cell Morphology. A Quantitative Assay for Measurement of Chemokinesis in *Tetrahymena*. **Part III. Reagents for Studying Cytoskeleton Protein Function.** Jasplakinolide: An Actin-Specific Reagent that Promotes Actin Polymerization. Site-Directed Antibodies as Tools For Investigating Structure and Function of Cytoskeleton Proteins. Direct Labeling of Components in Protein Complexes by Immuno-Electron Microscopy. Tat-Mediated Delivery of Antibodies into Cultured Cells. **Part IV. Cytoskeleton Dynamics.** Studying Cytoskeletal Dynamics in Living Cells Using Green Fluorescent Protein. Use of Green Fluorescent Protein to Study Cellular Dynamics: Constructing GFP-Tagged Motor Enzymes. Transient Transfections and Heterokaryons as Tools for the

Analysis of Keratin IF Dynamics. **Part V. Cellular Systems as Tools for Investigating Cytoskeleton Structure and Function.** Chromatophores as Tools for the Study of Organelle Transport. Centriole Duplication, Centrosome Maturation, and Spindle Assembly in Lysates of *Spisula solidissima* Oocytes. *Xenopus* Egg Extracts as a Model System for Analysis of Microtubule, Actin Filament, and Intermediate Filament Interactions. Detergent-Extracted Models for the Study of Cilia or Flagella. **Part VI. Genetic Approaches for Studies of Cytoskeleton Protein Function.** A Yeast Two-Hybrid Approach for Probing Cytoskeletal Protein Interactions. Manipulating Dynein Genes in *Tetrahymena*. Functional Analysis of Cytoskeletal Components in the Developing Visual System of *Drosophila*. Index.

Methods in Molecular Biology™ • 161
CYTOSKELETON METHODS AND PROTOCOLS
ISBN: 0-89603-771-1
<http://humanapress.com>

ISBN 0-89603-771-1



9 780896 037717

